Programming patchy particles to form complex ordered structures

A thesis submitted for admission to the degree of

Doctor of Philosophy

Daniel F. Tracey

Balliol College

Supervisor: Prof. Jonathan P. K. Doye

Physical and Theoretical Chemistry
Department of Chemistry
University of Oxford

Hilary Term, 2019

Abstract

Title: Programming patchy particles to form complex ordered structures
Name: Daniel F. Tracey
Degree: Doctor of Philosophy
College: Balliol College
Department: Physical and Theoretical Chemistry, Department of Chemistry
Date: Hilary Term, 2019

This thesis explores by numerical simulations the rational use of patchy particles to control material properties, by designing particles to either *assemble into* or *apply internal stress to* a target structure. Increasingly complex and fine-tuned patchy-particle assemblies are being reported, which may have a wide range of interesting properties and thus immense value for meso-scale materials, devices, and technologies. Understanding the behaviour of patchy-particle ensembles is also useful for understanding natural systems, such as viruses and condensed matter.

I introduce a systematic, rational design scheme for a set of patchy particles to form a unique periodic structure. Torsional restrictions encoded in my patches assist assembly, by controlling *second*-nearest neighbour bonding. As a proof-of-concept, I demonstrated the robust assembly of five complex, extended, three-dimensional targets. In contrast, previous structures assembled from patchy particles are mostly simple, two-dimensional, and/or finite. I also considered simplified versions of the successful designs (*e.g.* fewer patches, no torsional interactions), finding them sufficient in some cases but not others.

I further extend the structural complexity by assembling three-dimensional dodecagonal quasicrystals, building on earlier two-dimensional work [1–3] which was recently realised via DNA origami [4]. This is the first demonstration of the self-assembly of any three-dimensional quasicrystal from patchy particles. I use two systems: unary, with wide, non-selective patches; and ternary, with narrower, selective patches. Assembly is more complicated than in two dimensions (*e.g.* due to de-mixing), but robust nonetheless. I characterised the structures by their diffraction patterns. I unexpectedly observed screw dislocations in the unary system (the ternary system's narrower patches disfavour defects), and in an approximant.

Finally, I deliberately introduce internal stress into a helical, tube-like structure via imperfectly aligned patches. Recently [5], a new mechanism of cholesteric ordering was identified (in DNA origami filaments)—solenoidal shape deformations due to mechanical stress. However, the results for my tubes were inconclusive, with no clear trend in solenoidal shape deformations being yet apparent. This was at least partially due to the tubes' stiffness, which reduced the shape fluctuations, but may also reflect the complex network of axial and lateral interactions controlling the tubes' mechanics.

Acknowledgements and Statement of Contribution of Student

Funding. I am grateful for funding from the ESPRC Centre for Doctoral Training in Theory and Modelling in Chemical Sciences (TMCS), under grant EP/L015722/1 (with support from Prof. David Logan), and the James Fairfax-Oxford Australia Scholarship Fund (with support from Prof. John White).

Computational facilities. I acknowledge that: (1) Part of this work was performed using resources provided by the Cambridge Service for Data Driven Discovery (CSD3), operated by the University of Cambridge Research Computing Service (www.csd3.cam.ac.uk/). This facility is provided by Dell EMC and Intel using Tier-2 funding from the Engineering and Physical Sciences Research Council (capital grant EP/P020259/1), and DiRAC funding from the Science and Technology Facilities Council (www.dirac.ac.uk). (2) A small part of this work was performed using computational resources at Instituto de Química Física Rocasolano, Consejo Superior de Investigaciones Científicas (www.iqfr.csic.es). (3) A small part of this work was performed using the University of Oxford Advanced Research Computing (ARC) facility (http://dx.doi.org/10.5281/zenodo.22558).

Codes. I used two main simulation programs: oxDNA [6], and a currently-unpublished parallel Monte Carlo program by Dr. Eva González Noya. My involvement in implementing these programs for my purposes is described in detail in section 2.2.3. I also acknowledge my use of the following codes: (1) A code for calculating the number of particles in a cluster, once all pairs of bonded particles are known (section 3.4.1), by Dr. Lorenzo Rovigatti. (2) A code for calculating two-dimensional structure factors (section 4.3.4) by Dr. Aleks Reinhardt. (3) A code for measuring solenoidal shape fluctuations (section 5.4.5) by Mr. Maxime M. C. Tortora. (4) A code for calculating the persistence length of a flexible rod-like object (section 5.4.4) by Ms. Hemani Chabbra. I heavily adapted each of these four codes for my own applications—in the case of (2), I entirely rewrote it, making it applicable to a three-dimensional, finite cluster with arbitrary position and orientation.

Supervision. I gratefully acknowledge the guidance and support of my supervisor, Prof. Jonathan P. K. Doye, and of my collaborator, Dr. Eva González Noya.

I certify that this report contains work carried out by
myself except where otherwise noted.

Daniel F. Tracey
July 10, 2019

Personal Thanks

To my family and my friends and my God, without whom this would not have been possible, and for whose love and support I am hugely thankful.

This thesis is not my own, and I could not have completed it on my own. It is the product, directly and indirectly, of a whole network—just as 'it takes a village to raise a child'. Here, I have the chance to acknowledge and thank that network.

Firstly, thank you to my supervisor, **Jon**. Your wise guidance was extremely valuable. But equally, you left space for and encouraged my own initiative. Your feedback and assistance working through difficulties was clear and insightful, cutting through to the key ideas and problems. I have learnt a lot from you, about this subject area and more generally the process of research. You have been patient, supportive, and kind throughout. I am particularly grateful for your help in the final, busy weeks. Thank you also to **Eva** for your (voluntary) assistance and guidance. You were encouraging, patient, caring, approachable, and always willing to help. You worked through and explained problems and concepts carefully and methodically, helping me understand and make progress. It was a pleasure to work with you.

Secondly, thank you to all others who helped with my work and this thesis, including **Lorenzo**, **Max**, **Flavio**, **Domen**, **Jonathan**, and **Dom**. Your guidance and assistance was valuable—and was given freely and kindly. I greatly appreciate it. In addition, thank you to those with whom I shared **room 18.19**, and other members of the **TMCS**. I am grateful for your support, encouragement, and friendship. I also acknowledge the **Oxford Scriptorium**, a place and community which made the writing process more productive, wholesome, and enjoyable.

Thirdly, thank you to my family. **Mum** and **Dad**, you have selflessly given me immeasurable love and support, have made this opportunity possible, have made me who I am to do this, and have been alongside me all the way. Along with **Matt** and **Ben**, and am so grateful for your love, support, encouragement, and understanding.

Fourthly, thank you to my friends: for support, encouragement, listening, prayers, and advice regarding my DPhil; and for friendship more generally, making life during this time so much better—kindness, care, fun, bearing my burdens, helping me grow. I cannot possibly acknowledge all, and will no doubt miss some, but nonetheless I thank: **Steven**, **Ollie** & **Georgina**, **Jon**, **Mitch** & **Jess**, **LaRae**, **Ashley**, **Ruta**, **Emma**, **Lacey**, **John** & **Temple**, **Matt** & **Sarah**, **Tim** & **Danica**, **Sam** & **Katie**, and **Riggers**; and from home, **Matt**, **Singo**, **Matt**, **Eliza**, **Stu**, **Nat**, **Alison**, **Ed**, and **Tom**. Those who have gone before or alongside me in undertaking doctorates have been uniquely able to give special support. I thank the wider communities of **St Ebbe's Church**, **OUARFC**, and **Balliol MCR** as well.

Ultimately, I thank my **God**: Father, Lord, and Saviour. It is His world that I studied. And it was all by His loving grace, mercy, and kindness: the opportunities and abilities He has given me; the support He provided, carrying me through all difficulties; my whole life and every blessing in it and still to come.

Contents

Index and Definitions of Symbols, Acronyms, and Terms

Greek Symbols

Symbol	Definition ... Page number
$\alpha, \beta, \ldots$	Patches on particles ... 71
ε	Matrix of interaction strengths $\varepsilon_{\alpha\beta}$ in a designed system ... 72
$\varepsilon_{\alpha\beta}$	Interaction strength between patches α and β; usually 0 or 1, but can in principle take any real value. Dimensionless prefactor in Eq. 2.1 ... 72
ϵ_{LJ}	Minimum energy value of U_{ij}^{LJ}, *i.e.* depth of potential well for a pair of particles ... 71
η	Number of trial (MC) moves per unit time in a simulation ... 94
$\theta_{\alpha ij}$	Angle between patch vector $\hat{\mathbf{p}}_i^{\alpha}$ (patch α on particle i) and $\mathbf{r}_{ij}$ ... 72
ν	Thread (or inclination) angle; the angle between the normal to the axis of the object and the vector tracing the helical path ... 215
ρ^*	Reduced particle number density (number of particles per unit reduced volume), $\rho^* = N/V^*$ ... 94
σ-phase	Square-triangle tiling denoted (3^2, 4, 3, 4), based on the Frank-Kasper phase of the same name. ... 35
$\sigma_{\mathrm{ang},\alpha}$	Measure of the angular width of patch α (a Gaussian root-mean-square width, in radians). Usually the same for all patches in a system ... 72
σ'_{LJ}	Distance at which $U_{ij}^{\mathrm{LJ}'}$ passes through zero ... 71
σ_{LJ}	Distance at which U_{ij}^{LJ} passes through zero ... 71
$\sigma_{\mathrm{tor},\alpha\beta}$	Measure of the torsional 'width' for the patch pair α, β (a Gaussian root-mean-square width, in radians). Usually the same for all patch pairs in a system ... 73

$\phi_{\alpha\beta}$ Torsional angle for patches α and β: angle between the projections of the reference vectors for patches α (on particle i) and β (on particle j) onto a plane perpendicular to $\hat{\mathbf{r}}_{ij}$. See also 'torsional angle' 73

$\phi_{\alpha\beta}^{\text{offset}}$ Set of equivalent offset angles for patches α and β, *i.e.* preferred (minimum energy) values of the torsional angle, $\phi_{\alpha\beta}$. See also 'offset angle' 73

ϕ^{offset} Matrix of sets of offset angles $\phi_{\alpha\beta}^{\text{offset}}$ in a designed system 73

$\mathbf{\Omega}_i$ Orientation of particle i 71

Latin Symbols

Symbol	**Definition** ..... **Page number**
D	Diameter 234
$\mathrm{d}N_{\text{loop}}$,$N_{\text{loop}}^{\text{dis}}$	Distorted helix, as for $\mathrm{u}N_{\text{loop}}$ but with lateral patches positioned relative to each other as they are in $\mathrm{u}N_{\text{loop}}^{\text{dis}}$ helix 225
F	Helmholtz free energy 62
$\mathcal{H}$	Measure of circular helicity of a solenoidal conformation 241
$i, j, \ldots$	Particles 71
k	Wavenumber; in Fourier analysis of solenoidal conformations, reciprocal pitch 241
k_{B}	Boltzmann constant 74
L	Distance along the contour of a rod-like object that is used to calculate persistence length l_p 238
l_c	Contour length of a polymer chain 234
l_p	Persistence length of a rod-like object, given by Eq. 5.2 237
N	Number of particles in the system (simulation box) 71
n	New configuration (after Monte Carlo move) 83
N_{clu}	Number of particles in a cluster 191

T^*	Reduced temperature, $T^* = k_\mathrm{B}T/\epsilon_\mathrm{LJ}$ 74
T^*_init	Initial temperature (reduced) during a simulation 104
T^*_melt	Melting temperature (reduced) 94
U	Total potential energy in a system, given by Eq. 2.2 71
U_c	Potential energy of configuration c 86
U_{ij}	Interaction potential between particles i and j, given by Eq. 2.1 71
U_{ij}^ang	Angular modulation function in the interparticle potential, given by Eq. 2.5 72
U_{ij}^LJ	Lennard-Jones interaction potential between particles i and j, given by Eq. 2.3 71
$U_{ij}^\mathrm{LJ'}$	Cut-and-shifted Lennard-Jones interaction potential between particles i and j, given by Eq. 2.4 71
U_{ij}^tor	Torsional modulation function in the interparticle potential, given by Eq. 2.6 72
uN_loop	Undistorted helix (tight, tube-like, straight) with N_loop particles per 2π rad loop of the helix 223
V	Volume (of the simulation box) 82
V^*	Reduced volume, $V^* = V/\sigma^3_\mathrm{LJ}$ 94

Acronyms/Terms

Acronym/Term	**Definition** ..... **Page number**
1D	One-dimensional, or one dimension (depending on context) 197
2D	Two-dimensional, or two dimensions (depending on context) 2
3D	Three-dimensional, or three dimensions (depending on context) 2
6DH	Six (B-DNA) double helices, tightly cross-linked, parallel, in a honeycomb arrangement 218

BCC	Body-centred cubic (structure) 17
bp	Base pairs (in a DNA double helix) 212
ClaI	Clathrate type I; see Table 3.1 114
ClaII	Clathrate type II; see Table 3.1 114
CPU	Central processing unit (*cf.* 'GPU') 88
CUDA	Compute unified device architecture; NVIDIA's parallel computing architecture 92
Cycle	MC cycle, *i.e.* N attempted moves (a.k.a. sweep) 84
DDQC	Dodecagonal quasicrystal 140
FCC	Face-centred cubic (structure) 17
GLAD	Glancing angle deposition (patchy-particle synthesis method) 41
GPU	Graphics processing unit (specialised circuit architecture more efficient at processing data in parallel; *cf.* 'CPU') 88
H-phase	Square-triangle tiling denoted $(3^3, 4^2)$, based on the Frank-Kasper phase of the same name. 35
HCP	Hexagonal close-packed (structure) or hexagonal close packing, depending on context 17
IQC	Icosahedral quasicrystal 142
KF	Kern-Frenkel (patchy-particle model based on square-well potential) 79
LC	Liquid crystal, or liquid crystalline (depending on context) 211
LCLC	Lyotropic cholesteric liquid crystal 212
LJ	Lennard-Jones (interaction potential between particles) 71
MC	Monte Carlo (simulation type) 82
MD	Molecular dynamics (simulation type) 99
MPMC	Massively parallel MC; parallel MC algorithm in Ref. 7 88
NP	Nanoparticle 11

NPT	Isothermal-isobaric (thermodynamic ensemble): N (number of particles), P (pressure), and T (temperature) are specified and held constant in the simulation box 101
NVT	Canonical (thermodynamic ensemble): N (number of particles), V (volume of simulation box), and T (temperature) are specified and held constant in the simulation box 82
Offset angle	Preferred (minimum energy) value of the torsional angle for two patches. A set of equivalent offset angles is defined for each patch pair. See also '$\phi_{\alpha\beta}^{\text{offset}}$' 73
oxDNA	oxDNA simulation package [6], in which I implemented my interaction model and performed MC simulations 91
Particle type	Category of particles in a structure, based on structure's crystallographic symmetry. Particles of the same type have all the same properties (number of patches, patch vectors, and all patch properties) 107
Patch type	Category of patches in a structure, based on structure's crystallographic symmetry. Patches of the same type have all the same properties [interaction strengths with other patch types ($\varepsilon_{\alpha\beta}$), offset angles ($\phi_{\alpha\beta}^{\text{offset}}$), angular patch widths ($\sigma_{\text{ang},\alpha}$), and torsional patch widths ($\sigma_{\text{tor},\alpha\beta}$)] 108
Patch vector	Vector from centre of particle to patch. See also '$\hat{\mathbf{p}}_i^{\alpha}$' 72
PBC	Photonic band-gap crystal 19
PMC	Parallel MC program (for GPUs) developed by Dr. Eva González Noya 92
PMMA	Poly(methyl methacrylate) 39
PMW	Primitive model for water (patchy-particle model) 81
PS	Polystyrene 39
QC	Quasicrystal 20
Reference vector	A vector associated with each patch vector, used to calculate U_{ij}^{tor}; usually one of the other patch vectors for that particle 73
SC	Simple cubic (structure) 17

SHS — Sticky hard spots (patchy-particle model) 80

Torsional angle — The angle of relative rotation of particles i and j about the axis between them. Also known in stereochemistry as the *dihedral* angle (as in staggered or eclipsed ethane). See also '$\phi_{\alpha\beta}$' 73

Torsional — Relating to the relative rotation of two particles along the axis between them 23

WLC — Worm-like chain; idealised model for semi-flexible polymer 238

Wyckoff position — In simple and practical terms, a region of a unit cell defined by its distinct symmetrical environment. Unit cells may have a number of different Wyckoff positions, and each position may have multiplicity greater than 1, *i.e.* it has multiple instances within one unit cell. See Refs. 8,9 for technical definitions 107

List of Figures

List of Tables

Chapter 1

Introduction and Background

This thesis reports on patchy particles: their *rational design* to form target structures, their *self-assembly*, the *mechanical behaviour* of certain structures when under internal stress, and related behaviour. It aims to (partially) address a general, fundamental question: 'How can we design particles such that they assemble into a given ordered structure?'. This is the inverse question to—and far more difficult than—'Into what structure(s) does a given particle form?'. My research is relevant to the basic theoretical understanding of how *individual* particle interactions determine their *collective* structure and behaviour. It also addresses the design of patchy particles to invoke *internal mechanical stress* in a structure, and the use of such structures to study physical behaviour in complex systems—for the specific example of chiral shape fluctuations in rod-like objects. The *method* by which I studied these areas was numerical, *i.e.* computer modelling and simulation.

Complex structures composed of nano- and micro-scale particles have attracted great interest due to their potential for use in future materials, devices, and technologies. Their self-assembly is a promising means to their formation, moreso than top-down assembly (in which their arrangement is carefully manipulated). Patchy particles are one particular type of particle for which self-assembly into such structures is being actively explored. Thus, understanding patchy particles is crucial for the aforementioned applications. However, this research is relatively early-stage and has been predominantly theoretical. It has also tended to be less focussed on specific applications than on obtaining a general physical understanding, such as of the design principles to form target structures.

While patchy particles have received much attention over the past 15 years, and developments to date have been promising, the scope of research is still relatively limited in comparison

to the size of the challenge. Simulations have tended to focus on thoroughly understanding the behaviour of simple patchy particles (*e.g.* Janus particles). Although the structures assembled from patchy particles in simulations include some structures of widespread interest (*e.g.* cubic diamond), most of these structures are fairly simple (especially the extended structures), and more focus has been on two dimensions (2D) than three dimensions (3D). Experimental progress in synthesising patchy particles suggests complex, customisable particles will be possible, although much work remains. Thus, the assembly of actual particles has been limited, though some interesting structures have already been shown to form (again, moreso in 2D, *e.g.* kagome lattice). In both simulation and experiment, less of the work has considered the rational design of particles to form target structures; rather, most of the work observes and analyses the structures that form from a given system. My thesis extends previous work in a number of ways: I form a range of 3D, complex, extended target structures, both periodic and quasicrystalline, and I do this by rational design. My work thus offers a proof-of-concept of the potential to design patchy particles to form essentially any periodic target structure, and provides the first steps to showing how this can potentially be extended to quasicrystalline structures. In my work on patchy-particle nanotubes, I go beyond designing particles to form a particular structure, and investigate how the particle design can be used to control the nanotubes' mechanical properties. This aims to provide insights into the cholesteric ordering of rod-like chiral mesogens, a topic of recent interest. As far as I am aware, this is the first time patchy particles have been used to deliberately introduce internal stress and study its effects.

This chapter introduces the thesis, by way of explaining background concepts (section 1.1), applications (section 1.2), previous work (section 1.3), and the aims and scope (section 1.4). Background which is specific to each of the three component studies is given in the relevant chapter.

1.1 Basic concepts

In our progress, humanity continually seeks more effective ways to meet human needs and desires, both old and new, and to face challenges and problems that arise. One (small) part of this endeavour is new materials, devices, and technologies. Recently the focus on those at the nano-scale (*nanotechnology*, or *nano-engineering*) or micro-scale (or together, the meso-scale) has grown considerably. A promising but still immature approach towards developing such technology involves manipulating the individual properties of nano- or micro-scale particles, so that they arrange into a specific ordered structure. The ordering determines (alongside other factors, such as particle size) the material properties (*e.g.* electronic, optical, mechanical properties) [10]. So if the particles are well arranged—in a specific structure, typically far more complex than simple crystals—the structure may have useful properties for the required applications.

In this section, I identify and discuss the key concepts within this endeavour, in the context of my thesis. In summary, the goal is to rationally design patchy particles to self-assemble into targeted structures; invoking internal stress within a given structure is a related goal of interest. Both goals may allow control over material properties.

1.1.1 Self-assembly

In *self-assembly* processes, a collection of (initially disordered) component particles organises spontaneously to form an aggregate (at equilibrium)[†] with a well-defined, ordered structure [11–14]. The particles, often called '*building blocks*', may be of any kind: size (atomic or molecular scale, nanoscopic, microscopic, macroscopic), chemical composition, origin (natural or artificial), interaction type(s), *etc.*[‡] However, 'self-assembly' most commonly refers to particles larger than atoms and molecules but smaller than macroscopic (so invisible to the naked eye),

[†] An additional kind of self-assembly outside the scope of my thesis is *dynamic* self-assembly, in which systems are far from equilibrium and dissipate energy [11–13].

[‡] Indeed, the concept of self-assembly can be extended beyond small-scale particles to virtually any imaginable kind of particle organising into an ordered pattern. Some authors [11,13] even include among self-assembly systems of, for example, bacteria, fish, weather, and galaxies.

ordering predominantly via interactions other than covalent bonds. Essential to self-assembly is spontaneity, or autonomy: it occurs without external intervention or guidance, through the inherent properties (shape, charge, polarisability, magnetic dipole, surface properties, *etc.* [11]) of the individual particles and their resulting interactions, by enthalpic and entropic forces.[†] Also essential to ordered self-assembly is reversibility, since when particles aggregate irreversibly they tend to form a disordered glass rather than an ordered structure (particles collide at random, in disorder, and if they join irreversibly they are unable to then equilibrate or rearrange so as to gain order). Therefore, interactions involved in self-assembly are typically relatively weak—of the order of competing thermal energies. Self-assembly can occur in multiple stages over multiple length scales (*hierarchical* self-assembly) [13].

The potential utility of self-assembly for building ordered structures for future materials, devices, and technologies is huge; as such it has long been a central focus in science and engineering [11–13]. The utility has been demonstrated by nature, throughout which self-assembly occurs [11–13,16,22], for instance: the formation of atomic and molecular crystals, nucleic acid assemblies (through base-pairing and folding), virus capsids [23,24], microtubules [25], actin filaments [26], globular proteins (through the folding of polypeptide chains) [27], micelles, vesicles, and opals. Natural self-assembly indicates the possibilities that may one day be realised artificially (as well as offering valuable lessons, such as in assembly kinetics). Perhaps for this reason, the approach to artificial self-assembly is often to mimic nature: for example, the functional properties of DNA and RNA are widely employed in nanotechnology, offering exquisite control [20,28–36].[‡] Examples of self-assembly are also common in current artificial contexts [11,12], whether in physics (including condensed matter science), chemistry, biology, engineer-

[†] Self-assembly may also be influenced by the surrounding environment (*directed* self-assembly [13,15,16]), for example: electric or magnetic fields [17]; a solvent [18] or co-solute [19]; surfaces, interfaces, matrices, or templates [16,20]; or depletants causing depletion interactions [21]. But in this thesis I focus on cases where the surrounding environment does not play a significant role.

[‡] "The most mature and versatile non-biological self-assembly approach is clearly DNA nanotechnology. … Unsurprisingly perhaps, much of the work to develop a general-purpose directed self-assembly technology seeks to leverage DNA nano-technology to assemble other available synthetic nanoscale and microscale building blocks." [20]

ing, or materials science: *e.g.* micelles from surfactants or block copolymers [37], supramolecular complexes [38], liquid crystals [39], and self-assembled monolayers [40].[†] However, artificial self-assembly has not yet matched the precision, variety, robustness, and reproducibility of its natural counterpart. This gap must be narrowed if artificial self-assembly is to meet the goals proposed for it. Further discussion of specific potential applications of self-assembly can be found in section 1.2.

The strengths and advantages of self-assembly as a strategy for developing advanced nanotechnology applications include [11–14]:

(i) *Generality*, and thus *variety* and *complexity*, of assemblies: if one has enough control over the building block properties and interactions, then in principle one can build any ordered structure via self-assembly—finite and extended, simple and complex. One can use whatever particles one can sufficiently manipulate, which may include a wide range of sizes, compositions, and properties, giving further variety in assembly properties.

(ii) *Small scale*, compared to other nanotechnology assembly methods which face increasing difficulty manipulating particles of small sizes.[‡]

(iii) *Specificity*: a high level of control to form a specific product (via building block properties).

(iv) *Efficiency* or parallelism: many building blocks can organise simultaneously.

(v) *Simplicity* [41,42]: in general, self-assembly simply involves combining the particles in suitable conditions and allowing them to assemble—the assembly instructions are encoded into the building blocks. This is simpler than many other methods, which require complex manipulation using tools, techniques, and precision. Self-assembly is thus also usually cheaper.

Self-assembly may thus be able to produce structures that cannot be built any other way—or

[†] In many cases, the natural-artificial distinction is not useful, because natural self-assembly is artificially imitated and adapted.

[‡] The particle size range of interest in nanotechnology, from nanometres to micrometres, is too large to be manipulated by traditional chemistry processes, *i.e.* chemical bonding, and too small to be manipulated by traditional manufacturing processes [11,14].

at least produce them more easily. In particular, it may allow the kind of structures thought necessary for new, advanced materials, devices, and technologies. Self-assembly is a *bottom-up* approach, in contrast to *top-down* approaches in which particles are carefully (sometimes individually) manipulated so as to form the desired structure (*e.g.* photolithography) [15,43]. Top-down approaches generally compare poorly on all five points above (*e.g.* since photolithography stacks 2D sheets, it has limited ability to form 3D structures [11,12]); they are inherently serial, and continually size-limited.

Nevertheless, bottom-up self-assembly faces its own challenges, especially the (1) design and (2) synthesis of small-scale building blocks.[†] Regarding (1), the particle design principles to achieve a target structure are complex and relatively unexplored. But in theory, if these principles are adequately understood, a set of building blocks and conditions can be designed for any desired structure. Regarding (2), we currently lack sufficient control over synthetic particle properties, both in making one particle with the precise properties required, and in reproducing this across many particles to produce a homogeneous set of particles. Current procedures often yield polydisperse and imperfect (defect) products, which hampers self-assembly [13]. Section 1.3 discusses the current state of challenge (2) [and to some extent, also challenge (1)]. The focus of this thesis is on (1), particle design, for a specific kind of particle, patchy particles. In the next section, I further explore the idea of particle design.

It should be noted that this thesis is not only interested in self-assembly for the sake of its potential applications. Understanding self-assembly processes in general is of intrinsic value. For example, it will enable us to better understand life and living cells (in which self-assembly is fundamental) [11,12].

[†] A third challenge is the weakness of the interactions involved in artificial self-assembly, which makes defects common in assembled structures [14]. A fourth challenge is assembly kinetics, which depend on the free-energy landscape complexity (including any competing structures); assembly kinetics are sometimes sensitive to building block properties [19].

1.1.2 Rational design

In the context of self-assembly, '*rational design*' means rationally designing the building blocks so they are programmed to organise into a desired structure (which may in turn have desired properties) [17,20,33–35,44–47].[†] This requires understanding the principles connecting individual particle interactions with an assembled structure—that is, understanding *design principles*. Rational design differs from empirical methods, in which many possibilities are tested until suitable particles are found, and intuition or black-box artificial intelligence methods, in which suitable interactions may be discerned (by humans or computers, respectively) but the principles used to determine them are not elucidated.[‡] To predict the structure into which a given set of building blocks will self-assemble can be very difficult (and the more complex the set of building blocks, the more difficult it becomes) [49–56]. In many cases there are a large number of possible, similar structures that may form. The reverse challenge—to know what set of building blocks or interactions is needed for a target structure to assemble (as required for rational design)—is even harder. (The difficulty becomes greater again when one allows variation in system conditions such as temperature and pressure.)

Rational design is far more powerful than empirical, intuitive, or artificial intelligence methods: it makes it possible to deliberately form a wide range of structures. This paradigm shift from passive observation to active design [16] is essential to realise the potential of nanotechnology. Complete understanding of design principles would allow fabrication of any given target structure via self-assembly, purely by synthesising a particle with the correct properties. As for self-assembly, though, understanding design principles is also of interest in itself, for example in better understanding nature.

[†] One may also distinguish *positive design* from *negative design*: positive design favours a target structure, while negative design disfavours competing structures [48]. Rational design may include both.

[‡] Rational design is sometimes referred to as '*inverse design*', and empirical approaches as 'forward' strategies [43]. In forward strategies, a range of building blocks and assembly processes are examined, explored, and developed, and the subsequent structures are analysed; the strategy is then tuned to obtain desired outcomes. Rational or inverse design is a more natural approach than empirical forward strategies for achieving a desired application.

1.1.3 Patchy particles

My thesis focuses on the rational design for self-assembly of an increasingly broad class of particle known as 'patchy particles', which have attracted great interest over the past 15 years. In this section, I introduce some basic ideas necessary for understanding patchy particles, and in so doing clarify which kinds of systems are relevant to my thesis. Further information on experimental developments regarding patchy particles can be found in section 1.3.3. Note that, beyond the soft, nano- to micro-scale, near-spherical colloids, nanoparticles, and biological molecules discussed ahead, 'patchy particle' and related terms have been applied more broadly to hard and faceted particles [57], DNA [58], and smaller molecules [59,60], among other particles.

A *patchy particle* [15,17,26,49,61–65] has distinct regions on its surface (*patches*, or *interaction sites*), which interact in different ways with neighbouring particles: multiple 'surface functionalities'. That is, patches interact differently from the non-patch surface region. A classic, simple, patchy particle has discrete (perhaps point-like) patches at well-defined locations; these patches attract one another whereas the non-patch surface has little or no interactions (possibly only repulsions). But more generally, the patch regions may be less well-defined, two given patches may not attract but repel or not interact, each patch may interact differently with different patches (*e.g.* attract one but not interact with another), and the non-patch region may still interact.[†]

A great diversity of interparticle interactions are possible by varying the number, size (or width), and location of patches, as well as the kind and strength of interactions between pairs of patches. In the context of patchy particles, rational design concerns these variables, which may be finely tuned. Designing patchy particles gives control over the structures into which they assemble, via the local arrangement of (neighbouring) particles. Patchy interactions cover

[†] The term '*inverse patchy particle*' is sometimes used to refer to particles whose patches repel each other but attract the non-patch region, in contrast with conventional patchy particles whose patches attract each other but have no significant interaction with the non-patch region [15,66]. Inverse patchy interactions are usually caused by charged patches on oppositely-charged particles.

a wide variety of chemical and physical interactions: ion-ion, ion-dipole, dipole-dipole (including hydrogen bonding), dispersion and other van der Waals forces, hydrophobic or hydrophilic (or more generally solvophobic or solvophilic), other electrostatic interactions such as π-interactions, and magnetic. They are usually short-ranged, relative to the particle size.[†] Patchy interactions may also include covalent (coordination) bonds, or other forces that arise in a system [67], such as capillary forces and depletion interactions [21] (an entropic force), if the forces are made patchy.

For self-assembly of the complex structures needed in nanotechnology, a crucial (or at least, hugely valuable) element is *anisotropic* (or *directional*) interactions—those that vary with direction. Anisotropic interactions significantly extend the range of possible self-assembled structures, and the level of control over the self-assembled structure.[‡] Anisotropic interactions are crucial in atomic and molecular assemblies, for example diamond, in which carbon atoms have tetrahedral (sp^3-hybridised) covalent bonds; they are also crucial in protein assemblies. Patchy particles interact anisotropically, because of the patch interactions at specific directions. This makes patchy particles one of the most promising and most studied routes to anisotropic interactions for complex self-assembled structures. However other means are also promising, especially anisotropic shape (which is related to entropy) [17,44–46,49,55,56,58,61,63,67,70–84].[§] This thesis, though, focuses on spherical particles; however experimental particles are usually somewhat aspherical, and I do consider some non-spherical particles and their assemblies.[¶] [‖] I discuss this further in section 1.3.5.

Besides anisotropic interactions, other properties that make patchy particles useful as self-

[†] The strengths (and relative strengths) and ranges of the various interactions change as the sizes of the particles change [10]. Note also, since many of these interactions have a similar magnitude, in theory one can tune and control the net interaction.

[‡] Other valuable elements, besides anisotropy, include variation in particle size (*e.g.* [68,69]), but this is beyond my scope.

[§] Anisotropic media may also make interactions anisotropic.

[¶] In particular, from the realm of non-spherical colloidal particles I consider some *colloidal clusters* (or *colloidal molecules*) [44,85]. These are made from a cluster of spherical colloids or growth or decoration on one spherical colloid, in either case yielding an aggregate with a shape and behaviour somewhat resembling those of a molecule.

[‖] Of course, it is possible to have *both* patchiness and shape anisotropy, *i.e.* non-spherical patchy particles.

assembly building blocks include:

(i) Controlled (and limited) bonding *valence*: since the number of patches is controlled, and patches are (usually) the only interaction sites, the number of patchy 'bonds' (the coordination number) is controlled. This disfavours dense packing and agglomeration, better allowing open structures to form (which are common among the complex target structures of interest).

(ii) Controlled, well-defined *bond directions*: by specifying the locations of patches, the bonding direction is programmed, more precisely favouring target structures.

(iii) Patch *selectivity* (or *specificity*, or *complementarity*, or *orthogonality*): patches may interact (and bond) with other patches selectively, *i.e.* differently with different kinds of patches (depending on the interaction mechanism). This assists the self-assembly of complex structures by encoding into a particle further instructions regarding its favoured nearest neighbours and their relative arrangement. Note that henceforth I use the term 'selectivity' (of patches) to refer to any situation in which a patch interacts differently with different patches, and mostly avoid the similar terms 'specificity', 'complementarity', and 'orthogonality'.[†] The terms 'recognition' and 'lock-and-key' are also sometimes used to describe selective interactions.

Patchy particles most relevant to my work are colloidal particles, nanoparticles, and biological particles, as discussed in the next sections. These fall into the category of *soft matter*, and as such typically have the following features [10,87]:

(i) Interaction potentials (aside from patch interactions) are 'soft': strong repulsion at short distances (*i.e.* a repulsive core), and weak, short-ranged (relative to the particle size) attraction at larger distances.[‡] A variety of interaction types can be involved, and in competition with one another.

[†] Patchy selectivity is sometimes described using the term '*patch-antipatch*', whereby a patch only interacts with its complementary anti-patch [86].

[‡] Weak interactions are important for finding the free-energy minimum without becoming trapped in local minima (*i.e.* stuck with the first bond that forms) [56].

(ii) Particle length scales are mesoscopic, between nanometres and micrometres. Thus particle behaviour is classical, not quantum.

(iii) Particles are usually studied and manipulated in suspension (*i.e.* the dispersed phase of insoluble particles, liquid or solid, is within a liquid continuous phase). This means the particles move in Brownian motion (continuous and random), through thermal energy, without settling. It helps the system explore its phase space, and helps keep the system at thermodynamic equilibrium—which means particles join reversibly and so can separate or rearrange to find lower-energy structures—both of which assist self-assembly. The continuous phase, whose particles are much smaller, can usually be ignored or considered to first order as a continuum with effective interactions. Patchy particles usually disperse easily and homogeneously, due to their size [88]. In some cases, particles are studied at interfaces or on smooth surfaces [11,12].

(iv) Particle behaviour depends on physical, chemical, and biological principles, simultaneously.

1.1.3.1 Synthetic colloids and nanoparticles

Colloidal particles (or simply *colloids*) are particles with sizes between 1 and 1000 nm (*i.e.* mesoscopic), insoluble and dispersed and suspended in a continuous phase [87,89,90]. Patchy-particle colloids are typically solid, and the continuous phase is liquid; such a system is known as a suspension (or sol). Colloids can have various compositions, both organic and inorganic. Although colloids are usually somewhat amorphous, they most often adopt (and are most easily fabricated with) spherical shape, because a sphere minimises the interfacial free energy [90]. Colloids as building blocks are likened to atoms and molecules (albeit at a larger scale), and thus are expected to form a similar range of structures [49,88].

Nanoparticles (NPs) are typically defined to have dimensions between 1 and 100 nm [89]. They are usually inorganic (or metallic), rather than organic molecules; but they are normally

surrounded by an interfacial layer which may consist of inorganic or organic molecules (surface ligands, *e.g.* polymers or DNA, or surfactants) or of ions, and which stabilises them in solution (allowing them to be dispersed). The interfacial layer affects the particle's properties and behaviour, including assembly.[†] *Nanocrystals*, a type of NP, are single crystals of hundreds to thousands of metal or semiconductor atoms, or particles of magnetic or dielectric material, usually 1 to 20 nm in size. Ordered assemblies of nanocrystals are *superlattices*, typically 1 to 1000 μm large [16,75]. NPs may be colloids, but may also exist as solids outside a continuous phase. Although the term 'patchy particle' is traditionally and most often used of colloids but not NPs, for many NPs patchy particles are a good model.[‡]

In this thesis, for brevity, I often refer to colloidal particles and NPs collectively as 'colloids'.

Some of the means by which colloids may have patchy interactions include [17,63,93]:[§]

(i) Chemical or physical patterning of surfaces: patches may be attached (grafted) to, coated (decorated) on, or formed by chemical reaction on the particle surface, at particular locations, or at least with some uneven distribution. Examples include: ligands, polymers, or surfactants [94–98], (synthetic) DNA or RNA oligonucleotides [99–102], proteins/protein-based groups such as biotin-avidin or antibody-antigen pairs [103–105], or other organic tethers; deposited metal or metal oxide [106–110]; surface-charge patterns achieved through adsorption of polyelectrolyte [111–113]; surface chemistry [114–117]; and physical surface features such as roughness [118] or dimples (indentations) [119–121].

(ii) Particles made of multiple components with distinct interactions, structured so different components are positioned at different regions. Examples include: clusters of particles [122–129], possibly arranged with of one type, protruding at specific positions from an encapsulating material of another type [68,130,131]; a mixture of two polymers with dif-

[†] Typically, surface ligands are aliphatic chains of 8 to 18 carbon atoms, with a Lewis base end-group that anchors to the NP. However in many cases these native ligands are partially removed, by washing, before the particles are used or assembled. Both the core and the surface layer contribute to the net interaction between particles (and thus also their self-assembly), which can thus be complex [16].

[‡] Recently [91,92], patchy-particle models have more formally been connected with NPs.

[§] Note that the following categories are not mutually exclusive.

ferent properties [132,133]; monomer protrusions from a polymer [134]; micelles and vesicles formed from multicomponent particles like block copolymers, which may have regions dominated by different solvophilic or solvophobic groups [135]; telechelic (or 'end-functionalised') star polymers, which consist of multiple polymer chains with solvophilic end groups joined at a common centre, leaving their mutually attractive ends pointing outwards in different directions like patches [17,136]; DNA multi-arm structures (or 'star tiles'), in which a certain number of arms extend from a common centre, and the ends of the arms have specific unpaired DNA sequences which bond selectively with other arms [4,47,137–144].

(iii) Moieties, functional groups, or any components with different chemical interactions, within the particle itself. Examples include: different regions of a folded block copolymer [17], induced dipoles across the colloid, multipolar features, or other charge heterogeneities.

(iv) Frames or cages around the particles, which themselves (rather than the particles inside) interact with selectivity and directionality. Frames or cages have notably been formed by DNA origami [42,145–147].

Interactions between patches may be selective through the complementarity of the interacting groups. In particular, DNA interactions are, and protein interactions can be, selective—in the case of DNA, based on Watson-Crick base-pairing [28]. Metal coordination complexes have also been used to achieve selective bonding [148]. Targeted assembly using DNA selectivity is known as 'DNA-programmable assembly'.

It should be noted that in many of the above examples (and others), especially (ii), the particles are not perfectly spherical. Their shape may even fluctuate, or vary with the conditions, including solvent, acidity, and temperature. However, a sphere is still a reasonable first-order approximation, as has been shown, for example, for telechelic star polymers with many arms [149].

Colloids may assemble into ordered structures in a variety of ways [88]: at surfaces or in-

terfaces; by cooling, evaporation of the solvent, or sedimentation under gravity; through the strength of their attractive interactions; or perhaps through entropic forces. Historically, study of colloids has mostly considered only dispersed, gel, or close-packed periodic phases, but directional interactions offer a promising route to complex, ordered, open phases [56]. Moreover, the size of colloids is unique compared to that in most previously-assembled structures: larger than atoms and molecules, but smaller than macroscopic particles. This makes new properties and applications possible.

1.1.3.2 Biological molecules, in particular proteins

Although the term 'patchy particle' originated in connection with artificial colloids or NPs, it can be and is applied to many natural macromolecules, with reasonable accuracy [15,17,93].[†] Such molecules include proteins and clays. Just like artificial patchy particles, they self-assemble into complex structures through their anisotropic and (in some cases) selective interactions. (Thus, as is often the case, scientific models, understanding, synthesis, and technology related to patchy particles are merely following in nature's footsteps [88].)

Here I focus on proteins, which hold particular interest and are the most studied. Proteins are ubiquitous in biological material. They are the building blocks for a wide variety of structures, such as fibres, sheets, tubes, capsules (*e.g.* virus capsids), and channels, and essential to many biological processes. Many proteins assemble rapidly, spontaneously, and independently, with a high degree of accuracy.

Background: protein structure and interactions. In considering proteins as patchy particles, an understanding of their structure is important [154,155]. Proteins are macromolecules made up of one or more chains of amino acids (i.e polypeptide chains). The structure of a protein has four levels: sequence of amino acids (*primary* structure); characteristic local shapes from folding of parts of a polypeptide chain, most commonly α-helices and β-sheets (*secondary*); overall

[†] Indeed, some models used to represent biological molecules [150–153], before the term 'patchy particle' arose, are similar to or the same as those now used for artificial patchy particles [63].

shape of an entire folded chain, which may be complex (*tertiary*); structure of a complex of polypeptide chains and any non-polypeptide components (*quaternary*).[†] Anisotropic interactions in proteins arise through similar means as for colloids (section 1.1.3.1) [153]: functional groups at precise positions, which *e.g.* create directional hydrogen bonds; surface patterning and structuring, *e.g.* distinct regions of hydrophobic or hydrophilic groups; or uneven charge distributions.

How well does a spherical patchy particle represent a protein? Proteins are (usually) complexes of multiple components, but in most relevant contexts the complex is fixed and so proteins behave as one particle. The binding interface between proteins (as for individual polypeptide chains) is usually localised and well-defined, as for patchy particles, producing anisotropic (and often selective) interactions [17,154,155].[‡] Bonding between proteins (or polypeptide chains) normally takes the following types [156]: hydrogen bonding; covalent bonds (side groups on amines may bond with each other, *e.g.* forming disulphide bridges); hydrophobic or hydrophilic interactions (some side groups are hydrophobic or hydrophilic; in solution, like groups will come together); or charged interactions (some protein side groups are charged). All such bonds are directional and short-ranged [153], and thus are suitable to be treated as patchy interactions. Protein shapes vary (indeed, anisotropic shapes contribute to anisotropic interactions), but a sphere (as in a standard patchy particle) is a reasonable approximation for many globular proteins [153]. In any case, further studies could consider non-spherical patchy particles as models for non-spherical proteins. Hence, spherical patchy particles are reasonable models for many globular proteins.

[†] The actual structure of a polypeptide chain or protein may also depend on environmental factors, such as solvent, temperature, acidity, substrates to which the protein may bind, and other nearby proteins (protein *cooperativity*).

[‡] Note that I assume a stable tertiary structure while the quaternary structure (or protein complex) assembles. This in turn assumes that tertiary structures assemble more quickly than quaternary structures. This assumption is true for most protein complexes, but not all.

1.2 Applications: Why is this research valuable?

As raised in section 1.1, rational design of patchy particles to self-assemble into complex structures is a promising route to useful materials, devices, and technologies at the nano- and micro-scales. Likewise, properties can also be controlled by introducing internal stress into patchy-particle bonds. In this section, I further elaborate on the specific ways in which such research is worthwhile. It must be emphasised, however, that my research is at the general, theoretical level. As such, while it may contribute to developing applications, it is difficult to predict specific applications; moreover, it may be of value in other, unforeseen ways (which is less the case for research focussed only on one specific application). Regardless, understanding the principles of self-assembly and rational design, and of the influence of particle interactions on collective properties, is interesting in its own right.

1.2.1 Building new, complex structures

Self-assembly of patchy particles raises the possibility of building, in principle, any structure—and thus of achieving the properties these structures may possess. Patchy particles as building blocks (section 1.1.3) offer a limited number of bonds per particle (valence), selective interactions, and anisotropic interactions, all with control and tunability. Other possible building blocks compare less favourably: for example, atoms and molecules (studied in crystal engineering) allow little tunability and control [63], and any particles with isotropic interactions allow a smaller range of possible assemblies, with less complexity (higher symmetry) [157]. This limits their possible applications (given complex structures are essential for many applications [12]). As discussed earlier (section 1.1.1), self-assembly is an effective means of assembling patchy particles into these target structures.

With purely isotropic, non-selective interactions, most systems (of spherical components of uniform size) arrange into simple, dense, highly-coordinated (usually 12-fold), mechani-

cally strong arrangements (dense packing is thermodynamically favoured). These include the face-centred cubic (FCC) or hexagonal close-packed (HCP), body-centred cubic (BCC), NaCl, or $MgZn_2$ structures (or in 2D, HCP or a square lattice) [44,49,64,82,85]. That is, they mimic atomic crystals [20]. Systems with selective yet isotropic interactions mimic ionic, intermetallic, and alloy systems [20,158], while systems with anisotropic yet non-selective interactions (typically non-spherical particles) form a wide variety of crystal structures (and mesophases) [17,45,46,49,55,56,76,78,81–84]. Patchy particles provide both selective and anisotropic interactions. Thus, patchy particles are expected to reproduce all atomic, ionic, intermetallic, and alloy crystals, as well as achieving many others that do not form in these systems [15,20,159]. In particular, they may reproduce molecular crystals (molecular interactions are directional) and enable open (less dense), complex structures [*e.g.* simple cubic (SC), diamond, zeolites, clathrates, other microporous structures] [17].[†] Allowing multiple types of building blocks opens the door to almost any structure imaginable, finite or extended.[‡]

This promise of fabricating arbitrary structures is beginning to be fulfilled, with patchy particles having formed a range of finite and extended structures; see section 1.3.3.2 for a review. Already some new and interesting behaviour and properties has been observed in such patchy-particle assemblies [63]. As well as the specific applications discussed ahead, assembled colloidal structures could be useful throughout nanoscience and nanotechnology, for seemingly any area where nano-scale control is relevant [11,12,15–17,41,56,67,72,75]. Such applications include: templates for crystallisation; catalysts or catalysis assistants (imitating proteins), including for heterogeneous catalysis; (bio-)membranes (potentially with selective permeability), sieves, or filters; lenses in near-field optics [160]; photodetectors and photovoltaics (solar cells) for energy harvesting; light-emitting diodes; lasers; luminescence and displays including liquid crystal displays; energy transport materials; flash or magnetic data storage (hard disk drives);

[†] The packing densities of hard spheres in the FCC/HCP, BCC, SC, and diamond arrangements are 0.74, 0.68, 0.52, and 0.34, respectively.

[‡] "The limits on the complexity … within these assemblies, and the conditions for forming them … remains a major open question." [20]

field-effect transistors; physical, chemical, and biological sensors which respond to temperature, light, acidity, the presence of molecules/ions, *etc.* (via, *e.g.* surface plasmon resonance of noble metal nanocrystals); switches; surface-enhanced Raman scattering materials [67]; plasmonic materials; self-propelling (autonomous) motors or swimmers, for micro-scale robots [15]; imaging and diagnostic tools (*e.g.* for magnetic resonance imaging and photodiagnostic therapy); medical materials and biomaterials (*e.g.* for regenerative medicine, tissue engineering, and drug delivery [132,161–163]); materials for purification; structural materials of low density; in manufacturing and robotic assembly (as the assembling components become smaller); and in food manufacturing [164,165]. In addition to the structure, the scale (size of the particles) also affects an assembled material's properties. Forming structures with colloidal-size particles promises novel properties and behaviour, different to atomic or molecular assemblies and macroscopic assemblies.

1.2.2 Useful properties: Photonics, electronics, optics, *etc.*

Individual patchy particles may have interesting physical properties (electronic, optical, magnetic, mechanical, *etc.*) [67]. In an *assembly* of colloids or NPs, if the spatial and orientational ordering (and particle size) is appropriate, the particles may couple and their individual properties persist. In addition, assemblies of patchy colloids and NPs may have new, collective properties, again according to the structure [41,75].[†] For example, individual electrons, excitons, surface plasmons, or magnetic moments may interact or couple, leading to new and interesting properties, which can be tuned by particle arrangement, particle size, and assembly size (just as the band structure can be tuned in metals and semiconductors [72,75]). Since with designed patchy particles one has control over the collective structure, if one can also control individual particles (size, composition, *etc.*), this gives significant control over physical properties [75]. Surfaces are particularly important for controlling the assembly and collective properties of colloids

[†] Indeed, an assembly of NPs may have distinct properties to both the corresponding individual NP and the bulk material [41].

and NPs, because of the relatively high surface-to-volume ratio (especially the surface ligands of NPs, which can be varied to control interparticle spacing). Thus a desired property (for a desired application, to solve a given problem or challenge) could potentially be targeted by designing an appropriate patchy-particle system. Here I focus on a few of the most promising properties and their applications.

Certain complex colloidal assemblies are predicted to have useful photonic properties—specifically, they may be photonic band-gap crystals (PBCs) [90,166,167]. A PBC is a spatially ordered array of components with distinct dielectric constants, such that the refractive index varies in space periodically. PBCs prevent the propagation (in all directions, for 'complete' PBCs) of electromagnetic waves (of any polarisation) within a certain frequency range (the band-gap), just as a semiconductor has an energy band-gap that prevents the flow of electrons (because there is a gap between the highest-energy occupied electronic state and lowest unoccupied electronic state). Thus, PBCs can (for specific frequencies), for instance: stop photon propagation; confine photons in space; restrict photon emission in certain contexts (*e.g.* spontaneous emission); and guide photons along a path (as waveguides), possibly with no loss of energy. This makes them useful in many optical, optoelectronic, display, and other telecommunications technologies and devices (just as semiconductors are in electronic technologies), for example to miniaturise them.[†] For instance, PBCs could be used in: coherent light-emitting diodes and diode lasers; all-optical circuits, transistors, and logic gates [169]; optical fibres; displays; sensors; switches; and quantum electronic devices. Many of these may be useful in photonic computers, which would be faster and more powerful than their electronic counterparts, and which would avoid the need to convert between electronic and optical signals (information is increasingly transmitted by light, in optical fibres). Structures of interest for PBCs (many in all three dimensions) are open structures like: honeycomb (open hexagonal) [170–172], kagome [173], and pyrochlore [173,174] lattices; cubic diamond [166,174–177] (as opposed to hexagonal

[†] Photonic materials can also be found throughout nature, *e.g.* opals, feathers, butterfly wings, beetles [168].

diamond, a stacking hybrid); woodpile [177]; tetrastack [178]; various quasicrystals (QCs) [179–188]; and aperiodic or disordered structures [87,189]. Particles of colloidal size are predicted to have band-gaps in the range of visible light (because the periodicity of the structures is of the order of visible light wavelengths), making them particularly useful [177].

As well as photonics, colloidal assemblies may be useful in the more established fields of (micro)electronics and optics [12,14,190,191], such as thermophotovoltaics, energy storage, plasmon waveguides, optical switches, and light generators [16,17,41,75]. For example, self-assembly at the nanoscale offers a means to further miniaturise such systems; it also offers 3D systems, in contrast to photolithography, which is intrinsically 2D. Plasmonic [64], excitonic, and phononic (*e.g.* through the SC structure [192]) properties may also arise.

1.2.3 Understanding nature

Aside from specific applications, studying patchy particles and their self-assembly (or other behaviour) is of more general value for our scientific understanding of nature and biological processes. Patchy particles and self-assembly occur throughout nature, in far more diverse and complex ways than humans currently contemplate employing them. Already, some of the behaviour observed in patchy-particle systems has been novel and helped understand physical processes [63]. Understanding nature also presents an opportunity to design artificial systems that imitate natural ones [193].

1.2.3.1 Proteins

First and foremost, patchy-particle research has improved our understanding of proteins, which are essential in all life. Thus, models and ideas similar to those in colloidal patchy-particle research have been widely used in understanding proteins [63,71,73,194–206]. Protein crystallisation and more general phase behaviour is an area of intense research. Most proteins are notoriously difficult to crystallise; this is biologically valuable, as usually crystallisation would hinder

their functions. It would be useful to understand why crystallisation is difficult, and how and why proteins do crystallise in certain conditions (this would also help biochemists in protein structure determination). patchy-particle research is helping in this pursuit, showing the importance of anisotropic and selective interactions [63,194,198,200]. Other protein behaviours that have been better understood through patchy-particle research [63] include behaviour in solution, such as conformational stability, nucleation, aggregation, dissociation, condensation, and other phase behaviour [87,195,196,199,201]. Although isotropic models were used in early theoretical and computational research on proteins (with some success), most proteins interact anisotropically, and so those models have shortcomings and limits [153,198,207]. They cannot explain protein phase diagrams and behaviour, whereas anisotropic models can [153,194]. For instance, protein crystals have lower packing fractions than particles with isotropic potentials [208], and this can be replicated using anisotropic models [198,209].

One particular area of interest is virus capsids, which form quickly and accurately within a complex environment [24,73,202,205,210] (see also references in Ref. 211). Patchy-particle research continues to develop our understanding of virus capsids, and this may help design drugs that inhibit capsid assembly, or drug delivery vehicles that mimic capsids.

1.2.3.2 Other substances and processes

Aside from soft matter systems [17,63,212], patchy-particle systems are good models for many condensed matter systems—liquids and solids—of atoms and molecules (*i.e.* systems of much smaller scale). They have helped understand collective phase behaviour, such as phase transitions, crystallisation, and kinetics, as well as structural phenomena like defects and dislocations, and properties such as optical behaviour [44,87,88,213,214].[†] In particular, patchy-particle research has helped or can help in understanding [63,213]:

(i) liquid dynamics, including supercooled liquids and the formation of chemical and phys-

[†] The Brownian motion and thermodynamic behaviour of colloids in suspension mimics that of atoms, but since colloids are far larger and their dynamics are slower they are easier to observe. Colloids are also purely classical, so complex quantum effects are avoided [87].

ical gels (low density, kinetically arrested states) [215–221];

(ii) gas-liquid phase separation [222];

(iii) fluid-fluid transitions [153,223];

(iv) the formation of chains, networks, and other mesophases [217,224];

(v) liquid stability (in preference to crystallisation) [215,221];

(vi) competition between the formation of clusters and extended phases; and

(vii) other crystallisation or assembly behaviour.

Isotropic interactions were long used to model liquid systems, with some success; but isotropy is a very simple approximation, and anisotropy an important improvement [63].

1.3 Previous work (literature review)

This section reviews the extensive patchy-particle research performed to date. I begin with research by numerical simulations (section 1.3.2) and then consider experimental research (section 1.3.3)—both in synthesising patchy particles, and studying their self-assembly.

Before beginning, I state explicitly the value of modelling (be it for theoretical analysis or numerical simulation) alongside experiment [93].[†] First, modelling enables one to quickly and (relatively) easily study a large number of systems, which is not feasible by experiment. Given the vast range of possible systems (*e.g.* different building block designs or system conditions) and great difficulty of predicting the structure into which building blocks assemble, or of knowing the required building blocks for a given structure (section 1.1.2), this is hugely valuable. The overall landscape can be scanned, before focusing on areas of interest. In particular, synthesising patchy-particle building blocks is often difficult and costly, so if the predictions of modelling can guide experimentalists in designing promising building blocks, this will save much work and speed up research progress [15]. Second, modelling enables study of arbitrary systems,

[†] There are of course also disadvantages and limitations to modelling: smaller systems, smaller timescales, an imperfect representation of reality, difficulty in knowing whether a result is physically realistic, *etc.*

and so it allows one to study systems that cannot currently be studied experimentally (whether this be due to safety, technology, cost, or any other factor). If promising results are found, efforts can be made to make these systems experimentally possible. Finally, modelling enables far more detailed understanding of systems than experiment, by providing precise information about individual particles at small time intervals (position, orientation, energy, *etc.*). For example, the full phase diagram can be studied, giving the relative stability of competing structures [225].[†] Hence, modelling has been heavily pursued in patchy-particle self-assembly research, and has made a large contribution, even predicting novel, interesting behaviour and thus inspiring experimentalists [212]. A good example of complementary modelling and experimental research was in the study of patchy particles forming a kagome lattice, where simulations [225,226] [Fig. 1.1(d)] confirmed experimental [227] (Fig. 1.3) results and provided further information, notably a complete phase diagram.

Continual developments in both experiment and theory inspire each other. Thus, an important motivation of this thesis is to guide experimentalists in further research of synthesising and assembling patchy particles, via predicted structures and behaviour, and general design principles.

1.3.1 Definitions: Torsional interactions, Janus and triblock particles, depletion interactions

At this point I must introduce some concepts. The *torsional* arrangement of two particles relates to their relative rotation along the axis between them. The torsional angle specifies this relative rotation, and is known in stereochemistry as the *dihedral* angle (as in staggered or eclipsed ethane). I use the term '*torsional interactions*' to refer to interparticle interactions which include a '*torsional component*', *i.e.* for which the torsional arrangement matters. If an interaction potential includes a torsional component, two configurations can have the same pair of bonded particles

[†] A further advantage of coarse-grained modelling, like mine, is that it gives general results which apply to a range of real systems, and so helps identify the key features in these systems that lead to observed behaviour.

in the same relative position with the same pair of patches pointing at each other, but different interaction energies because of different torsional arrangements. This adds an extra layer of complexity and specificity to a patchy interaction: not only must two particles bond with the correct pair of patches in the correct position, but the particles must have their preferred torsional orientation. My patchy-particle model potential includes a torsional component.

Janus particles have two hemispheres with distinct properties and interactions [15,88,228–234].[†] They can be thought of as the simplest type of patchy particle (with one patch, whose width is half the particle, and the other hemisphere being a non-patchy region). *Triblock* (sometimes called *triblock Janus*) particles have three regions: large patches on opposite poles, with a non-patchy region around the equator.

Depletion interactions or forces arise when (larger) colloids are mixed in solution with (smaller) particles, called depletants. Compare two arrangements: in the first, two colloids are near but not in contact; in the second, they are in contact. In both cases, the closeness of the colloids prevents the depletants occupying space between them. However in the latter there is more available space away from the two colloids (because they are closer). Thus the configurational entropy of the depletants is larger in the latter, because they have more possible configurations (more possible positions they can occupy). Thus the system entropically favours arrangements in which the colloids are closer, through an effective attraction between them [see Fig. 1.2(g)].

1.3.2 Simulation

A range of increasingly complex patchy-particle simulations have been performed, which explore the variety of behaviour and assembled structures these particles exhibit, and reveal design principles to form target structures. Some analytical theoretical research has also been performed, but that is not my focus. For recent overviews of numerical simulations (and theoretical analysis) of the behaviour and self-assembly of patchy particles, consult Refs. 15,17,63,66,88.[†]

[†] They are named after the Roman god, who had two faces on opposite sides of his head.

[†] Ref. 63, in particular, summarises thermodynamic behaviour and assembly results obtained using the Kern-Frenkel and Doye-group models for patchy particles, which are discussed in section 2.1.

Spherical patchy particles are typically modelled as a core with short-range repulsion and surface patches with longer-range attraction (or repulsion), giving an overall anisotropic pair interaction potential [15]. I explain my model and compare it with other models in section 2.1. However, other approaches have also been used, including: models designed for specific particles (*e.g.* proteins, water molecules); models comprising many distinct 'atoms' per particle, some of which represent patches; and a density functional theory approach in which particle interactions are anisotropic [15].

Table 1.1 summarises (non-exhaustively) previous simulation studies on the assembly of patchy particles into complex structures, along with some analytical studies. It reports, in particular, the patchy-particle models used, patch designs studied, assemblies observed, and other results of interest. It omits many studies, including studies on: (1) non-spherical particles (studies and reviews considering non-spherical particles include Refs. 17,44–46,49,55,56,58,61,63,67,70–73,75–79,81–84) including grafted or tethered particles in which the graft is modelled explicitly [235–238], and telechelic star polymers [239]; (2) self-assembly dependent on external system conditions (*e.g.* a cosolute [19]); (3) thermodynamics with no consideration of assembled structures (*e.g.* [240]); and (4) only liquids, not stationary phases. The table includes only a few studies focused explicitly on biological self-assembly; see Refs. 24 and references cited in Refs. 202,211 for simulation and analytical studies focused on virus capsid self-assembly. A selection of structures assembled by patchy particles is shown in Fig. 1.1.

Simulations thus far have demonstrated the basics of patchy-particle self-assembly: anisotropic interactions cause particles to arrange in controlled structures. In some cases, structure growth occurs via direct nucleation, and in other cases via rearrangement from disordered aggregates. Simpler systems (fewer distinct particles, fewer patches, less patch selectivity, smaller patches, *etc.*) assemble correctly more easily and quickly. Many patchy design parameters have been varied: number, position, and width of patches; interaction strength; interaction range; patch selectivity (in a few cases); and torsional interactions (in very few cases) [63]. Some parameters

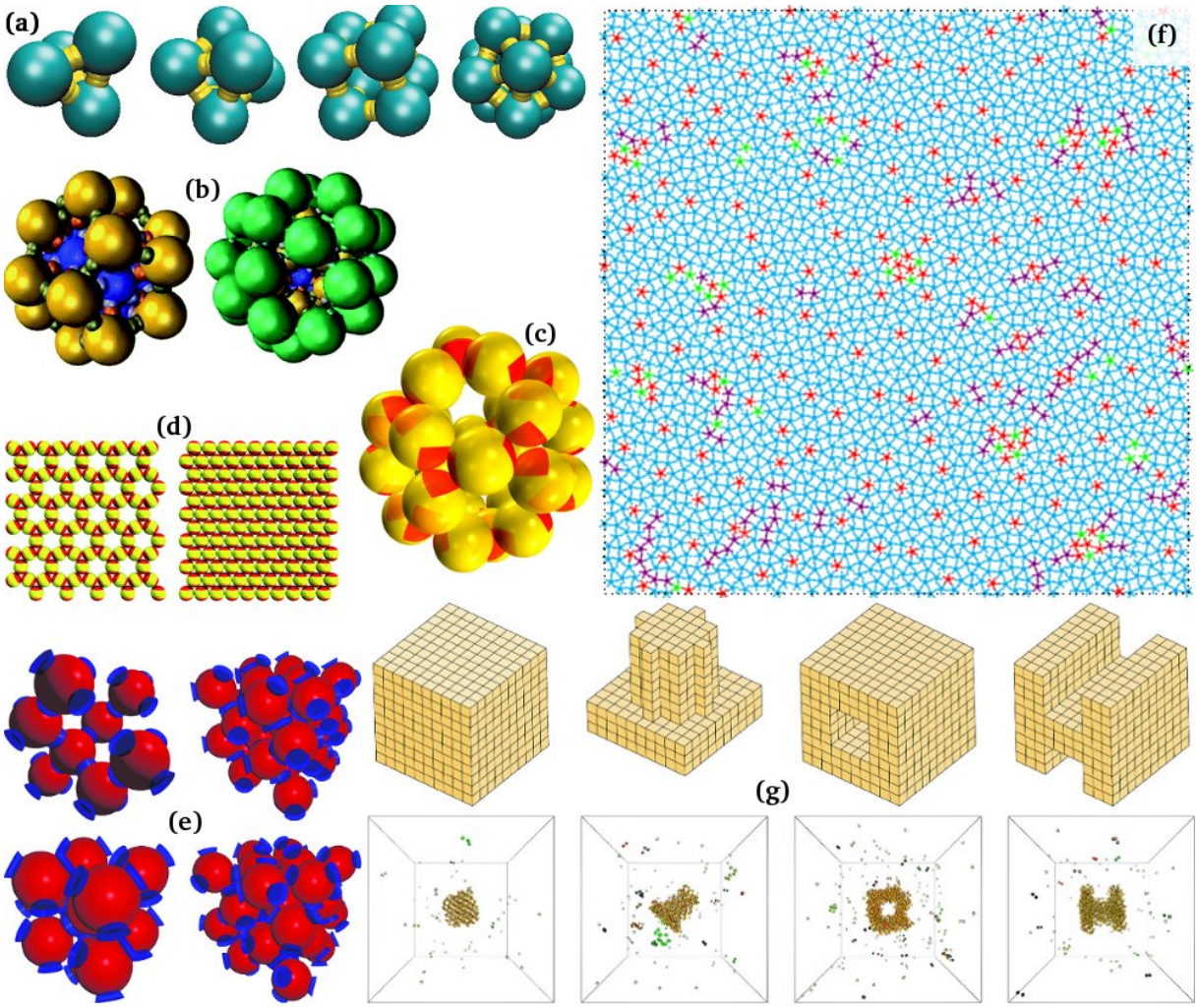

Figure 1.1: Collage of structures self-assembled from patchy particles in simulation. **(a)** Finite clusters, left to right: tetrahedron, octahedron, cube, icosahedron; dodecahedron (not shown) did not form. Formed from particles with 3, 4, 3, and 5 suitably-arranged patches, respectively. **(b)** Multi-shell clusters from templated assembly, left to right: $A_{12}B_{20}$ (dodecahedron surrounding icosahedron); $A_{12}B_{20}C_{30}$ (icosidodecahedron surrounding dodecahedron surrounding icosahedron). Formed from particles with various complex arrangements of selective patches. **(c)** An icosidodecahedron, the basic unit of clathrate lattices, formed from particles with 2 triangular patches, with staggered orientations. **(d)** Left to right: 2D kagome and HCP lattices. Formed from particles with 2 patches at opposite poles, wide enough to allow two bonds per patch. Replicated and studied experimental assembly in Ref. 227 (Fig. 1.3). **(e)** Clockwise from top left: cubic diamond (1 unit cell, 8 particles); FCC ($2 \times 2 \times 2$ unit cells, 4 particles each); orientationally disordered FCC ($2 \times 2 \times 2$ primitive cells, 4 particles each; randomly oriented patches); BCC (8 particles at the vertices of a cube around the central particle). All formed from particles with 4 tetrahedrally-arranged patches. **(f)** 2D dodecagonal QC, $N = 2500$. Formed from particles with 5 equally spaced, non-selective patches. Colours for local environments: cyan=σ-phase, purple=H-phase, red=HCP, green=other. **(g)** Cube ($N = 396$), cylinder on slab ($N = 489$), structure with central cavity ($N = 806$), 'H'-shape ($N = 696$); top row shows design, bottom shows self-assembly. All formed from particles with 4 tetrahedrally-arranged, selective patches, with each particle distinct (modelling 'DNA bricks').
(a,b,c,d,e,f,g) reprinted with permission from Refs. 211,241,242,226,243,2,244 respectively, © American Institute of Physics, The Royal Society of Chemistry, Macmillan Publishers Limited, The Royal Society of Chemistry, American Institute of Physics, American Physical Society, The Royal Society of Chemistry, respectively.

Table 1.1: Summary of simulation studies of patchy particle assembly, and some analytical studies. Studies are ordered by year of publication (of first study in each row, from oldest to most recent).

Dimensions	Patchy model[a]	Patchy design(s)	Assembled structure(s)[b]	Other comments	Reference(s)
3D	Other	4 patches (equally spaced around equator), 6 patches (octahedral). Pairs of complementary patches.	n/a	Modelled proteins. Studied phase behaviour, including fluid-fluid phase transition. Results help understand the difficulty of protein crystallisation.	[151]
3D	KF	2 patches (opposite poles), 4 (tetrahedral), 6 (octahedral). Patch width and interaction range vary.	n/a	Studied phase behaviour, in particular fluid-fluid coexistence	[153]
3D	Other	6 patches (octahedral), 12 (arranged for FCC). Pairs of complementary patches. Interaction strength varies.	EXT. SC (6 patches), FCC (12).	Studied phase behaviour to understand protein crystallisation.	[209]
3D	Other (many 'atoms' per particle)	2 patches (opposite poles), 4 (equally spaced on equator), ring patches (patchy region all around equator; sometimes patterned, *i.e.* different patch types), double rings (adjacent ring patches of different types, around lines of latitude), line patches (along sections of lines of longitude; patterned). Patches sometimes selective.	EXT & MESO & FIN. Chains (2 patches), sheets (4, ring patches), 5- or 6-particle rings (line patches), icosahedra (double rings), square pyramids (double rings), tetrahedra (double rings).	Phase transitions from higher to lower temperatures vary between structures.	[61]
3D	KF	4 patches (tetrahedral).	EXT. Cubic diamond.	Only achieved reliable self-assembly when began from seeds or included a torsional component.	[249]
3D	Other (similar to Doye)	3, 4, 5 patches. Selective patches. (Arrangement and selectivity designed to form targets.)	FIN. Icosahedron, dodecahedron (virus capsid shapes).	Modelled virus capsid self-assembly dynamics and pathways.	[210]

Continued on next page

Table 1.1 (*Continued from previous page*)

Dimensions	Patchy model[a]	Patchy design(s)	Assembled structure(s)[b]	Other comments	Reference(s)
3D	SHS	2, 3, 4, 5 patches (equally spaced, *i.e.* 2 at opposite poles, 3 equally spaced on equator, 4 tetrahedral, 5 similar to square pyramid); also studied binary mixtures of particles with different numbers of patches. Also, 4, 5, 6 patches at random positions.	n/a	Helped understand supercooled liquids. Studied phase behaviour, in particular gas-liquid coexistence, liquids, gels, disordered states (including possible 'empty liquid', *i.e.* gel network/homogeneous disordered phase, stable at equilibrium at low density; occurs with low number of patches). Agreement with Wertheim theory of associating liquids [250–253].	[215,254]
3D	PMW	4 patches (tetrahedral, but 2 patches under surface). 2 pairs of complementary patches.	n/a	Studied thermodynamics and phase behaviour, including dynamics in supercooled states, density anomalies, gas-liquid phase separation, and critical point.	[216,218]
3D	Doye	3 patches (within same hemisphere, arranged either to form tetrahedra, cubes, or dodecahedra), 4 (for octahedra), 5 (for icosahedra), or ring patches (passing through icosahedral patch sites).	FIN. Platonic solids: tetrahedra (3 patches), octahedra (4), icosahedra (5), cubes (3).	Studied thermodynamics and dynamics of self-assembly, thoroughly. Ref. 202 included torsional component, which assisted self-assembly of targets. For icosahedra: identified optimal patch width and temperature for self-assembly; assembly was robust despite polydispersity in patch positions (within a limit); assembly was reversible; assembly occurred both through direct nucleation and indirectly through disordered intermediates. Relates to virus capsid formation (especially with torsional interactions). See Fig. 1.1(a).	[197,202,211]

Continued on next page

Table 1.1 (*Continued from previous page*)

Dimensions	Patchy model[a]	Patchy design(s)	Assembled structure(s)[b]	Other comments	Reference(s)
3D	SHS	2 patches (opposite poles); also studied binary mixture of 2- and 3-patch particles (3 patches equally spaced on equator).	MESO. Chains (unbranched for monodisperse system, branched for mixture, and forming a fully connected network, *i.e.* gel, if sufficient 3-patch particles).	Studied thermodynamic properties and phase behaviour, including percolation transition, thermodynamic instability, structural and dynamic properties of gels. Agreement with Wertheim theory, which authors combine with Flory-Stockmayer approach to gels [255].	[217,256,257]
3D	KF-related	1 patch, 2 (opposite poles). Wide patches.	n/a	Studied phase behaviour, in particular fluid-fluid coexistence and percolation line. Agreement with Wertheim theory.	[223]
2&3D	Doye	2D: 4, 5, 6 patches (equally spaced). 3D: 4 patches (tetrahedral), 6 (octahedral).	EXT. 2D: square crystal (4 patches), HCP (4, 5, 6), σ-phase[c](5), H-phase[c] (5). 3D: SC (6 patches), partial crystallisation and clusters (4 patches).	2D: 5-patch assemblies show frustration (local order incompatible with global).	[198]
3D	Doye	6 patches (octahedral).	EXT. SC, BCC, FCC (FCC either orientationally ordered or disordered/plastic).	Studied phase behaviour.	[258]
3D	KF-related	General (non-specific).	n/a	Analytical, no simulations. Modelled lysozyme. Studied phase behaviour and solubility.	[200]
2&3D	Doye	2D: 2 patches (arranged to form square cluster). 3D (arranged to form cubic cluster): 3 patches. Pairs of complementary patches.	FIN. Clusters of 2, 3, 4, 8 particles.	Modelled self-assembly of homomeric protein complexes (to understand their evolution). Studied thermodynamics and dynamics. Torsional interactions.	[203]
3D	SHS-related	3 patches (equally spaced on equator). Selective: 2 patches of one type, 1 of another, with different interaction strengths.	MESO & FIN. Chains, including branched (and 'hyperbranched polymers'), and clusters.	Analytical (including Wertheim theory), no simulations. Studied phase diagram, in particular liquid-vapour critical point.	[222,259]
3D	KF	1 patch. Patch width varied, from hemisphere (*i.e.* Janus particle) to entire surface (*i.e.* isotropic attractive potential).	MESO & FIN. Micelles, vesicles, and other clusters; lamellar phase.	Studied phase behaviour. Similar to experimental Janus particle systems, *e.g.* [260–263].	[264,265]

Continued on next page

Table 1.1 (*Continued from previous page*)

Dimensions	Patchy model[a]	Patchy design(s)	Assembled structure(s)[b]	Other comments	Reference(s)
3D	KF	4 patches (tetrahedral).	EXT. BCC, FCC (orientationally ordered or disordered/plastic), hexagonal and cubic diamond (and their stacking hybrids).	Studied phase behaviour. Varied interaction range and patch width. Cubic diamond favoured at low temperature, low pressure, short interaction range, and small patch width. Studied competition between crystallisation and glass formation, including nucleation barriers to crystals; nucleation barrier the same for both diamond structures and their stacking hybrids. Studied polydispersity in patches (width/position/interaction strength); little effect on crystallisation (within an experimentally realisable limit). See Fig. 1.1(e).	[243,266–269]
3D	Doye	*Ditto*	*Ditto*	*Ditto*. Also, showed seed assisted diamond assembly.	[207]
3D	KF	2 (opposite poles). Patch width varied from entire surface (*i.e.* isotropic attractive potential) to zero.	EXT & MESO. Interconnected planar square lattices (patch width allows 4 bonds per patch), interconnected planar triangular lattices (3 bonds per patch), independent planar triangular lattices (2 bonds), chains (1 bond).	Studied phase behaviour.	[270]

Continued on next page

Table 1.1 (*Continued from previous page*)

Dimensions	Patchy model[a]	Patchy design(s)	Assembled structure(s)[b]	Other comments	Reference(s)
2D	Doye-related	3 patches (either equally spaced, or one of two isosceles triangle arrangements), 4 patches (either equally spaced, or one of two rectangular arrangements), 5 patches [equally spaced; either all attractive (denoted '5*') or with selective patches ('5^-'): two types, each type attracts unlike patches and repels like patches], equimolar binary mixture of 2- and 3-patch particles (both equally spaced).	EXT. Honeycomb lattice (3 patches; elongated hexagons for isosceles arrangements, low pressure; irregular hexagons for binary mixture, low pressure), HCP (3, 4, 5*, or 5^- patches, or binary mixture, all high pressure; both 5-patch lattices are distorted; or 4 patches, medium pressure but wider patch width), 'square lane' and 'zig-zag lane' lattices (3 patches in one isosceles arrangement), open square/rhombus lattice (4 patches, low pressure; rhombuses for rectangular arrangements), σ-phase[c](5* patches, low pressure), intermediate between σ-phase and HCP (5* patches, medium pressure), H-phase-like structure[c](5* patches, small patch width), intermediate between open and close-packed hexagonal lattices (binary mixture, medium pressure), open lattice with triangular tiles (5^- patches, low pressure), semi-close-packed lattice with elongated hexagonal tiles (5^- patches, medium pressure).	Used genetic algorithm approach to find lowest energy structures—no simulations. Modelled at $T = 0$. Non-trivial, ordered, structures; some open.	[271]
3D	Doye	3 patches (within same hemisphere, arranged to form dodecahedra), 5 (for icosahedra). Various complex multi-patch designs for multi-shell cluster structures.	FIN. Icosahedra and dodecahedra formed around spherical core particle. Multi-shell structures form around icosahedra and dodecahedra.	Templating assisted self-assembly, enabling dodecahedra to form, reducing aggregation. Relates to virus capsid formation. See Fig. 1.1(b).	[241]

Continued on next page

Table 1.1 (*Continued from previous page*)

Dimensions	Patchy model[a]	Patchy design(s)	Assembled structure(s)[b]	Other comments	Reference(s)
2D[d]	KF	2 (opposite poles). Patch width allows up to 2 bonds per patch.	EXT. 2D kagome lattice and HCP.	Replicated and studied experimental assembly in Ref. 227 (Fig. 1.3). Kagome lattice stable at low temperature and pressure. See Fig. 1.1(d).	[226]
2D	Doye	Various (3–12 patches, arranged to form Archimedean and Platonic tilings, both with particles at centres and at vertices of tiles). Some systems use particles of different sizes.	EXT. All Archimedean and Platonic tilings except trihexagonal assembled from either the centre or vertex design.	Used genetic algorithm approach to find lowest energy structures—no simulations. Studied phase behaviour at $T = 0$, in particular stability over a range of pressures.	[272]
3D	KF	2 patches (opposite poles).	MESO. Chains and rings (for suitable patch width).	Agreement with Wertheim theory.	[273]
3D	Doye	4 patches (regular and irregular tetrahedral arrangements)	EXT. FCC- and HCP-like, BCC-like, hexagonal double layers—competing structures.	Used evolutionary algorithm approach to find lowest energy structures, combined with simulations. Studied phase behaviour and thermodynamic properties of competing structures.	[54,274]
3D	KF	3 or 5 patches (equally spaced, *i.e.* 3 patches around equator, 5 arranged similar to square pyramid).	EXT. 3 patches: independent, honeycomb planes; interpenetrating hexagonal planes; FCC. 5 patches: bonded hexagonal planes, FCC.	Studied phase behaviour.	[275]
2D	Doye	5, 6, or 7 patches (equally spaced); Ref. 3 uses mixtures of particles with different numbers of patches, and various (designed) selective patches.	EXT. Dodecagonal QC, σ-phase[c], H-phase[c], HCP.	Studied phase behaviour. Open crystals form at low pressure with small patch widths. QC forms on cooling, in region between hexagonal and open structures. QC formation robust and stable over a range of conditions and model parameters; entropically stabilised against periodic approximants. Ref. 3 related patchy particles to multi-arm tiles, and simulated the assembly of such tiles into QC. See Fig. 1.1(f).	[1–3]

Continued on next page

Table 1.1 (*Continued from previous page*)

Dimensions	Patchy model[a]	Patchy design(s)	Assembled structure(s)[b]	Other comments	Reference(s)
3D	KF	4 patches (tetrahedral). Three configurations of patch selectivity: all patches identically attractive, all distinct and only self-attractive, 2 pairs of complementary patches).	EXT. Cubic diamond, BCC.	Studied phase behaviour. Studied effect of patch selectivity: selectivity assisted diamond formation.	[86]
3D	KF (adapted for non-circular patches)	2 patches (opposite poles). Patch shapes triangular, staggered orientations of patches on each particle.	EXT & FIN. Cubic tetrastack lattice, clathrate-like structure, sometimes in smaller clusters.	Tuned patch width and shape to control number of bonds and favour a target structure (reducing competition with other structures, including polymorph packing hybrids). Studied polydispersity in patches (width/position); target assembly was robust (within limits). See Fig. 1.1(c).	[242]
3D	KF	4 patches (tetrahedral).	EXT. Gels, BCC, FCC (orientationally ordered or disordered/plastic), cubic diamond.	Studied phase behaviour, in particular relative stability of crystals and low-temperature fluids; difficulty of crystallisation makes gels stable, even as $T \to 0$.	[221]
3D	Other	2 patches (opposite poles). Patch- and non-patch regions are oppositely charged, so unlike regions attract and like regions repel (*i.e.* 'inverse patchy particles').	EXT. Uniformly charged wall confines particles to quasi-2D arrangement. Microcrystalline gels (branched networks of triangular- or square-crystalline domains), disordered aggregates.	Tuned system conditions, interparticle interactions, and interactions between particles charged wall, to control assembly.	[276,277]
3D	Other	2 patches (opposite poles). Patch width allows multiple bonds per patch.	EXT. Tetrahedral or octahedral motifs, arranged into open lattices (competing with FCC): pyrochlore, hexagonal tetrastack, perovskite-like.	Analytical, no simulations. Studied phase behaviour. Varied patch width. Entropy (orientational and vibrational) favours open lattices.	[278]

Continued on next page

Table 1.1 (*Continued from previous page*)

Dimensions	Patchy model[a]	Patchy design(s)	Assembled structure(s)[b]	Other comments	Reference(s)
2D	KF	Various (3–5 patches, arranged to form semi-regular Archimedean tilings). Patch selectivity: each patch has one complementary patch, which may be itself.	EXT. All 8 semi-regular Archimedean tilings.	Minimal design strategy (*i.e.* least selectivity/fewest distinct interaction types). Patch selectivity was essential for forming targets.	[279]
3D	KF	4 patches (tetrahedral). Patch selectivity (designed to form target structures): each particle distinct (modelling 'DNA bricks').	FIN. Various complex, large clusters (*e.g.* cube, cylinder on a slab, cube with cavity, 'H'-shaped prism).	KF model parametrised to experimental data. Results compared to experimental data. See Fig. 1.1(g).	[244]
3D	KF-related	1, 2, 3, 4 patches (equally spaced, *i.e.* 2 at opposite poles, 3 equally spaced on equator, 4 tetrahedral).	MESO & EXT. Helices (1 patch), hexagonal columnar and body-centred tetragonal (2 patches), honeycomb (2D sheets; 3 patches), cubic diamond (4 patches).	Combines KF model with more complex and realistic model for soft particles, allowing deformations and polydispersity.	[280]
2D	Doye	8, 10, or 12 patches (equally spaced).	EXT. Octagonal QC, decagonal QC, and dodecagonal QC.	Octagonal and decagonal QCs only metastable, and former only so when simulation begins in that structure (*i.e.* not self-assembly).	[281,282]

[a] All patches are attractive, non-selective (*i.e.* attract all other patches equally), and circular, unless stated otherwise. 'KF' = Kern-Frenkel; 'Doye' = Doye research group; 'SHS' = sticky hard spots [hard spheres with short-range, narrow (spot-like), square-well attraction between patches]; 'PMW' = primitive model for water (essentially, a specific case of SHS, to model water). See section 2.1.3 for further details of patchy-particle models.

[b] 'EXT' = extended structure; 'MESO' = mesophase structure (intermediate phase between liquid and solid); 'FIN' = finite structure (*i.e.* cluster).

[c] σ-phase and H-phase are tilings (local packings) of squares and equilateral triangles. They are formally denoted as $(3^2, 4, 3, 4)$ and $(3^3, 4^2)$, respectively [245]. This notation refers to the sequence of triangles ('3') or squares ('4') around each vertex (indices denoting multiples of the same shape). They are labelled σ and H, as originally in Ref. 198, by analogy to the Frank-Kasper phases [246,247] of the same name. The σ and H Frank-Kasper phases are periodic approximants of dodecagonal QCs, but in two (of three) dimensions can be thought of as square-triangle tilings [248].

[d] Particles are constrained to 2D when assembling, but have 3D orientational freedom (as in the associated experiment).

(mostly patch width, interaction strength, and interaction range) have been tuned and optimised for certain contexts. Small (narrow) patches and stronger interactions thermodynamically favour the target structure, but make it kinetically less accessible, as it is harder to find the correct structure, and rearrangement from incorrect bonds is more difficult. However, few studies have rationally designed patchy particles to form a target structure; most have simply observed the structures that form from a given particle design.

In general, more work has been done in 2D than 3D, more on finite structures and mesophases than extended structures, more on liquids and disordered phases than ordered phases, and more on simple systems than complex systems [20,63,271]. Studies in 3D of extended, ordered, complex phases are fairly limited. Studies on finite structures (often modelling virus capsids, or forming custom clusters) have achieved far greater local complexity [*e.g.* Refs.241,244; Figs. 1.1(b,g)] than studies of extended structures. In principle, one could achieve any arbitrary finite structure, given suitable conditions and sufficient time, using distinct particles with selective bonding. Studies on mesophase-like assemblies have focused on chains, rings, helices, gels, networks and other similar structures (*e.g.* [61,217,222,256,257,259,264,265,270,273]).

Regarding studies on extended, ordered structures, many have yielded common close-packed structures (*e.g.* FCC/HCP, BCC). But these are of less interest than open structures, due to the latter having more potential applications (section 1.2) and a greater variety of structures [66]. In particular, cubic diamond is of great interest and so has been well studied [86,207,221,243, 249,266–269,280] [Fig. 1.1(e)]. For particles with tetrahedral patches, there is strong competition with cubic diamond, including from hexagonal diamond, BCC, dodecahedral clusters, disordered networks or gels, and liquid phases; the phase diagram is rich and complex [66,254,274]. In general, more complex particle designs (*e.g.* torsional interactions [242,249], patch selectivity [86]) allow greater control over the favoured structure; this, alongside tuning the system parameters (*e.g.* interaction range, temperature/pressure/density), has assisted diamond formation (as has seeding [207,249]). However even diamond is a relatively simple structure compared to

the kinds of structures hoped for in nanotechnology, albeit more complex than FCC/HCP, BCC, and SC. More complex structures assembled in simulation include tetrastack and a clathrate-like structure [242] [Fig. 1.1(c)]. While QCs have been formed [1–3,281,282] [Fig. 1.1(f)], this was only in 2D, and only dodecagonal QCs were stable.[†] In summary, the structures formed thus far from patchy particles in simulations are of limited complexity.

1.3.2.1 Torsional interactions

Given my interaction potential includes a torsional component, I now discuss the few other simulation studies with torsional interactions.

Refs. 202,203 used a similar torsional interaction to mine. Torsional interactions increased the ease of target structure assembly. Without torsional interactions, cubes did not assemble easily and octahedra did not assemble; with torsional interactions, both assembled [202]. Torsional interactions raised the free energy of competing structures, including disordered aggregates, and also the energy barrier to their formation—thus they favoured the target structure both thermodynamically and kinetically. Aggregates were mostly avoided. Without torsional interactions, when a second particle joins a first, it can do so with any torsional orientation, and thus the third particle that joins with the second may do so with an incorrect relative position to the first; there are thus many ways for clusters to misform. With torsional interactions, the relative orientation of each particle that adds to a cluster is controlled so that the next particle must bond in the correct configuration; the cluster cannot misform. In other words, torsional interactions control *second*-neighbour bonding. The cluster grows by the stepwise addition of monomers, and kinetic traps are avoided. The free-energy landscape is 'funnel-like', in that it continually guides the growing cluster to the correct structure.

The effect of reducing competition with alternative structures (or equivalently, reducing the number of competitor structures) is more significant when there are more competitors, or they

[†] In 2D, the kagome lattice, σ-phase, H-phase, and Platonic and Archimedean tilings are among the more complex extended structures formed.

are closer in structure or energy. This means that, in general, torsional interactions are more important for forming more complex structures (which are less entropically favourable). Thus, torsional interactions—like patch selectivity—increase the range of *accessible* target structures, as more complex structures may not form due to competing structures [211].

Torsional interactions in Ref. 249 were included via an additional term in the interaction potential. The authors found this greatly helped tetrahedral particles to assemble into cubic diamond.

I am not aware of any other studies that used torsional interactions (consistent with the relative simplicity of the structures assembled thus far). In a similar approach to torsional interactions, Ref. 242 used *patch shape* to control the torsional orientation of bonded particles [and second-neighbour bonding; Fig. 1.1(c)]. This again reduced competition between structures, and improved assembly kinetics. However, this approach offers less flexibility than torsional interactions: it is unclear how to design the shapes of a pair of interacting patches to achieve an arbitrary torsional angle, whereas controlling torsional angles themselves does this directly.

1.3.3 Experiment

I now review experimental developments regarding patchy particles, which I divide into two parts: *synthesis* of patchy particles (section 1.3.3.1), and their *assembly* into structures (section 1.3.3.2). The division is not always clear, with many studies both synthesising a collection of particles and observing their assembly. More work has been done on synthesis than on assembly [64]—hardly any 3D structures were assembled from patchy particles before 2010 [15]. Naturally, assembly requires synthesis first; but besides that, synthesis is judged to be the greater challenge, while it is thought assembly will be reliable and versatile once given adequate building blocks [12]. Many reviews have been published on both synthesis and assembly of patchy colloids and NPs [10,15–17,26,64–66,75,87,88,283,284], or covering only synthesis [44,49,72,82] or

only assembly [41,67,214].[†] While my focus is on spherical particles (section 1.1.3), I consider some shape anisotropy; I comment further on this in section 1.3.5.

1.3.3.1 Synthesis of patchy particles

The synthesis of colloids and NPs has been refined over many decades. Experimentalists have long been able to produce (*non-patchy*) spherical colloids which are monodisperse in size and properties (both bulk and surface), from a range of materials [traditionally, mostly silica or polymer latex, *e.g.* polystyrene (PS) or poly(methyl methacrylate) (PMMA)] and in a range of sizes; Ref. 90 provides a good review. Similarly, non-patchy NPs of controlled size and properties can be produced relatively easily, *e.g.* nanocrystals.[‡] More recently, much focus has been on expanding the range of synthetic colloids and NPs and increasing their complexity: particles of many shapes, compositions, and functionalities can now be produced [10,49]. A large part of this focus has been on *patchy* particles; the methods and techniques used in their fabrication are continually developed. A variety of chemical, physical, and even biologically-inspired methods are used [235]. Progress has been made on controlling patchy particle size (and reducing it—currently below the micrometre scale, but rarely down to tens of nanometres [98]), patch width, patch shape, and patch positioning, on introducing multiple patches, and on purifying the synthesised particles (*i.e.* making them monodisperse) [65]. Many types of colloidal patchy building blocks can now be made with sufficient quality and in sufficient quantity to study their self-assembly [88]. Likewise, the production of NPs has been refined to produce various sizes, shapes, and compositions with better uniformity [16]. Lately, focus has been on more diverse inorganic cores and surface ligands, in particular anisotropic patterning [82].

Nonetheless, the challenge of synthesising patchy particles is huge. The variety, precision, and homogeneity of synthetic patchy particles is currently far from what is desired (or what is seen in their biological counterparts). We do not have the control or tunability over patch

[†] Refs. 16,41,67,72,75,82 focus on NPs only, not colloids more broadly.
[‡] NP compositions include chalcogenides, nitrides, arsenides, oxides, elementary metals and semimetals; there are also core-shell particles or other multicomponent NPs [10].

designs and properties (number of patches, patch positions, widths, shapes, and interaction strengths) we need. Thus far, most synthesis methods produce particles with only one or two patches, patches with the same functionality, and/or regularly arranged patches (*i.e.* without flexibility over precise patch positions). Regarding patch selectivity, other than via complementary DNA interactions, little progress has been made. Regarding torsional interactions, these have not yet been demonstrated for traditional patchy particles, but some creative approaches have been attempted. Thus, experiment lags behind simulation. Most individual developments are small and specific, not versatile—each synthesis method only allows the production of a limited range of patchy particles, not widely customisable patchy particles [88]. Further, for most synthesis methods thus far, some or all of the following are true: production is difficult, costly, or time-consuming; the yield of particles is low, and the method not scalable (thus it is unsuitable for large assemblies or applications); the range of possible particle sizes and compositions is low; they produce polydisperse particles; and/or particles are not easily dispersed (important for subsequent self-assembly) [65].[†]

The remainder of this section surveys patchy-particle synthesis methods—first for colloids, then NPs—and the types of patchy particles that can be synthesised—with a special section on DNA-based particles—before addressing patches with torsional interactions.

Synthesis methods—colloids. The following is a (non-exhaustive) categorised list of demonstrated techniques for fabricating patchy colloidal particles, based on the reviews in Refs. 15,17, 64,65,88.[‡]

I. **Surface modification methods.** The surface of an existing (non-patchy) colloid is treated to become patchy, with distinct surface regions that have different interactions. Since colloids are usually homogeneous, creative strategies are required for regio-selective modification. In one common strategy, some *template*, *mask*, *matrix*, or *substrate* is used (*e.g.* gel, wax, poly-

[†] Unfortunately, those methods which are more easily scaled typically fare poorly on other criteria, such as allowing multiple patches, and vice versa [15].

[‡] Note that the following categories are not mutually exclusive.

mer), and only the template-free part of the particle surface is treated. The template may be carefully designed (*e.g.* a curved shape) to fine-tune the deposited surface region. Similarly, particles can be modified at an *interface* (*e.g.* air-liquid, liquid-liquid, air-solid, liquid-solid), such that if the treatment occurs in one phase then only one side of the particle is modified. If the precise position of the particle at the interface can be controlled (*e.g.* [115]), the region of surface modification is tunable.

(i) *Physical deposition* [64]: regio-selective deposition or coating, *e.g.* of metal or metal oxide, in liquid or vapour phase.[†] The simplest regio-selective case, in which deposition occurs from above on a layer of particles, yields Janus particles (*i.e.* deposition only occurs on the top half) [228]. Deposition can be regio-selective via:

a. A template, with the layer of treated particles bound to it, partially embedded in it, or masked by it [260,261,285]. In one technique ('colloidal lithography'), one or two layers of a colloidal crystal act as a mask for the treated layer(s) underneath them. Coating only occurs on the lower layers' unbonded surface regions, or only through the interstices of mask layers. Colloidal lithography produced 2 to 5 gold nanodot patches in symmetric arrangements [106–108]; reactive ion etching of the mask layer led to further control and variety in the patch patterns [107]. When multiple layers are modified simultaneously, particles in different layers are coated differently, so they must then be separated. An external mask can be used instead, with deposition occurring only through its grooves.

b. An interface: similarly, deposition occurs on one side of particles at an interface.

c. 'Glancing angle deposition' (GLAD) [109,110]: vapour deposition is applied at an angle to a monolayer, so that only certain regions of each particle are coated, since particles partially mask their neighbours. Varying the monolayer arrangement and

[†] General liquid deposition techniques include chemical, electrochemical, electroless, and layer-by-layer methods. General vapour deposition techniques include chemical vapour deposition, molecular beam epitaxy, and physical vapour deposition; a vapour may be obtained thermally or by electron-beam sputtering.

the relative angle of deposition changes the width and shape of patches (one deposition can cover 3.7–50% of a particle's surface [109]). Multiple depositions can create multiple distinct patches on the same hemisphere (perhaps overlapping, with an overlap area down to 1.6%)[†]; if particles are inverted between depositions, patches can be formed on both hemispheres [110]. Thus GLAD gives flexibility and control in patch properties, alongside relative accuracy and precision. For example, it is possible to achieve two triangular patches with orientations staggered relative to each other, as in the simulations of Ref. 275.

(ii) *μ-contact printing* (or *stamping*): a soft, treated elastomer stamp (usually polydimethylsiloxane) is pressed onto a monolayer, printing its treatment (either by physical forces, *e.g.* electrostatic, or chemical bonding [105] which is more permanent) onto the surface region that it contacts. For instance: (1) hydrophobic cationic surfactants were printed onto negatively charged PS latex particles [94]; (2) polymers based on poly(aminoethyl (meth)acrylate) were printed onto aldehyde-functionalised PS-sulfonate [105]). Printing can be repeated (possibly with different treatments) if the particles adhere to the first stamp, and a second stamp is applied on the other side [286]. Patch width can be controlled by stamp stiffness, stamping pressure, and the quantity of 'ink' on the stamp.

(iii) *Chemical* methods: regio-selective chemical treatments, *e.g.* reactions or binding of ligands, achieved via templates or at interfaces (so the chemical treatment takes place on only part of the surface). Examples include the following. (1) 'Particle lithography': PS particles covered in cationic polyelectrolyte were bound to glass, and anionic polyelectrolyte was regio-selectively adsorbed on the unbound surface, yielding an anisotropic surface charge; the width of the (single) patch was controllable [111,113]. Multiple adsorbed layers were also built up, with further control over patch width and shape [112].

[†] The advantage of overlapping depositions is that it may create patches of smaller width and/or new functionality, through the combination or connection of distinct depositions.

(2) Silica or PS particles in a colloidal crystal were modified respectively with sulfuric acid or 3-(trimethoxysilyl)propyl methacrylate, only on their unbonded surface regions [114]. (3) Silica particles in water were partially adsorbed in molten wax, the wax solidified, and the water-phase side of the particles treated with dichlorodimethylsilane [115]. (4) A monolayer of PS particles on a metallic thin film underwent reactive ion etching to reduce their size and separate them, and were bonded to the film [287]. The part of the film between particles was removed, so that when the particles were broken off they had metal caps on one side. (5) A PS solution was applied to a silica layer frozen in a gel, such that after solvent evaporation the silica particles were encapsulated in a PS membrane with only their two poles exposed. The poles were treated with (3-aminopropyl)trimethoxysilane and Rhodamine B isothiocyanate, before the PS was selectively dissolved [116]. (6) Positively charged amidine-functionalised PS particles were confined at an air-water interface [117]. Hydrolysis in the water phase converted the amidine groups to carboxylic acid which was then deprotonated, leaving that side of the particle surface negatively charged. (7) Polymers were encapsulated in DNA cages, before cross-linking the polymer and denaturing the DNA, leaving on the polymer a controlled number of DNA strands (those from the cage that were originally bound to it) [102].

(iv) *Swelling* or *deswelling* methods: polymer particles were swollen with a similar monomer, and the monomer phase separated in a number of distinct protrusions on the polymer surface [134]. The morphology of the two phases varied and could be tuned. If there are many small protrusions of monomer, the surface is rough, which affects the particle's depletion interactions. In another approach [120], PS particles at high temperature were swollen with oil and then cooled, so that the oil phase-separated. Once the oil was selectively removed (*e.g.* by evaporation), the particles were left with dimpled shapes (with dimples where the oil used to be). (See also Refs. 119,121 for different approaches

to similar outcomes.)

(v) *Heterogeneous nucleation* or *polymerisation*: silver heterogeneously nucleated on the surface of silica particles [288], or gold on cationic PS particles [289], and then grew via surface diffusion. Another approach is (seeded) emulsion polymerisation, in which nucleation and growth or polymerisation occurs on a particle surface to produce a colloid with small satellite particles—like a cluster. (1) Based on inorganic surface chemistry, PS latex (or PMMA) nucleated on silica seeds (or TiO_2 seeds) whose surface was functionalised with grafted methacryloxymethyltriethoxysilane [128,129]. Although particles with different numbers of patches were produced in each batch, some improvements to monodispersity were made. The yield was also increased (2×10^{15} clusters per litre, with 70% of clusters having the same number of protrusions). (2) One smooth PS satellite grew on a rough-surfaced PS particle, forming a dimer [118]; the rough and smooth parts interact differently due to depletion interactions.

(vi) *Direct writing*: using means such as electron beam lithography or a rigid stylus, patterns can be 'written' on the surfaces of some particles.

(vii) *Photolithography*: standard photolithography can be applied using templates to modify a surface regio-selectively.

II. **Direct synthesis.** A colloid is fabricated with regions—whether just on the surface, or through the particle core—of distinct chemical or physical properties. Suitable synthesis conditions may be required to attain the patchiness.

(i) *'Colloidal cluster'* (or *'colloidal molecule'*) methods: numerous approaches have been used to produce clusters of colloidal particles, through physical (*e.g.* van der Waals forces, electrostatic interactions, depletion interactions, capillary forces) or chemical means; a thorough review is in Ref. 44.[†] Some approaches are:

[†] Other methods, even beyond those in the cited review, have been used to form clusters. However many of these other methods are less precise and controlled, or only produce shape anisotropy, not patchiness.

a. 2D geometrical confinement: a controlled number of PS or silica particles were captured in a shallow cavity etched onto a substrate [122]. Through capillary forces (and due to their confinement) they aggregate into quasi-2D clusters of specific geometries. The clusters remain when the solvent is evaporated.

b. 3D geometrical confinement: similarly but more powerfully, while encapsulated in emulsion droplets, systems of 2–15 PS particles arranged into clusters, which remain after emulsion evaporation [123–125]. Mixing particles of different sizes [68,130] or different materials (*e.g.* PS and silica) gives greater flexibility to cluster morphology; *e.g.* a partial covering of very small particles over a few large particles left projections (patches) of the large particles at precise locations [68] [Fig. 1.2(f)]. The clusters can be subsequently swelled with (partly encapsulated in) monomer until only the outermost parts of the cluster extend beyond the monomer, and the monomer can later be polymerised [68,130,131], as in Fig. 1.2(a). This not only yields a more spherical shape, but gives chemically distinct patches (the outer parts of the original cluster, amidinated PS). Components of the cluster can also be independently functionalised before joining together, giving further flexibility in patch distinction [56]. An alternative route to similar clusters used photocurable, particle-stabilised, Pickering oil-in-water emulsions [290].

c. Coalescence: PS particles with a liquid protrusion, or PMMA particles surrounded by a wetting layer, aggregate into clusters through coalescence of their liquids, which are then polymerised [126,127] [Fig. 1.2(e)]. Various numbers of particles may join, and the cluster geometry can be tuned—beyond regularly spaced patches—with good control.

d. Reorganisation: randomly-shaped aggregates of polymer spheres reorganised into uniformly-shaped clusters of up to five spheres, by swelling with an apolar solvent and allowing the clusters to minimise their interfacial energy [291].

(ii) *Microfluidic* and *capillary flow* methods: multiple polymers are combined in liquid phase and then polymerised within one particle. For example: (1) simultaneous electrohydrodynamic jetting of two polymer solutions, with assistance from an electric field, formed biphasic (*e.g.* Janus) or triphasic particles of the two polymers [132,133]; (2) multiphase droplets in an oil-in-water emulsion were photocured [292]; (3) multiple emulsions were solidified into particles [293]; (4) two dissimilar polymers in a solvent were precipitated and phase separated in a confined droplet, through mixing with a non-solvent in a jetting process, producing particles with two or more distinct surface regions [294].

(iii) *(Micro)-phase separation of polymers*: linear block co- and ter-polymers may take on sphere-like conformations (as some proteins do). The two components may spatially separate, for instance by partial dewetting (for immiscible phases), or because of different affinities for the solvent. Thus, careful design of copolymer components and structure (along with the choice of solvent and conditions) can produce particle regions of distinct properties. Monomer-embedded polymers may also phase-separate [17]. Block copolymers can alternatively aggregate into micelles or vesicles, which may also show patchiness through the separation of their components, as above (*i.e.* there are regions where one component prevails) [135]. However, the shape and patch arrangements of these polymer particles usually fluctuates. In another approach, some core-shell particles or polymers phase-separate (*e.g.* by chemical reaction, solvent evaporation, annealing, polymerisation) to form one large particle with a distinct 'satellite' particles [44].

(iv) *Phase separation of ligands*: a mixture of two polymer ligands on silica particles phase-separated to form rippled and 'raspberry' morphologies (many distinct clumps of ligands), through reduction in solvent quality [97]. The authors had some control over ligand arrangement.

(v) *Heterogeneous growth*: a silica core, which was surrounded by PS particles forming a cluster of controlled morphology, was heterogeneously grown around the PS particles. Selectively dissolving the PS left the core, which had dimples or facets at the PS particle positions. Functionalisation of its surface could be site-specific, either at or away from the dimples. Particles with 1–4, 6, and 12 patches were produced [295,296], and 8-patch particles were proposed [66].

(vi) *'Colloidal fusion'*: in a similar process to II(v) heterogeneous growth, first a cluster was formed of a liquid core (silicone-based emulsion droplet) surrounded by solid but malleable PS spheres of a controlled number and arrangement [297]. Next, through wetting and surface energy minimisation, the cluster compacted into a sphere, with the droplet deforming to protrude between the PS particles. This left a PS sphere with patches of protruding emulsion. These patches can bond with similar patches on other particles (and the liquid bonds could be cured), or with distinct particles [to form colloidal clusters, as in II(i)]; or they can be further modified; or the emulsion can be hardened and the PS selectively dissolved, leaving the anisotropically-shaped core [as in II(v)].

(vii) *Magnetic composite particles*: magnetic NPs can be positioned anisotropically within or on the surface of larger colloids by: (1) dispersing NPs and silica microbeads in oil, emulsifying, then removing the oil [298]; (2) growing polymer (3-(trimethoxysilyl) propyl methacrylate) droplets around hematite cubes, which are encapsulated but sit on one edge of the droplet [299].

In some cases [*e.g.* II(ii) microfluidics], the patchy or non-patchy regions can be subsequently treated, functionalised, or etched (to reshape or resize them). For example: (1) on 1 μm-sized, negatively charged sulphate PS, gold patches produced via GLAD [I(i)c] were functionalised with a monolayer of *n*-octadecanethiol, becoming attractive hydrophobic patches with tunable widths [227,300] (Fig. 1.3); (2) on PS, printed block copolymer ink [I(ii)] was function-

alised with an amine and active ester, an alkyne and azide, or biotin and avidin, in each case yielding orthogonal, 'click-type' biorecognition interactions [105]; (3) gold hemispheres deposited onto PS using a template [I(i)a] were made charged by applying *N*,*N*,*N*-trimethyl-(11-mercaptoundecyl)ammonium chloride [260,261]; (4) gold was selectively deposited [I(i)] on the sides of rod-shaped particles, avidin was adsorbed over the whole surface, and the gold was etched leaving avidin only at the ends [103]; (5) patches in monomer-swelled clusters from 3D confinement [II(i)b] were functionalised (*e.g.* with biotin and then two types of single-stranded DNA sticky ends [131,301], one on the patches and one on the non-patchy regions [Fig. 1.2(a)]; or with metal coordination complexes which bond selectively [148]). Some surface modification processes can also be repeated multiple times to attain multiple patches, as noted for printing [I(ii)] and GLAD [I(i)c] [227,300], but also for deposition methods more broadly. (Practical difficulties mean most processes cannot be accurately repeated more than once.)

What is the relative usefulness—current and potential—of the above methods, in general? Firstly, methods that produce batches of particles typically produce smaller yields than continuous fabrication methods, and are less scalable. It is also difficult to maintain consistency of output particles from batch to batch. Batch methods include deposition [I(i)] and printing [I(ii)]; continuous methods include some microfluidic methods [II(ii)]. Secondly, methods that use templates are typically more robust and versatile (*e.g.* the number of patches can be varied) than those that do not, but produce smaller yields and are harder to scale (because they depend on the template). Template methods also require additional steps (thus often additional time and cost): design and production of the template, application of the template, and removal of the template after modification. The production and application of the template may apply further limitations.[†] Only since 2010 could template methods achieve more than one patch [15]. Thirdly, techniques based on existing methods, especially conventional industrial methods

[†] However, using *particles* as a mask, as in colloidal lithography, rather than an external template, avoids some of these difficulties such as template fabrication. It also decreases the patch pattern resolution to the length scale of the particles, down to around 50 nm (compared with templates of around 520 nm) [106].

[*e.g.* emulsion polymerisation [I(v)], swelling [I(iv)] [64]], are more easily scaled. Fourthly, techniques at emulsion interfaces [*e.g.* emulsion polymerisation [I(v)], 3D confinement [IIb]] have potential to be scaled with high uniformity, as well as flexibility of patch position and width. Identical particles sit at identical positions at an interface, because the position depends precisely on surface tension; the surface tension can be altered by adding chemical species. Two patches could be achieved by double emulsions, with the particles spanning the continuous phase, outer droplet, and inner droplet, and different chemical modification occurring in different phases [15]. Finally, most techniques produce polydisperse particles (dispersity in, *e.g.*, particle size, or the number, width, shape, or position of patches), meaning they must subsequently be sorted—which can be difficult. In particular, for methods that produce clusters [II(i) and I(v)], the number of particles per cluster varies in any batch; clusters of different sizes can be separated by density-gradient centrifugation.

Overall, surface modification (I) rather than direct synthesis (II) is currently the main patchy-particle synthesis route [88]. In general it is more versatile, allowing more flexibility in particle size and composition, and patch width, shape, and composition. However colloidal cluster methods [II(i) and I(v)] show great potential, albeit producing non-spherical particles. In general, they allow larger numbers and more varied geometries of patches than most other techniques, with good control (albeit not fully customisable geometries); they also give high yield. Four of the most promising individual techniques are: (1) GLAD [I(i)c] [109,110], and three cluster methods, namely those via (2) 3D confinement in an emulsion [II(i)b] [68,123,125,130,131], (3) coalescence of protrusions [II(i)c] [126,127], or (4) emulsion polymerisation [I(v)] [128,129]. Of these, (2–4) produced particles of smallest size [100 nm–1 μm, with potential to go smaller; (1) produced particles of 1–9 μm, again with potential to go smaller]. (4) is most scalable, followed by (2) and (3). (4) has most control and flexibility over patchy-particle properties, followed by (1) and (2), with (2–4) having already shown the greatest variety of patch arrangements [44,66]; a limitation of (1) is the dependence of patch shape and width on the monolayer orientation,

which may vary between production batches. Regarding other techniques, chemical methods [I(iii)] have the downsides of long production times, difficulty in creating multiple patches, and poor scalability. Some microfluidic methods [II(ii)] allow multiple distinct functionalities (from the distinct polymers), but have poor control over particle size, and are unable to produce non-patch surface regions (*i.e.* regions not of the component polymers). Particle lithography [I(iii)] [111–113], templated deposition [I(i)a] [260,261], and capillary flow methods [II(ii)] [132,133,292] give relatively high yields and are scalable.

Synthesis methods—nanoparticles. Synthetic techniques are somewhat different for patchy NPs. Here I summarise them more briefly, following the reviews in Refs. 16,26,41,67,72,75,82. In comparison to colloids, in general, NP (especially nanocrystal) synthesis is relatively simple and controllable; particles are also smaller [16].[†] The following are some approaches to synthesise patchy NPs.

(i) *Multi-ligand systems*: mixtures of surface ligands (*e.g.* amines, alkylphosphines, phosphine oxides, phosphonic acids) are common in NP synthesis [16]. Usually, different ligands mix evenly across the surface; it is difficult to cause ligands to bind regio-selectively. However some approaches have been demonstrated to cause ligands to phase separate, giving different surface properties at different positions. For instance, two thiol ligands, one hydrophobic and one hydrophilic, on 4 nm gold or silver NPs ordered themselves on the surface in regular patterns, including ripples, down to 5 Å [95,302] [Fig. 1.2(d)]. Surface curvature is thought to be an important factor in ligand arrangements. The ligands at particle poles can also be selectively replaced with other thiol ligands [302].

(ii) *Uneven ligand distributions*: changing the solvent quality (adding water to dimethylformamide) thermodynamically drove a uniform covering of self-attractive polymer ligands on gold and silver NPs to aggregate into precise patches on the surface, leaving uncov-

[†] Synthesis of nanocrystals is typically performed in solution: this gives good control to make monodisperse products, can be used for many materials, and is simple and cheap [75].

ered regions [98]. The authors had some control over the number, width, and positioning of these patches, and their arrangement can be preserved by photo-cross-linking. This method was versatile across various NPs and ligands. In another system, ligands were replaced at 1–6 specific positions with DNA oligonucleotides on modified gold NPs [303].

(iii) *Regioselective surface blocking*: in a two-step process [304], block copolymers were first used to block (cover) specific areas of the NP surface, by fine control of interfacial free energies; then, the polymer-free surface regions were modified with single-stranded DNA, giving selective interactions. The method was versatile across a range of NP compositions, sizes, and shapes.

(iv) *DNA-capped* or *-framed NPs*: DNA oligonucleotides have long been used to replace or attach to surface ligands on NPs [305–308]. Their dangling ends can be freely chosen to achieve selective interactions/bonds.[†] Even when spread isotropically across the surface, DNA caps have been used to control the crystallisation of NPs (into *e.g.* BCC, FCC) [309–311]. Recently, DNA caps were placed anisotropically by using templates [99,100], which opens the possibility for further control over crystallisation. Janus NPs [312], with two different sides, provide another route to anisotropic DNA caps. DNA frames or cages (often via origami) [42,145–147,313] around NPs are another approach, as the frame or cage can provide the anisotropic interactions not present in the particles.

(v) *Faceted particles*: anisotropic growth of nanocrystals is common. It leads to different reactivity and behaviour of the different facets, which can be used to functionalise these surfaces differently (*e.g.* through deposition or ligand binding) [82].

(vi) *Clusters*: similarly to heterogeneous nucleation on colloids [I(v)], nucleation and growth of satellites can produce an anisotropic cluster (*e.g.* epitaxial inorganic nanocrystal growth on an existing nanocrystal) [44].

Further approaches to patchy polymer ligands [beyond (i) and (ii)] are reviewed in Ref. 96.

[†] If necessary, the surface oligonucleotides can be bound to DNA linkers.

Particle types. Having considered the *methods* developed to produce patchy particles, I now consider the *kinds* of particles these methods have been able to produce: firstly, by a few categories of interest; secondly, by numbers of patches.[†]

The simplest patchy particles are Janus particles, which have received much focus. Experimentalists can now produce with good control a wide variety of Janus particles—composition (*e.g.* silica, PS), size, interactions, distinction between the two hemispheres (*e.g.* [94,115,132,260–263,285]. See reviews in Refs. 228–234 for further information. However, most Janus particle synthesis techniques do not extend to more complicated patch arrangements [15,17], with some exceptions (*e.g.* [285]). Regarding biphasic *polymer* particles, accessible designs include Janus [262], triblock, striped, or even multiple separate patches [17]; *telechelic* star polymers enable many patches, with a some control over their number and arrangement, but with a soft conformation [17,136]. Controlled binding of *ligands*, DNA, or proteins at specific positions is difficult, although two or three types of ligands can be patterned around a particle in various ways (*e.g.* [302]) [63]. In particular, particles with one *DNA patch* have been made easily [100], whereas particles with a variety of controlled patch positions and distinct, selective DNA grafts on each were more arduous [131] [Fig. 1.2(a)]. More recent techniques are getting more flexible and controlled [17]. In *lock-and-key* particle pairs (as in enzymes), one particle (the 'lock') has a dimple (or concavity) into which its complementary pair (the 'key') fits; these can be fabricated for 1–7 dimples [119–121] [Fig. 1.2(g)]. *NPs* (with surface ligands) are mostly limited to two patches, ripples of ligands [*e.g.* [95], Fig. 1.2(e)], or a 'raspberry' ligand morphology (many distinct clumps of ligands; *e.g.* [97]) [98].

Consider now particles according to their number of patches, as in Ref. 66. Numbers of patches from 2 to 15 have been produced via the colloidal cluster approach [II(i) under 'Synthesis methods—colloids']; these are usually arranged in simple geometries. For example, the multi-step process in Ref. 131, from clusters to patchy particles to DNA decorations [Fig. 1.2(a)],

[†] The reviews in Refs. 17,66 are respectively organised by particle types and number of patches.

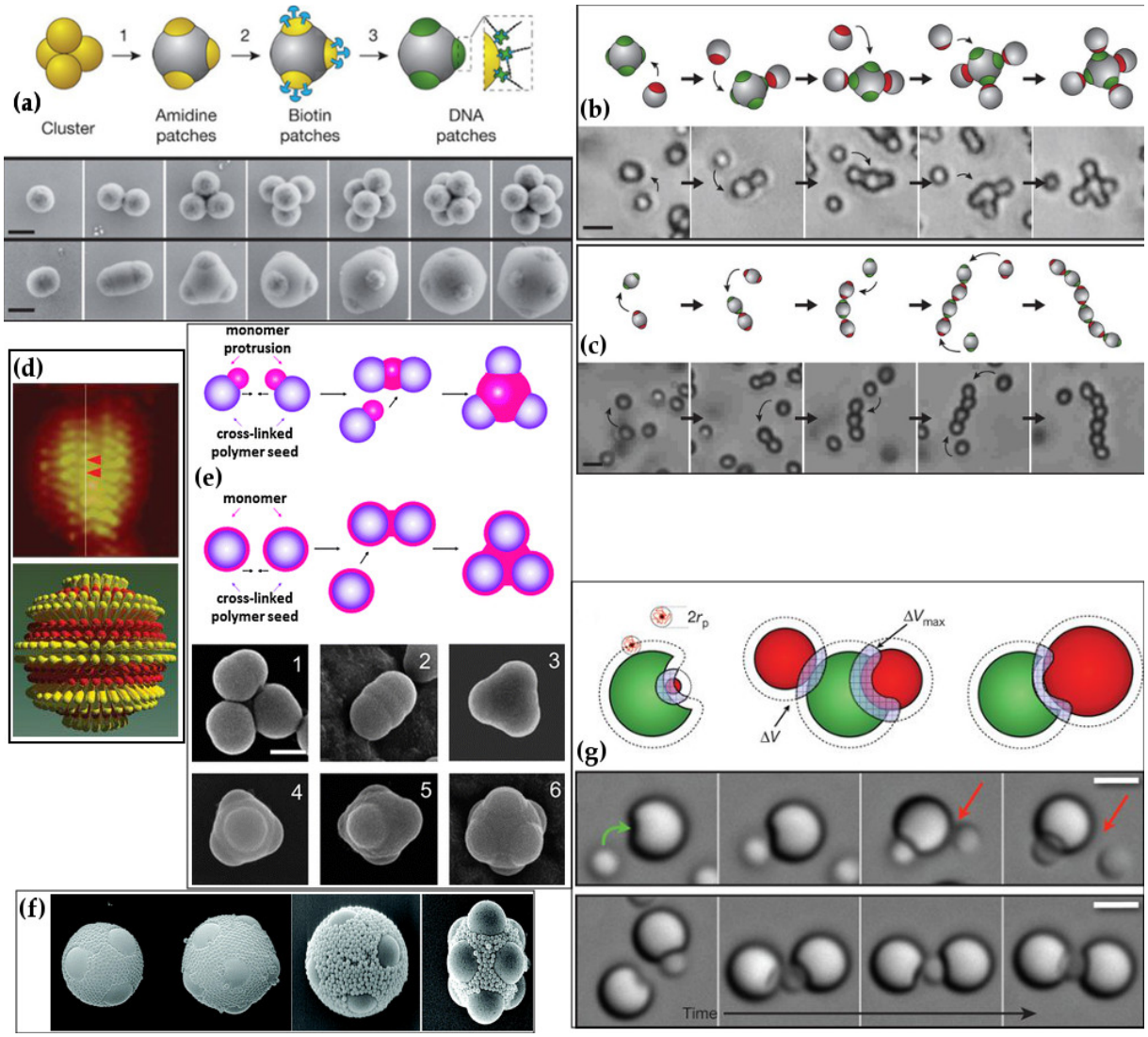

Figure 1.2: Collage of patchy particles synthesised in experiment. **(a)** Top row: schematic of functionalising 4-patch particle with DNA. (1) Cluster of four amidinated PS microspheres, formed in emulsion droplets which are later evaporated, is swollen with styrene, leaving protruding PS patches. The styrene is then polymerised. (2) Patches are functionalised with biotin. (3) DNA oligomers with biotin bind to biotin patches by streptavidin bridge. Middle row: electron micrographs of amidinated PS clusters, of 1–7 spheres (with controlled symmetry). Bottom row: electron micrographs after swelling with PS. (Scale bars 500 nm.) **(b)** Schematic (top-row) and snapshots (bottom row) of step-wise process of 1-patch particles joining with 4-patch particle to form AB_4-type 'colloidal molecule' cluster (Bent arrows point towards point of attachment; straight arrows denote time advancement; scale bar 2 μm.) **(c)** As for (b), but for complementary 2-patch particles forming chain. **(d)** Monolayer-protected gold nanoparticles with two thiol ligands that phase-separated into ripples. Top: STM image of gold nanoparticle (scale bar 10 nm). Bottom: schematic drawing (different colours for different ligands). **(e)** Schematics of liquid protrusions (row 1) or wetting layers (row 2) of monomer on different cross-linked polymer spheres coalescing to form colloidal clusters; liquid is then polymerised. SEM images (rows 3 & 4) of clusters of 1–6 vinyl acetate-coated PS spheres formed by merging styrene liquid protrusions (scale bar 200 nm). **(f)** SEM images of clusters of n silica spheres (left to right: $n = 6,7,8,8$), surrounded by smaller spheres of $1/10$ their size, formed by confinement within water-in-oil emulsion droplets (scale bar 2 μm). Protrusions of larger spheres, at controlled positions, act as patches. **(g)** Top row: schematic of 'lock-and-key' particle pairs, where one particle fits into the complementary concavity of another, and so preferentially binds there due to depletion interactions. The depletion interaction (depletants shown in left image) betw-

(Caption continued on next page.)

Figure 1.2: *(Caption continued from previous page.)* een two particles is proportional to ΔV, the overlapping excluded volume; hence the bond on the right side of the middle image is preferred to all other bonds shown. The dimples can be thought of as patches. Middle and bottom rows: snapshots of assembly of lock-and-key particles. Green (red) arrows point out successful (failed) binding. (Scale bars 2 μm.)
(a–c,d,e,f,g) reprinted with permission from Refs. 131,95,44,68,119, respectively, © Macmillan Publishers Limited, Nature Publishing Group, The Royal Society of Chemistry, American Chemical Society, Macmillan Publishers Limited, respectively.

produces particles that mimic atoms and molecules in bonding directionality and valence (sp, sp^2, sp^3, sp^3d, sp^3d^2 and sp^3d^3). Aside from clusters, though, patch numbers are limited. *1-patch* particles can be made as Janus particles or lock-and-key particles (as discussed in the previous paragraph), but with the patch occupying a precise, small region (*e.g.* [100,105,117]). *2-patch* particles can take the form of triblock particles (sometimes with two distinct patches, and in the case of GLAD [I(i)c] with controlled relative orientations) [133,227,231,285,300], or two small patches, which are usually on opposite poles. There are few reports of synthesising particles with *3 or more* distinct, precisely located patches (other than by cluster methods). These include colloidal fusion [II(vi)], which formed particles with four and eight patches [297], and (ii) replacement of 1–6 NP ligands at specific positions with DNA linkers [303]. This is a significant but important challenge for experimentalists; and the challenge is greater when one considers distinct patch types and interactions.[†] Nonetheless, other patchy designs have been created, including rings (at the equator or elsewhere) [285], ripples [95] [Fig. 1.2(d)], and many-patch particles [97,134]. Telechelic star polymers [17,136] and DNA multi-arm tiles [4,47,137–144], albeit non-spherical and more amorphous, can also behave as patchy particles.

DNA particles. The variety, bonding selectivity, orientational specificity, and strength of binding between two single-stranded DNA sequences with complementary base pairs makes them highly promising for synthesising patchy particles for controlled assembly of target structures. So I survey here the current approaches to the incorporation of DNA in patchy colloids and

[†] However it is worth noting that to achieve limited valence and open structures, typically a small, discrete number of patches is desired. So the lack of patch numbers greater than two is not as large a problem as it may seem.

NPs, following reviews in Refs. 20,31,33,34.

(i) *Grafting DNA onto particles*: various approaches have been used to site-selectively bind DNA (as described earlier), such as: via colloidal clusters [131,301] [this method enables binding of two different types of DNA strands; Fig. 1.2(a)], by masking particles to selectively attach oligonucleotides [99,100], by sequential ligand replacement and DNA electrostatic repulsion [303], by charged surfaces [261], or by imprinting within DNA cages [102]. Alongside routes to site-selective DNA binding, general progress is being made on versatility and control of (non-selective) DNA binding: for example, the variety of types of particles to which DNA can be bound continues to increase through more general experimental approaches [314].

(ii) *DNA origami*: DNA origami has been used to form DNA frames (or cages) around colloids, and the frames provide directional and selective interactions to the encapsulated particles [42,145–147]. In one case [147], the DNA at each vertex in the cage was different, allowing highly selective bonding. DNA has also been used to completely encapsulate particles in a thick DNA origami layer (a 'nanoflower'), whose bonding valence and directionality can be controlled by the number and location of sticky ends protruding from the flower [313]. In another case [315], an 'L'-shaped DNA origami belt was bound to one colloidal particle, wrapping around its surface and enabling further binding of (distinct) particles at the vertex and two tips of the 'L'.

(iii) *Emulsion droplets*: in an innovative approach [316], DNA strands at the interface of emulsion droplets were free to diffuse around the interface when droplets with complementary strands made contact. Thus, two droplets bind via a patchy region enriched in DNA; but the patchy region is mobile. Some control was possible over the number and width of these patches.

(iv) *All-DNA particles*: DNA wireframes [47] and multi-arm tiles [4,137–144] can be viewed as patchy particles.

DNA nanotechnology, *e.g.* DNA origami, can in principle assemble any arbitrary structure by using a set of unique building blocks with selective interactions, if given sufficient time and conditions. However, this has not yet been extended to the self-assembly of *particles* that directed by DNA interactions [20].

Selective interactions have also been achieved with protein/protein-based interactions, such as biotin-avidin [103–105].

Torsional interactions. Torsional interactions have not yet been demonstrated in experiment for first-generation patchy particles. Some natural patchy interactions are torsionally restricted, especially in biological molecules. Notable examples include: DNA oligonucleotides; proteins, which are used to form virus capsids; and antibody-antigen pairs. The complex structure of biological interfaces can be orientationally-specific, such that two interfaces are complementary not only in shape but also in torsional angle (i.e. connected interfaces must have the correct relative orientation [241]). (In nature this property usually controls protein *complexes* rather than *crystals*.)

The most promising approach to synthesising patchy particles with torsional interactions is functionalising colloids and NPs by incorporating patches based on the above molecules (both natural and engineered). This demands creative approaches. DNA patches have been popular; in particular, one successful strategy is multi-armed DNA motifs (star tiles) with selective interactions between arms. Torsional angles between tiles can be either 0 or π rad as the interaction is between two DNA helices.[†] The 3–6-armed DNA building blocks developed by the Mao [4,138–142] and Yan [137,143,144] groups can assemble into a range of 2D lattices and 3D clusters. Note however that because DNA tiles are quite flexible, it is difficult to control the orientation of their arms. Larger origami multi-arm tiles, with rigid angles, have thus far only been used to form finite structures. Another approach [315] is DNA origami belts [approach (ii) under 'DNA par-

[†] Specifically, the relative orientation of the building blocks is controlled by the number of turns of the DNA double helix along each arm [202].

ticles']. Given the prevalence of proteins and DNA structures as colloidal patches (as discussed earlier), there are likely to be further developments of torsional interactions.

Another potential approach towards torsional interactions may be to combine shape (*e.g.* lock-and-key molecules) and patches (in other words, both entropic and enthalpic interactions), as proposed in Ref. 81 and pursued in Ref. 296. Or, for patchy particles made of a cluster of colloids, a surface charge on the colloids could provide a repulsive electrostatic interaction which varies with the relative orientations of two bonded colloids (as in the antibonding interaction in ethane between hydrogens on opposite carbons) [249]. Finally, a patterned (or otherwise complex) patch structure, for example through many surface ligands, can be imagined in which certain bonding orientations are preferred [249]. Overall, control and flexibility over torsional interactions seems some way off, but not impossible.

1.3.3.2 Assembly of patchy particles

As noted, experimental progress on the assembly of patchy particles is considerably less than on their synthesis [64]. Here I review the range of structures achieved in experimental patchy colloid and NP systems. With purely isotropic, non-selective interactions, most systems (of one, spherical component) arrange into simple,[†] dense, mechanically strong crystals such as FCC or HCP, BCC, NaCl, or $MgZn_2$ (or in 2D, HCP or square lattices); that is, they mimic atomic crystals [20]. Systems with selective yet isotropic interactions mimic ionic, intermetallic, and alloy systems [20,158], while systems with anisotropic yet non-selective interactions (typically non-spherical particles) form a wide variety of crystal structures (and mesophases) [17,45,46,49,55,56,74,76,78,81–84]. Patchy particles provide both features (without requiring non-spherical shapes), so patchy interactions enable open (less dense), complex structures. Hence here I focus less on the numerous studies in which simple isotropic-interaction structures formed.

Assemblies are typically formed in solution and through solvent evaporation or cooling (as

[†] The simplicity or complexity of a periodic crystal can be crudely measured by the size of the unit cell.

in conventional atomic or molecular crystallisation), or sometimes by reducing the quality of the solvent.[†] Some assemblies form at interfaces or surfaces, which confines the structure to 2D. While much research has been performed on *directed* assembly using templating, temperature, light, or electric, magnetic, or shear fields [15,16,41,64,65,67,75], I do not review such systems, focusing only on those where the patchy interactions control the assembly.[‡§]

Mesophases and *finite clusters* are ubiquitous in self-assembled systems (especially Janus particles): chains, wires, or strings (branched or unbranched) [64,94,104,117,119,131,148,261,302, 304,318] [Fig. 1.2(c)]; helices or tubes [263]; rings; networks and films [131,302]; clusters (*e.g.* dumbbells, dimers, trimers, tetrahedra, octahedra, triangular bipyramids) [100,119,120,131,145,260, 261,286,304,318]; micelles and vesicles [118,260–262]; and microcapsules [319]. For example, by joining single-patch spherical particles at each patch on a multi-patch particle, tetrahedral patchy particles led to methane (AB_4)-like colloidal molecules [131] [Fig. 1.2(b)]; similarly, single-patch particles led to AB, 2-patch to AB_2 (trans- and cis-)ethylene, and 3-patch to AB_3. Some clusters (especially those employing DNA interactions) are quite complex and precise, such as a model of da Vinci's *Vitruvian man* [42]. The formation of many finite assemblies can be adjusted by varying patch shape and width (or system conditions).

More complex, *extended* assemblies are rare, and were reportedly unobserved before 2010 [15]; reasons include the lack of a sufficient quantity of monodisperse patchy particles of suitable design. However some examples have appeared more recently. A much-reported study [227] formed a kagome lattice (an open structure, and the 2D analogue of diamond) from triblock colloidal particles, via hydrophobic interactions, as shown in Fig. 1.3.[¶] The open structure is stabilised by patchy attractions and entropy, since particles can vibrate and rotate on their lattice

[†] More specifically, nanocrystal assembly methods include: solvent evaporation (drop-casting, evaporating from a tilted vessel, evaporating over a polar liquid), solvent destabilisation (gradual increase of the solution's polarity through a non-solvent, either by non-solvent diffusion or by enrichment via solvent evaporation), gravitational sedimentation, and confinement perhaps in a droplet or at an interface [16].

[‡] However I do still consider studies where somewhat-unavoidable interactions are at play, such as those related to the solvent, depletion interactions, or entropy (and packing).

[§] Note also that I do not consider studies of the assembly of multiple, significantly-different components, such as the range of binary NP superlattices achieved in Ref. 317.

[¶] Alongside the kagome monolayer, some related structures also formed, including two parallel kagome layers, with octahedral local arrangements.

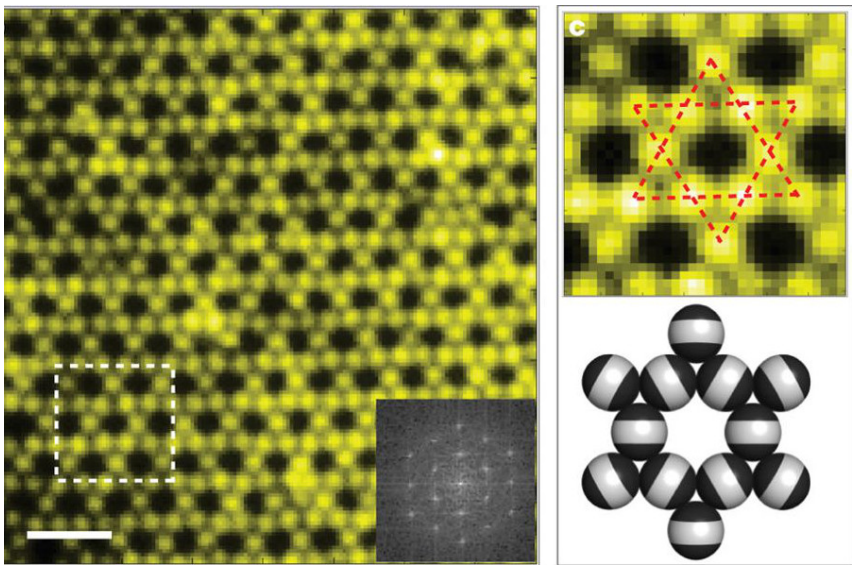

Figure 1.3: 2D kagome lattice, assembled in solution from layer of 3D particles with 2 hydrophobic patches at opposite poles ('triblock'), wide enough to allow 2 bonds per patch. Left: Fluorescence image; scale bar 4 μm; inset is Fourier transform. Top right: close-up of dashed square on left, highlighting structure (staggered triangles). Bottom right: illustration of particle arrangement. The assembly was replicated in simulation [226] [Fig. 1.1(d)]. Reprinted with permission from Ref. 227, © Macmillan Publishers Limited.

positions [320,321]. This study was the first to demonstrate not only a novel structure, but also the *design* of patches to target and achieve a structure. An important feature of the design was to use 2 patches which each allow 2 bonds, rather than 4 single-bond patches, to make the synthesis easier; the patch width was therefore crucial in achieving the structure. In a related study [300], from similar particles, a honeycomb lattice formed.

DNA approaches beyond conventional patchy particles have achieved other interesting structures. One study [146] used DNA cages around NPs to assemble the elusive (3D) diamond structure and related structures (FCC and zincblende). In another [313], the valence of patchy nanoflowers was tuned to attain 2D hexagonal and square lattices; and the concept could possibly be extended to 3D [20]. Using DNA multi-arm tiles [4,47,137–144], a wider range of complex structures have been formed. The more interesting structures include: 2D finite patterns based on Archimedean tilings, Penrose tilings, or QCs, and curvilinear arrays (as well as quasi-3D structures from their folding); 2D lattices like honeycomb, six-coordinated arrays, kagome, and σ-phase; an extended 2D dodecagonal QC; 3D finite structures like cubes, tetrahedra, dodeca-

hedra, icosahedra, cuboctahedra (an Archimedean solid), snub cubes, and bucky balls. Recently [101], the most complex structures yet were formed using DNA—clathrate structures—however the building blocks were non-spherical.[†]

1.3.4 Summary

Overall, previous work on patchy particles is extensive, and shows potential, but has only made small progress in the overall goal of assembling an arbitrary structure. This is understandable, given the size of the challenge. In *simulations*, a few systems (*e.g.* Janus particles, two-patch particles, tetrahedral-patch particles) have been well studied, and many others have been studied less thoroughly. Most studied systems are simple (in particular, with small numbers of patches—4 or less—that are regularly arranged and non-selective), and many are in 2D. The structures formed are also relatively simple. Moreover, there have been few cases of *rational design* of patches to form particular target structures; 2D targets have been somewhat complex—they notably include dodecagonal QCs—while 3D targets have been quite simple. Also, only a few studies have considered *torsional* interactions (and their design).

In *experiment*, significant work has been done on synthesising patchy particles over the past two decades, and this ability has improved significantly. Progress has been made on varying and controlling particle size and composition, number of patches, patch position, and patch width; more generally, uniformity of output has improved. But much work remains to meet the goals of patchy-particle self-assembly. Few techniques produce more than a few patches, or fully controlled patch positions or widths. Selective interactions are limited and torsional interactions still to be demonstrated. Experimental assembly is logically dependent on synthesis, so awaits further synthesis developments. Many mesophases and finite clusters have been formed, some rationally targeted, but few complex extended phases. Experimental assembly of patchy particles into extended 2D phases is currently at a basic level, with mostly fairly simple

[†] Many more structures have assembled from non-patchy particles isotropically covered in DNA: reportedly, over 500 different crystals of 36 different symmetry groups [101].

structures; the kagome lattice is a notable exception, alongside a dodecagonal QC from DNA multi-arm tiles. In 3D, no such extended phases have been reported [66], beyond those relying on complex DNA strategies. Greater understanding is required of the efficiency and success of the self-assembly process. Another challenge is stabilising assembled structures (which often form weakly, and may rely on the presence of other particles such as a resin filler for NPs [16]), including in the environments where the structures may be used (*e.g.* biological environments).

1.3.5 Other progress in patchy-particle understanding

Here, I review other aspects of the design and assembly of patchy particles into target structures, that have been learned over decades of research.

Polydispersity. Given the likely applications of self-assembled patchy particles, for example technological contexts, a high degree of perfection in the assembled structures is likely necessary (*i.e.* few defects). If this required highly monodisperse building blocks, this would be hard to achieve, given the difficulty of patchy-particle synthesis. However, while minor polydispersity in colloidal *particle size* is known to frustrate assembly,[†] this is not necessarily the case for polydispersity in *patch width*, *arrangement*, and *interaction strength*. (Monodispersity in the *number* of patches, in contrast, is likely to be important.) No experimental studies have been performed, but in the few simulation studies a reasonable amount of patch polydispersity did not hinder self-assembly [197,242,269]. A more relaxed requirement in particle monodispersity is encouraging: it makes the kind of complex patchy particles I study more experimentally realistic. It also seems that a lower level of perfection (or monodispersity) is required in macroscopic biological self-assembly than in molecular self-assembly [12], which may carry over to patchy-particle self-assembly.

[†] For the successful assembly of nanocrystals, it is estimated that the standard deviation of the size distribution must be less than 10% [75].

Thermodynamics, entropy, and assembly stabilisation. Systems of patchy particles follow standard statistical thermodynamics [16,87]. A system at equilibrium and constant temperature seeks to minimise its Helmholtz free energy F, which is given by $F = U - TS$, where U is the total internal energy of the system (the sum of the kinetic energy, which is constant, and the potential energy, in this case predominantly from interactions between particles), T is the temperature, and S the entropy. Thus, the driving force to self-assembly is a reduction in F, which can be achieved by a decrease in U or an increase in S; the relative importance of these two components depends on T. In a patchy-particle system, U is minimised chiefly by correctly aligning (both in distance and orientation) as many patches with each other as possible. Entropy is made up of a number of components, including: configurational (determined by the number of possible arrangements of particles in a configuration, or the number of ways of exchanging particles, ignoring local effects; it relates to disorder), vibrational, and rotational (the latter two components are respectively related to the ability of the particles to locally vibrate and rotate around their equilibrium positions).

Thermodynamics is important when considering the assembly of patchy particles: assembly is not purely an energetic minimisation, but entropy can be significant. One important factor in maximising *configurational* entropy is simpler, less specific patchy designs—fewer particle types, fewer patch types, less (or no) patch selectivity, and/or less (or no) torsional restrictions. Systems with less specific designs have greater configurational entropy: fewer particle types means more interparticle exchanges are possible; fewer patch types or less patch selectivity allows more equivalent orientations of a given particle (it can vary which of its patches bonds to a neighbour) [86]; fewer torsional restrictions means more equivalent configurations of bonded particles. Regarding *orientational* and *vibrational* entropy, larger angular and torsional patch widths allow particles to rotate more freely. Open structures often allow particles greater local motion (vibrational and rotational); this has been shown to stabilise open structures against denser structures with more patchy bonds [278,320,321]. For example, the experimentally-

assembled 2D kagome lattice [227] (as well as various related clusters) is stabilised against HCP by vibrational and rotational entropy. The high rotational entropy comes from the large patch width (each of the two patches is large enough for two bonds), which allows much particle rotation without disrupting bonding [225]. This result is further encouragement for my goal of assembling complex, open structures: entropy may assist their formation and stability.

Assembly kinetics. The above factors may not only entropically stabilise a structure, but also assist assembly kinetics. Less specific designs with less particle types and patch selectivity mean the favoured structure is more probable and easier to find in configuration space [56]; it thus forms faster [202]. However, there may also be more traps—competing structures—in which the system can become stuck. Larger patch widths and more open structures make traps less 'sticky', since particles are more free to move, making it easier to correct any crystallisation defects by thermal energy (as for the 2D kagome lattice [225]).

Design principles. Design principles (section 1.1.2) for patchy particles, *i.e.* principles enabling one to design a set of particles to assemble into an arbitrary structure, are much sought after [49,214]. Here I mention a few of the general principles uncovered by analysing previous work.[†] First, more patches makes an interaction more anisotropic and specific, better favouring the target structure [211]. However, there is a limit: too many (identical) patches, and the net particle interaction approaches an isotropic interaction [56]. Second, as in the preceding paragraph, the more complex the system—more distinct particles, more complex patch designs (number of patches, patch selectivity)—the more kinetically difficult it may be for the system to assemble into the correct structure [56]. Third, as in the paragraph on thermodynamics, the more complex the system the less entropically stabilised is the target structure (it has less configurational entropy) [86]. (However, a more complex and specific design will often *enthalpically* stabilise the target structure.) Similarly, narrower patch widths and less open target structures

[†] See also Refs. 322,323 for principles specific to NP assemblies from DNA-based interactions.

allow less vibrational and rotational freedom to entropically stabilise the target structure [56].

Patchy-particle classification. Patchy particles have been classified in many ways in the literature, including some of the categories mentioned earlier: Janus particles, triblock particles, inverse patchy particles; categories based on composition such as polymers (including telechelic star polymers), DNA-coated colloids, DNA-cage or -frame particles, DNA multi-arm tiles; nanocrystals. Patchy particles have also been classified according to the number of patches [66]. However, probably the most useful and general classification is based on various 'patchy dimensions', each of which can vary smoothly over a range, and which can be combined in different ways [49,81,134].[†] Such dimensions include: surface coverage (proportion of the particle surface covered in patches), number of patches (or more generally pattern quantisation, which allows for example ring patches, for which the number of rings is counted), patch width and shape (which may vary between patches), patch arrangement (regular or irregular, close or far), and patch interactions (selective interactions, interaction strength, interaction type). In my patchy-particle model, I enable inputs to be general across most of these dimensions.

Particle shape. As mentioned in section 1.1.3, this thesis focuses on particles with spherical shape. However, it is important to note the relationship between patchiness and shape: non-spherical particles have anisotropic interactions, just like patchy particles, and so can be related to equivalent patchy particles (in other words, they behave similarly). Thus, Ref. 81 considers non-spherical shape ('directional entropic forces') as a form of patchiness. The authors designed shapes equivalent to particles with 4, 6, or 8 regularly-arranged patches (typically by cutting facets or concavities into spheres) that assembled into diamond, SC, and FCC or sheared BCC crystals, respectively. In other work [20,324], (small, ordered, non-spherical) clusters of particles are considered as 'functionally equivalent' to patchy particles (even when the cluster is uniformly functionalised), with each component particle a patch creating anisotropic interac-

[†] The dimensions in these references cover more broad features than patchiness, most notably particle shape.

tions. Thus, shape and patchiness are related. So although I simulate purely spherical particles, the experimental synthesis and assembly of non-spherical particles—especially clusters of particles [68,118,122–131,290,291], dimpled particles [119–121,295,296] [Fig. 1.2(g)], or particles with protrusions [134]—is still relevant.

1.3.6 Isotropic potentials for assembling complex structures

Aside from patchy particles, how else may complex colloidal structures be made? Many competing approaches are possible, such as non-spherical particle shapes, or systems with particles of different sizes; here I consider one. *Isotropic* interaction potentials which are more complex than standard hard or soft interactions can yield complex structures, periodic and quasicrystalline. Such potentials can be precisely tuned to achieve a desired long-range ordering. For example, a range of complex open structures have been formed by simulation in 2D (*e.g.* triangular, square, rectangular, honeycomb, kagome, rectangular kagome, truncated square, truncated hexagonal, and truncated trihexagonal lattices) and 3D (*e.g.* FCC, BCC, SC, wurtzite, diamond, CaF_2, γ-brass, β-tin, Frank-Kasper phases such as σ-phase and A15, clathrate type I, porous mesophases) [325–338]; see also reviews in Refs. 43,339. Various disordered structures have also been formed in 2D and 3D: glasses with icosahedral local order [340,341], icosahedral clusters (large and small) [342,343], decagonal and dodecagonal QCs or their periodic approximants such as the σ-phase [344–348].[†] Recently [349–351], 3D decagonal, dodecagonal, octagonal, and icosahedral QCs were formed from complex isotropic potentials; a range of 2D QCs [352] were also formed from a relatively simple, hard-core/square-shoulder potential.

However, *rational* design of these potentials is difficult, because the relationship between potential and structure is not obvious. A common approach [326–336,338] is inverse design methods which draw on statistical mechanical optimisation, or use black-box artificial intelligence. Otherwise, a suitable potential is obtained empirically by testing many different poten-

[†] Many of the assembled QCs are only metastable.

tials [349,351]. In a process of discovery, parameter space is explored for families of suitable potentials—informed trial and error. Careful fine-tuning may be involved [352]. Physical reasoning and intuition may also be used, but is usually not fully rationalised and understood [325,340–348,350,351,353].

The main difficulty with these potentials, though, is in realising them experimentally [43]. While some control over interaction range, well depths, and the distance between minima is possible through soft matter physics and chemistry (for example through tailoring the ligands or polymer brushes surrounding a particle, or tailoring the solvent [43]), the kinds of potentials proposed are currently out of reach, and it is not clear how they may be achieved. Some (*e.g.* for the 3D QCs [349,351]) involve multiple minima and control of interactions out to the third coordination shell. Others involve discontinuities in potential or gradient. Additionally, there are limits to the accessible structures when using isotropic potentials, because very similar potentials produce different structures [43].

1.4 Aims and outline

1.4.1 Scope

I restrict my scope to modelling the behaviour of patchy particles of the following kinds:

(i) *Shape*: as mentioned sections 1.1.3 and 1.3.5, I only consider spherical particles.

(ii) *Attractive patches* on *repulsive particles*: my particles are weakly repulsive and my patches are purely attractive. This excludes a minority of systems studied (both by simulation and experiment) in the literature, including inverse patchy particles and charged particles (see Ref. 63 for discussion on the latter).

(iii) *Small* but *non-infinitesimal patches*: my patches are neither point-like (as in some models and experimental realisations)—they have a width—nor large (covering a large proportion of the particle surface, as in a Janus or triblock particle). In particular, they only allow

one bond per patch; this excludes many patches studied in simulation or produced in experiment.[†]

(iv) *Non-hierarchical*: *hierarchical* assembly occurs throughout nature [354] and has great potential for artificial systems (as demonstrated in biology and DNA technology) [56]. In hierarchical assembly, particles assemble into intermediate structures (substructures of the target) at a higher temperature, and these intermediates join together into the target itself at a lower temperature. (There may in fact be more hierarchical steps.) This may involve using multiple different (patchy) interaction strengths. However, I restrict my approach to non-hierarchical, single-step assembly. Thus, all interaction strengths are equal (except for some minor differences, explained at the time), and all interactions are simultaneously 'active'. I discuss my non-hierarchical approach from a methodological perspective in section 2.2.5.2.

(v) *Monodisperse particles*: I do not consider any polydispersity or imperfection among particles (of the same kind) or patches.

(vi) *Uniform particle size*: although particle size can easily be varied in both simulation and experiment, and this allows a greater variety of accessible structures, all my particles have the same size.

Limits must be drawn at some point, in order to allow a focused, thorough, and deep study (without unnecessary complexity)—even though there is surely much of interest outside these limits.

1.4.2 Aims

The main aim of this thesis is the following:

(i) To *demonstrate* the *self-assembly* of *complex*, *extended*, *3D* target structures from *patchy particles*. As noted (section 1.3.2), there have been few studies of such structures; more studies

[†] The maximum number of bonds for a Janus patch which covers half the particle surface is six [56], as seen for example in Ref. 263.

have focused on simple (*e.g.* FCC, SC), finite, and/or 2D target structures. However, for the proposed applications of colloidal systems, complex, extended, 3D structures are required. Thus, it is necessary to extend and develop previous work, and that is my aim: to show such structures can assemble from patchy particles. This main aim is to provide a proof-of-concept, rather than an in-depth study of patchy particles and their self-assembly. The complexity of the systems I study makes analytical approaches too difficult, and a thorough study of particle behaviour too expansive; thus I use simulations and focus on the assembled structures over broader assembly behaviour. This complexity also limits the number of different systems I can study, due to the computational cost of simulating them. In other words, to study systems of unprecedented complexity, I must compromise in the detail of the study. Note that I am not dealing with global minimum structures (at zero temperature), but only thermodynamically stable structures at finite temperatures.

In fulfilling this aim, I also intend to better understand other areas, including:

(ii) The *kinetics* of self-assembly for complex systems of patchy particles, such as kinetic traps, and how the rate of assembly varies in different systems;

(iii) The *thermodynamics* of complex patchy-particle systems; and

(iv) The *design principles* for patchy particles to form complex structures (section 1.3.5).

By using a simple patchy-particle model, I aim to understand general behaviour and principles, rather than those specific to a particular system (*e.g.* PS particles with ligands). Further information on the model and its applicability is given in section 2.1.

A further aim, relating more to my study of nanotubes (Ch. 5), is:

(v) To investigate the effects of varying the patchy design on the mechanical properties and behaviour of a system. More specifically, I aim to observe the effects of *stressed* designs (*i.e.* those in which the patchy interactions cannot be perfectly satisfied) in tube-like objects. I consider how the tubes respond to stresses by writhing, and analyse their thermal shape fluctuations.

In fulfilling this aim, I also aim more broadly:

(vi) To demonstrate the potential of simple patchy-particle models to model the behaviour and properties of complex systems.

In each case, I hope this thesis will contribute to experimental advances, for example in suggesting particle designs to form target structures, or better understanding self-assembly kinetics and thermodynamics.

1.4.3 Thesis outline

This thesis is organised as follows. Ch. 2 addresses the model I use to represent patchy particles, and the simulations I use to study them. I explain some theoretical background, compare with alternative models and methods, and justify my approach. The next three chapters report on three distinct but related studies on patchy particles. Ch. 3 concerns the self-assembly of systems of patchy particles into complex, extended, 3D, periodic phases. I explain my patchy-particle designs, and report on the successful assembly of periodic structures more complex than previously assembled via patchy particles (with kinetic and thermodynamic observations). I also consider alternative, simpler designs for the same structures. Ch. 4 goes beyond Ch. 3 to report on the assembly of 3D dodecagonal QCs; it extends previous work on patchy-particles assembling into 2D dodecagonal QCs. As in Ch. 3, this chapter reports on the designs, kinetics, and final structures; it also discusses the phenomenon of screw dislocations which arises in some systems. Ch. 5 is concerned with tube-like structures, in which patch designs apply stress to the ideal tube so as to cause chiral, thermal shape fluctuations. This chapter is motivated by recent work observing and studying chiral fluctuations in DNA origami structures (both in simulation and experiment); it is an example of the use of patchy particles to model more complex systems in a simple way. Finally, Ch. 6 summarises and ties together the research in this thesis, and considers the outlook for future research and developments.

Chapter 2

Methods

This thesis aims to design patchy particles that either assemble into a target structure, or apply internal stress to a structure. It investigates the behaviour of a system of particles by numerical simulations; this chapter explains the methods. The two main components of the method are the model interaction potential used to represent patchy particles, and the simulation method—namely, Monte Carlo. Section 2.1 concerns the former, and section 2.2 concerns the latter. In both cases, I *describe* my approach, *explaining* the theoretical background where necessary,[†] and then *compare* it with possible alternatives (covering the most common methods used elsewhere) and *justify* my choices. In the case of the Monte Carlo simulations, I also describe thermodynamic details of my *implementation* to simulate patchy particles assembling from a dilute fluid (section 2.3). Details for each specific application of the model and simulation method can be found in the relevant chapters. Section 2.4 ends the chapter by describing my approach to design a set of patchy particles programmed to form a particular target structure. It works through the scheme for one example structure.

2.1 Model interaction potential

2.1.1 Description of potential

2.1.1.1 Overall potential

The potential is a single-site potential (*i.e.* each particle is represented by a single site, with position and orientation). Interactions between particles are pairwise. The repulsion is isotropic, but

[†] In some cases, standard background information (including derivations) is omitted. However the main text includes more basic and detailed information for methods that are less well-known or where my choice of method was open for question.

the attraction depends on the relative orientation of the two particles. The interaction potential between particles i and j, U_{ij}, is given by

$$U_{ij}(\mathbf{r}_{ij}, \mathbf{\Omega}_i, \mathbf{\Omega}_j) = \begin{cases} U_{ij}^{\mathrm{LJ}'}(r_{ij}) & : r_{ij} < \sigma'_{\mathrm{LJ}} \\ U_{ij}^{\mathrm{LJ}'}(r_{ij}) \max\limits_{\text{patch pairs } \alpha,\beta} \left[\varepsilon_{\alpha\beta} U_{ij}^{\mathrm{ang}}(\hat{\mathbf{r}}_{ij}, \mathbf{\Omega}_i, \mathbf{\Omega}_j) U_{ij}^{\mathrm{tor}}(\hat{\mathbf{r}}_{ij}, \mathbf{\Omega}_i, \mathbf{\Omega}_j) \right] & : r_{ij} \geqslant \sigma'_{\mathrm{LJ}} \end{cases}, \tag{2.1}$$

where $\mathbf{r}_{ij}$ is the interparticle vector, r_{ij} is the interparticle distance, $\hat{\mathbf{r}}_{ij}$ is the direction of the interparticle vector, $\mathbf{\Omega}_i$ and $\mathbf{\Omega}_j$ are the respective orientations of i and j, α and β are patches on particles i and j respectively, and σ'_{LJ} is a constant defined in the next paragraph. For a system of N particles, the total potential energy, U, is given by the sum of all two-body terms:

$$U = \sum_{i<j}^{N} U_{ij}(\mathbf{r}_{ij}, \mathbf{\Omega}_i, \mathbf{\Omega}_j). \tag{2.2}$$

The potential is based on a standard Lennard-Jones (LJ) potential,

$$U_{ij}^{\mathrm{LJ}}(r_{ij}) = 4\epsilon_{\mathrm{LJ}} \left[\left(\frac{\sigma_{\mathrm{LJ}}}{r_{ij}} \right)^{12} - \left(\frac{\sigma_{\mathrm{LJ}}}{r_{ij}} \right)^{6} \right]. \tag{2.3}$$

σ_{LJ} and ϵ_{LJ} are, as usual, respectively the interparticle distance at which $U_{ij}^{\mathrm{LJ}} = 0$ and the minimum value of U_{ij}^{LJ} (*i.e.* the depth of the potential well for a pair of particles, at $r_{ij} = 2^{1/6}\sigma_{\mathrm{LJ}}$). U_{ij}^{LJ} is truncated (at cutoff distance r_{cut}) and shifted to give $U_{ij}^{\mathrm{LJ}'}$, as follows:

$$U_{ij}^{\mathrm{LJ}'}(r_{ij}) = \begin{cases} U_{ij}^{\mathrm{LJ}}(r_{ij}) - U_{ij}^{\mathrm{LJ}}(r_{\mathrm{cut}}) & : r_{ij} < r_{\mathrm{cut}} \\ 0 & : r_{ij} \geqslant r_{\mathrm{cut}} \end{cases}. \tag{2.4}$$

I set $r_{\mathrm{cut}} = 2.5\sigma_{\mathrm{LJ}}$. σ'_{LJ} in Eq. 2.1 corresponds to the distance at which $U_{ij}^{\mathrm{LJ}'}$ passes through zero.[†]

The overall potential U_{ij} (Eq. 2.1) has two regimes (but is continuous, by design). In the shorter-distance regime ($r_{ij} < \sigma'_{\mathrm{LJ}}$), the potential is simply the isotropic LJ repulsion. In the

[†] For $r_{\mathrm{cut}} = 2.5\sigma_{\mathrm{LJ}}$, $\sigma'_{\mathrm{LJ}} \approx 1.00068\sigma_{\mathrm{LJ}}$.

longer-distance regime ($r_{ij} \geqslant \sigma'_{\mathrm{LJ}}$) the LJ interaction is modulated by a dimensionless prefactor, $\varepsilon_{\alpha\beta}$, which may be specific to the two patches involved, and two orientationally dependent functions, U_{ij}^{ang} and U_{ij}^{tor}. For any pair of particles i and j, only the pair of patches α (on i) and β (on j) that maximises $\varepsilon_{\alpha\beta}U_{ij}^{\mathrm{ang}}U_{ij}^{\mathrm{tor}}$ is considered to interact (yet the potential is still continuous as a function of the orientations of i and j).

2.1.1.2 Components of patchy attraction

In this work, $\varepsilon_{\alpha\beta}$ mostly takes binary values, 1 if α and β attract or 0 if they do not, but sometimes takes other (positive) values in order to vary the strength of different patch-patch interactions. In principle it could take any real value. To define $\varepsilon_{\alpha\beta}$ for all patch pairs, one therefore requires a (square) *matrix* of values, ε.[†]

The angular modulation term, U_{ij}^{ang}, is a measure of how directly the patches α and β point at each other; maximum interaction occurs when they point directly towards each other. It is based on a product of two Gaussian functions:

$$U_{ij}^{\mathrm{ang}}(\hat{\mathbf{r}}_{ij}, \boldsymbol{\Omega}_i, \boldsymbol{\Omega}_j) = \exp\left(-\frac{\theta_{\alpha ij}^2}{2\sigma_{\mathrm{ang},\alpha}^2}\right) \exp\left(-\frac{\theta_{\beta ji}^2}{2\sigma_{\mathrm{ang},\beta}^2}\right). \tag{2.5}$$

$\theta_{\alpha ij}$ is the angle between the patch vector $\hat{\mathbf{p}}_i^{\alpha}$, representing the patch α on particle i, and $\hat{\mathbf{r}}_{ij}$. $\sigma_{\mathrm{ang},\alpha}$ is a measure of the angular width of patch α (a Gaussian root-mean-square width, in radians; the full width at half maximum of the Gaussian is $2\sqrt{2}\sigma_{\mathrm{ang},\alpha}$). In this work, unless otherwise noted, it is the same for all patches in a system (hence I usually write 'σ_{ang}' for brevity). It controls the constraint on the preferred angular alignment of a pair of patches.

The torsional modulation term U_{ij}^{tor} describes the variation in the potential as either of the particles i and j is rotated about the interparticle vector $\mathbf{r}_{ij}$. That is, it is a function of the tor-

[†] In practice (see section 2.4.1), I divide patches into *types*. (Each patch of a given type has the same properties.) So I define a matrix only for all pairs of patch types.

sional angle of the particle pair. Analogously to U_{ij}^{ang}, U_{ij}^{tor} is given by

$$U_{ij}^{\mathrm{tor}}(\hat{\mathbf{r}}_{ij}, \boldsymbol{\Omega}_i, \boldsymbol{\Omega}_j) = \exp\left\{ -\frac{\left[\min\limits_{i \in \phi_{\alpha\beta}^{\mathrm{offset}}} (\phi_{\alpha\beta} - i)\right]^2}{2\sigma_{\mathrm{tor},\alpha,\beta}^2} \right\}. \tag{2.6}$$

To define the *torsional angle* (like the *dihedral angle* in stereochemistry), $\phi_{\alpha\beta}$, I specify a unique *reference vector* for each patch (usually one of the other patch vectors).[†] $\phi_{\alpha\beta}$ is then the angle between the projections of the reference vectors for patches α and β onto a plane perpendicular to $\hat{\mathbf{r}}_{ij}$. I also define a set of *offset angles* for each patch pair, $\phi_{\alpha\beta}^{\mathrm{offset}}$ (via a matrix of sets ϕ^{offset})[‡]. This allows me to specify one or more preferred (minimum-energy) values of the torsional angle, $\phi_{\alpha\beta}$, possibly non-zero, each favouring some relative torsional rotation. If multiple equivalent offset angles are in the set $\phi_{\alpha\beta}^{\mathrm{offset}}$ (corresponding with the site symmetry of the particle in the target structure), I find the minimum value of $\phi_{\alpha\beta} - i$ for $i \in \phi_{\alpha\beta}^{\mathrm{offset}}$ (*i.e.* across the set of equivalent offset angles).

U_{ij}^{tor} is maximised when the torsional angle $\phi_{\alpha\beta}$ matches one of the offset angles, *i.e.* the relative twist of α and β around $\mathbf{r}_{ij}$ matches one of the preferred orientations for those patches. (In the case $0 \in \phi_{\alpha\beta}^{\mathrm{offset}}$, U_{ij}^{tor} is maximised when the projections of both patches' reference vectors onto the plane perpendicular to $\mathbf{r}_{ij}$are parallel.) Twisting around the interparticle vector, away from $i \in \phi_{\alpha\beta}^{\mathrm{offset}}$, is penalised. Thus, the torsional component of the potential ensures bonded patches have the correct relative orientation. $\sigma_{\mathrm{tor},\alpha\beta}$ is the torsional 'patch width' and controls the constraint on the preferred torsional alignment of two patches. As for $\sigma_{\mathrm{ang},\alpha}$, unless otherwise noted, it is the same for all patch pairs in a system (hence I often write 'σ_{tor}' for brevity).

[†] Preferably, a reference vector should not be nearly parallel to its patch vector, because that complicates the calculation of $\phi_{\alpha\beta}$. This condition is usually fulfilled by choosing another patch vector as the reference vector.

[‡] As noted for $\varepsilon_{\alpha\beta}$, I divide patches into *types*. (Each patch of a given type has the same properties.) So I define a matrix only for all patch type pairs (see section 2.4.1).

2.1.1.3 Parameters and units

As in Ref. 202, I typically set $\sigma_{\text{tor}} = 2\sigma_{\text{ang}} = 0.6$ rad, but in some cases (where noted) I use $\sigma_{\text{ang}} \neq 0.3$ rad. $\sigma_{\text{ang}} = 0.3$ rad means that the interaction is half as strong if one patch angle is 20° away from perfect alignment (the other patch being at perfect alignment). $\sigma_{\text{tor}} = 0.6$ rad means the interaction is half as strong if the torsional angle is 40° away from perfect alignment. As $\sigma_{\text{ang}} \to \infty$ and $\sigma_{\text{tor}} \to \infty$, the isotropic LJ potential is recovered.

I use reduced units. σ_{LJ} and ϵ_{LJ} are the reduced units of length and energy, respectively, and $T^* = k_{\text{B}}T/\epsilon_{\text{LJ}}$ is the reduced temperature unit.

2.1.2 Justification of potential

2.1.2.1 Development of model

The above coarse-grained model interaction potential derives from Ref. 202, which itself derives from a simpler, well-used model [1,2,54,197,198,202,203,207,211,241,258,271,272,274,281,282].[†] (The potential used in the latter references, except Ref. 203, does not include a torsional component.) It has been referred to as the 'orientational Lennard-Jones' model [17].

I generalised the original potential of Ref. 202 in two main ways:

(i) The original model did not include the prefactor $\varepsilon_{\alpha\beta}$. $\varepsilon_{\alpha\beta}$ gives selectivity (*i.e.* specificity and variety) in the interaction strengths between patches. Experimentalists are improving their ability to control patch selectivity (section 1.3.3.1).

(ii) The original model only allowed preferred torsional angles of 0° (for a given reference vector), *i.e.* it did not include offset angles ($\phi_{\alpha\beta}^{\text{offset}}$), let alone multiple equivalent offset angles. In real (natural or artificial) systems with torsional interactions, the preferred angle could take an arbitrary value other than 0°. Practically, introducing $\phi_{\alpha\beta}^{\text{offset}}$ also makes it easier to match the particle design to the symmetry of the target structure.

[†] Refs. 2,282 vary the LJ exponent. Ref. 282 modifies U_{ij}^{ang} to be the sum of two similar terms with distinct angular patch widths. In Ref. 281, and in some simulations of Ref. 282, the $r_{ij} \geqslant \sigma'_{\text{LJ}}$-regime in Eq. 2.1 applies across *all* r_{ij}—*i.e.* patches can interact 'within' a particle.

2.1.2.2 General justification

The model balances physical realism with simplicity (*e.g.* few parameters), efficiency (low computational cost), and generality across many types of patchy interactions, including colloids, NPs, and biological molecules like proteins. That is, its simplicity allows one to study patchy-particle behaviour common to many systems, rather than behaviour specific to a certain type of particle. Yet it is still complex enough to account for the main, essential features of a real system; patchy-particle models like the current one have replicated a range of complex behaviours of real patchy particle systems seen in experiment. In any case, models with much greater detail are not computationally feasible, given the size of patchy particles and the timescale on which self-assembly occurs, and given the vast range of design and phase space I explore. Coarse-graining (a 'toy model') is necessary, but any first-order, general principles should still be observable. While each experimental system has its own complications (*e.g.* for DNA interactions [20,56])[†] these can be investigated later in the research process. It is advantageous that the model is based on the well-characterised LJ potential, as comparison with other systems is easier.

The model's flexibility (*e.g.* number of patches, torsional interactions) allows a wide range of interactions and behaviours. If required, these variables could be tuned to represent specific particles. For instance, the model accounts for most observed behaviour of DNA multi-arm structures, but to accurately represent them a narrow patch width should probably be used, in order to capture their fixed valence (*i.e.* each patch can only make one bond) [3]. (Moreover, patch vectors that can change under the influence of an internal potential could be used, to represent the internal flexibility of these motifs.)

[†] "[T]he [field is in a] current exploratory stage . . . , concerned with global features of the phase diagram and possible assembled structures, [so] the accuracy of the DNA-induced potential model is sensibly not a major concern. . . . Parameterising the spatial and angular extent of the interactions (and optionally binding valence, dihedral angle constraints, *etc.*) between building blocks, and defining the matrix of relative energetic strengths of the attractions between different particle populations should suffice for mapping out phase behaviour and structure formation; with the phase boundaries presumably only being weakly sensitive to the exact form chosen for the potential." [20]

Suitability for colloids. Colloidal interaction potentials are complex and varied.[†] The LJ potential is suitable for some colloids (*e.g.* [356]), especially those with longer-ranged potentials. Moreover, it is a general, well-studied potential. The model does not include explicit solvent molecules (colloids, NPs, and biological molecules typically self-assemble in solution). Thus, a 'fluid phase' in the model corresponds to a dilute solution [241]. It also does not explicitly include surface ligands, ubiquitous on NPs and common on colloids. Rather, the effect of the solvent and ligands on the interaction potential is treated implicitly. Additional simplifications of the model (beyond those of a standard LJ potential) include:

(i) Repulsions are purely isotropic and do not consider the effects of patches. In soft matter systems, core repulsion is usually strong so would indeed overshadow patchy interactions.

(ii) U_{ij}^{ang} is unrealistically symmetric [271]. Consider two nearby particles, i and j, with patches α and β respectively. Consider a configuration in which i, j, α, and β are all in the same plane, and $\theta_{\alpha ij} = \theta_{\beta ji} = 20°$, *i.e.* both patches are at $20°$ to the interparticle vector. There are two possibilities: α and β are both on the same side of $\mathbf{r}_{ij}$ (top row of Fig. 2.1), or they are on opposite sides of $\mathbf{r}_{ij}$ (one above, one below; bottom row). In the first case α and β are nearer each other, and thus might be expected to interact more strongly; in the latter they are further apart. However, in Eq. 2.5 both cases give the same value of U_{ij}^{ang}, and so have the same interaction energy. This simplification applies more generally to any other angles $\theta_{\alpha ij}$ and $\theta_{\beta ji}$, including configurations where i, j, α, and β are not in the same plane. Note, though, that in all cases, the model favours two patches to improve their alignment.

(iii) Only one patch per particle can be involved in a bond—there is no 'double bonding' between two particles. Double bonding is unlikely in interactions between real patchy colloids and NPs, but is possible in biological interactions (*e.g.* through hydrogen bonding).

Some such simplifications are necessary, and these ones are unlikely to have significant effects

[†] Indeed, colloidal potentials are sometimes (*e.g.* for inorganic nanoparticles) non-additive, so they cannot be modelled as an explicit sum of the components of the interaction [355].

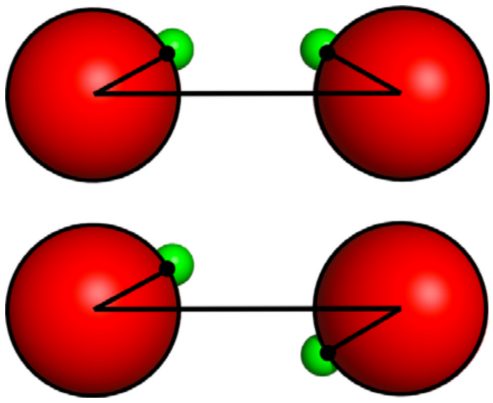

Figure 2.1: Two patchy-particle configurations with the same energy according to the model, illustrating a simplification of the model [point (ii)]. Reprinted with permission from Ref. 271, © Institute of Physics.

on the behaviour.

Torsional interactions. The inclusion of torsional interactions in the potential distinguishes the model from most others (sections 2.1.3 and 1.3.2.1). Torsional interactions are included because they assist the assembly of complex structures. The major limitation of patchy (or any other directional) interactions is that they only determine the *local* neighbourhood—the nearest neighbours. Local neighbourhoods progressively grow to give the overall structure. In contrast, complex isotropic interaction potentials can also control *second*-nearest neighbours (and *third*-nearest neighbours, *etc.*), through their longer range. Thus, such isotropic non-patchy interactions can control *multiple* coordination shells, which can be helpful in forming complex structures. For example, cubic diamond has tetrahedral particle coordination, but many other structures also have tetrahedral coordination, such as hexagonal diamond and many cage structures [274]. Moreover, many structures can form from particles with tetrahedrally-arranged patches, such as BCC (two interpenetrating diamond lattices). Thus, it is difficult to find conditions which uniquely yield cubic diamond from tetrahedral patchy particles [207,243,249,266–269].

Torsional patchy interactions help overcome this difficulty. Torsional interactions control the relative orientation of two particles, and therefore control the position at which a *second* neigh-

bour binds to the nearest neighbour. Thus, torsional interactions control the second neighbour shell. Torsional interactions in the nearest-neighbour shell in turn direct the *third* neighbour shell, and so on. As noted (section 1.3.2.1), torsional interactions were shown in simulations to assist—both thermodynamically and kinetically—the formation of cubic diamond [249], and cubes and octahedra [202,203]. They reduce competition with alternative structures, and thus increase the range of accessible target structures. Indeed, it is hypothesised that torsional interactions are essential for some biological self-assembly [197,202,211]. Of course, the torsional component of the potential can be switched off ($U_{ij}^{\mathrm{tor}} = 1, \forall i, j$) to model non-torsional interactions; this may be more appropriate for current patchy colloids and NPs [49,202].

I discussed experimental realisations of torsional angles in section 1.3.3.1 (under 'Torsional interactions'); particles with torsional interactions may be achievable.

2.1.2.3 Choice of parameters

Regarding patch widths, Refs. 197,198 showed the value of $\sigma_{\mathrm{ang}} = 0.3$ rad to be reasonable to achieve reliable patchy-particle self-assembly. It balances (or optimises between) two competing requirements: energetic (narrow patches better favour one specific target structure) and kinetic (wide patches maintain kinetic accessibility of the target structure, because the system can more easily break out of incorrect configurations) [197].[†] In any case, results are relatively insensitive to the precise values (or ratio) of σ_{ang} and σ_{tor}, as shown in Ref. 202. The values used here are typical of those in the studies cited in section 2.1.2.1 that used the same model. In cases where the choice is important, I discuss this further at the relevant point. Setting $\sigma_{\mathrm{tor}} = 2\sigma_{\mathrm{ang}}$ is physically reasonable because angular and torsional degrees of freedom are likely coupled in some systems; moreover, this effectively eliminates one parameter (making the model simpler). The ratio of 2 is chosen because torsional angles do not usually need to be so constrained to achieve specificity, and as noted wider patches improve kinetic accessibility.

[†] In general (regarding all model parameters), "The interactions … need to be specific enough to prevent [incorrect assemblies] while maintaining kinetic accessibility" [202]. If the patches are too narrow, the system (at low temperatures) forms a vapour of clusters; if the patches are too wide, it behaves like an isotropic LJ fluid.

My value of the LJ cutoff distance, $2.5\sigma_{\mathrm{LJ}}$, is typical for similar studies, balancing computational efficiency with accuracy [357,358]. Long-range interactions are unrealistic for colloids and biological molecules—even $r_{\mathrm{cut}} = 2.5\sigma_{\mathrm{LJ}}$ is quite high [63,359].[†]

Given real colloids and biological molecules tend to interact over a shorter range than the distance of the well in the standard LJ potential [359], some researchers consider a generalized LJ potential with exponents of 20 and 10 (rather than 12 and 6, as in Eq. 2.3). Ref. 197 compared results using these two sets of exponents for my model, and overall the trends were similar and the differences small. Self-assembly progressed more slowly for a 20-10 LJ potential,[‡] with initial yields of the target structure (in this case, an icosahedral cluster) smaller; but given time, the yields more closely matched those for a 12-6 LJ potential.

2.1.3 Comparison with other potentials

Many other patchy-particle models have been used to represent colloids, NPs, and/or biological molecules. Most have in common with my model the combination of an isotropic repulsive potential from spherical cores, with an orientation- (and distance-) dependent patchy attraction, which is due to a small number of precisely-defined sites on the surface [15,63,212]. Some other patchy models are similar to mine, typically those that represent biological molecules (*e.g.* deoxygenated haemoglobin assembling into sickle cell fibres [196], viral capsid assembly [210]), but also those that represent polymers (*e.g.* supramolecular polymers assembling and bundling [224]).

The most widespread alternative patchy-particle model is the Kern-Frenkel (KF) model [153]. The KF model has been well used (*e.g.* [19,86,200,221,223,226,240,243,249,264–267,269,270,275,279,280,361,362]).[§] In the KF model, the basic interaction is a hard-sphere, square-well (rather

[†] Using a cut-and-shifted potential is standard practice. Otherwise, the potential extends infinitely, or at least in practice to the size of the simulation box, which is computationally expensive [357]. The effect of the cut-and-shift is minimal: for $r_{\mathrm{cut}} = 2.5\sigma_{\mathrm{LJ}}$, U_{LJ} shifts to higher energy by $0.016\epsilon_{\mathrm{LJ}}$ and the crossover distance (at which the potential passes from positive to negative) shifts to a larger distance by $0.00068\sigma_{\mathrm{LJ}}$ (*i.e.* $\sigma'_{\mathrm{LJ}} \approx 1.00068\sigma_{\mathrm{LJ}}$).

[‡] This is because for a shorter-range potential: (1) particles are statistically less likely to be within each other's attractive potential wells, in order to form bonds; and (2) the energy barrier to rearrangement once a bond forms is higher [360].

[§] Some studies use a continuous version of the KF model, in order to perform molecular dynamics simulations

than LJ) potential. But this is modulated by an orientationally-dependent term to represent attractive patches: it takes the value 1 if the interparticle vector passes through a patch on the surface of both particles, or 0 if it does not. Thus, to attract, two particles must both be close together and have patches that "face each other"—*i.e.* there is a separate radial and angular requirement for patchy interaction (as for my model). Each requirement is controlled by one parameter: the interaction range, and the patch width, respectively. The interaction energy is the well depth if particles attract, infinite if they overlap, or 0 otherwise (rather than being a product of smooth Gaussians).

The KF model is simpler than mine, which brings some advantages,[†] but is less realistic overall. One important difference is that due to the square-well nature of the KF angular term (and, if included, a torsional term), the KF model specifies a preferred *range* of angles, rather than a specific preferred angle. Particle orientations move freely within this range, with no energy penalty. (One can crudely think of the system as 'rattling' around between the walls of the well.) This is physically unrealistic, because both biological and synthetic patchy systems are likely to have an optimum angular arrangement. (The corresponding image is of 'vibrating' around the preferred angle.) Thus, the KF model may fail to adequately encourage particles to form the correct arrangement, which is important for more complex structures like those considered here. Nonetheless, Ref. 207 reported that the two models behave similarly (for the case of diamond assembling from tetrahedral patchy particles).

Other patchy/anisotropic particle models in the literature include:

(i) Sticky hard spots (SHS) or point-like patch models [215,217,256,257][‡]: particles are hard spheres, and patches are also (small) hard spheres; patches interact with each other if they are within a short distance (full interaction if so, no interaction if not). One parame-

(*e.g.* [19]). Ref. 223 uses the orientational dependence of the KF model, with a different model for the base interaction (the 'Baxter model'). Ref. 200 uses an attractive Yukawa-type potential rather than the square well, to model lysozyme. Ref. 280 combines the KF model with a more complex and realistic model for soft particles, allowing deformations and polydispersity.

[†] For example, hard-sphere, square-well models like the KF model are easier to treat analytically, enabling comparison between theoretical and simulation results [63].

[‡] Ref. 257 uses a continuous version of the SHS model.

ter controls patchy bonding (there is no explicit angular term), so the radial and angular components of the interaction cannot be tuned independently (as in the model I use and the KF model).

(ii) Primitive model for water (PMW) [216,218,363]: a specific version of the SHS model (the SHS model was derived from the PMW model), designed to model water. Four patches, two for hydrogen atoms and two for lone pairs, are tetrahedrally arranged, with the lone pair sites under the particle surface. Unlike patches attract, like patches do not interact.

(iii) A primitive model for silica [364]: similar to the PMW model, a specific version of the SHS model, but for silica.

(iv) A model for dipolar interactions [222,259]: like the SHS model, but to model dipolar fluids. Hard-sphere particles have dissimilar patches (three patches, two of one type and one of another), with various interaction selectivity.

(v) Models involving many distinct atoms: in one approach [61,71,73], some atoms represent patches, and interact differently from other atoms which represent the particle core. This allows full flexibility in patch positions, sizes, and interactions. In another approach [235–237], some atoms represent a NP, and others one or more tethers (*e.g.* polymers) attached to its surface.

(vi) Models of gels [365,366].

(vii) Models of proteins [71,73,150,151,367].

Some of these models bear similarities with mine or the KF model; but most are inappropriate for my work. They may be inappropriate because they: are overly simple or less realistic (*e.g.* the SHS model); are used not as a general model but to model a specific system [*e.g.* associating and network-forming fluids such as water (ii) and silica (iii),[†] gel-forming systems (vi), proteins (vii)] [63]; and/or have been rarely used, and thus offer limited comparisons. Some key

[†] These are the first systems for which anisotropic potentials were used [63].

differences between my model and other inappropriate models are that mine has: (1) a longer interaction range, (2) a continuous potential, (3) extended (rather than point-like) patches, and (4) the restriction of one bond per particle pair [63]. Point-like patches are less realistic for soft matter systems than extended patches [63,271]. See Refs. 15,63,153,212 for more thorough discussions of patchy-particle potentials used elsewhere and section 1.3.2 for my review of previous patchy-particle simulation studies.

Ultimately, the potential that best represents a specific patchy system (whether colloids, NPs, or biological molecules) depends on the system. In particular, for colloids it depends on particle size, composition, and how the surface is functionalised to give patchy interactions. And for a given synthetic colloid, the best model will not be known until that colloid is produced. Thus, my decision to use a general model (section 2.1.2.2) is reasonable.

2.2 Monte Carlo simulations

2.2.1 Background

To simulate the assembly of patchy particles, I use Metropolis [368] Monte Carlo (MC) simulations in the canonical (NVT) ensemble [357,358]. In the canonical ensemble, N (the number of particles in the system/simulation box), V (the volume of the simulation box), and T are held constant. Traditionally, and most naturally, MC simulations in physics, chemistry, and biology are used to determine averages of thermodynamic properties of a system at equilibrium (*e.g.* entropy, free energy, pressure, chemical potential, specific heat) [368]. However they can also be used to simulate the configurations into which a system arranges, and to represent dynamics and self-assembly (discussed further in section 2.2.5.2).

In this section, I provide a brief introduction and theoretical background to canonical MC simulations in the context of this thesis. This section draws on two standard texts, Refs. 357,358, to which the reader should refer for further information.

2.2.1.1 Basics of MC

MC simulations do *not* directly simulate the dynamical evolution of a system; rather, they sample its configuration space stochastically [357,358]. To this end, a sequence of stochastic moves (changes in the configuration) is performed, causing the system to evolve in a *random walk*. Some moves are accepted and others are rejected (returning the system to the configuration before the move). Average system properties (including any preferred configuration into which the system settles) across a MC simulation correspond to physical averages—provided the simulation meets the criteria of: (1) ergodicity, and (2) balance (the latter criterion is discussed in section 2.2.1.2). An *ergodic* simulation is one which can access all possible configurations of the system; an ergodic simulation that runs for a very long (but still finite) time will visit all configurations. In other words, there is a finite pathway between any two points in configuration space. (If, for example, the system's free-energy landscape is such that two free-energy minima are separated by a large barrier, the simulation may not be able to access both these minima.) If a simulation meets both criteria (1) and (2), the system will tend towards the actual configurations of its physically-realised equivalent. Running such a simulation for sufficiently long will yield the global optimum configuration; the difficulty is that one cannot know in advance how long is sufficient for a given system.

The basic MC algorithm is as follows [357,358]:

1. **Initialise:** set up an initial configuration of particles, which is the first *old* configuration, o.

2. **Move:** make a random move from o, to arrive at a *new* configuration, n.

3. **Accept** or **reject:** accept or reject the move from o to n, according to some probabilistic criteria. If the move is rejected, return to o (*i.e.* n is erased and o remains as it was); if the move is accepted, n becomes o.

4. **Iterate:** repeat steps 2 and 3 until the simulation is complete (usually determined by the

number of moves).

An MC *cycle* (also known as a *sweep*) is a sequence of N (the number of particles in the system) attempted moves (whether accepted or rejected). The randomness—both in generating moves (step 2; this includes choosing the particle(s) to move, the type of move, and the size of the move) and accepting them (step 3)—gives rise to the name 'Monte Carlo', and requires repeated random number generation. Since new configurations are chosen randomly, without any memory of previous configurations, the sequence of configurations is a *Markov chain* (or *drunkard's walk*).

2.2.1.2 Probabilities, balance, and the Metropolis acceptance criterion

The probability of *generating* a trial move from o to n (step 2) is $P_{\text{trial}}(o \to n)$. The probability of *accepting* the trial move from o to n (step 3), known as the *acceptance probability*, is $P_{\text{acc}}(o \to n)$. Thus the probability of *actually moving* from o to n (taking it as a given that the system begins in o), known as the *transition probability*, is $P_{\text{trans}}(o \to n)$:

$$P_{\text{trans}}(o \to n) = P_{\text{trial}}(o \to n) P_{\text{acc}}(o \to n). \tag{2.7}$$

At equilibrium (a stationary distribution), by definition, the probability of being in a given configuration and moving to any other configuration must be the same as the probability of being in any other configuration and moving to the given configuration [357]. That is, the total flux away from the given configuration must be the same as the flux into that configuration. This applies for all configurations. Mathematically,

$$P_o \sum_{n \in C \setminus o} P_{\text{trial}}(o \to n) P_{\text{acc}}(o \to n) = \sum_{n \in C \setminus o} P_n P_{\text{trial}}(n \to o) P_{\text{acc}}(n \to o) \qquad \forall o, \tag{2.8}$$

where P_o is the probability of being in configuration o, the sum is over all configurations in the total space of possible configurations C (but not including o), and thus n here can be *any* new configuration. This condition is known as *global balance* (or simply *balance*). Satisfying global

balance ensures the system converges to the correct equilibrium configuration, whatever the initial configuration.

However, enforcing global balance in practice is complicated, as it requires simultaneous knowledge of very many configurations (due to the summations in Eq. 2.8). Therefore the condition of *detailed balance* (related to *microscopic reversibility*) is typically enforced instead. Detailed balance [357] imposes the balance condition independently on every pair of possible configuration transitions. The probability of being in a given old configuration and moving to a given new configuration is the same as the probability of being in the given new configuration and moving to the given old configuration:[†]

$$P_o P_{\text{trial}}(o \to n) P_{\text{acc}}(o \to n) = P_n P_{\text{trial}}(n \to o) P_{\text{acc}}(n \to o) \qquad \forall o, n. \tag{2.9}$$

In other words, for every move, there exists a reverse move with the same probability. Detailed balance only requires knowledge of two configurations at a time, o and n, and thus is more easily implemented. However, it is more stringent than global balance, and imposing it is not actually necessary for a correct MC simulation [369].

To meet the requirement of detailed balance, I use the following common practice [357]. For all moves, it is equally likely to generate a move and its reverse move, *i.e.* $P_{\text{trial}}(o \to n) = P_{\text{trial}}(n \to o)$ for all o, n (or in other words, the *transition matrix* of trial moves is symmetric). Thus $P_{\text{trial}}(o \to n)$ and $P_{\text{trial}}(n \to o)$ cancel in Eq. 2.9, which can then be rearranged to give the desired ratio of acceptance probabilities:

$$\frac{P_{\text{acc}}(o \to n)}{P_{\text{acc}}(n \to o)} = \frac{P_n}{P_o}. \tag{2.10}$$

[†] Note, therefore, that if in any situation it is impossible for a reverse move to occur (one which precisely reverses the previous move), then detailed balance (but not global balance) is broken. This means the selection of which particle to move in step 2 cannot be systematic; it must be possible for the same particle to be moved twice in a row. So although on average each particle is moved once per cycle, the choice of particle for each move is entirely random, under detailed balance. It also means the maximum move size must be constant (and not, *e.g.*, in proportion to a value that changes); otherwise, if it reduces between two moves, the second move may not be large enough to return to the original configuration.

The probability distribution of configurations in the canonical ensemble follows the canonical Boltzmann distribution (using the canonical Boltzmann factor, $\exp\left(-U/k_BT\right)$):

$$P_c = \frac{1}{Z}\exp\left(-\frac{U_c}{k_BT}\right), \tag{2.11}$$

where U_c is the potential energy of configuration c,[†] and Z is the canonical partition function (which is constant for a given system at a given thermodynamic state). So P_n/P_o in Eq. 2.10 can be related to the canonical Boltzmann factor, giving:

$$\frac{P_{\text{acc}}(o \to n)}{P_{\text{acc}}(n \to o)} = \exp\left(-\frac{U_n - U_o}{k_BT}\right). \tag{2.12}$$

To satisfy the above ratio of acceptance probabilities, many schemes are possible. I use the Metropolis [368] criterion for the canonical ensemble, which is widely used and efficient (both in computational cost, and statistical accuracy):

$$P_{\text{acc}}(o \to n) = \min\left\{1, \exp\left(-\frac{U_n - U_o}{k_BT}\right)\right\}. \tag{2.13}$$

That is, in MC step 3 all moves that lower the potential energy are accepted (the exponent in Eq. 2.13 is positive, and the exponential greater than 1), and some moves that increase the potential energy are accepted (the exponent is negative, and the exponential between 0 and 1). In the latter case, the acceptance probability decreases with the size of the potential energy difference between the configurations, and also decreases as T decreases.[‡] This acceptance scheme is a *Markov-chain* MC scheme, in which the probability of the system being in a given configuration depends only on the previous configuration.

[†] In principle, one should consider the *total* internal energy, which also includes the kinetic energy, when calculating these probabilities. However, if the temperature is constant, as is the case for the canonical ensemble I sample (see section 2.3), then the average kinetic energy of the system is also constant. So typically the kinetic energy is (safely) ignored, and only the potential energy considered.

[‡] To decide computationally whether to accept a move with acceptance probability less than unity, I follow standard practice: I compare the probability to a random number between 0 and 1, and if the random number is less than the probability, I accept the move; if not, I reject it.

The Metropolis acceptance criterion *biases* the system's walk through configuration space according to energy. Over many small, discrete moves (step 2), the system tends towards lower energy configurations. (Such sampling of configuration space is referred to as '*importance sampling*', and differs from random sampling by weighting lower-energy configurations more strongly.) But accepting some moves which increase the energy ensures configuration space is properly sampled: simulations in which energy can never increase become stuck in local minima (which may not be the global minimum), unable to cross free-energy barriers.

As discussed ahead (section 2.3), in most simulations I slowly reduce the temperature. Reducing T does not necessarily mean the system is far from thermodynamic equilibrium [370], as long as the decrease in T is sufficiently gradual. To be certain the decrease in T is sufficiently gradual, one would need to know the configuration space energy landscape (among other things). This is impossible to know in advance. Moreover, decreasing T gradually enough is sometimes prohibitively expensive. Therefore, as in most implementations, I decrease T slowly, and repeat (stochastically) the simulation a number of times (beginning from different initial configurations). If all repetitions yield similar outcomes, this suggests (but does not guarantee) the cooling was sufficiently gradual.

2.2.2 Parallel MC

Serial computing performs a series of tasks, one after another; in contrast, *parallel* computing performs tasks independently and simultaneously, in parallel *threads*. MC computations have traditionally been run in serial, because the stochastic sampling procedure—moving from one configuration to the next (section 2.2.1.1)—is naturally serial. Each step randomly chooses a new configuration, and accepts or rejects it; the acceptance of a move depends on the configuration of neighbouring particles resulting from previous moves, so in general moves cannot be computed independently. When the interaction is short-ranged, however, it is possible to efficiently parallelise MC, and I make use of parallel MC for simulating larger systems. In this

section, I describe the basic elements of my parallel MC approach; for further information, the reader should consult Ref. 7.

Parallel computations are usually more efficient when run on a single graphics processing unit (GPU), as opposed to a network of multi-core central processing units (CPUs) [371]. Effective GPU algorithms split a computation into thousands (or more) of independent, identical *threads*. Various parallel MC algorithms have been created (see the references given in Ref. 7). The most powerful, simplest, and most reliable is the *chequerboard* algorithm [372,373], recently implemented for GPUs by Anderson *et al.* [7] and named 'MPMC' (for 'massively parallel MC').

MPMC breaks down the MC procedure into parallel threads by splitting the system (simulation box) into a chequerboard of cells (cubic and equally sized) as in Fig. 2.2(a), and using *cell lists* [357,358] to keep track of which particles are in each cell. MC moves can proceed independently and concurrently within sets of cells that are far enough apart to avoid affecting each other by their moves. This condition is achieved by ensuring the cell width is greater than the interaction range [Fig. 2.2(b)], in my case $r_{\rm cut}$,[†] and rejecting moves in which a particle leaves its cell; thus two particles which have a cell in between them cannot interact. In 3D (2D), therefore, moves can proceed in one eighth (quarter) of the volume of the simulation box at a time [*i.e.* there are eight (four) distinct sets of cells]. The cells that evolve simultaneously at any time are 'active' cells, and they are separated by 'inactive' cells, which are unchanged. After a number of moves, active cells become inactive, some of the inactive cells become active, and the cycle repeats; all cells are active at some point. MPMC uses one thread to perform moves in each active cell.

The MPMC algorithm [7] can be summarised as follows :

1. **Chequerboard:** Randomly divide the system into a chequerboard.
2. **Choose set:** Randomly choose a set of cells to be active.
3. **MC**: Simultaneously for all cells in the active set, perform a given number of standard MC moves (randomly choosing the order of moved particles in each cell, and without allowing

[†] Ideally (for maximum parallelisation), the cell width is only slightly larger than the interaction range [Fig. 2.2(a)], but the optimal width also depends on the total box size [7].

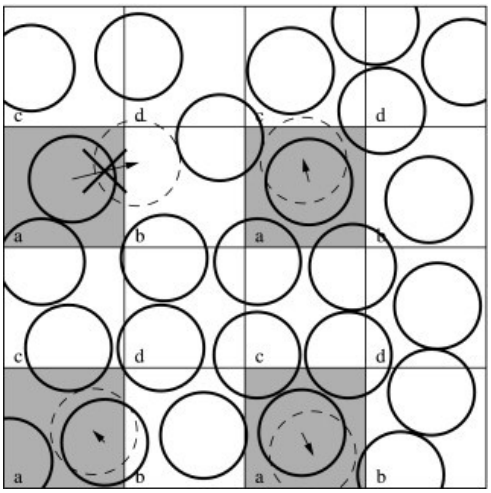

(a) Chequerboard division

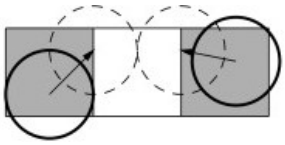

(b) Cell width condition

Figure 2.2: (a) The simulation box (here in 2D) is divided into a chequerboard of cells. The cells are separated into sets, here labelled 'a', 'b', 'c', 'd'. MC moves occur concurrently in one set of cells, the 'active' cells, here shaded. Moves in which a particle leaves its cell (*e.g.* top left move) are rejected. **(b)** If the length of cell side is greater than the interaction range (shown by the circles), concurrent MC moves within separate active cells cannot cause particles to interact. Reprinted with permission from Ref. 7, © Elsevier.

a particle to leave its cell).

4. **Iterate sets:** Repeat steps 2 and 3 until each set has been active once.

5. **Iterate chequerboard:** Repeat steps 1–4 until the simulation is complete (usually determined by the total number of moves).

MPMC satisfies detailed balance (section 2.2.1.2) and maintains randomness, despite the partial ordering of particle moves (due to division into cells). The conditions which guarantee detailed balance are: (1) random ordering of which cell set is active (step 2); (2) random ordering of which particles are moved (within each cell; step 3); and (3) rejecting moves in which a particle leaves its cell. Ergodicity (section 2.2.1.1) is achieved by periodically splitting the simulation box into a new chequerboard (along new, random lines; step 1).

2.2.3 Implementation

In this section I describe my implementation of Metropolis MC simulations in the canonical ensemble, in order to simulate patchy particles under my interaction model (section 2.1.1) in 3D.

I begin with features uniform across both implementations (section 2.2.3.1), and then discuss my serial (section 2.2.3.2) and parallel (section 2.2.3.3) implementations. I end by briefly discussing my validation of these implementations (section 2.2.3.4).

2.2.3.1 Both serial and parallel

I initiate each system in a random configuration (both particle positions and orientations)[†] in a rectangular prism (almost always cubic) simulation box with *periodic boundary conditions* [357, 358].[‡]

All my moves are single-particle moves. I choose a particle to move at random, and then choose the move type. The possible move types are translations and rotations (but not combinations of the two), and these are equally likely. Translations are to a position randomly chosen from a cube centred on the selected particle. Mathematically,

$$\mathbf{r}_i^{\text{new}} = \mathbf{r}_i^{\text{old}} + \Gamma \begin{pmatrix} \mathcal{R}_1 - 0.5 \\ \mathcal{R}_2 - 0.5 \\ \mathcal{R}_3 - 0.5 \end{pmatrix} \tag{2.14}$$

where $\mathbf{r}_i^{\text{old}}$ and $\mathbf{r}_i^{\text{new}}$ are the positions of particle i before and after the translation (respectively), $\mathcal{R}$ is a random number in the range $[0, 1]$ ($\mathcal{R}_j$ is determined separately for each j), and Γ is the side length of the translation cube. Thus, $\mathbf{r}_i^{\text{new}}$ is chosen from an even distribution in a cube with length Γ centred on $\mathbf{r}_i^{\text{old}}$. Rotation moves differ between serial and parallel implementations. I use the maximum move size (*e.g.* for translations, controlled via Γ) to target an MC rotation and

[†] Trial positions and orientations are generated one particle at a time. The procedure is slightly different for my serial and parallel implementations. In *serial*, when each particle is generated, its interaction energy with all other particles is calculated. The trial position and orientation is rejected if any interaction energy is greater than $100\epsilon_{\text{LJ}}$, otherwise it is accepted. In *parallel*, the trial position is rejected if the interparticle distance is less than σ_{LJ}. In either case, if rejected, a new position and orientation is generated, and so on until one is accepted.

[‡] To simulate a system of particles one must first define the simulation box (the space in which the particles exist). When using periodic boundary conditions, the simulation box is repeated infinitely on both sides in all dimensions [357]. This means that a particle's nearest neighbours, with whom it interacts, may be in a different box (but really they are on the opposite side of the same box). Particles that move across a box boundary, into a new box, reappear on the opposite side of the original box. Periodic boundary conditions avoid 'edge effects'—any unphysical effects from the artificial edges of a finite simulation box—without the difficulties and cost of a large box and/or a large number of particles. The box shape must be a space-filling polyhedra, to be infinitely repeatable in all directions.

translation move *acceptance ratio* (the proportion of trial moves that are accepted in step 2 of the MC algorithm) of around 0.3–0.4. This helps achieve good sampling of configuration space.[§]

After each proposed move, I calculate the energy of the new configuration and accept or reject it according to the Metropolis criterion in Eq. 2.13. Actually, one need not calculate the interparticle energy of all particle pairs in the system after every move, but only of the moved particle and those particles possibly affected by the move. I use the *cell list* method [357,358] to determine relevant particle pairs. The simulation box is split into a number of cells, whose side length is greater than r_{cut}. After a move, interactions are calculated between a particle and other particles in the same cell or the neighbouring 26 cells (in 3D), because particles cannot interact with any further cells (given the side length). The list of particles in each cell is periodically updated. If the system is sufficiently large—at the very least more than 27 cells, but in practice significantly larger, due to computational overheads—the cell list method improves efficiency. The calculation of interactions using cell lists scales as $\mathcal{O}(N)$. This compares with: $\mathcal{O}(N^2)$ for a naïve algorithm which checks all particle pairs; or $\mathcal{O}(N^2)$ to $\mathcal{O}(N^{5/3})$ for the *Verlet list* (or *neighbour list*) method [374], which keeps lists of nearby particles (up to a distance slightly greater than r_{cut}). The overall computational efficiency of the cell list method depends on other factors (*e.g.* total cell size), but typically the computational overhead becomes worthwhile for $N \gtrsim 1000$ (*i.e.* all of my systems) [358].

Given the calculation of interparticle interactions is the most time-consuming part of MC, the algorithm scales overall as $\mathcal{O}(N)$ [357,358].

2.2.3.2 Serial

In serial, to run on a CPU, I implemented my patchy model in the existing oxDNA simulation package [6], written in the C++ programming language. oxDNA already contained all necessary (serial) MC infrastructure. I provided flexibility in the input of individual patchy-particle

[§] The optimum acceptance ratio is simply the one that samples configuration space most efficiently, and this varies between systems. Typically, values between 0.2 and 0.5 are efficient [357].

designs.

A particle's orientation is specified as a (3×3) rotation matrix. The new matrix after a candidate rotational move is produced by choosing a random vector as an axis and rotating the particle around it for a random angle, as in Ref. 358.[†] oxDNA does not adjust the maximum translation or rotation move sizes during a simulation,[‡] meaning the respective acceptance ratios vary from start to finish;[§] I manually refined the move sizes for each system before simulating.

oxDNA generates pseudo-random numbers through Linux's `drand48()` function [375], which uses the linear congruential algorithm and 48-bit integer arithmetic.

2.2.3.3 Parallel

In parallel, to run on a GPU, the patchy-particle model is implemented in a currently-unpublished code written by a collaborator, Dr. Eva González Noya, with minor assistance from me. Henceforth I refer to this program as 'PMC' (for 'parallel MC'). PMC is written in the Fortran 90 programming language (with some subroutines in C that serve as interface between the CPU and GPU), and uses the well-established NVIDIA CUDA Toolkit [376,377].

A particle's orientation is specified as a *quaternion* (a set of four scalar values). Quaternions reduce the redundancy of orientation matrices (to specify an orientation, only three independent values are needed, whereas a 3×3 matrix has nine), but also avoid the gimbal lock and singularities that may arise in the equations of motion when using Euler angles (another alternative orientation representation) [358]. To generate a random change in orientation, the procedure is analogous to rotation matrices in oxDNA (section 2.2.3.2): first choose a random

[†] Over the course of a simulation, floating-point arithmetic can corrupt the orthonormality of rotation matrices [212]. oxDNA uses checks and safeguards to ensure this does not occur.
[‡] This is important for obeying detailed balance (section 2.2.1.2).
[§] This causes some inefficiency during my simulations, because the acceptance ratio is high in the initial, gas-phase stage, and low in the later, cluster-gas equilibrium phase.

vector as an axis, then rotate by a random angle [358]. Mathematically, for quaternions,

$$\begin{aligned} \mathbf{a}_i^{\text{new}} &= (\cos\tfrac{1}{2}\psi, \hat{\mathbf{s}}\sin\tfrac{1}{2}\psi) \otimes \mathbf{a}_i^{\text{old}}, \\ \psi &= (2\mathcal{R} - 1)\psi_{\max}, \end{aligned} \tag{2.15}$$

where $\mathbf{a}_i^{\text{old}}$ and $\mathbf{a}_i^{\text{new}}$ are the orientations of particle i before and after the rotation (respectively), $\hat{\mathbf{s}}$ is the unit vector of the random rotation axis, ψ is the random rotation angle, and $\psi_{\max}$ is the maximum MC rotation angle. PMC maintains an acceptance ratio of 0.4, by adjusting Γ and $\psi_{\max}$ during each simulation (as is standard practice [357,358]).[†]

PMC differs from MPMC as published [7]; the differences improve efficiency by increasing parallelisation. In particular, MPMC runs one parallel thread per active cell (section 2.2.2). Each thread checks moves in one 3D cell against particles in the same cell and the 26 neighbouring cells ($3^d - 1$ neighbouring cells in dD, where d is the number of dimensions). In contrast, PMC runs 27 (3^d) threads per active cell. Each thread checks moves in one cell against particles in *one* of the neighbouring cells or the cell itself (*i.e.* a thread computes the interaction energy of the moved particle with particles in only one cell).[‡]

PMC generates a separate stream of pseudo-random numbers for each active cell. It does so with CUDA's cuRAND library [376], which uses various random number generation algorithms.

For further details of the implementation of MPMC, see Ref. 7.

2.2.3.4 Validation of implementations

To check the output of these implementations, I performed a number of tests, including:

[†] Although this strictly means PMC simulations disobey detailed balance (section 2.2.1.2), the failure is small, and less important for non-equilibrium simulations like mine. It is important, though, that the move size remains small, in order for MC dynamics to be physically realistic (section 2.2.5.1).

[‡] To provide further computational detail, a *warp* is a group of 32 threads that run the same code and have the same execution path. To maximise efficiency an algorithm should group threads in blocks of size n warps, for some integer n. In 3D, for each active cell, PMC uses a block of size 1 warp. Thus there are $32 - 27 = 5$ unused threads per block; nonetheless, PMC is still more efficient than when using one thread per active cell. One of the threads is the "master"; it performs the MC move, collects the energies calculated by the "slave" threads, and checks whether the move is accepted.

(i) I calculated the energy at $T^* = 0$ of various simple periodic structures with perfect patchy-particle designs. For a perfect structure with n patchy bonds per particle (on average), all of the same length, according to Eq. 2.1 the energy per particle is $-(n/2)\epsilon_{\mathrm{LJ}}$. Both oxDNA and PMC calculate the correct energies.

(ii) I simulated patchy particles designed to form the following simple structures, beginning from configurations already arranged in these structures, at temperatures slightly below the melting point (T^*_{melt}): finite clusters (*e.g.* tetrahedra, cube) and simple extended crystals (*e.g.* SC, cubic diamond, zincblende, wurtzite). The structures were stable during these simulations.

(iii) I simulated the assembly of the patchy particles in (ii), beginning from the fluid phase. The target structures formed successfully.

(Section 2.4.1 explains how I designed patchy particles for the structures in these tests.)

I confirmed that both programs agree on the energies of a number of (stationary) configurations, as well as on the average energies for simulations in the canonical ensemble under a range of conditions.

2.2.4 Parallel MC speedup

In this section, I consider the computational speedup of parallel MC, compared with serial MC. I begin with comments applicable to MPMC in general (including prior testing of MPMC; section 2.2.4.1), and then consider the efficiency of my specific MC implementations in oxDNA and PMC (section 2.2.4.2).

2.2.4.1 Speedup of MPMC in general

Aside from overheads, the number of trial moves per unit time, η, is constant while N varies. The overheads of MPMC (most importantly, the launch of GPU kernels) are large, meaning MPMC is only faster than serial MC for large N.

Anderson *et al.* [7] tested the performance of MPMC on a GPU against a serial CPU MC algorithm. They ran the tests for hard disks in 2D at reduced particle number density $\rho^* = N/V^* = 0.698\ \sigma_{\mathrm{LJ}}^{-3}$ (where $V^* = V/\sigma_{\mathrm{LJ}}^3$ is the reduced volume). At their respective peak efficiencies, MPMC on a GPU was 148 times faster than serial MC (as measured by the number of MC moves per unit time). At peak efficiency, per *socket* MPMC on a GPU was 37 times faster than serial MC, per *node* it was 20 times faster, per *unit currency* it was 27 times cheaper, and per *Joule* it was 13 times more efficient.

Although these efficiency gains of MPMC are significant, they were only realised at peak efficiency in a particular 2D system. In that system, peak efficiency for MPMC on a GPU occurred for $N \gtrsim 10^6$; for serial MC, efficiency was fairly flat, at least for $N \gtrsim 5 \times 10^3$. Of course, the efficiency of MC (both serial and parallel) varies with a number of factors, including hardware, software, and details of the system simulated (*e.g.* number of dimensions, simulation box size, density, interaction range, interaction potential—which in my case includes the number of patches per particle and the presence or absence of U_{ij}^{tor}). The number of active cells running in parallel decreases from roughly $N/8$ for hard disks in 2D to roughly $N/144$ for a 3D system of LJ interactions with $r_{\mathrm{cut}} = 2.5$, like my systems [7]. Given GPUs require at least 10^4 parallel threads to run at peak efficiency, this implies $N \gtrsim 1.44 \times 10^6$ particles are needed for MPMC to run at peak efficiency, for systems like mine (according to Anderson *et al.*). Since I study systems of $N \lesssim 2 \times 10^4$ particles, this raises the question of whether MPMC as published is worthwhile for me.

2.2.4.2 Speedup of my parallel implementation

Here I explain and empirically verify that PMC is indeed faster than my oxDNA serial algorithm, for the larger systems I study.

Explanation. Firstly, PMC is even more efficient than MPMC. Anderson *et al.* [7] suggest the improvement that PMC implements, described in section 2.2.3.3 (27 threads per active cell),

lowers the number of particles necessary for peak-efficiency MPMC to $N \gtrsim 5.3 \times 10^4$. Secondly, rather than *peak* efficiency, what I require is simply for parallel MC to be faster than serial MC in *my applications*. (In Anderson *et al.*'s tests on 2D hard disks, this occurred for $N \gtrsim 5 \times 10^3$.) Thirdly, as mentioned in section 2.2.4.1, the exact efficiency of an MC algorithm depends on many factors, in particular density. The efficiency of MPMC is greater at lower densities, as described in the next paragraph. Given Anderson *et al.*'s tests were performed at $\rho^* = 0.698\ \sigma_{\mathrm{LJ}}^{-3}$ whereas typically in my systems $\rho^* = 0.1\ \sigma_{\mathrm{LJ}}^{-3}$, MPMC is comparatively faster for my systems than Anderson *et al.*'s tests suggest.

MPMC is relatively more efficient (compared to serial MC) at low densities than high densities because at low densities, more MC moves can be performed simultaneously.[†] After dividing the system into a chequerboard of cells, parallel MC moves can be performed in one eighth of the cells—the maximum fraction of active cells when ensuring all active cells are separated by inactive cells, so their particles cannot affect each other (section 2.2.2). For a given N, at low density there are more cells than at high density, thus more moves can be performed in parallel. However, this argument relies on the density being relatively homogeneous throughout the system (*i.e.* the particles being evenly spread). If particles are concentrated in a smaller region, the density in this region is higher; the actual efficiency of MPMC is more like that corresponding to this higher density, because the slowest (high-density) thread determines the efficiency.[‡] In my simulations the efficiency changes over time. My systems typically begin in the gas phase—with low, homogeneous density ($\rho^* = 0.1\ \sigma_{\mathrm{LJ}}^{-3}$)—so MPMC is very efficient (relative to serial MC). After assembly, however, cluster(s) grow, making the density inhomogeneous. In the clusters, the density is typically around 0.4–0.6 $\sigma_{\mathrm{LJ}}^{-3}$ (while the fluid around them has $\rho^* < 0.1\ \sigma_{\mathrm{LJ}}^{-3}$); MPMC performs with roughly the (lower) efficiency it would at these higher densities.

[†] Calculating the interaction energy between a particle and its neighbours is also cheaper at lower densities. This is because at low density, particles have fewer neighbours within r_{cut}. However this advantage applies to both serial MC and MPMC, so does not improve the relative efficiency of MPMC.

[‡] In the inhomogeneous case, there are also regions of very low density—cells containing few or even no particles—alongside the cluster(s). These low-density cells can make few or no MC moves, and so they finish running sooner than the high density cells. But MPMC does not wait for the high density cells to complete their MC moves; rather, it proceeds from the completed low-density cells to new cells among the active cell set, as soon as they finish.

Verification/testing. Dr. Noya performed preliminary testing against a standard serial MC code (which used cell lists). She ran both the serial code and her parallel code on the same machine. Dr. Noya compared the codes on a system of patchy particles designed to form the clathrate type I structure (Table 3.1), beginning from the crystal at $\rho^* = 0.4125186\ \sigma_{\mathrm{LJ}}^{-3}$ (as noted, this is representative of the densities of target structures in my work). Performing simulations of an equilibrium state (as when simulating the crystal) means there is less probability that the serial and parallel trajectories diverge, which would make the results less comparable. She found that for $N = 1242$, serial MC (a standard implementation, not oxDNA) is 1.4 times faster, but for $N = 9936$, PMC is 10 times faster (and for $N = 268272$ it is 48 times faster).

I performed further testing on the speeds of oxDNA and PMC at various N. Note there are differences between the algorithms [*e.g.* representation of orientations, adjustment of move sizes (sections 2.2.3.2 and 2.2.3.3)], as well as the programming languages and compilers, so the two codes are not directly comparable. Similarly, the computational hardware and system architecture on which the codes are run necessarily differ. For this reason, my tests are not designed to compare the codes' *theoretical* efficiencies, but rather to compare their efficiencies *in practice* in my context, for the purpose of knowing the faster code for given N.

I studied a system of patchy particles designed to form the cP4 structure (structure described in Table 3.1, particle design in Table 3.2), beginning from two configurations: (1) a random configuration at $\rho^* = 0.1\ \sigma_{\mathrm{LJ}}^{-3}$, to represent the early low-density gas phase of my self-assembly simulations; and (2) a random configuration at $\rho^* = 0.6\ \sigma_{\mathrm{LJ}}^{-3}$ (slightly less than the density of the cP4 crystal, $\rho^* \approx 0.6506\ \sigma_{\mathrm{LJ}}^{-3}$) which is then placed in a larger box, giving $\rho^* = 0.1\ \sigma_{\mathrm{LJ}}^{-3}$, to represent the later cluster-gas equilibrium stage of my assembly simulations. I performed simulations at $T^* = 0.122$ (just below T^*_{melt}) for 5×10^4 MC cycles,[†] for a variety of N. For oxDNA, I used (fixed) move sizes representative of those used in actual simulations [note that these give different acceptance ratios for systems (1) and (2)]; for PMC I adjusted the move sizes to target

[†] For systems with $N = 3.2\times10^4$ particles, on the Tesla K40m GPU (see caption of Fig. 2.3), computation time limits meant I could only run 2.5×10^4 MC cycles. The trends in the results suggest this had little effect.

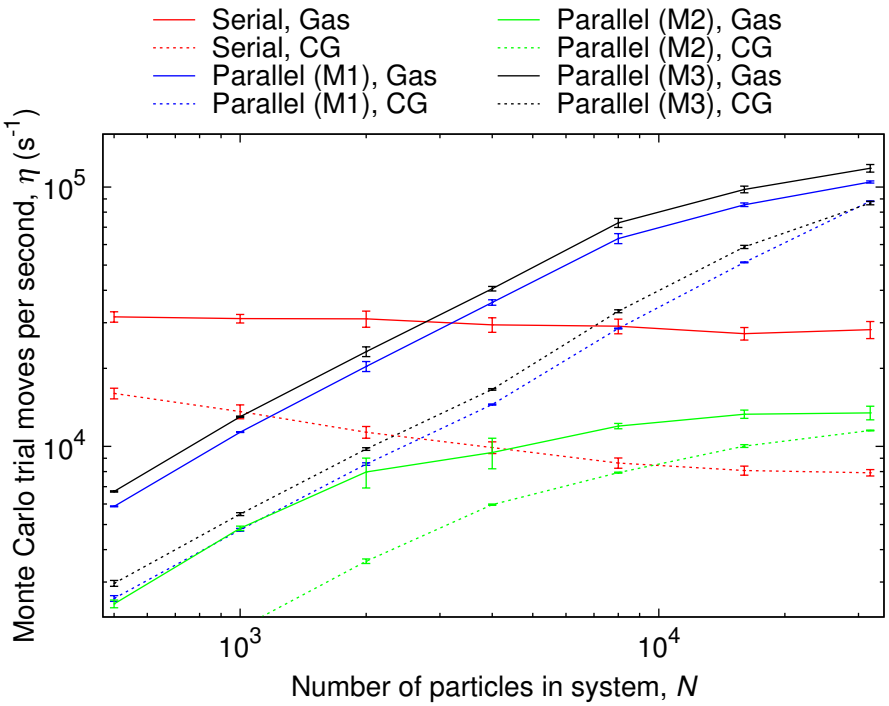

Figure 2.3: Monte Carlo simulation speeds (number of MC trial moves per second) for serial (oxDNA) and parallel (PMC) codes at a range of system sizes. The patchy particles simulated were designed to form cP4. Solid curves mark random configurations at $\rho^* = 0.1\,\sigma_{\mathrm{LJ}}^{-3}$, representing a low-density gas phase. Dashed curves mark random configurations at $\rho^* = 0.6\,\sigma_{\mathrm{LJ}}^{-3}$ which were then placed in a larger box to give $\rho^* = 0.1\,\sigma_{\mathrm{LJ}}^{-3}$, to represent a cluster-gas equilibrium (CG). Curves of the same colour were run on the same machine. The results plot averages over five trials, with error bars representing standard deviations. The machine details are as follows. Serial: Intel Xeon E5-2450 v2 2.5 GHz, 4 GB RAM. Parallel (M1): NVIDIA Tesla P100 GPU, 16 GB memory, Intel Xeon E5-2650 v4 2.2 GHz 12-core processor, 96 GB RAM. Parallel (M2): NVIDIA Tesla K40m GPU, 12 GB memory, Intel Xeon SandyBridge 2.0 GHz 16-core processor, 64 GiB RAM. Parallel (M3): NVIDIA Tesla V100 GPU, 12 GB memory, Intel Xeon SandyBridge 2.0 GHz 16-core processor, 64 GiB RAM. Note that M2 performed slowly, having an older GPU microarchitecture.

an acceptance ratio of 0.4 (for both translations and rotations). I timed the simulations and calculated the computation speed, η. I repeated tests five times for each system, and calculated the respective averages. The results are shown in Fig. 2.3.

Fig. 2.3 plots η against the number of particles, both on logarithmic axes. Different curves represent results for different systems [(1) or (2)] and different machines. For a typical plotted curve, η should be low at small N (for small systems, overhead costs are large relative to actual computation time), but increase as N increases, until the curve flattens once η hits peak efficiency. (Total computation *time*, rather than η, is proportional to N at peak efficiency.) In my results, the increase with N is relatively steady. The serial (oxDNA) computations peak at

relatively small N (below the range tested), as they have small overheads, and thus have relatively constant speed across the plot. The parallel (PMC) computations have large overheads, and so peak at greater N—towards the upper end of the tested range, or beyond it. At smaller N, parallelisation is not fully utilised. There is a crossover point at which parallel computations become faster than serial (as observed in Dr. Noya's preliminary testing). The exact value of N at which this occurs depends on the machine used, but for the two main machines I used (M1, Tesla P100, and M3, Tesla V100), it occurs at $N \approx 3 \times 10^3$.

Comparisons between serial and parallel, or different parallel machines, can only be made for the same starting configuration (low-density, or cluster-gas equilibrium), *i.e.* only between solid curves, or only between dashed curves. Low-density simulations are faster than cluster-gas equilibrium simulations (discussed previously in this section, under 'Explanation'). But for all machines, the difference is similar, so the results described above hold for both types of systems.

Comparing the three pairs of parallel runs, their slopes are all quite similar—they scale the same with N—as they use the same algorithm. The main difference is the machine architecture.

Thus, PMC is significantly faster than oxDNA for my larger systems (but not my smaller ones). I used oxDNA for systems with $N \lesssim 2000$, and PMC for systems with $N \gtrsim 10000$.

2.2.5 Comparison of MC with alternative simulation methods, and justification

In this section, I consider first alternatives to MC itself (section 2.2.5.1), and then alternative MC methods (section 2.2.5.2). In each case, I explain the reasons for my choices. See Refs. 212,357,358 for further discussion of patchy-particle modelling methods.

2.2.5.1 Alternatives to MC

Molecular dynamics. The main alternative type of simulation to MC is molecular dynamics (MD). In MD simulations, the direct dynamic evolution of a system over time is simulated by

numerically integrating Newton's laws for each particle [357]. MD has the following advantages, compared to MC:

(i) MD is more easily parallelised than MC, making simulations of large systems faster.

(ii) MD simulations directly simulate physical trajectories and dynamics, whereas MC simulations do not. (MC simulations were initially designed for, and are most suited to, calculating average thermodynamic properties for a system at equilibrium.)

(iii) MD simulations allow (real) cooperative motion of particles, which aids cluster growth, unlike single-particle move MC. My simulations involve the assembly of particles from a low-density fluid into a dense cluster. During assembly two phases coexist: fluid (gas) and nucleated cluster(s). For a cluster to grow, it must collide with fluid particles. But in MC simulations, particles move individually, so a cluster cannot move collectively towards a fluid particle. (If one particle in a cluster moves while the remainder of the cluster does not, whether by translation or rotation, the move will likely weaken that particle's patchy interactions and increase its energy. Such moves are usually rejected under the Metropolis criterion; it is unlikely for one particle to 'pull' the cluster with it towards a fluid particle. Thus, other than small vibrations, there is little cluster movement in MC simulations.) Further, individual fluid particles may take a long time to move towards a cluster (especially as they are equally likely to move away from it). Thus, cluster growth in MC is slow. However in MD, clusters naturally move collectively, reducing the time for clusters to collide with fluid particles and grow.

However, MD requires calculating the derivative of the interaction potential, in order to implement forces [357]. This calculation is costly [especially for a complex potential like mine; a naïve MD algorithm scales as $\mathcal{O}(N^2)$], making MD more expensive than MC [in which interaction calculations scale as $\mathcal{O}(N)$]. In general, the higher the dimensionality and lower the density (as in my systems), the greater the relative efficiency of MC. Also, anisotropic interactions are more complicated in MD simulations; calculating the torque involved in patchy-particle inter-

actions, as is needed for MD, can be difficult. Using moves that are strictly unphysical, as in MC, can also be advantageous: it can search configuration space more efficiently than when using only physical moves [357].

I have reduced disadvantage (i) by using PMC.[†] Furthermore, MC simulations can, if performed appropriately, reasonably approximate diffusive dynamics—addressing disadvantage (ii). MC moves are not physical—in this thesis they are stochastic, uncorrelated jumps in a particle's position and orientation—and thus MC simulations do not in general imitate dynamics [368]. However, MC simulations in the fluid phase and in which the moves are physically meaningful—typically, small (local), single-particle translations and rotations—do represent a system's diffusive dynamics (in which the mean squared displacement of a particle is proportional to time) [378–382].[†‡] This has been tested in a number of systems (*e.g.* for proteins [383], for colloidal crystallisation [380,384], for LJ liquids [385], for a binary LJ glass-forming mixture [386], for the long-time equilibrium dynamics of silica [387], for hard spheres [388]). Such MC simulations agree well with MD simulations. Thus, they can reasonably represent Brownian motion of particles, such as colloids, NPs and biological molecules, in solution—the kind of systems modelled in this thesis. Moreover, they do not require the presence of solvent particles (which would increase the computational cost), unlike MD simulations [211]. For this reason, MC as performed here can give a qualitative understanding of the dynamical evolution of a system. In any case, I do not need to precisely equate MC dynamics with a real system, but I only consider the general dynamical behaviour and the final structures into which particles assemble. MC simulations have been used in many previous cases to study patchy-particle dynamics (*e.g.* [207,249,267]).

[†] Still, parallel MD would likely be faster than PMC, and faster than serial MD at smaller N than N at which PMC is faster than oxDNA.

[†] The simulation timescale, in units of MC cycles, is proportional to real time; the proportionality constant depends on the acceptance ratio [380,381]. 'Small' translations are less than 10% of the particle diameter.

[‡] If, for some reason, a system behaves on sub-diffusive timescales, then MC is a poor approximation.

Other approaches. A related approach to simulating the *assembly* of particles is to more thoroughly search the space of possible ordered configurations and find those with *lowest energy* (*i.e.* stable, thermodynamic products). There are two main efficient ways of doing this for patchy particles [212], both typically in the isothermal-isobaric (NPT) ensemble:

(i) The 'floppy box' (or 'variable box') method: simulate a small number of particles in a box with variable shape [51].

(ii) Using genetic or evolutionary algorithms to identify candidate structures, and then further testing them [271,274].

However this approach is more useful for understanding phase behaviour than self-assembly, as it neglects kinetics. Hence, I did not pursue it.

2.2.5.2 Alternative simulation methods

Virtual Move MC. The underrepresentation of cooperative motion in single-particle-move MC simulations [point (iii) in section 2.2.5.1] means the relative diffusion rates of different-sized clusters are physically incorrect: larger clusters diffuse too slowly. This reduces the accuracy of MC dynamics, and can cause unphysical kinetic traps. One solution is to use the virtual move Monte Carlo (VMMC) algorithm [382,389,390]. VMMC allows collective motion by introducing 'virtual' moves (as well as, not instead of, standard moves), which enable whole clusters to move together. This corrects the relative diffusion rates of different-sized clusters, giving more realistic diffusive dynamics, and speeds up the assembly process. Unlike some other cluster move algorithms, VMMC satisfies detailed balance (section 2.2.1.2). However, for systems in which the main mechanism of cluster growth is monomer addition at low density (as opposed to cluster-cluster aggregation)—like mine—the benefit of using VMMC is limited [382,391], as tested for the current model in Ref. 211.

Biased moves. At low temperatures and pressures, MC simulation of patchy-particle clusters is quite inefficient, as evidenced by low acceptance rates for MC moves (even when, as in PMC, the move size varies to compensate) [212]. For this reason, some simulators use *biased moves* [357], such as aggregation-volume-bias [392,393]. However, I did not find this added complexity necessary, as my simulations were sufficiently fast.

Hierarchical assembly. When initially having difficulty with assembly kinetics, I considered hierarchical self-assembly. Hierarchical assembly helps the correct structure form both kinetically and thermodynamically. If an intermediate forms quickly, the system is more likely to avoid forming aggregates or competing structures (even if the competing structures have similar free energies to the target structure), because once the intermediate forms there are few assembly pathways other than that to the target. In the sorts of systems I consider, it is common for particles to aggregate kinetically at a similar temperature to that at which they form the correct structure. If such kinetic aggregates could be avoided by a hierarchical pathway, this would improve the yield of the target structure.

However, hierarchical assembly in general introduces more complication into simulation. For example, interactions between particles (*e.g.* number of patches, patch strengths) are usually more complex than for the corresponding one-step pathway. In a one-step pathway, if incorrect bonds form they can break and particles can reassemble correctly. But in a hierarchical pathway, incorrect bonds in the intermediate structure cannot easily dissociate, because the intermediate is more stable than individual particles and its bonds are stronger than those which form in the second assembly stage. Hence, after each hierarchical stage, complete purity of products is required, with no defects (otherwise these defects can become fixed). So, one may need to design more specific interactions to ensure this is achieved. The multi-step simulation protocol is also more complicated. Williamson [394] found hierarchical pathways no more successful than non-hierarchical, in the case of patchy particles forming complex clusters. And of course,

replicating hierarchical assembly in experiment is more challenging. Therefore, I did not use hierarchical assembly.

2.3 Simulation thermodynamics

2.3.1 Temperature

For self-assembly simulations, I *anneal* from higher to lower temperatures. Simulations begin at a starting temperature, T^*_{init}, corresponding to the stable low-density fluid (gas) phase, then gradually cool to the two-phase (fluid and cluster coexistence) region. Note that I do not expect my patchy particles to have a stable liquid phase, because torsional interactions inhibit the formation of low-energy disordered configurations. For simulations using oxDNA, annealing is not continuous, but rather stepwise (*i.e.* the temperature does not decrease after each MC cycle, but after a fixed number of cycles). However the temperature jumps are small enough to approximate continuous annealing. For simulations using PMC, annealing is continuous.

The precise melting point differs for each system studied. It cannot be known with accuracy in advance, and must be found empirically. Moreover, the temperature window is narrow for good nucleation and crystal growth from the fluid (as discussed further in section 3.4.2). Given the above, for each system I typically begin with preliminary simulations at a faster annealing rate across a larger temperature range. Cluster growth occurs at $T^* < T^*_{\text{melt}}$ in these simulations. This is because in the temperature window for good crystal growth, the rate of nucleation is low; so if the time spent in this window is short (*i.e.* when annealing is fast), nucleation is unlikely. Only once the temperature is lowered below T^*_{melt} does nucleation become more likely.[†] Multiple clusters form in these preliminary simulations—the faster annealing rate causes quenching. Nonetheless, these faster simulations help me empirically find a lower limit for T^*_{melt} (and the temperature window for good crystal growth) for each system. Subsequently, slower anneal-

[†] Moreover, hysteresis is common in phase transitions in simulations—the observed nucleation temperature is below the true value of T^*_{melt}.

ing simulations over a smaller temperature range are used for production runs—beginning and ending as close as possible to T^*_{melt}. However considerable simulation time can still be spent in the fluid phase, because nucleation is stochastic and may not occur immediately.

In some cases, the structure rearranges from the arrangement that first forms from the fluid (which may be disordered), and the target structure is not the higher-temperature condensed phase. Slowly cooling from the gas to the target structure, as above, would then require simulating over a much larger temperature range: begin in the gas phase, cool to the higher-temperature condensed phase, and continue to cool to the lower-temperature condensed phase. A few approaches to reduce the computational cost are possible:

(i) Use a faster annealing rate throughout. In this case, this system will be further from thermodynamic equilibrium, increasing the likelihood of multiple nucleation, and reducing the quality of the structures formed.

(ii) Begin at lower T^*_{init}, below T^*_{melt}, and anneal over a smaller temperature range from the higher- to the lower-temperature condensed phase. As for (i), multiple nucleation in the higher-temperature condensed phase is likely, reducing the quality of the structures formed. But given more time at the lower temperatures, the aggregated clusters may rearrange into the target structure.

(iii) Use a faster annealing rate, as in (i), but only between the formation of the higher-temperature condensed phase and rearrangement into the lower-temperature condensed phase. That is, follow the usual protocol from the gas to the higher-temperature condensed (at a slow annealing rate), then speed up the annealing rate (across the temperature range in which little reordering occurs), but slow it down again before the structure rearranges into the lower-temperature condensed phase. This approach is more complex to implement, and it is hard to know the temperatures at which to adjust the cooling rate.

In practice, I found approach (i) the best balance of simplicity and computational cost.

2.3.2 Density

I chose to assemble large clusters from gases (low density fluids), in the two-phase region, rather than to assemble extended phases (at higher densities), because this is typical of the conditions under which colloids, NPs, and biological molecules assemble. Forming clusters rather than extended phases avoids requiring the crystal orientation to be commensurate with the simulation box. Also, at high density, particles have more difficulty diffusing through the simulation box to find a thermodynamically favourable position—which is important for systems of multiple kinds of particles.

I perform self-assembly simulations at reduced particle number density $\rho^* = 0.1\,\sigma_{\mathrm{LJ}}^{-3}$ (which corresponds to a concentration in solution). Whilst this density is higher than in typical experimental studies involving colloids or biological molecules, this was previously shown to have little effect [197]. Higher concentrations are necessary because otherwise assembly will not occur on the timescale accessible in a simulation, which is far shorter than in experiment. My density is low enough for particles to form an aspherical cluster without the cluster interacting with its periodic images, and high enough to minimise the difficulty of gas-phase particles finding the cluster.

2.3.3 Other

In MC simulations, a system may fail to adequately explore configuration space if it becomes trapped in a local free-energy minimum, and thus may not find the global minimum configuration. This is more common if the energy landscape is rough, with many distinct minima of similar energies—as is likely for my complex systems. To avoid this problem, I ran multiple simulations for each system.

N, the number of MC cycles, and the temperature schedule (T^*_{init}, final temperature, and cooling rate), all vary between systems. I did not perform any equilibration steps.

2.4 Patchy-particle design

To design a set of patchy particles that forms a target structure, I developed the following scheme. In section 2.4.1 I outline the scheme in general terms, and then in section 2.4.2 I apply it to an example target.

One way to build an arbitrary structure would be for every building block to be unique, occupying a specific position with specific neighbours. This would be hugely challenging both synthetically (*i.e.* to synthesise a large number of distinct particles) and kinetically (*i.e.* for all particles to find their correct positions).[†] More generally, a criterion for a design scheme is to use a minimal, or at least limited, number of different components. Here, I satisfy this criterion by taking advantage of symmetry.

2.4.1 General approach

2.4.1.1 Particles

For each particle in the target structure, I define patch vectors pointing at its nearest-neighbour coordination shell. I divide the patchy particles in the unit cell into *types*, based on the structure's crystallographic symmetry, with particles of the same type having all the same properties (number of patches, patch vectors, and all patch properties). I then include the appropriate number of particles of each type in the simulation box.

In general, particles are of the same type if they map onto each other by the symmetry operations of the structure's space group; but there is an exception. By way of explanation, the particles in the target structure's unit cell can be categorised by the *Wyckoff positions* [8,9] they occupy. Distinct particles in a unit cell occupying the same Wyckoff position map onto each other by the group's symmetry operations. Each occupied Wyckoff position—each category of particles—corresponds to either one or two *types* of patchy particles, in my scheme. For space

[†] However, this approach has some potential for finite structures, in which the number of components is manageable, *e.g.* via DNA bricks [244,395].

groups without mirror planes or improper rotations, each occupied Wyckoff position corresponds to *one* patchy-particle type. For space groups with mirror planes or improper rotations, occupied Wyckoff positions which lie on a mirror plane or improper rotation axis correspond to *one* patchy-particle type; but other occupied Wyckoff positions correspond to *two* patchy-particle types, because particles that map onto each other by mirror planes or improper rotations have enantiomeric environments. In the latter case, there are equal numbers of particles of each type, and the two patchy-particle types are enantiomeric—they are the same except for equal and opposite offset angles ($\phi_{\alpha\beta}^{\text{offset}}$) on all pairs of corresponding patches.

Note that splitting *one* Wyckoff position into *two* particle types is only necessary because the particles have patches. Patch arrangements depend on surrounding particles in the structure, which differ in different enantiomeric environments (as created by mirror planes or improper rotations).

2.4.1.2 Patches

Just as for particles, I categorise patches into *types*. Patches of the same type have the same properties (interaction strengths with other patch types, $\varepsilon_{\alpha\beta}$, and offset angles, $\phi_{\alpha\beta}^{\text{offset}}$). On a given particle, patches that are related by the site symmetry (at that Wyckoff position) are usually equivalent and so are of the same patch type. The exception is patches that are *only* related by a mirror plane or improper rotation; these patches are of different patch types, but differ only in their offset angles, which are equal and opposite. Otherwise, patches are of distinct types.

For each patch α, I define $\varepsilon_{\alpha\beta} = 1$ for all patches β to which α points in the target structure. As noted in section 2.1.1, in some cases I set $\varepsilon_{\alpha\beta}$ to a value other than (but typically close to) 1, for finer control of the patchy interaction strength. For all other β, I define $\varepsilon_{\alpha\beta} = 0$—these patch pairs do not interact in the target structure. In some cases, for one patch α I define $\varepsilon_{\alpha\beta} > 0$ for multiple patches β—*i.e.* one patch type can interact with multiple other patch types. This is to target a disordered structure, by allowing greater flexibility in interparticle bond networks.

For each patch, I choose a reference vector from one of the other patch vectors on that particle; where possible the reference vector chosen lies on a symmetry axis or plane. For each complementary (*i.e.* interacting) patch pair $\alpha\beta$, I calculate the offset angle(s) $\phi_{\alpha\beta}^{\text{offset}}$ in the target structure. An offset angle is obtained from the torsional (dihedral) angle for a sequence of four coordinating particles: the two particles interacting via their patches, and the particles to which the two corresponding reference vectors point. If the chosen reference vector is a patch vector for which other patches on that particle are of the same patch type, then any of these symmetry-equivalent patches could have been used as the reference vector; to capture this symmetry when using a single reference vector I allow multiple offset angles, one for each of the equivalent possible reference vectors. Thus each offset angle corresponds to a symmetry-equivalent orientation of the particle in the target structure.

2.4.1.3 General comments

The patchy interactions specified by the above rules are *only* satisfied when all particles have all their patches bonded, and thus when the structure they form has the same network topology of nearest neighbours as the target structure. That is, the rules *fully* specify the target structure, thermodynamically favouring its formation. This outcome is achieved because the ε matrix of interaction strengths gives selectivity in patchy interactions, with the specified patch vectors ensuring coordination occurs at the correct geometry. But I also highlight the role of the matrix of ϕ^{offset} values: this provides selectivity in *sequences* (not just pairs) of particles, by ensuring nearest neighbours bond with the correct relative orientation.

In most of the structures I target, a particle has similar bond distances with each of the particles its first coordination shell. Nonetheless, there are small differences in bond distances between pairs of coordinating particles, both across different structures and sometimes also between coordinating particles in a given structure. My model gives no consideration to different distances (*e.g.* by varying the particle size or bond strength). I discuss the implications of this

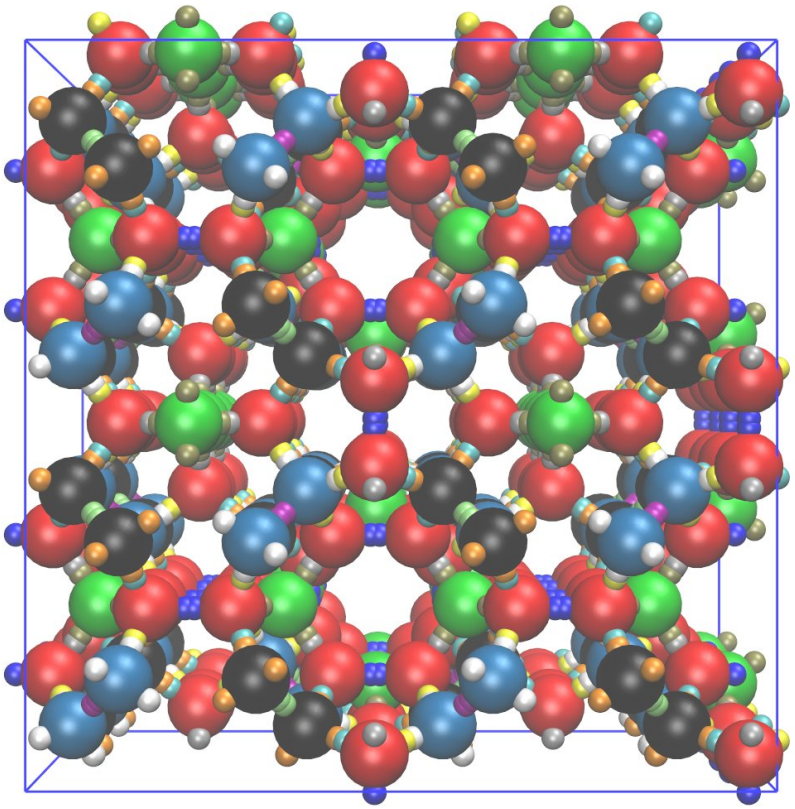

Figure 2.4: Clathrate I structure, depicted with patchy particles. Different colours correspond to different types (for both particles and patches). Red particles occupy Wyckoff site 24k, blue and black occupy site 16i, and green occupy site 6d [in space group $Pm\bar{3}n$ (no. 223)].

where relevant.

2.4.2 Application to example structure

One of the target periodic structures (Ch. 3) is clathrate type I (ClaI). This structure is shown in Fig. 2.4. Here I illustrate the above scheme (section 2.4.1) for ClaI. Table 3.1 gives further information on the structure, and full details of the set of patchy particles designed to form it are given in Table 3.2.

Clathrate I is in in space group $Pm\bar{3}n$ (no. 223) and has 46 particles in its unit cell, located at three Wyckoff positions: 24k (red in Fig. 2.4), 16i (blue and black), and 6d (green). (The label number denotes how many particles occupy this position in a unit cell; the label letters are sequential from lower to higher symmetry). ClaI is in space group $Pm\bar{3}n$ (number 223), which contains mirror planes and improper rotation axes. Positions 24k and 6d lie on mirror planes,

so each corresponds to one patchy-particle type, whereas position 16i does not so corresponds to two particle types that are enantiomeric. Thus, I define four types of patchy particles, with 8 particles in the unit cell for each of the two 16i types.

All particles coordinate with four others, so have four patches. On the *24k* particles, one patch interacts with a patch on another 24k particle, one with a 6d particle, and one with each of the two types of 16i particles. The latter two patches map onto each other only by a mirror plane, and so are of different types, with equal and opposite offset angles; no other patch pairs are related by symmetry, so all are of different types. For all the patches, I choose as reference vectors one of the two patch vectors that lie on the mirror plane (those to 6d and 24k particles). The patches on the *6d* particles each interact with a patch on a (different) 24k particle, and map onto each other by the site symmetry (D_{2d}). The patches are all of the same type, and the reference vector for each patch is chosen to be the vector for the patch that is related by both a 2-fold rotation and a mirror plane. On the *16i* particles, one patch is unique and interacts with another 16i particle (of the same particle type, not its enantiomer). The other three patches interact with 24k particles, and map onto each other by a 3-fold rotation so are therefore of the same type. The patch vectors of any of the three symmetry-related patches could be used as the reference vector for the unique patch; I choose one but have three equivalent offset angles to account for the symmetry. I use the unique patch, which lies on a 3-fold axis, as the reference vector for all the other three patches. The two types of 16i particle are identical except for having equal and opposite offset angles for all patches.

Chapter 3

Periodic Structures

This chapter presents a study of the rational design and self-assembly of patchy particles—with torsional interactions—into complex, extended, 3D, periodic phases. Using the patchy-particle design scheme in section 2.4, I report on the successful assembly of a range of periodic structures more complex than previously assembled via patchy particles. This is a demonstration of one approach to the rational design of particles to form target structures, as a proof-of-concept. The approach can also be adapted to *aperiodic* structures, which I consider in Ch. 4.

The chapter is structured as follows. I begin with an introduction (section 3.1), and I then describe the five periodic target structures assembled (section 3.2). Next, I detail the methodological aspects specific to this chapter (section 3.3). The bulk of the chapter is my observations and discussion of the assembly of the patchy-particle systems (section 3.4). This includes the thermodynamics and kinetics of their assembly (section 3.4.2), and the differences in behaviour for different target structures, especially systems containing particles with different numbers of patches (section 3.4.3.1). I then explore one particular area of interest, namely the possibility of alternative, simpler designs for patchy-particle systems to form the same structures (section 3.5). I end with some conclusions and a discussion of future work (section 3.6).

3.1 Introduction, background, and aims

As discussed in section 1.3.2, simulations of patchy particle assembly to date have been relatively simple (at least compared to the potential complexity of such systems). The range of extended 3D structures formed is limited; they include SC, FCC, BCC, cubic diamond, cubic and hexag-

onal tetrastack, pyrochlore, and clathrate-like and perovskite-like structures.[†] Most of these are fairly simple; but complex structures tend to be more promising for patchy-particle applications (section 1.2).[‡] Correspondingly, the sets of patchy particles used to form these structures were also mostly relatively simple [*i.e.* few types of particles (usually just one), few patches (usually 4 or less), regularly arranged patches, little or no patch selectivity, no torsional interactions]. Often, complex particles assembled into phases with inherent disorder, rather than into extended, ordered phases [396]. While (non-patchy) particles with complex, isotropic interaction potentials (section 1.3.6) have formed more complex, extended 3D structures (*e.g.* CaF_2, γ-brass, β-tin $tI4$-Sn, A15-type $cP8$-Cr_3Si, clathrate type I, σ-phase $tP30$-CrFe, porous mesophases; decagonal, dodecagonal, octagonal, and icosahedral QCs), these particles are less promising for experimental realisation (and for rational design).

Thus, here I aim to demonstrate that patchy particles can be used to form more complex, extended, 3D structures than previously considered, using more complex systems of patchy particles. Moreover, I demonstrate my systematic design scheme (section 2.4) for a set of patchy particles to form a unique and specific periodic target structure; few studies have rationally, systematically designed particles for target structures. Rather than an in-depth study, here I provide a proof-of-concept, for a few selected structures. I do not aim for analytical results, or a thorough understanding of all aspects of particle assembly. My study is general, rather than focused on a particular type of patchy particle. I also consider the kinetics and thermodynamics of self-assembly, and particle design principles.

By way of background, historically, a *crystal* is distinguished by translational symmetry (*i.e.* periodicity) in all of its dimensions: its constituent particles are arranged in a lattice which

[†] The range and complexity of extended patchy-particle structures formed in *experiment* (section 1.3.3.2) are less, due to limitations in particle synthesis. The 2D kagome lattice and a recent DNA origami dodecagonal QC are the main notable examples.

[‡] More complexity has been achieved in 2D (*e.g.* Archimedean and Platonic tilings, kagome lattice, H-phase, σ-phase, dodecagonal QC) than in 3D, and more for finite clusters (*e.g.* Platonic solids) or mesophase structures than extended structures. However, extended, 3D structures are far more relevant to the possible applications of patchy-particle self-assembly.

repeats periodically [397,398].[†] The *unit cell* is the smallest section of the crystal that can reproduce the whole crystal by being copied and translated in all directions. The unit cell contains all structural and symmetry information of the crystal (*i.e.* all symmetry operations of the crystal's space group are present within the unit cell). The *primitive cell* (or *asymmetric unit*) is as small or smaller than the unit cell. It does not contain all symmetry information; by applying the symmetry operations of the crystal space group to the primitive cell, one recovers the unit cell.

3.2 Target structures and designs

I chose five complex, 3D, extended crystals as target structures: clathrate type I (ClaI), BC8, clathrate type II (ClaII), cP4, and A15. These are pictured in Fig. 3.1, and full structural details are given in Table 3.1. I chose these structures for the following reasons:

(i) They are complex (*i.e.* they have a large number of particles in the unit cell), open (*i.e.* low-density) structures of the kind that may be used in patchy-particle applications, potentially having useful photonic, electronic, optical, *etc.* properties (section 1.2). Clathrate structures, for example, involve large polyhedral cages (or pores). Their 'host-guest' structure gives colloidal clathrates possible applications in imaging and sensing (*e.g.* MRI), chemical separation and storage (*e.g.* of pollutants, or carbon or methane for environmental reasons, or hydrogen for energy storage), and electronic and thermoelectric materials (*e.g.* electronic band gaps) [101,400–403].

(ii) These structures are expected to be difficult to form. In particular, previous work has shown that many similar structures form from particles with tetrahedral patches [*e.g.* BCC, FCC (orientationally ordered or disordered), cubic and hexagonal diamond, dodecahedral clusters, gels, liquids], and thus there is a high level of competition in their assembly [86,207,221,243,249,266–269]. Frustration (an incompatibility between the preferred local

[†] The term '*crystal*' has been redefined more broadly by IUPAC and IUCr to include aperiodic ordered structures (such as QCs) [89,399]. On this definition, crystals are ordered (but not necessarily periodic) in all dimensions, as manifested in a discrete diffraction pattern (*i.e.* sharp Bragg peaks). In this chapter, I use 'crystal' as shorthand for 'periodic crystal'.

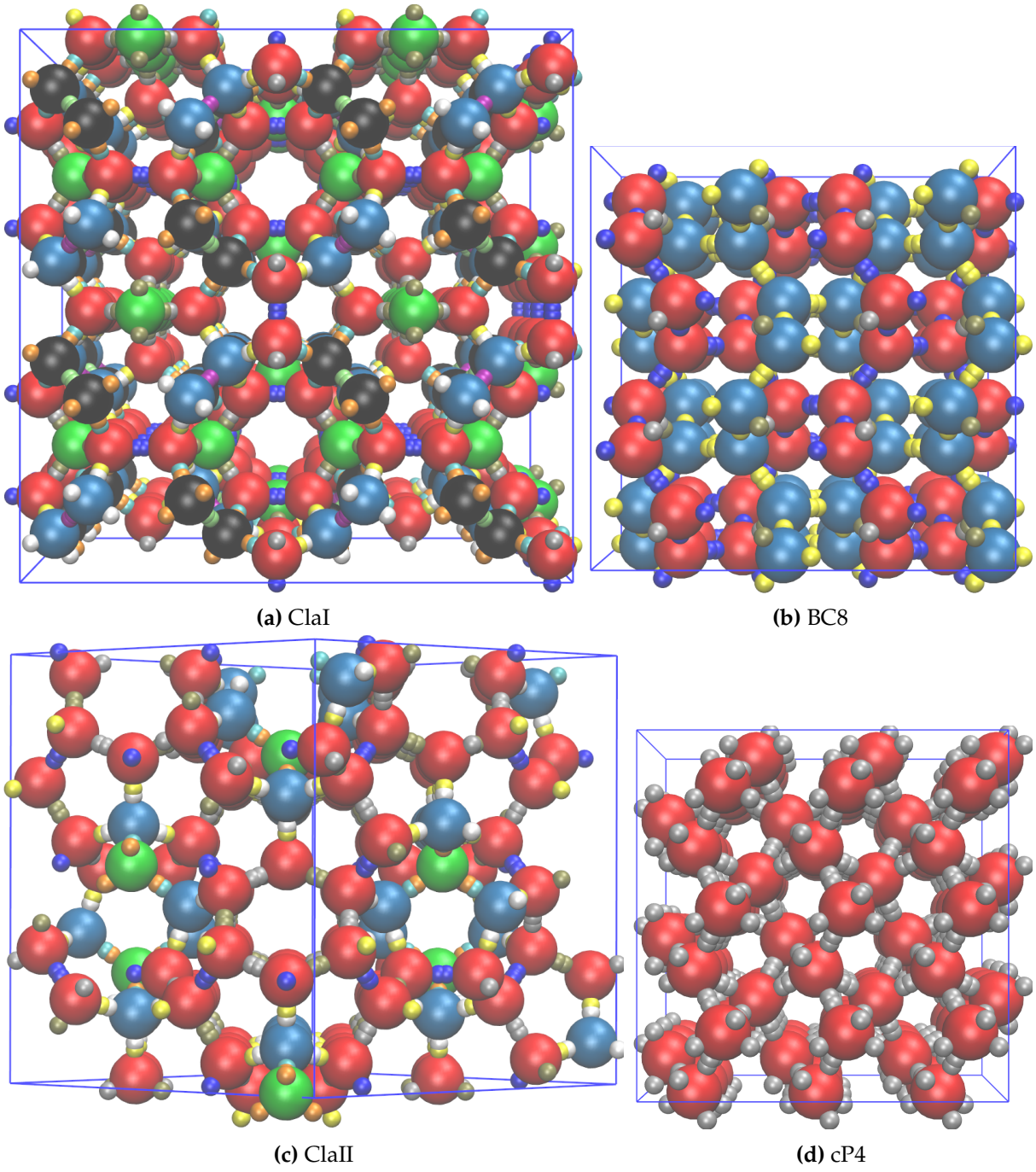

(a) ClaI **(b)** BC8

(c) ClaII **(d)** cP4

Figure 3.1: Crystal structures of the **(a)** clathrate type I, **(b)** BC8, **(c)** clathrate type II, and **(d)** cP4 targets, depicted with patchy particles. Details of each structure are given in Table 3.1. Different colours represent different *types* of particles and patches (particle and patch types are explained in section 2.4, and are based on the crystal's symmetry). Particle details are specified in Table 3.2. Particle sizes are simply pictorial (particle interactions are soft, so particles are not hard spheres as shown). For clarity, patches are shown as spheres (protruding from the particle surface), rather than as surface regions; patch sizes do not correspond to patch widths. *(Continued on next page.)*

order and 3D crystallinity) can arise [258]. Three of my targets, ClaI, BC8, and ClaII, have roughly tetrahedral local coordination for all particles. Thus it is challenging to assemble

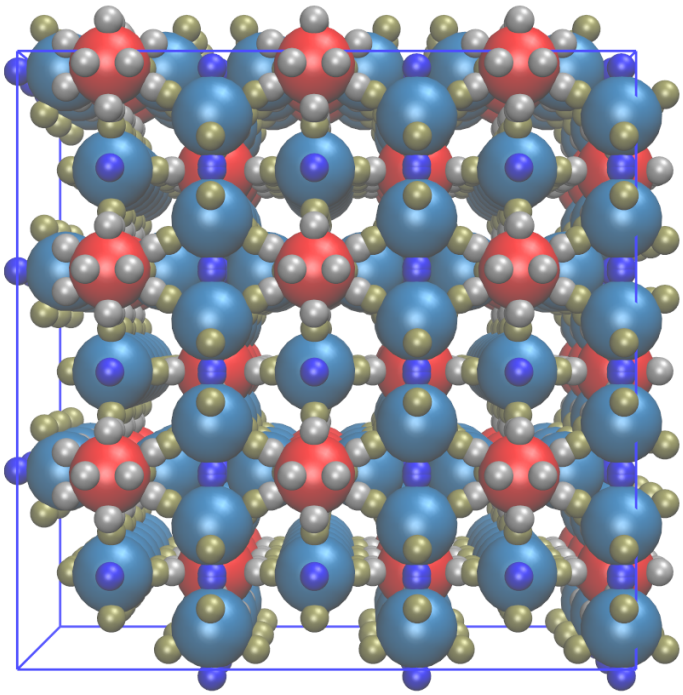

(e) A15

Figure 3.1: *(Continued from previous page.)* Crystal structure of the **(e)** A15 target.

these structures over other competitors.

(iii) There is some variety across my set of targets. In particular, particles in cP4 have a coordination number of 6, and particles in A15 have coordination numbers of 6 and 12 (depending on one's definition of coordination—the nearest-neighbour distance is similar to the second-nearest-neighbour distance).

(iv) The first four structures were found to be stable in potential parameter space near to an icosahedral QC [349] (for a one-component system with an isotropic potential having multiple minima). Some are approximants of the icosahedral QC.[†] Thus, understanding the design of patchy-particle systems to form these structures, and understanding their self-assembly, may be useful for subsequently designing a system to assemble into an icosahedral QC.

I designed a set of patchy particles to form each structure, following the procedure in sec-

[†] An *approximant* of a QC is a periodic structure with similar local arrangements of particles to the QC (but distinct from the QC over longer range) [404]. Thus, approximants are competitor structures to QCs during assembly.

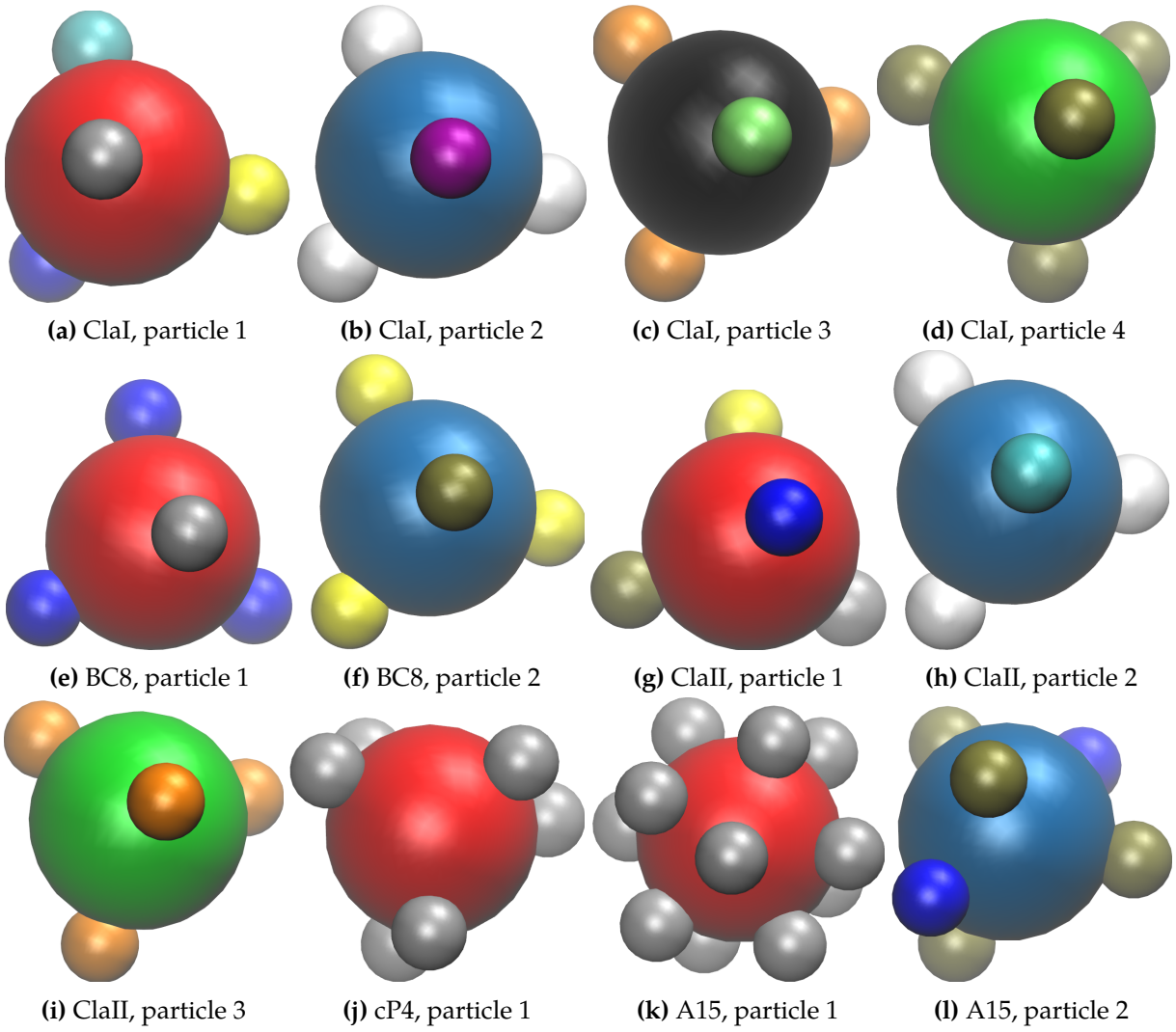

(a) ClaI, particle 1 **(b)** ClaI, particle 2 **(c)** ClaI, particle 3 **(d)** ClaI, particle 4

(e) BC8, particle 1 **(f)** BC8, particle 2 **(g)** ClaII, particle 1 **(h)** ClaII, particle 2

(i) ClaII, particle 3 **(j)** cP4, particle 1 **(k)** A15, particle 1 **(l)** A15, particle 2

Figure 3.2: Images of each type of patchy particle designed to form each target structure, as specified in Table 3.2.

tion 2.4. Full details of the designs are given in Table 3.2, and the particle sets are pictured in Fig. 3.2.

3.3 Methods

I simulated systems of $N \approx 1000$, in serial. I normally chose N as a cubic multiple of the number of particles in the target structure's unit cell. In annealing, I lowered T^* by 2×10^{-4} every 2.2×10^5 MC cycles (stepwise, but quasi-continuous). The total number of MC cycles varied between structures: roughly 2×10^7 for ClaI, BC8, ClaII, and cP4, and roughly 4×10^7 for A15. I repeated the assembly protocol five times for each target structure (each time beginning

Table 3.1: Structural details for the target structures considered in this chapter.

Name	Notes/description/references	Pearson symbol[a]	Space group	Prototype	Lattice parameters	Occupied Wyckoff positions[b]	Cage types[c]	Frank-Kasper dual
ClaI	Structures for ClaI and ClaII are given in Ref. 400. Also known as sI (or SI) phase. ClaI and ClaII have been formed experimentally from (non-spherical) colloids [101]. ClaI and ClaII, with guest sites unoccupied, have been shown to form from water molecules [402] and patchy colloids [242] [Fig. 1.1(d)] in coarse-grained simulations. ClaI was also formed via a complex isotropic potential [405]. Roughly tetrahedral coordination.	$cP46$[d]	$Pm\bar{3}n$ (No. 223)	Si_{46} clathrate (guest sites unoccupied)	a	6d 16i 24k	2×5^{12} $6 \times 5^{12}.6^2$	A15 (Pearson symbol $cP8$, prototype Cr_3Si)
BC8	Structure is given in Refs. 406,407. Also known as Si (III) phase. Metastable (albeit with a long lifetime), high-pressure (~ 8 GPa), low-temperature state of silicon found experimentally on cooling [408–413] and recently crystallised from NPs via a colloidal route [414]. [Also: metastable, high-pressure state of germanium [415]; predicted high-pressure ($\gtrsim 1100$ GPa) phase of carbon [416].] Found in first-principles calculations [406]. Roughly tetrahedral coordination. Structure can be understood as a periodic tiling of interpenetrating prolate and oblate Penrose rhombohedra.	$cI16$[e]	$Ia\bar{3}$ (No. 206)	Si	a	16c	n/a	n/a
ClaII	See notes for ClaI. Also known as sII (or SII) phase. (Stable) samples of ClaII with guest sites almost entirely unoccupied have been produced from silicon [401]. Roughly tetrahedral coordination.	$cF136$[f]	$Fd\bar{3}m$ (No. 227)	Si_{34} clathrate (guest sites unoccupied)	a x_1 x_2 z	8a 32e 96g	16×5^{12} $8 \times 5^{12}.2^4$	C15 Laves (Pearson symbol $cF24$, prototype $MgCu_2$)

Continued on next page

Table 3.1 (*Continued from previous page*)

Name	Notes/description/references	Pearson symbol[a]	Space group	Prototype	Lattice parameters	Occupied Wyckoff positions[b]	Cage types[c]	Frank-Kasper dual
cP4	Theoretically proposed high-pressure ($\gtrsim$ 300 GPa) lithium phase [417] (unknown in nature or experimentally). Chiral space-group; one of only two known elemental phases adopting $P4_132$. Coordination of three equilateral triangles around each Li atom.	$cP4$	$P4_332$ (No. 212)[g]	n/a (theoretical)	a	4a	n/a	n/a
A15	Structure is given in Ref. 418. Also known as Q223 phase. A Frank-Kasper phase [246,247]. Formed in various soft matter systems, supported by computations [157,419–427]. Formed from non-spherical particles in simulation [55]. Body-centred packing of edge-sharing icosahedra. Structure can be understood as BCC unit cell with dimers on each face (those in different planes are orthogonal).	$cP8$	$Pm\bar{3}n$ (No. 223)	Cr_3Si, β-W	a	2a 6c	n/a	n/a

[a] The Pearson symbol gives the Bravais lattice along with the number of particles per unit cell.
[b] The numeral in a Wyckoff position label is the number of particles occupying this position per unit cell.
[c] Cage type notation $n \times i^a.j^b$: n is the number of such cages in the unit cell; $i, j, \ldots$ are the number of vertices on a face; $a, b, \ldots$ are the number of such faces in cage. (Cage types only applicable to clathrates.)
[d] Guest sites unoccupied ($cP54$ with guest sites occupied).
[e] 8 particles per primitive cell, hence the name 'BC8'.
[f] Guest sites unoccupied ($cF160$ with guest sites occupied). 34 particles per unoccupied primitive cell.
[g] The enantiomeric space group is $P4_132$ (No. 213). Either structure can form spontaneously from non-patchy particles. My design (arbitrarily) targeted $P4_332$.

Table 3.2: Design details for the sets of patchy particles used to form each target structure. Images of each particle are shown in Fig. 3.2. The design procedure is described for the example of ClaI in section 2.4.2. cP4's space group ($P4_332$) contains no mirror planes or improper rotations, so its occupied Wyckoff position corresponds to one particle type. Space groups for all other structures do contain a mirror plane or improper rotation axis. For ClaII and A15, all occupied Wyckoff positions coincide with a mirror plane, so each corresponds to only one patchy-particle type. For BC8, Wyckoff position 16c does not coincide with a mirror plane, so corresponds to two enantiomeric patchy-particle types (with equal and opposite offset angles).

Structure	**Particle type**	**Wyckoff position**	**Patch details**					
			Number	Unit vector	Patch type	Interacts with (type)[a]	Reference vector number	Offset angle(s) (rad)[b]
ClaI	1	24k	1	$(1.0, 0.0, 0.0)$	1	2	2	0.0
			2	$(-0.568260, 0.822849, 0.0)$	3	3	1	0.0
			3	$(-0.277449, -0.540955, 0.793971)$	4	5	1	0.216
			4	$(-0.277549, -0.541146, -0.793806)$	6	7	1	-0.216
	2	16i	1	$(1/\sqrt{3}, 1/\sqrt{3}, 1/\sqrt{3})$	8	8	2	$-2.368, -0.274, 1.821$
			2	$(1/\sqrt{3}, -1/\sqrt{3}, -1/\sqrt{3})$	5	4	1	0.216
			3	$(-1/\sqrt{3}, -1/\sqrt{3}, 1/\sqrt{3})$	5	4	1	0.216
			4	$(-1/\sqrt{3}, 1/\sqrt{3}, -1/\sqrt{3})$	5	4	1	0.216
	3	16i	1	$(1/\sqrt{3}, 1/\sqrt{3}, 1/\sqrt{3})$	9	9	2	$-1.821, 0.274, 2.368$
			2	$(1/\sqrt{3}, -1/\sqrt{3}, -1/\sqrt{3})$	7	6	1	-0.216
			3	$(-1/\sqrt{3}, -1/\sqrt{3}, 1/\sqrt{3})$	7	6	1	-0.216
			4	$(-1/\sqrt{3}, 1/\sqrt{3}, -1/\sqrt{3})$	7	6	1	-0.216
	4	6d	1	$(1/\sqrt{3}, 1/\sqrt{3}, 1/\sqrt{3})$	2	1	2	0.0
			2	$(1/\sqrt{3}, -1/\sqrt{3}, -1/\sqrt{3})$	2	1	1	0.0
			3	$(-1/\sqrt{3}, -1/\sqrt{3}, 1/\sqrt{3})$	2	1	4	0.0
			4	$(-1/\sqrt{3}, 1/\sqrt{3}, -1/\sqrt{3})$	2	1	3	0.0
BC8	1	16c	1	$(1.0, 0.0, 0.0)$	1	2	2	$-\pi/3, \pi/3, \pi$
			2	$(-0.158279, 0.987394, 0.0)$	3	3	1	1.893
			3	$(-0.158279, -0.493690, 0.855113)$	3	3	1	1.893
			4	$(-0.158279, -0.493690, -0.855113)$	3	3	1	1.893
	2	16c	1	$(1.0, 0.0, 0.0)$	2	1	2	$-\pi/3, \pi/3, \pi$
			2	$(-0.158279, 0.987394, 0.0)$	4	4	1	-1.893
			3	$(-0.158279, -0.493690, 0.855113)$	4	4	1	-1.893
			4	$(-0.158279, -0.493690, -0.855113)$	4	4	1	-1.893

Continued on next page

Table 3.2 (*Continued from previous page*)

Structure	Particle type	Wyckoff position	Patch details					
			Number	Unit vector	Patch type	Interacts with (type)[a]	Reference vector number	Offset angle(s) (rad)[b]
ClaII	1	96g	1	$(1.0, 0.0, 0.0)$	4	5	2	0.0
			2	$(-0.308353, 0.951272, 0.0)$	3	3	1	0.0
			3	$(-0.268752, -0.422917, 0.865398)$	1	1	1	2.005
			4	$(-0.268752, -0.422917, -0.865398)$	2	2	1	-2.005
	2	32e	1	$(1.0, 0.0, 0.0)$	6	7	2	$-2.094, 0.0, 2.094$
			2	$(-0.297442, 0.954740, 0.0)$	5	4	1	0.0
			3	$(-0.297442, -0.477357, 0.826837)$	5	4	1	0.0
			4	$(-0.297442, -0.477357, -0.826837)$	5	4	1	0.0
	3	8a	1	$(1.0, 0.0, 0.0)$	7	6	2	$-2.094, 0.0, 2.094$
			2	$(-0.333330, 0.942810, 0.0)$	7	6	1	$-2.094, 0.0, 2.094$
			3	$(-0.333330, -0.471397, 0.816502)$	7	6	1	$-2.094, 0.0, 2.094$
			4	$(-0.333330, -0.471397, -0.816502)$	7	6	1	$-2.094, 0.0, 2.094$
cP4	1	4a	1	$(1.0, 0.0, 0.0)$	1	1	2	0.0
			2	$(0.5, \sqrt{3}/2, 0.0)$	1	1	1	0.0
			3	$(-1/6, -\sqrt{3}/6, -2\sqrt{2}/3)$	1	1	4	0.0
			4	$(-5/6, \sqrt{3}/6, -\sqrt{2}/3)$	1	1	3	0.0
			5	$(-1/6, -\sqrt{3}/2, \sqrt{2}/3)$	1	1	6	0.0
			6	$(-1/3, 0.0, 2\sqrt{2}/3)$	1	1	5	0.0
A15	1	2a	1	$(1.0, 0.0, 0.0)$	1	2	11	π
			2	$(0.600001, 0.799999, 0.0)$	1	2	12	π
			3	$(0.399997, -0.799996, 0.447223)$	1	2	9	π
			4	$(0.399997, -0.799996, -0.447223)$	1	2	8	π
			5	$(0.399997, 0.199998, 0.894429)$	1	2	6	π
			6	$(0.399997, 0.199998, -0.894429)$	1	2	5	π
			7	$(-0.399997, -0.199998, 0.894429)$	1	2	10	π
			8	$(-0.399997, 0.799996, -0.447223)$	1	2	4	π
			9	$(-0.399997, 0.799996, 0.447223)$	1	2	3	π
			10	$(-0.399997, -0.199998, -0.894429)$	1	2	7	π
			11	$(-0.600001, -0.799999, 0.0)$	1	2	1	π
			12	$(-1.0, 0.0, 0.0)$	1	2	2	π

Continued on next page

Table 3.2 (*Continued from previous page*)

Structure	**Particle type**	**Wyckoff position**	**Patch details**					
			Number	Unit vector	Patch type	Interacts with (type)[a]	Reference vector number	Offset angle(s) (rad)[b]
A15 (*continued*)	2	6c	1	$(1.0, 0.0, 0.0)$	2	1	5	π
			2	$(-0.200001, 0.979796, 0.0)$	2	1	6	π
			3	$(-0.200001, -0.653199, 0.730295)$	2	1	6	π
			4	$(-0.600001, -0.326600, -0.730295)$	2	1	5	π
			5	$(0.447213, -0.365147, -0.816497)$	3	3	1	$0.0, \pi$
			6	$(-0.447213, 0.365147, 0.816497)$	3	3	2	$0.0, \pi$

[a] Patches of each type selectively interact with patches of only one patch type (which may be the same type).
[b] For the interaction between patch α on particle i and patch β on particle j, offset angles are measured clockwise when looking along $\mathbf{r}_{ij}$ from i to j. They are in the range $[-\pi, \pi)$.

from a different random configuration).

3.4 Results and observations

3.4.1 General

All five target structures successfully self-assembled from their respective patchy-particle systems. I confirmed structures visually (by viewing them in cross-section, aligning particles, with the assistance of colouring by particle type). To observe the gas-cluster transition (cluster nucleation and growth), I used a simple yet useful order parameter: the number of particles in the largest cluster in the system. In this context, a *cluster* is any network of sequentially bonded particles; I define two particles as *bonded* if the magnitude of the interaction energy between them is $\geq 20\%$ of the maximum possible value, *i.e.* $U_{ij} \leq -0.2\epsilon_{\mathrm{LJ}}$. (The interaction energy between a pair of particles, i and j, at the optimal distance $2^{1/6}\sigma_{\mathrm{LJ}}$, with perfectly aligned patches, and in their preferred torsional orientation, is $U_{ij} \approx -\epsilon_{\mathrm{LJ}}$.) Figs. 3.3(a–e) plot this order parameter over simulation time (*i.e.* MC cycles), for each of the five repetitions for each structure. They show that by the end of most simulations, the largest cluster contains all or almost all N particles in the simulation box. In every case this did not occur, I observed one (or sometimes two) additional, smaller cluster(s), rather than unbonded particles, or many small clusters. Visual inspection of the configurations confirms the target structure correctly formed in all cases—both the largest clusters, and any smaller clusters. That is, all patchy bonds occur between correct patch pairs, at the correct angles, and at the preferred torsional orientations; so all particles were in their correct crystal positions. Thus, even when the largest cluster does not contain all particles, but multiple clusters form, there was no fundamental failure in the self-assembly of patchy particles into the target structure; the difficulty was kinetic (as discussed in the next section).

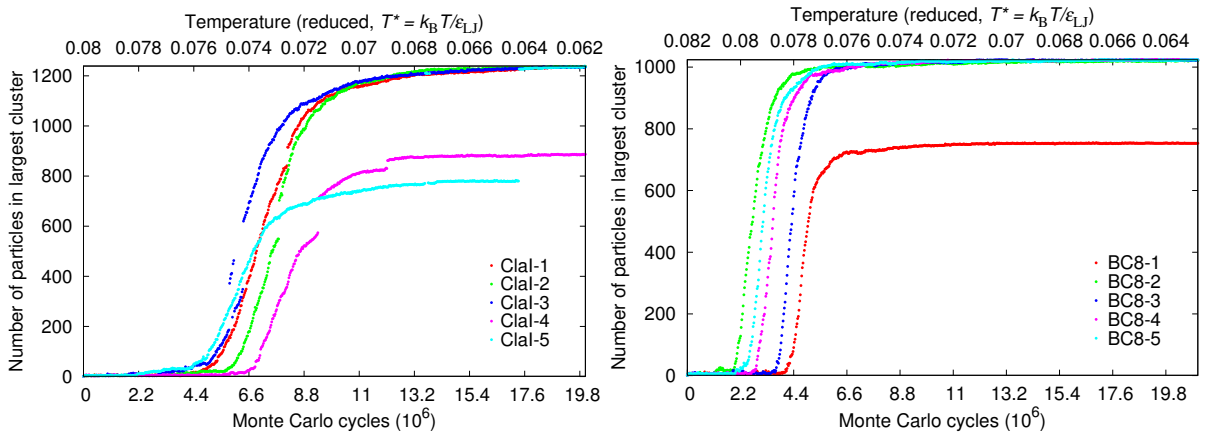

(a) Clathrate I

(b) BC8

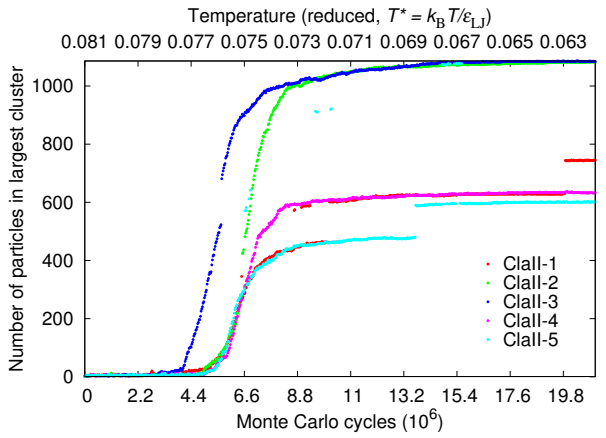

(c) Clathrate II

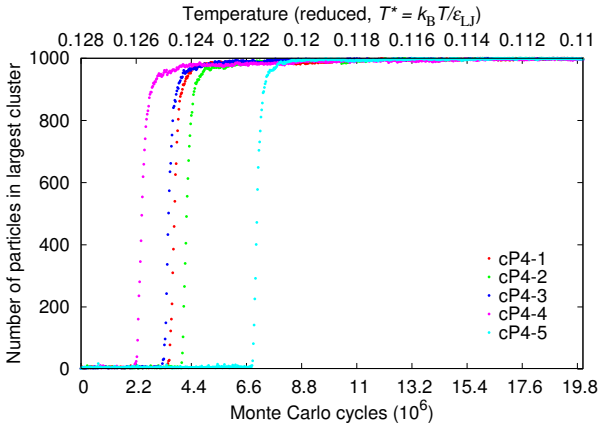

(d) cP4

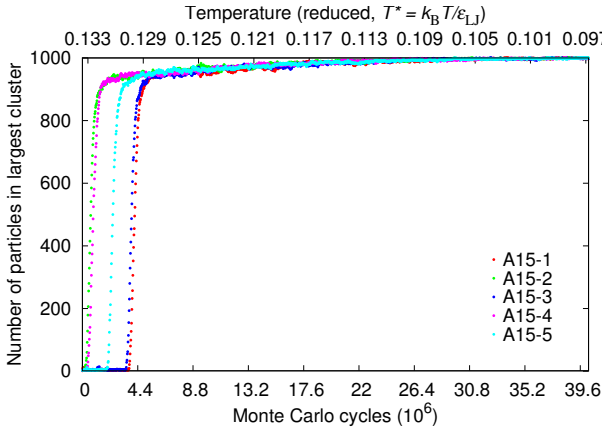

(e) A15

Figure 3.3: Cluster nucleation and growth during annealing simulations for the systems designed to form **(a)** clathrate I, **(b)** BC8, **(c)** clathrate II, **(d)** cP4, and **(e)** A15. Five distinct simulations are plotted for each design. The vertical axis is my order parameter, the number of particles in the largest cluster in the system (as defined in section 3.4.1). The maximum value on the vertical axis in each plot is N (total number of particles) for that simulation. The horizontal axis corresponds to both MC cycles (bottom axis, increasing left to right) and reduced temperature (top axis, decreasing left to right). The annealing rate was the same for all simulations, although the simulated temperature range varied between structures.

3.4.2 Assembly thermodynamics and kinetics

The thermodynamic and kinetic behaviour was as expected. As the temperature decreases, a first-order phase transition occurs from the monomeric gas (fluid) phase to the two-phase [gas and solid (cluster) coexistence] region. Nucleation appears consistent with classical nucleation theory [428–435]. Assembly progresses by the addition of monomers (and occasionally small clusters) onto growing clusters, always in the correct arrangement. Disordered aggregates, incorrect structures, and other kinetic traps were not observed. These are features of assembly when torsional interactions are included and were previously observed in Ref. 202 (the free-energy landscape is 'funnel-like'). (Disordered aggregates are more common in systems without torsional interactions, sometimes being both thermodynamically and kinetically favoured [197,211,241].) Snapshots from the self-assembly of the system designed to form BC8, as an example, can be seen in Figs. 3.4(a–c): (a) shows the gas phase, (b) the nucleation of a cluster (towards the bottom right), and (c) the final cluster, containing all particles.

Some patchy-particle studies [197,211,241] have observed nucleation in one metastable (but kinetically favoured, via a lower free energy barrier to nucleation) structure, then rearrangement to another.[†] However, given my patchy designs fully specify a target structure (via patch positions, patch selectivity, and torsional interactions) and incorrect structures were not observed, this phenomenon is disallowed.

There is a narrow temperature window for good nucleation and crystal growth from the gas (section 2.3.1), in which a single, large cluster forms, rather than multiple small clusters. Within the two-phase region, at *high* temperatures, the free energy barrier to nucleation is high, so it does not occur on practical timescales; entropy dominates. Within the same region, at *low* (supercool) temperatures, the free energy barrier is low, multiple nucleation occurs, and many clusters grow. Since they nucleate and grow randomly, these clusters are unlikely to have complementary shapes so as to fit together to grow into a larger cluster (with the correct structure).

[†] This phenomenon is also observed in other, experimental contexts (*e.g.* [152,436–438]).

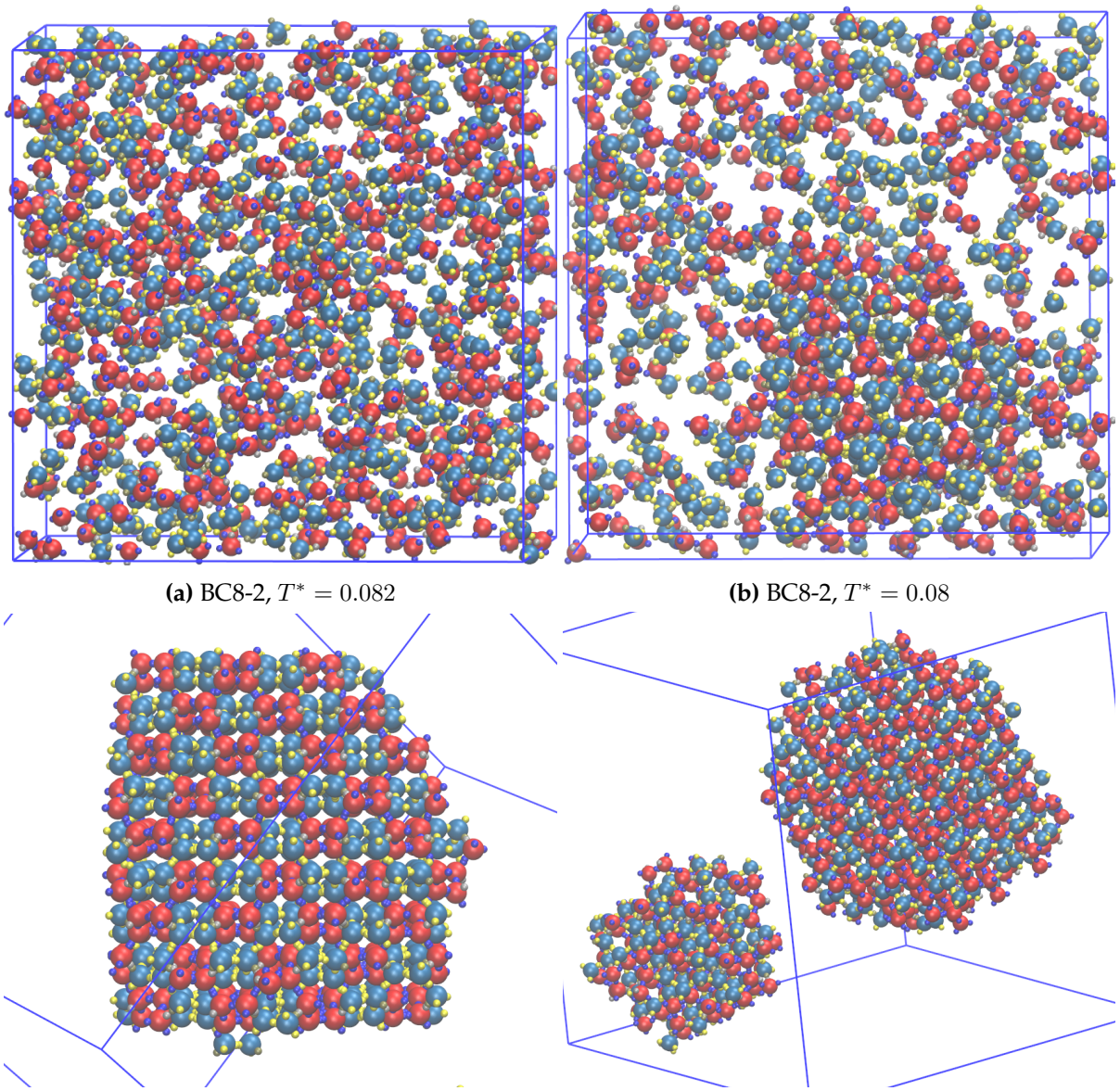

(a) BC8-2, $T^* = 0.082$ **(b)** BC8-2, $T^* = 0.08$

(c) BC8-2, $T^* = 0.063$ **(d)** BC8-1, $T^* = 0.063$

Figure 3.4: Simulation snapshots showing: **(a)**–**(c)** three stages in the self-assembly of repetition 2 [as in Fig. 3.3(b)] for the BC8 design [**(a)** gas phase, **(b)** nucleation, **(c)** final cluster]; and **(d)** the final state of repetition 1 for the BC8 design.

(This is especially so the more complex the target structure, hence it is likely for my structures.) However these clusters cannot easily break apart and reassemble, because the low temperature offers limited thermal energy to break bonds; the system is kinetically trapped. Thus, it retains separate clusters, rather than a single large cluster; this can be seen in Fig. 3.4(d) for the BC8 design. (Note, however, that even when multiple nucleation occurs, all clusters form in the correct structure, rather than forming the disordered kinetic aggregates which are common without torsional interactions [197,211,241]. Hence low temperatures are undesirable not because the

wrong structure forms, but simply because the right structure forms less neatly.) Within the two-phase region, in the *intermediate* temperature window for good crystal growth, nucleation occurs but is rare—the free-energy barrier can be crossed, but is not insignificant, so there is an equilibrium between nucleation and dissociation of nuclei. The rate of growth is much greater than the rate of nucleation, so once a cluster does nucleate, it grows relatively rapidly, and it is unlikely other clusters will nucleate in this period. Thus, only one large cluster grows.

In preliminary simulations, I used a faster annealing rate. Crystallisation typically occurred at lower temperatures than in simulations with a slower annealing rate. This is because in the temperature window for good crystal growth, nucleation is rare and takes longer to occur; if annealing is fast, nucleation is unlikely within the short time spent in the narrow temperature window (section 2.3.1). Only once the temperature is further lowered does nucleation become more likely.[†] Thus, typically nucleation occurred at low temperatures, and multiple clusters formed, in these preliminary simulations (*i.e.* quenching occurred). Nonetheless, these quicker simulations help *find* a lower limit for the temperature window for good crystal growth.

In Fig. 3.3, among repeated simulations for the same design, clusters nucleated at a range of temperatures (*e.g.* at $0.122 \lesssim T^* \lesssim 0.126$ for the cP4 design). This is because nucleation is a stochastic process. The highest observed nucleation temperature for each structure is a lower bound on the actual nucleation temperature.

The effect of my fast annealing is the imperfect growth noted in section 3.4.1 (*i.e.* multiple clusters). The best cluster growth (*i.e.* that which leads most directly to a cluster containing all particles) usually occurred at higher temperatures. As an example, the cluster in repetition 1 for BC8 nucleated at lower temperatures than those in other BC8 simulations, and this was the only BC8 simulation in which the final largest cluster did not contain all particles [as shown in Fig. 3.4(d)]. Other simulations which showed multiple nucleation are ClaI-4,5 and ClaII-1,4,5; the largest cluster stopped growing (*i.e.* the corresponding cluster-growth plot becomes flat)

[†] Moreover, hysteresis is common in phase transitions in simulations—the observed nucleation temperature is below the true value of T^*_{melt}.

without containing all particles. In some cases of multiple nucleation, the largest cluster did not combine with others, and so the largest cluster at the end of the simulation did not contain all particles (*e.g.* ClaII-4). In other cases, the largest cluster combined with other cluster(s), as manifested in discontinuous jumps in its size (*e.g.* ClaI-4 at $T^* \approx 0.0715$ and $T^* \approx 0.069$). When two separate clusters join, the bond may only be weak (perhaps involving only a few particles). Thus, the joined clusters may later break apart (*e.g.* ClaII-5 twice forms a larger cluster of ~ 900 particles at $T^* \approx 0.072$, but it soon breaks apart).[†] Note that when bonds formed between separate clusters in my simulations, they did so with both clusters in the correct alignment. This is an unlikely outcome for clusters without the angular and torsional constraint forced by my patchy model. (Of course, though, when clusters join by only a few patches there may still be some defects, because the bonds are weak and flexible; *e.g.* they may be missing particles at the cluster-cluster interface.)

3.4.3 Differences between target structures

It is apparent in Fig. 3.3 that some structures formed more rapidly and successfully than others. cP4 forms most easily: in all simulations, the final largest cluster contained all particles, and it grew over relatively few steps (*i.e.* the slope during cluster growth is steep). Similarly, A15 forms easily, and BC8 forms almost as easily, with multiple clusters forming in only one instance (repetition 1). The reason these structures form more easily is most likely that they and their patchy-particle designs are simpler: there are fewer particles in the unit cell (4 for cP4, 8 for A15, 8 for BC8), fewer particle types (1, 2, and 2, respectively; related to the number of Wyckoff positions), and fewer patch types (1, 3, and 4). Thus, for these structures, there are fewer configurations for the system to explore, and it can find the correct ones more quickly. In contrast, for both clathrates, at the end of many simulations the largest cluster did not contain all particles (as described in section 3.4.2), and cluster growth was slower (the slope is flatter). ClaII and

[†] My definition of cluster size is in this sense naïve: if two distinct clusters form a bond by one pair of patches (on one pair of particles), my definition classifies them as now being one cluster. Of course, such a bond is weak, and easily breaks apart.

ClaI have, respectively, 34 and 46 particles in their unit cells, and their patchy-particle designs have 3 and 4 types of particles, and 7 and 9 types of patches. A system has more configurations to explore to find these more complex structures.

Whereas particles in ClaI, ClaII, and BC8 have 4 patches per particle, those in cP4 and A15 do not: cP4 has 6 patches per particle, and A15 particles has on average 7.5 patches per particle (per unit cell, 2 particles with 12 patches and 6 particles with 6 patches). In my model, a particle's energy is the sum of the energies of its patchy bonds. Thus a particle with more patches can achieve a lower energy than one with fewer patches. Therefore, structures containing particles with more patches are more energetically stable, and have higher melting points. This can be seen by the different nucleation temperatures in Fig. 3.3: $T^* \approx 0.078$ for the ClaI and ClaII designs, $T^* \approx 0.081$ for BC8, $T^* \approx 0.126$ for cP4, and $T^* \approx 0.133$ for A15.[†] These temperatures are roughly in proportion to the (average) number of patches per particle in each structure.[‡]

The more successful assembly of some structures than others, discussed in the first paragraph in this section, may also be explained by the differences in nucleation temperatures. The best cluster growth occurs at higher temperatures, because particles rearrange more easily and quickly to find correct configurations. Nucleation temperatures are higher for cP4 and A15 than for BC8, ClaI, and ClaII, hence the more successful assembly of the former.

In particles with large numbers of patches, neighbouring patchy interactions may overlap with each other (section 1.3.5, under 'Design principles'), hindering correct assembly. But I did not observe this, even for the A15 particles with 12 patches. (If this did occur, it could be prevented by using narrower angular patch widths, σ_{ang}.)

[†] The stated temperatures are approximate *highest observed* nucleation temperatures (across all five repetitions); these are given by the highest temperature below which the number of particles in the largest cluster *continuously* exceeds 10.

[‡] The nucleation temperatures are not perfectly proportional to the numbers of patches per particle; for instance, BC8 has a slightly higher nucleation temperature than the clathrates, despite both having 4 patches per particle. Likely reasons are: (1a) nucleation is stochastic, and moreover (1b) the complexity of patchy designs varies, and this affects nucleation kinetics (as in the previous paragraph); and (2) the bond distance varies between structures (and within structures), and this affects bond energy.

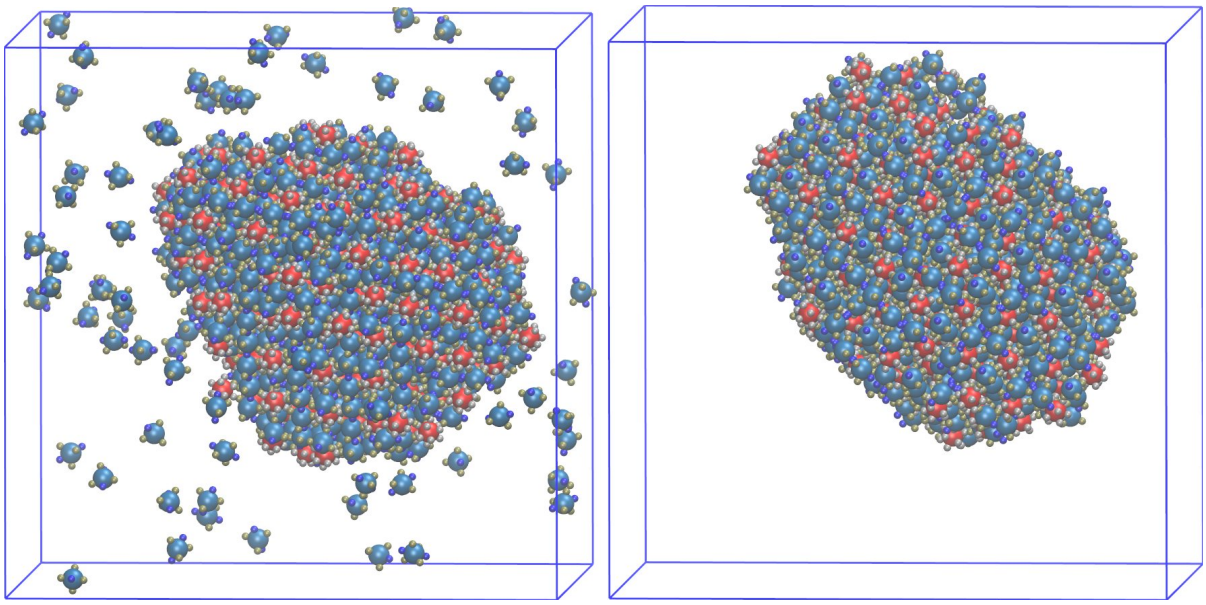

(a) A15-5, $T^* = 0.13$ **(b)** A15-5, $T^* = 0.097$

Figure 3.5: Simulation snapshots showing the final stages of assembly in repetition 5 [as in Fig. 3.3(e)] for the A15 design.

3.4.3.1 Mixed-coordinate systems

The mixed coordination (or valency) of the patchy particles in my design for A15 gives rise to different behaviour from other structures, under my interaction model. Assembly occurred over two 'stages', shown in Fig. 3.5. At first, the interior of the structure forms, incorporating *all* 12-patch particles but only *interior* 6-patch particles (*i.e.* all those not on the surface). This left a sea of unbonded 6-patch particles around the growing cluster [Fig. 3.5(a)]—a monomer-cluster equilibrium. Then, as the temperature further decreased, the unbonded 6-patch particles joined onto the outside [Fig. 3.5(b)]. This behaviour can also be seen in Fig. 3.3(e): after the steep period of cluster growth, the curves do not become flat (as they do for most other structures), but have a slightly positive gradient. In this period, the largest cluster's size continues growing as more 6-patch particles add on. The reason for this behaviour is that, as noted in section 3.4.3, in my model a particle's energy is the sum of its patchy bond energies. The energy of a fully bonded 12-patch particle is twice as low as that of a fully bonded 6-patch particle, because twice as many patches are satisfied. Therefore, there is a temperature window in which fully bonded

12-patch particles are favourable, but not fully bonded 6-patch particles—especially not those on the surface, where not all patches can be satisfied. (But still, in this window, the *interior* 6-patch particles are required to enable 12-patch particles to fully bond.)

This behaviour is no problem, however, because the interior of the cluster still grows with the correct structure (with both particle types), and the 6-patch particles later join in their correct positions and orientations.

3.4.4 Bond distances

As noted (section 2.4.1.3), in my patchy-particle designs, I give no consideration to different bond distances in the target structure. The system does not know that one pair of patches should bond at a different distance to another pair. The ClaI, ClaII, BC8, and A15 structures, have, respectively 6, 4, 2, and 2 different first-coordination-shell bond lengths; the longest such bond is 2.1%, 1.4%, 3.7%, and 11.8% greater than the shortest, respectively for each structure. (All first-coordination-shell bonds in cP4 are the same length.) All structures assembled successfully despite these different bond lengths.

3.5 Reduced structural information

A patchy-particle design encodes structural information, which programs the particles to self-assemble into the target structure. For instance, patch locations program the relative positions of neighbouring particles. One point of interest is the *minimal* structural information required to stabilise (favour) a target structure. Can complex target structures form with less information than specified by my patchy-particle design scheme (section 2.4)? For example, one could use fewer particle types, fewer patches, fewer patch types, less (or no) patch interaction selectivity, or less (or no) torsional interactions.[†] This chapter has so far shown a design that is *sufficient* to stabilise each target structure, but perhaps some or all will still form with less encoded infor-

[†] The first may be the most problematic—usually distinct particles are needed for different symmetry environments.

mation. Less information corresponds to simpler patchy designs, which are attractive because they make experimental realisation easier. Simpler designs: (1) improve thermodynamic stabilisation of the target structure, with respect to the gas phase, by increasing its configurational entropy (there are more possible configurations that still achieve the correct structure) [86]; and (2) improve kinetic accessibility of the target structure, because it is easier to find in configuration space. But simpler designs may also: (3) reduce thermodynamic stabilisation by increasing the relative energetic stabilisation of related, competing structures (*i.e.* the design may not *fully* determine the target structure); and (4) reduce kinetic accessibility by increasing the number of kinetic traps (competing structures). (See section 1.3.5, under 'Thermodynamics', 'Kinetics', and 'Design principles', for further discussion.) For example, there are many similar tetrahedral structures [point (ii) in section 3.2], and the less information encoded in the design to specify one over the others, the more competition between them. Thus, there is a trade-off when reducing structural information. The minimum structural information to stabilise (and make accessible) a given structure will vary between structures.[†]

3.5.1 Fewer patches

Intuitively, structures with high coordination environments (*e.g.* A15) are good candidates for reducing structural information in their designs. Their large number of patchy bonds may overspecify the structure. Indeed, my original A15 design already ignores some structural information: it includes all 2a-6c[‡] nearest-neighbour bonds (4 per 6c particle, 12 per 2a particle; bond length 2.544 Å in Cr_3Si) and the shorter 6c-6c nearest-neighbour bonds (two per 6c particle; 2.275 Å), but not the slightly longer 6c-6c bonds (8 per particle; 2.786 Å). Patches for the former two bond types—including positions, patch selectivity, and offset angles—were sufficient to yield A15, without patches for the latter bond type. So, can the information content be reduced further still?

[†] Minimal design strategies were pursued in Ref. 279, but for relatively simple 2D structures.
[‡] The labels refer to particle Wyckoff positions, as in Table 3.1.

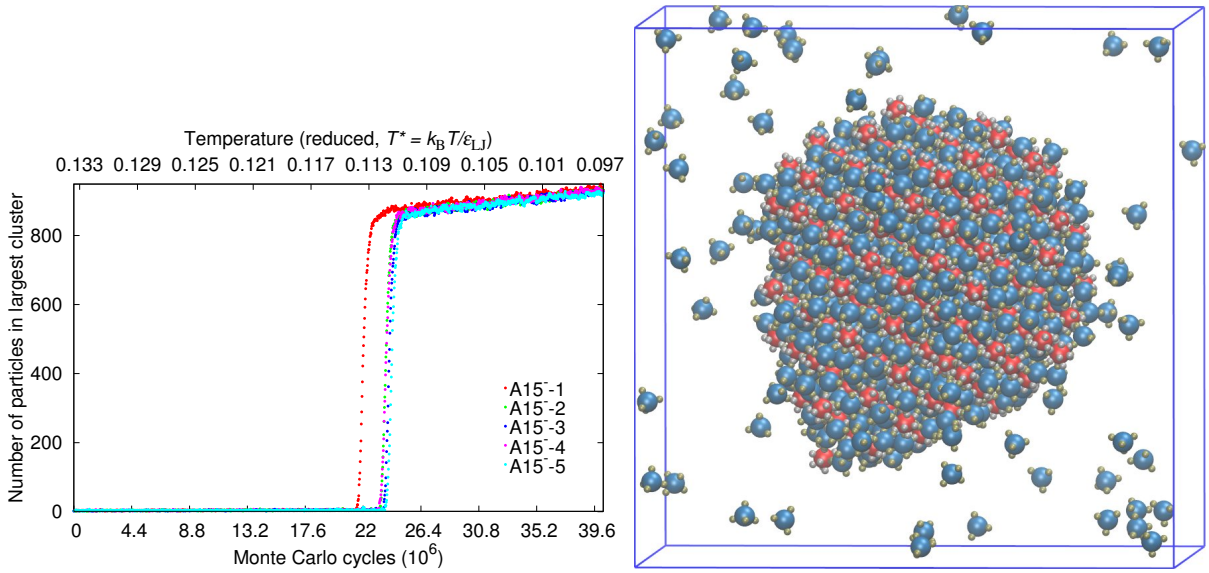

(a) Cluster growth

(b) $A15^-$-1, $T^* = 0.097$

Figure 3.6: For simulations of the system designed to form A15 with fewer patches (labelled '$A15^-$'): **(a)** Cluster-growth plot (as in Fig. 3.3); and **(b)** example final configuration.

I designed a system with no 6c-6c patches, only patches for 2a-6c bonds: the design is the same as that in Table 3.2 and Fig. 3.2(k–l), except 6c particles have only 4 patches. (Patch numbers 5 and 6, both of type 3, are omitted.) This system correctly formed A15 (all simulation details were the same as before). The results for this test are shown in Fig. 3.6(a). Crystallisation occurred at a lower temperature than in the original simulations in Fig. 3.3(e) ($T^* \approx 0.113$, previously $T^* \approx 0.132$). Also, at the end of the simulations ($T^* = 0.097$), the surface 6c particles had still not bonded to the cluster, as shown in Fig. 3.6(a) by the largest cluster sizes not reaching their maximum (N), and pictured in the final configuration of an example simulation in Fig. 3.6(b). These observations are explained by the lower number of patches on the 6c patches, which raises their energy (when fully bonded), thus decreasing the enthalpic stabilisation of A15 and lowering its melting point. Further, the temperature difference between the two stages of self-assembly is larger, because the difference in the number of patches on the two particle types is greater.

3.5.2 Torsional interactions

Another approach to reducing structural information is eliminating the torsional component of the interaction potential (*i.e.* setting $U_{ij}^{\mathrm{tor}} = 1$). This approach is appealing, given that torsional interactions are difficult to implement experimentally (section 1.3.3.1, under 'Torsional interactions'). Torsional interactions may sometimes be redundant, if patch positioning or selectivity already requires the particles to bond in the correct torsional orientation. However, eliminating torsional interactions is likely to make self-assembly more kinetically difficult (section 1.3.2.1). For instance, as discussed in section 1.3.2, it is difficult for cubic diamond to form without torsional interactions [86,207,243,249,266–269]; however it is possible under some conditions (in particular, by using a seed [207,249] or via selective interactions [86]).

To this end, I simulated designs with no torsional interactions (but with all other design details the same) for two sample structures, ClaI and BC8. The annealing rates were slightly faster (T^* decreased by 2×10^{-4} every 2.9×10^5 MC cycles for ClaI and 2×10^{-4} every 4.5×10^5 MC cycles for BC8) and the temperature ranges narrower. The results for these simulations are shown in Fig. 3.7. ClaI assembled with roughly equal success compared to when torsional interactions were included [a sample final configuration is shown in Fig. 3.7(c); and Fig. 3.7(a) is similar to Fig. 3.3(a)]. However, BC8 did not. Rather, a somewhat disordered, liquid-like phase formed from the gas. On further cooling, a different ordered structure formed, nucleating from the liquid-like phase: hexagonal diamond [an example final configuration is shown in Fig. 3.7(d)]. Hexagonal diamond formed in wide, short clusters, due to its quasi-layered nature (the two particle types occupy alternating layers, which each have a honeycomb arrangement). In hexagonal diamond, the patches were imperfectly aligned (they were optimised for BC8), so the energy of hexagonal diamond is higher than that of BC8 (and there is some structural distortion). Therefore, the former is likely to be a kinetic product that is thermodynamically less stable. Often, defects were present in the hexagonal diamond phase. Sometimes, liquid-like regions remained

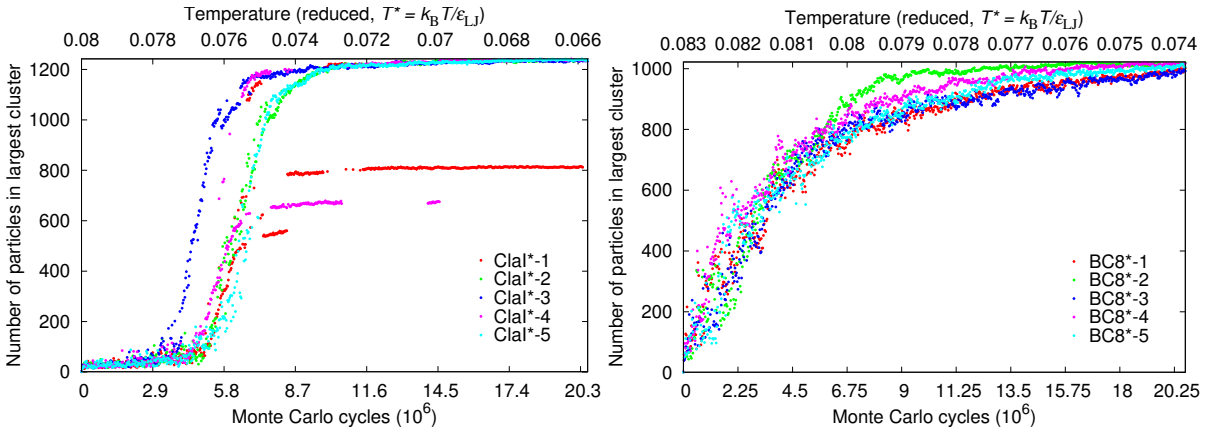

(a) ClaI* **(b)** BC8*

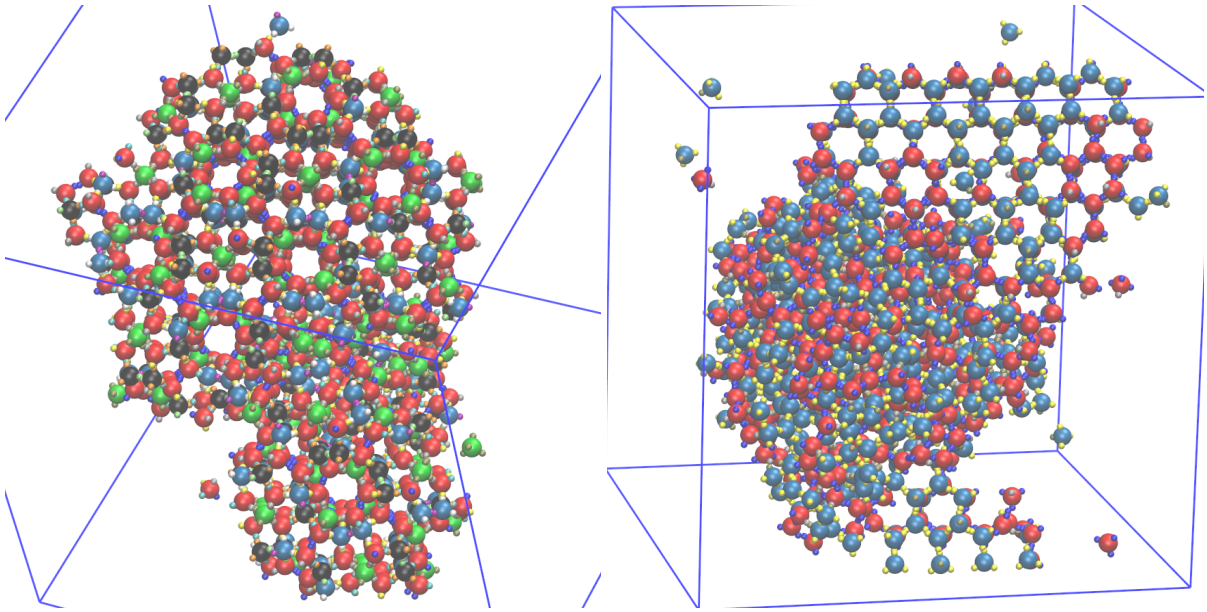

(c) ClaI* simulation 2, $T^* = 0.066$ **(d)** BC8* simulation 1, $T^* = 0.074$

Figure 3.7: (a) and **(b)** Cluster-growth plots (as in Fig. 3.3), and **(c)** and **(d)** final configurations, for simulations of the systems designed to form **(a,c)** clathrate I and **(b,d)** BC8, but for which the torsional component of the interaction potential was not included (denoted with an '*'). Note the hexagonal diamond structure at the top and bottom of **(d)**, with a liquid-like disordered phase in between (and connected).

[as in Fig. 3.7(d)]. Sometimes, BC8 motifs were present. These three observations indicate a degree of disorder remained in the hexagonal diamond phase, consistent with it being a kinetic product formed from a liquid, with imperfectly aligned patches.

Cluster growth for the BC8 design without torsional interactions [Fig. 3.7(b)] is slower than with torsional interactions [Fig. 3.3(b)], as shown by the gradients in the respective cluster-growth plots. Moreover, the data series in Fig. 3.7(b) is 'fuzzy'—the clusters did not grow smoothly. This is because multiple liquid-like clusters (droplets) nucleate from the gas, rather

than an ordered cluster. The droplets regularly join together and break apart, and particles evaporate from them more easily than from an ordered phase (being less strongly bonded). Thus, the size of the largest cluster in the system fluctuates. Growth occurs via Ostwald ripening [436,439], in coarsening dynamics. The number of particles in the largest cluster in the system is a worse order parameter for such assembly of a disordered phase, compared to direct nucleation of an ordered phase.

The formation of disordered aggregates was also observed in Ref. 202 when assembling complex clusters without including torsional interactions, but not with torsional interactions. In addition, competition between structures from particles with tetrahedrally arranged patches (without torsional interactions) has been well reported (*e.g.* [243,274]). It seems that assembly without torsional interactions is more difficult for some structures than others. Particles are not as clearly guided when joining onto the cluster, and may bond incorrectly.

The implication of these results is that for some structures, but not all, torsional interactions are redundant, and a structure can be stabilised and form without them. I hypothesise that they are redundant for ClaI but not BC8 because the ClaI design is already more specific—more particle and patch types, more patch selectivity—and this specificity only allows the correct torsional arrangement of the target structure. My BC8 design has only 2 particle types and 4 patch types, and other particle arrangements can (partially) satisfy it.

3.6 Conclusions

I have demonstrated a clear and systematic scheme to design patchy particles that assemble into a given periodic structure. The scheme ensures the target structure is the free-energy global minimum structure below some cutoff temperature, with no nearby competing structures (even though the specificity of the designs may reduce the configurational entropy of the respective target structures). Kinetic accessibility is not a problem (at least for the example structures I considered). The scheme is robust in forming the correct structure across a variety of complex

structures (and also across a range of bond distances, for a single structure). The specificity encoded by precise patch positions, patch interaction selectivity, and restrictions on torsional orientations, program the system to assemble in the correct structure. Torsional interactions are the most novel feature of my designs; they give a significant kinetic advantage, in disfavouring disordered kinetic aggregates which are common elsewhere, especially for complex structures, open structures (for which denser packings would be preferred), and structures with many competitors (*e.g.* tetrahedrally coordinated structures).

Possible further work includes:

(i) Thorough investigations of the minimal structural information required in a patchy design to form a target structure. Each aspect of the design could be systematically tested:

   a. What is the minimum number of patches required to form the target structure? (Moreover, are some patches more essential than others? If so, which?)

   b. Can the patch positions be simplified? (*e.g.* For the structures with roughly tetrahedral coordination, would they form if the patches were precisely positioned on a tetrahedron, rather than pointing precisely at neighbouring particles?)

   c. What is the least patch selectivity required (*i.e.* how few patch types, and how many other patch types can each interact with)?

   d. What are the smallest torsional restrictions required (*i.e.* how few patches require torsional interactions, and for those that do how many equivalent offset angles are acceptable)?

   These investigations could be completed for many structures, to reveal general principles. Thus far, I have only demonstrated some reduction in information is possible for a limited number of cases, but have not systematically explored this.

(ii) Studies on the effect of patch polydispersity on successful self-assembly. Previous work suggests reasonable polydispersity in patchy design does not hinder assembly (section 1.3.5,

under 'Polydispersity'), however this may not be the case for more complex, 3D designs.

(iii) Assembling specific structures, which have specific properties, to be used for specific applications. For a given structure, the design could be optimised for experimental realisation (*e.g.* maximally simplified), and used in more accurate models of colloids or NPs.

Chapter 4

Dodecagonal Quasicrystals

In the previous chapter, I demonstrated the rational design and self-assembly of a range of complex, extended, 3D, periodic phases. An obvious next step, but greater challenge, is to assemble ordered but *aperiodic* target structures. Can 3D quasicrystals (QCs) form from patchy particles? It may be that achieving the complex *global* ordering of QCs is more suited to a complex isotropic potential, rather than local ordering via patchy interactions. My patchy-particle approach, as demonstrated in Ch. 3, works well for periodic targets because controlling the *direction* of bonds fully specifies the *nearest*-neighbour arrangement, and controlling the *torsional angle* specifies the *next*-nearest-neighbour arrangement (*i.e.* together, they determine the local configuration and how it extends). But the structure of QCs does not periodically repeat—rather, there is some disorder, and a large variety of local configurations (coordination environments). However, in many cases the local configurations are similar, so it is possible that a patchy-particle design for one configuration may be suitable for multiple configurations. (It may even be the case that one design applies to environments with different coordination numbers. For example, a 6-patch particle may forgo one bond and assemble in a 5-coordinate environment.) Targeting QCs also gives further motivation for minimising the complexity (or information content) in my patchy-particle designs (section 3.5); the design complexity required to individually specify the numerous environments in QCs is potentially very large, and would make design, simulation, and experimental implementation prohibitively difficult.

Assembly of QCs from patchy particles has been addressed in very few studies [1–3,281,282]; these showed the successful formation of 2D dodecagonal QCs (DDQCs)—and in the most recent case [282], metastable 2D octagonal and decagonal QCs. To my knowledge, patchy particles have never formed 3D QCs (of any symmetry) in simulation, let alone experiment. In this chap-

ter I successfully pursue one particular 3D target QC, a DDQC, thus extending the aforementioned 2D studies. As was the previous chapter, this chapter is a proof-of-concept, hopefully opening the door to further and more detailed studies.

I begin with an introduction to QCs (section 4.1.1): their relevance and possible applications (section 4.1.2); and their formation in soft matter systems (section 4.1.3.1), in simulations of non-patchy particles (section 4.1.3.2), and in simulations of patchy particles (section 4.1.3.3). I first assemble a σ-phase, which is a periodic approximant of a DDQC (section 4.2). I then progressively discuss designs and assembly behaviour of systems of one, two, or three patchy particles that are programmed to form DDQCs (sections 4.3.1, 4.3.2, 4.3.3). I characterise the potential quasicrystallinity of the structures formed by their diffraction patterns (section 4.3.4). Finally, I report on the unanticipated presence of screw dislocations within the assembled structures (section 4.3.5). I end with conclusions and discussion of future work (section 4.4).

4.1 Introduction and background

4.1.1 Quasicrystals

'*Quasicrystal*' is a portmanteau of 'quasiperiodic crystal'. QCs are neither periodic (like periodic crystals), nor disordered (like amorphous solids) [398,440–442]. They are aperiodic (their structure does not repeat periodically); but they have long-range order, thus their Bragg diffraction patterns are discrete rather than continuous (*i.e.* they have a finite number of sharp Bragg peaks).[†] More specifically, QCs do not have *translational* symmetry (*i.e.* a translated copy cannot perfectly overlay the original), but only quasiperiodicity: the density function can be expressed as a finite sum of periodic functions, some of which have incommensurate periods. But QCs are *orientationally* ordered: they have long-range correlations in bond angles. The orientational

[†] The terms '*quasicrystalline*' and '*quasiperiodic order*' essentially mean 'having the order of a QC'. The related terms '*aperiodic*' and '*non-crystalline*' are broader, meaning 'lacking translational periodicity'; they include disordered phases. The term '*crystal*' was redefined by IUPAC and IUCr to refer to any structure with a discrete diffraction pattern; it thus now includes QCs (and other aperiodic crystals) [89,399].

order can be seen from the alignment of bonds in specific directions [398]. QCs can display (as shown in their diffraction patterns) any rotational symmetry orders, including orders forbidden to periodic crystals—*i.e.* anything other than 2-, 3-, 4-, and 6-fold symmetry.[†] Thus, they have well-defined, discrete point group symmetries. Their forbidden symmetries were previously thought to be incompatible with continuous filling of space (the crystallographic restriction theorem [443,444]), yet QCs do just that.

QCs can be obtained as projections or cuts from a periodic lattice in a higher-dimensional space (*i.e.* mD QCs are projections from nD space, for $n > m$). 3D QCs may be periodic in zero, one, or two dimensions (and quasiperiodic in the others). *Axial* (or *planar*) QCs (*e.g.* octagonal, decagonal, dodecagonal) are periodic—have stacked layers—in one (axial) dimension and quasiperiodic within each layer. Only icosahedral QCs (IQCs) are quasiperiodic in 3D.

QCs were first reported [445] in 1984 after 10-fold rotation symmetry was observed in the diffraction pattern of a rapidly-cooled Al-Mn alloy, indicating icosahedral symmetry.[‡] A theoretical understanding was proposed in the same year [446]. The experimental work earned the 2011 Nobel Prize in Chemistry. Since 1984, hundreds of QCs have been produced from (mostly binary and ternary) intermetallic compounds, with various symmetries and compositions [398,441,442,444,447–450]. While the first QCs were not thermodynamically stable equilibrium structures, and the Bragg peaks had finite widths, QCs that were stable and had sharp peaks were later discovered. Other materials found to have QC structure include chalcogenides [451] and perovskite ultra-thin films [452,453]. QCs have more recently been discovered in nature, in particular in meteoritic material, with icosahedral and decagonal symmetry [454–456].

The thermodynamic stability of QCs is the subject of much debate [457]. It has been difficult to prove that a QC structure has lower free energy than all other structures (especially its many approximants), at a given set of conditions. Stabilisation may be either energetic (*i.e.* the QC is

[†] These are the only rotation operations compatible with infinite translation in 2D or 3D (without causing overlap).
[‡] Orders of symmetry forbidden in periodic crystals had been observed earlier in diffraction patterns, but were explained in other ways, and not recognised as indicating a new phase.

the minimum-energy structure) or entropic (*i.e.* the QC's greater entropy outweighs its higher energy). For further discussion and analytic studies, see Refs. 458,459.

4.1.2 Interest and applications of quasicrystals

General applications of complex, extended structures were discussed in section 1.2.2, and many of these applications apply to QCs. In particular, QCs are candidates for photonic band-gap crystals (PBCs) [182,460], in part due to their higher order rotational symmetry (forbidden for periodic crystals) [181]. While icosahedral [181,184,186], octagonal [187,188,461], and pentagonal [183,187,188] QCs all show promise (alongside others), DDQCs are among the most studied, having very high symmetry [179,180,185,441]. Large, complete photonic band-gaps, in all directions (*i.e.* isotropic), for light of any polarisation, are possible. Most periodic PBCs only satisfy a few of these properties. In particular, in many periodic crystals the periodicity varies with the dimension, which means the band gap may also vary with the direction—and be small or non-existent in one or two directions. Since QCs have higher-dimensional symmetry, their band gaps are more likely the same in all directions [181,462]. PBCs could be used in a range of applications (section 1.2.2), and colloidal PBCs are especially promising because their band-gap is in visible-frequency ranges [441,463]. (QC photonic materials have been fabricated by methods other than colloidal self-assembly with band-gaps in the microwave [181], near-infrared [179], infrared [184], and visible [186] regions.) Other photonic and optical properties of QCs besides band-gaps are also of interest, with relevance to photoluminescence, plasmonics, lasers, light transport, and reflectivity [464]. The disorder of QCs may, surprisingly, enhance rather than suppress wave transport [465]. Reviews of photonic properties of QCs and their applications can be found in Refs. 464,466.

More generally, the distinct structures of QCs (compared to more widely known periodic or disordered materials) potentially give rise to different properties and functions, which could be exploited via rational design [426,464,467–469]; materials of new structure can have unex-

pected applications. One of the first large-scale applications of intermetallic QCs was non-stick coatings on frying pans [470–472]. They have since been used as an additive (for hardness or reinforcement) to steel for needles, dentistry instruments, and razor blades, and to other alloys (usually for specialised applications). QCs are suitable because of their low friction, lightness, low surface reactivity, hardness, thermal conductivity, non-stick-ness, non-toxicity, stability, and wear-resistance. Electronic [442,473], phononic [466], mechanical, vibrational, light absorption, adhesion, and physico-chemical (*e.g.* corrosion resistance, catalysis) properties of QCs may also be useful [440,469]. Reviews of properties and applications of intermetallic QCs can be found in Refs. 450,469. Some of these properties may extend to colloidal QCs, and in any case they indicate that novel properties of *some* kind may be found in colloidal systems as well. Colloidal QCs have reached the popular media [474], with speculation of their application for camouflage or invisibility, or in shape-shifting robots.

Understanding the formation of QCs, and how to control their structure and properties, is the first stage in being able to exploit their potential applications. Studying colloidal QCs may also improve our (incomplete) theoretical understanding of QCs in general [468]. For example, a QC diffraction pattern with 18-fold symmetry has only recently been observed, in a colloidal (polymeric) system [475]; it may therefore reveal more about QC formation in general, and why certain symmetries arise when they do (or do not). As another example, the principles for the formation (*e.g.* nucleation, stabilisation, dynamics) of QCs may be better understood through colloidal systems; since these are much larger than metallic systems, the quantum-mechanical principles thought to explain metallic QCs cannot apply [463].

4.1.3 Review: Assembly of quasicrystals

4.1.3.1 Soft matter systems

Colloidal and NP QCs were first fabricated only relatively recently, in 2004; however since then a diverse and growing range of QCs have been produced. Table 4.1 presents key details for

most of the soft matter (and supramolecular) QCs fabricated to date.[†] Reviews can be found in Refs. 442,463,468,476,477. Typical length scales for QCs are: 50–80 nm for copolymer systems, 50 nm for colloids, 20 nm for NPs, and 10 nm for dendrimer and molecular systems (compared with 0.5 nm for intermetallic compounds and 2 nm for chalcogenides) [463]. Most experimental observations of colloidal QCs have involved a significant element of chance, although some have involved rational design (*e.g.* tuning parameters for a system that formed approximant structures, replicating the interactions of one QC-forming system in another, or following the predictions of simulations [4]) [426].

The presence of two incommensurate length scales is considered important (if not essential) for the formation of QCs in one-component systems, both in experiment and in simulations of particles with isotropic interactions (section 4.1.3.2) [352]. This is supported by Table 4.1. The polymer systems typically comprise a well-defined hydrophobic core surrounded by a shell of hydrophilic, flexible arms. This produces two length scales in their interaction potentials. Similarly, the dendrimer systems have one length scale for the backbone and another for the ends of the branches. All reported NP systems are binary, but those with components of the same composition have two length scales due to different particle sizes. I am not aware of any QCs formed from mixtures of colloids (as is common for metallic QCs).

Almost all soft matter QCs reported to date have dodecagonal symmetry. The only exceptions in Table 4.1 are those formed by directed assembly (which are thus beyond the scope of this thesis) [478–486], and an 18-fold polymeric QC [475]—the only experimental example of a QC with this symmetry. No reported soft matter QCs have icosahedral symmetry [349]. The case for intermetallic QCs is very different: most are icosahedral, and few are dodecagonal (or octagonal or decagonal) [248,398,441,442,444,447–450].[‡] (The two naturally occurring QCs found

[†] In addition to the soft matter QCs I report, many soft matter systems have produced related periodic structures—including approximants—such as Frank-Kasper phases [246,247], or other structures such as disordered states. Moreover, in many soft matter experiments, QCs formed *alongside* approximants.

[‡] As at 2012, "there is one, probably stable, semimetallic dodecagonal QC known, $Ta_{1.6}Te$, with a lubricant-like layer structure [451]" [442]. One hypothesis for the different symmetries of intermetallic and soft matter QCs is as follows [282]. Metallic systems have sharp favoured bonding angles (as in narrow patch widths), which better stabilise octagonal and decagonal—and possibly icosahedral—QCs. Soft matter systems, in contrast, have less

Table 4.1: Summary of published assembly of QCs in soft matter (and supramolecular) systems. Publications are ordered by year (of first study in each row, from oldest to most recent).

System class[a]	System and assembly details	QC diffraction rotational symmetry(ies)[b]	Reference(s)
DEN	Nearly-spherical micelles (supramolecular structures), which self-assembled from conically-shaped, organic, single-component dendrimers. Formed *liquid* (quasi)crystals.	12-fold	[182,423,491]
SIL[c]	Silica spheres (1.53 μm, dielectric). QCs formed in aqueous solution using holography (providing an external field, to optically trap particles).	5-fold, 7-fold, 8-fold	[478]
POL[c]	Polymer-dispersed liquid crystal (mixture of aliphatic urethane resin oligomers, nematic liquid crystal, and surfactant). QCs formed in solution using multi-beam holographic lithography exposure (interference of multiple coherent laser beams), providing an external field. Able to switch between symmetries.	5-fold, 7-fold, 9-fold	[479]
POL	Three-arm micelles, which self-assembled from triblock (ABC) star-shaped copolymer [polyisoprene, PS, and poly(2-vinylpyridine), linked at a junction], or a blend of the copolymer and PS homopolymer.[d]	12-fold	[490,492]
PS[c]	Monolayer of colloidal PS spheres (1.45 μm, negatively charged). Formed pseudomorphic phase with both periodic and quasicrystalline structure. QCs formed in solution under a weak 10-fold [480–482] or 7-fold [481] quasiperiodic potential, via an external field produced by optical standing-wave patterns from 5 [480–482] or 7 [481] interfering laser beams.[e]	7-fold [481], 10-fold [480–482]	[480–482]
DEN	Nearly-spherical, chiral micelles, which self-assembled from dendrimers (triphenylenes functionalized with benzyl ether and phenyl propyl ether dendrons). Formed *liquid* (quasi)crystals.	12-fold	[493]
NP	Binary systems of surfactant-coated, inorganic nanocrystals (13.4 nm Fe_2O_3 & 5 nm Au, 12.6 nm Fe_3O_4 & 4.7 nm Au, and 9 nm PbS & 3 nm Pd). QCs self-assembled in solution.	12-fold	[488]
NP	Binary systems of surfactant-coated, inorganic nanocrystals (11.2 nm PbS & 5.2 nm/3.8 nm Au). QCs self-assembled in solution.	12-fold	[494]
POL	Nearly-spherical micelles, which self-assembled from linear diblock copolymers [poly(isoprene-*b*-ethylene oxide)]. QCs self-assembled in aqueous solution.	12-fold, 18-fold	[475]
MESO	Mesoporous silica. QCs produced via self-assembly of anionic surfactant micelles (*N*-myristoyl-L-glutamic acid) with a co-structure-directing agent (*N*-trimethoxysilylpropyl-*N*,*N*,*N*-trimethylammonium chloride); silica encages micelles.	12-fold	[495]
POL	Nearly-spherical micelles, which self-assembled from linear tetrablock copolymers [poly(styrene-*b*-isoprene-*b*-styrene-*b*-ethylene oxide)]. QCs self-assembled at high temperature.	12-fold	[496]
NP	Binary systems of surfactant-coated, inorganic NPs (2.9 nm polyoxomolybdate clusters & 8.1 nm PbS/CdSe nanocrystals). QCs self-assembled in solution.	12-fold	[497]

Continued on next page

Table 4.1 (*Continued from previous page*)

System class[a]	System and assembly details	QC diffraction rotational symmetry(ies)[b]	Reference(s)
MOL[c]	Monolayer of hydrogen-bonded pentamers of ferrocenecarboxylic acid (FCCOH), combined with FCCOH dimers. QCs assembled on Au(111) surface.	10-fold	[483]
MOL[c]	Monolayer of fullerenes (C_{60}) or pentacene ($C_{22}H_{14}$). QCs assembled on Al-based QC substrates (Al-Ni-Co, Al-Cu-Co, Al-Cu-Fe, Al-Pd-Mn, Ag-In-Yb). Substrates act as templates: certain preferred adsorption sites trap particles.	5-fold, 10-fold	[484,485]
PS[c]	Monolayer of colloidal PS spheres (3.9 μm, negatively charged). QCs formed using 1D quasiperiodic potential, via an external field produced by a laser beam.[e]	1D quasiperiodicity	[486]
NP	Binary system of surfactant-coated, inorganic, magnetic nanocrystals [9 nm ferromagnetic single-domain (HCP) Co & 4 nm polycrystalline Ag]. QCs self-assembled via magnetic forces.	12-fold	[498]
NP	Binary system of surfactant-coated, inorganic nanocrystals [11.9 nm Ag & 5 nm Ag].[f] QCs self-assembled in solution.	12-fold	[499]
POL	Nearly-spherical, nanoscale micelles, which self-assembled from linear diblock copolymers [poly(1,4-isoprene-*b*-DL-lactide)]. QCs self-assembled on rapid cooling from disordered liquid state. Metastable (rearranged over long time into 3D Frank-Kasper σ-phase).	12-fold	[500]
COOR[c]	2D metal-organic, porous coordination network (involving 4-, 5-, and 6-fold vertices) of Eu and *para*-quaterphenyl-dicarbonitrile. QCs assembled on Au(111) substrate, directed by Eu.	12-fold	[501]
POL	Giant surfactants, consisting of (hydrophilic) polyhedral oligomeric silsesquioxane cages, onto which (hydrophobic) PS tails tether at the vertices. (Surfactants self-assembled via nanophase separation between hydrophilic and hydrophobic parts.)	12-fold	[426]
NP	Binary systems of surfactant-coated inorganic nanocrystals (6.8 nm $CoFe_2O_4$ & 12 nm Fe_3O_4, 6.2 nm FePt & 11.5 nm Fe_3O_4, 8.8 nm Fe_3O_4 & 14.6 nm Fe_3O_4, and 5.8 nm Au & 9.7 nm Fe_3O_4). QCs assembled as thin-film, from slow drying of hexane solution on an immiscible liquid subphase (diethylene glycol).	12-fold	[502]
MOL[c]	Monolayer of fullerenes (C_{60}). QCs assembled by interactions with $Pt_3Ti(111)$ substrate, terminated by two layers of Pt.	12-fold	[503]
DNA	Binary system of 5- and 6-arm DNA motifs, with balance between rigidity and flexibility of arms (via bridges between adjacent arms). Rationally designed, following computational studies [3], and finely-tuned conditions.	12-fold	[4]

[a] 'COOR' = coordination network, 'DEN' = dendrimers (tree-like, repeatedly-branched macromolecules), 'DNA' = DNA multi-arm structures (star tiles), 'MESO' = mesoporous, 'MOL' = molecular, 'NP' = nanoparticle, 'POL' = polymer, 'PS' = polystyrene, 'SIL' = silica.
[b] All reported QCs are axial.
[c] *Directed* assembly, rather than *self*-assembly.
[d] The structure reported in Ref. 490 may be an approximant, rather than the QC. But the authors state it may be possible to form the QC by tuning parameters (*e.g.* length ratio of polymer star arms).
[e] The quasiperiodic potential plays the role of a substrate, guiding self-assembly.
[f] First assembly of QCs from NPs of same composition.

thus far have decagonal and icosahedral symmetries [454–456].) An explanation is required. The drivers for QC formation are different in soft matter and intermetallic compounds, as their interaction potentials are very different [487]. Atoms in intermetallic compounds have strong attractive and quantum mechanical interactions. Colloidal particles have weak, short-ranged attractions; QC stability may instead come entropically, via phason flips, or from the aforementioned two length scales. While an answer has not been conclusively proven, it has been argued that in some cases (*e.g.* for NPs) DDQCs have the highest entropy [488]; see further discussion of the stability of DDQCs in Refs. 468,489.

Thus, colloids are certainly capable of forming QCs; indeed, they are more promising than intermetallic compounds for single-component QCs [504]. However, their formation is not yet fully understood, and thus is not yet controllable. An exception is DNA nanotechnology approaches [4], over which a high degree of control is possible.

4.1.3.2 Simulations: Non-patchy particles

Theoreticians and simulators have long attempted to model QCs of colloid-like particles. Most attempts have been for particles with isotropic (non-patchy) potentials; very few have been for patchy particles (see ahead in section 4.1.3.3). Table 4.2 reports most of the simulation studies in which QCs formed from particles with isotropic potentials, along with some analytical studies of QC stability and growth.[†] Further information can be found in review articles [351,353,441, 463]. Most simulations (especially the earlier ones) were in 2D. In the majority of simulations, QCs self-assembled from random initial configurations [351]. In some of the earlier studies, the evidence for the presence of quasicrystallinity is not fully convincing, due to issues such as a small system size and poorly-converged diffraction patterns.

As for the QCs assembled experimentally in soft matter systems (section 4.1.3.1), the ma-

sharp bonding angles, which stabilise DDQCs.

[†] As for Table 4.1, in addition to the QCs I report, many simulations yielded approximant structures, such as the Frank-Kasper phases [246,247], or other structures such as disordered states. Moreover, in many simulations, QCs formed *alongside* approximants.

Table 4.2: Summary of published assembly of QCs in simulations—and some analytic studies—for particles with isotropic (non-patchy) interaction potentials. Publications are ordered by year (of first study in each row, from oldest to most recent). Unless noted, all systems are one-component.

Dimensions	System and methodological details, assembly details, and comments	QC diffraction rotational symmetry(ies)[a]	Reference(s)
2D	2 components of different sizes. LJ potential. Lattice model (Penrose tiling). Energy calculations.	10-fold	[523]
2D	2 components of different sizes. Decoration of Penrose tiling.[b] MD simulations. Studied stability and phase transitions.	10-fold	[524,525]
2D	2 components of different sizes. LJ potential. MC simulations.	10-fold	[526,527]
2&3D	Local growth: particles were sequentially added to a seed, following certain rules. 2D [514,515], 3D [516].	10-fold [514,515], icosahedral [516]	[514–516]
2D	2 components of different sizes. LJ potential. MC simulations.	12-fold	[528]
2D	Lattice model (rhombus Penrose tiling)[b]. Renormalisation group methods and MC simulations.	10-fold	[529]
3D	Effective metallic pair (pseudo)potential. Energy calculations. (Analytical study.)	Icosahedral	[507]
3D	Potential with two length scales [340]: LJ potential plus additional maximum. MD simulations. Further analysis [530] performed by MD simulations and thermodynamic perturbation theory.	12-fold[c]	[344]
2D	Lattice model (square-triangle tilings). MC simulations. Developed a (phason) elastic theory.	12-fold	[531]
3D	2 components of different sizes. LJ potential. MD simulations.	10-fold[d], icosahedral[d]	[512,513]
3D	2 components of different sizes. Complex, oscillating potential with multiple length scales. Local growth: particles were sequentially added to a seed, following certain energetic rules.	Icosahedral	[509]
3D	Charged colloids, modelled by effective pair potentials combining electrostatic repulsion with polymer depletion or van der Waals attraction. Thermodynamic perturbation theory, to model freezing. (Analytical study.)	Icosahedral	[508]
2D	Potential with two length scales: hard core plus linear ramp. MC simulations.	10-fold	[532]
2D	Potential with two length scales: LJ potential plus additional Gaussian maximum (similar to [344]). MD simulations. Formed approximant, not perfect QC [346].	12-fold	[345]
2D	Potential with two length scales: square well. MD simulations and free-energy calculations. QC formed after quenching liquid phase to an amorphous phase, then heating the amorphous phase.	10-fold	[533]
3D	2 components of different sizes. Complex, oscillating potential with multiple length scales. MC simulations of local growth: particles were sequentially added to a seed, following certain energetic rules.	12-fold, icosahedral	[510]
2D	Three-arm micelles, self-assembled from triblock (ABC) star-shaped copolymers.[e] Lattice model. MC simulations. Formed approximant, not perfect QC.	12-fold	[534]
2D	Potential with two length scales: LJ potential plus additional Gaussian maximum (similar to [344]). MD simulations.	10-fold, 12-fold	[346,535]

Continued on next page

Table 4.2 (*Continued from previous page*)

Dimensions	System and methodological details, assembly details, and comments	QC diffraction rotational symmetry(ies)[a]	Reference(s)
2D	Potential with two length scales: LJ potential plus additional maximum (same as [344]). MC simulations.	12-fold[c]	[536]
2D	Charge-stabilised colloids in substrate potentials with various (mostly quasicrystalline) symmetries (*i.e. directed* assembly, not *self*-assembly)[f]. MC simulations.	5-fold, 8-fold, 10-fold, 12-fold, 20-fold	[517,537]
3D	Hard (non-spherical) polyhedra: tetrahedra [538,539], truncated tetrahedra [79,81], triangular bipyramids [540], truncated triangular bipyramids [541], truncated octahedra [502][g]. MC (or MD [502]) simulations and free-energy calculations.	12-fold	[79,81,502, 538–541]
3D	Potential with two length scales: LJ potential plus additional maximum (similar to [344]). 8-fold QC did *not* actually form; it was proposed based on outcomes of MD simulations.	8-fold	[511]
3D	Bilayer of water molecules [542] or silicon [543][h], confined between parallel, non-hydrogen-bonding walls (which did not act as templates). MD simulations. Studied phase diagram; stable in a narrow region.	12-fold	[542,543]
3D	Models of deformable micelles: spherical micelles, dimers of micelles (providing shape polydispersity), and tethered NPs. Mobile surface features (mimicking polymers). Repulsive effective pair potential. MD simulations and free-energy calculations.	12-fold	[544]
2D	Potential with two length scales: LJ potential plus additional Gaussian maximum (same as [346]). MD simulations.	12-fold, 18-fold	[545]
2D	Potential with two length scales: soft-core particles. Free-energy calculations and MD simulations.	10-fold, 12-fold	[546,547]
2D	Potential with two length scales: softened, hard core plus square well. Langevin dynamics simulations.	Unspecified	[548]
2D	Potential with two length scales: soft-core particles. Density functional theory and Brownian dynamics simulations.	12-fold	[347,348]
2D	Potential with two length scales: soft-core particles. Dynamical phase field crystal model; QCs grown from seed(s).	10-fold, 12-fold	[549,550]
2D	Potential with two length scales: hard disks (no attraction) with step-like square-shoulder (*i.e.* core-shell particles). MC simulations. Stability and phase behaviour further studied [551,552] by MC simulations and free-energy calculations.	10-fold, 12-fold, 18-fold, 24-fold	[352]
quasi-2D	Model of nematic fluids of colloidal pentagonal platelets. Phenomenological numerical modelling based on minimization of Landau-de Gennes free energy.	10-fold	[553]
2D	2 components of different sizes. Potential with two length scales: square well. MC simulations.	12-fold	[554]

Continued on next page

Table 4.2 (*Continued from previous page*)

Dimensions	System and methodological details, assembly details, and comments	QC diffraction rotational symmetry(ies)[a]	Reference(s)
2D	Heptagons ('faceted nanoplates') of systematically transformed shape (other polygons did not form QCs). Complex attractive potential, depending on relative positions and orientations. MC simulations.	12-fold	[57]
3D	Potential with two length scales: soft repulsion with shoulder (no attraction; core-shell particles). MD simulations.	10-fold	[506]
3D	Complex, oscillating potential with three wells [555]; empirical, fitted to *ab initio* data (for intermetallic compounds); extends to third-neighbour shell. MD simulations.	8-fold[i], 10-fold[j], 12-fold[k], icosahedral[l]	[46,349,351]
2D	Potential with two length scales: hard disks (no attraction) with rounded and ramped step-like shoulder (*i.e.* core-shell particles)—more complex than potential in Ref. 352. MD simulations. Studied assembly and phase behaviour.	10-fold, 12-fold, 18-fold, 24-fold	[505]
3D	Complex potential: purely repulsive, with two minima. MD simulations.	12-fold[d]	[556]
3D	Potential with two length scales: soft-core particles. Dynamical phase field crystal model.	Icosahedral	[350]
3D	Four potentials with multiple length scales: (1) LJ potential plus additional maximum (two length scales, same as [344]); (2) Complex, oscillating, potential with three wells (same as [349]); (3) Soft repulsion with shoulder (two length scales, same as [506]); (4) Embedded-atom model potential for aluminium. MD simulations.	12-fold	[557]
2D	Potential with only one length scale: soft repulsive disks (no attraction). MD simulations.	8-fold, 12-fold	[504]
2D	Potential with two length scales: LJ potential plus additional Gaussian maximum (same as [346]). Brownian dynamics simulations; sequential deposition of particles from vapour onto surface layer in QC arrangement.	10-fold [558], 12-fold [281]	[281,558]

[a] All reported QCs are axial, except for those with icosahedral symmetry.
[b] Penrose tilings are projections from a higher dimension onto a 2D plane. See Refs. [518–522].
[c] Kinetically stable (*i.e.* long-lived), but thermodynamically only metastable (*i.e.* not lowest energy structure).
[d] Note that the system was too small to definitively verify the structure formed.
[e] Modelled the experimental system and reproduced the results of Ref. 490.
[f] Substrate potential can be achieved via laser interference, as in experiments [479–482,486].
[g] First reported assembly of QC in simulation from non-spherical particles.
[h] First reported QC assembled from water. First reported QC assembled from silicon—and first reported single-element atomic QC.
[i] Unusual structure: "has a relationship to β-Mn but incorporates pairs of helices of equal handedness at the location of the tile vertices" [351].
[j] Unusual structure: "contains pentagonal spirals with handedness that break ten-fold rotational symmetry" [351].
[k] Unusual structure: "consists of narrow lamellae with hexagonal crystal structures in two layers that are rotated relative to one another by multiples of 30°" [351]. Structure has smectic layers, axially stacked, giving rise to global dodecagonal symmetry.
[l] First reported assembly of single-component IQC. Only reported assembly of body-centred IQC (all other reported IQCs are primitive-icosahedral or face-centred-icosahedral) [349].

jority of QCs assembled in simulations were dodecagonal; of those that were not, most were decagonal. The only exceptions in Table 4.2 are 2D 18- and 24-fold QCs [352,505], an octagonal QC [504], and icosahedral and octagonal QCs [349,351]. Furthermore, simulations showing reliable (*i.e.* large system sizes, robust assembly) self-assembly of *3D non-dodecagonal* QCs from spherical particles are arguably [351] limited to octagonal, decagonal, and icosahedral QCs [349,351], and a decagonal QC [506]. (Regarding 3D symmetries other than dodecagonal, noted in Table 4.2: two studies [507,508] of IQCs were analytical, rather than simulations, so they showed stability but not formation of QCs; two other studies [509,510] of IQCs were not physically realistic assembly simulations but employed sequential addition of particles to a seed, fixing particle positions; one study [511] proposed but did not assemble an octagonal QC; and three early studies [509,512,513] of IQCs were for systems of two components with different sizes, which are not within the scope of my thesis. Regarding 2D symmetries other than decagonal or dodecagonal: three studies [514–516] of IQCs employed sequential addition of particles to a seed; and the icosagonal QC [517] (20-fold symmetry) was formed via directed assembly rather than self-assembly.)

As for experimental colloidal QCs, assembly of QCs in simulations has mostly been by trial-and-error or even accident [351]—as in the first 3D QC observed [344]. Thus, rational design of QC-forming systems is at an early stage; advances in understanding could have great value.

Most studies introduced two (or more) incommensurate length scales into their interaction potential, via one (or both) of the following [441]: (1) mixtures of components with different sizes (with a tuned size ratio), or (2) complex potentials. The former approach, which follows metallic alloy systems, is outside the scope of my thesis (section 1.4.1). The latter approach follows the core-shell structure of many soft particles, which gives rise to two length scales (section 4.1.3.1). The argument for the stabilisation of QCs by two incommensurate length scales has been well developed [347,348,352,441,468,504,507,546,547,559].[†] (At least) two length scales are

[†] The self-assembly of QCs from non-spherical particles (*e.g.* [79,81,538–541]) may also rely on the multiple length scales inherent in their steric interactions [504].

present within the structures of 2D QCs (*e.g.* 5-, 8-, 10-, and 12-fold [560,561]). A second energy minimum at a larger length scale favours interparticle bonds at a selected, non-close-packed distance; or a maximum disfavours a certain distance. All simulated single-component, spherical-particle systems in Table 4.2 involve multiple length scales: the Dzugutov potential and its relatives [281,344–346,511,530,535,536,545] (LJ potentials with additions); hard- or soft-core potentials with additions such as shoulders or wells [347,348,350,352,506,532,533,546–550]; potentials modelling colloids [508,534,544,553]; and other complex potentials, often related to metallic potentials [46,349,351,507,556]. Many of these potentials were carefully tuned. However, it was recently shown [504] that having two length scales is not necessary (even in a one-component system): octagonal and dodecagonal QCs assembled with a purely repulsive, smooth potential. Note, however, that the potential was still tuned. The same study and another [506] also showed that an attractive potential is not necessary.

The main difficulty of these QC-forming potentials—as acknowledged [349]—is experimental realisation. The more complex potentials, with multiple minima and maxima, are currently beyond the realm of possibility. While the shape of some of the simpler potentials is possible for colloidal particles, even then they were carefully tuned (to favour the QCs over similar structures), and fine-tuning colloidal potentials can be difficult. Thus, despite the success of these simulations, other approaches to QC assembly are of value.

4.1.3.3 Simulations: Patchy particles

One alternative approach to QC assembly is to use patchy particles, which can specify quasicrystalline local configurations through patch angles.[†] Patchy particles may be experimentally more realisable than complex interaction potentials (section 1.3.3.1). Few studies [1–3,281,282] have considered QC assembly from patchy particles. All were in 2D and formed DDQCs, except

[†] Note that this approach, like the multi-component mixtures and complex potentials discussed in section 4.1.3.2, also (implicitly) introduces two length scales [504]. This is because, in defining bond angles (and torsions), the positions of multiple shells of particles are determined, and thus second, third, *etc.* neighbour distances are implied.

Ref. [282] which formed metastable 2D octagonal and decagonal QCs.

By way of background, the (3D) σ- and H-phases are Frank-Kasper phases [246,247]. They correspond to the 2D square-triangle tilings denoted (3^2, 4, 3, 4) and (3^3, 4^2), respectively (and thus these tilings were labelled 'σ' and 'H' in Ref. 198).[†] Local environments for (2D) σ-, H-, and HCP-phases are shown in Figs. 4.1(a–c). The σ- and H-phases (both 3D and 2D) are periodic approximants of DDQCs.

Van der Linden *et al.* [1] performed MC simulations on systems of particles with 5 or 7 regularly arranged, non-selective patches (all patches attracted one another equally).[‡] Patches interacted with the same potential as that which I use (section 2.1), but without torsional interactions. Whilst HCP [in which the tiling comprises of only triangles, and no squares; (3^6)] is thermodynamically favoured at high pressures and wide patch widths, the lower density σ-phase becomes more favourable at lower pressures and narrower patch widths. In the region where the σ-phase is lowest in entropy, but near the boundary with the HCP-phase ($\sigma_{\text{ang}} \approx 0.45$ rad), a DDQC formed robustly, on cooling—for both 5- and 7-patch particles [Fig. 1.1(f)]. Reinhardt *et al.* [2] subsequently performed free-energy calculations to determine phase diagrams for the 5-patch system. They showed the DDQC is thermodynamically favourable compared to its periodic approximants, for a wide range of conditions (temperature, pressure, patch width, LJ exponent). It is entropically stabilised, by vibrational entropy and configurational disorder. The relatively wide patch width was essential to the DDQC's stabilisation as this then allowed the one-component system to exhibit both 5- and 6-coordinate sites. The growth dynamics of DDQCs from 5-patch particles was further studied using Brownian dynamics simulations [281].

A later study [3] performed MC simulations on mixtures of particles with 5 and 6 regularly-spaced patches, with the same patchy interaction potential, but a narrower patch width ($\sigma_{\text{ang}} =$

[†] This formal notation [245] refers to the sequence of equilateral triangles ('3') or squares ('4') around each vertex. Indices denote multiples of the same shape.

[‡] These systems were chosen based on observations from earlier simulations [198,271] in which 5-patch particles either did not crystallise due to frustration, or formed the QC-approximant (2D) σ- or H-phases. Even if only local motifs, rather than extended phases, of σ- or H-phases were observed, the local motifs alone are associated with DDQCs [531].

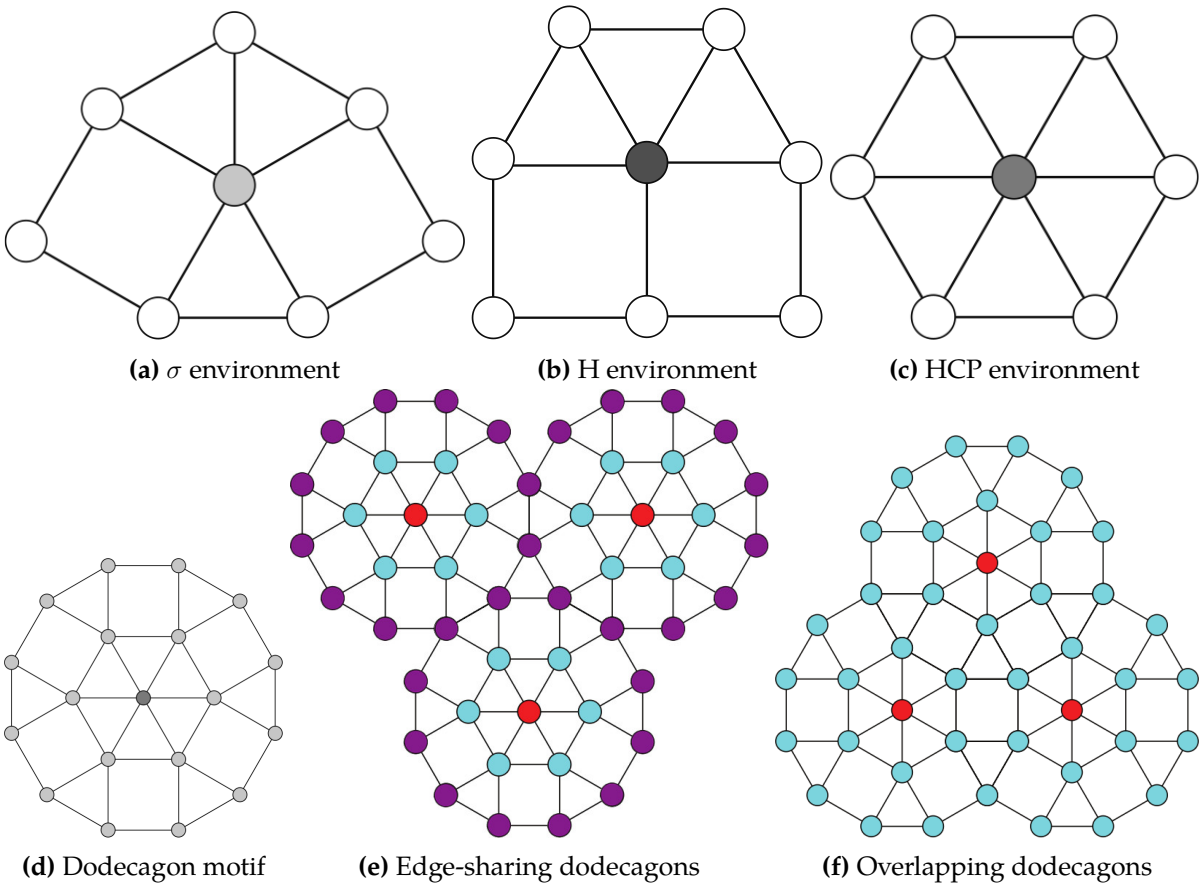

(a) σ environment **(b)** H environment **(c)** HCP environment

(d) Dodecagon motif **(e)** Edge-sharing dodecagons **(f)** Overlapping dodecagons

Figure 4.1: Depiction of environments and motifs found in DDQCs (and some approximants): **(a–c)** local environments (for the shaded particles); **(d–f)** dodecagon and two ways of arranging nearby dodecagons (with red particles at the centre of dodecagons). Colours in **(e,f)** correspond to the particle types of the DDQC-3 (section 4.3.3.1) and DDQC-3* (section 4.3.3.2) designs (*cf.* Table 4.3): purple for type 1, cyan for type 2, and red for type 3. Adapted and reprinted with permission from Ref. 1, © American Institute of Physics.

0.3 rad). In the first system, interactions were non-selective—all patches attracted all other patches equally—and the ratio of 5- to 6-patch particles was 12:1.[§] A DDQC formed robustly on cooling, and free-energy calculations (similar to the previous study [2]) confirmed it was thermodynamically stable, not just a kinetic product. Since the system contained both 5- and 6-patch particles, the patch width did not need to be tuned to stabilise both DDQC environments (as in the previous one-component systems [1,2]). However using two components introduced the potential complication of de-mixing into one-component σ- (5-patch particles) and HCP- (6-patch particles) phases.

To discourage de-mixing, and because non-selective patchy interactions slow the assembly

[§] This ratio was chosen because it is the ratio of σ (5 neighbours) and HCP (6) environments in a DDQC approximant, namely the crystal of edge-sharing dodecagon motifs [Fig. 4.1(e)].

kinetics (as particles must find their correct environments stochastically), the authors studied three additional selective systems. The second and third systems had fully selective patches, designed to form two DDQC approximants: crystals of edge-sharing dodecagon motifs [Fig. 4.1(e)] and of overlapping dodecagon motifs [Figs. 4.1(f)], respectively. The second system had two types of 5-patch particle and one type of 6-patch particle, in a ratio 6:6:1; the third had one 5-patch particle and one 6-patch particle in a ratio 6:1. Each distinct bond in the approximants corresponded to a selective, exclusive patchy interaction (*i.e.* each patch type only interacted with its complement). As expected, these designs formed their respective approximants, with some defects (gaps between periodic domains with different orientations, due to multiple nucleation), rather than a DDQC. Thus, the authors designed a fourth system with intermediate selectivity, finding a balance between the non-selective (first) and selective (middle two) systems. That is, some selectivity improved formation kinetics, but some interaction freedom allowed the disorder of QCs. The design was between the second and third systems, allowing more patches on the two 5-patch particles of the second system to interact. This introduced competition between edge-sharing and overlapping dodecagon motifs. The selectivity guided the 6-patch particles to the centre of dodecagons, whereas the freedom allowed dodecagons to coordinate in various ways—thereby allowing disorder. This system formed a DDQC on cooling, showing motifs from both dodecagonal approximants (and others). Free-energy calculations again confirmed thermodynamic stability.

This later study [3] further pursued the experimental realisation of 2D DDQCs by performing coarse-grained simulations of DDQC motifs formed from DNA multi-arm motifs (star tiles; section 1.3.3.1, under 'DNA particles'). DNA sequences allow selective interactions. The authors showed that individual dodecagons, and edge-sharing and overlapping dodecagon motifs, were structurally stable at room temperature.[†] Their predictions were recently confirmed in experiment [4], indicating that the patchy particle approach—like in this thesis—is experi-

[†] On a surface, the structures held their shape, but in solution they were distorted. Nonetheless, the network topology—all bonds—remained.

mentally realisable, or at least useful for guiding experiments.

Most recently [282], using a similar potential to that which I used, 2D patchy particles with 8 or 10 symmetrically arranged, non-selective patches, were studied via MC simulations. Octagonal and decagonal QCs, respectively, were metastable when the simulations began with their respective structures, and when simulation parameters were tuned (*e.g.* LJ exponent, patch widths—narrow widths were required, $\sigma_{\text{ang}} \approx 0.02$–$0.03$ rad). When the simulations began with a random configuration (*i.e.* self-assembly), only metastable decagonal QCs were obtained (not octagonal), and even then only after a protocol of cooling then reheating. Nonetheless, this represents the first stabilisation of non-dodecagonal QCs from patchy particles.

It is also worth mentioning that patchy-particle studies (*e.g.* [197,202,211]) have demonstrated the assembly of small, finite, 3D clusters with non-crystallographic symmetries [*e.g.* icosahedral; Fig. 1.1(a)].

4.1.4 Aims and expectations

This chapter extends (or generalises) the work of the three previous studies (section 4.1.3.3) on assembling DDQCs from 2D to 3D. 3D DDQCs are axial (*i.e.* dodecagonal layers are stacked periodically). Extending from 2D to 3D might therefore seem simple. But this is the first attempt at assembling DDQCs in 3D, and as such there are many unknowns. For example, there may be differences between 2D and 3D, in:

(i) patchy designs [patch width, patch selectivity and interaction strengths, torsional interactions (which were not included in the 2D simulations), *etc.*];

(ii) thermodynamic stability;

(iii) assembly kinetics (on which axes will growth be fastest, and what 3D shapes will large clusters take?); or

(iv) other areas.

I aim to explore such questions.

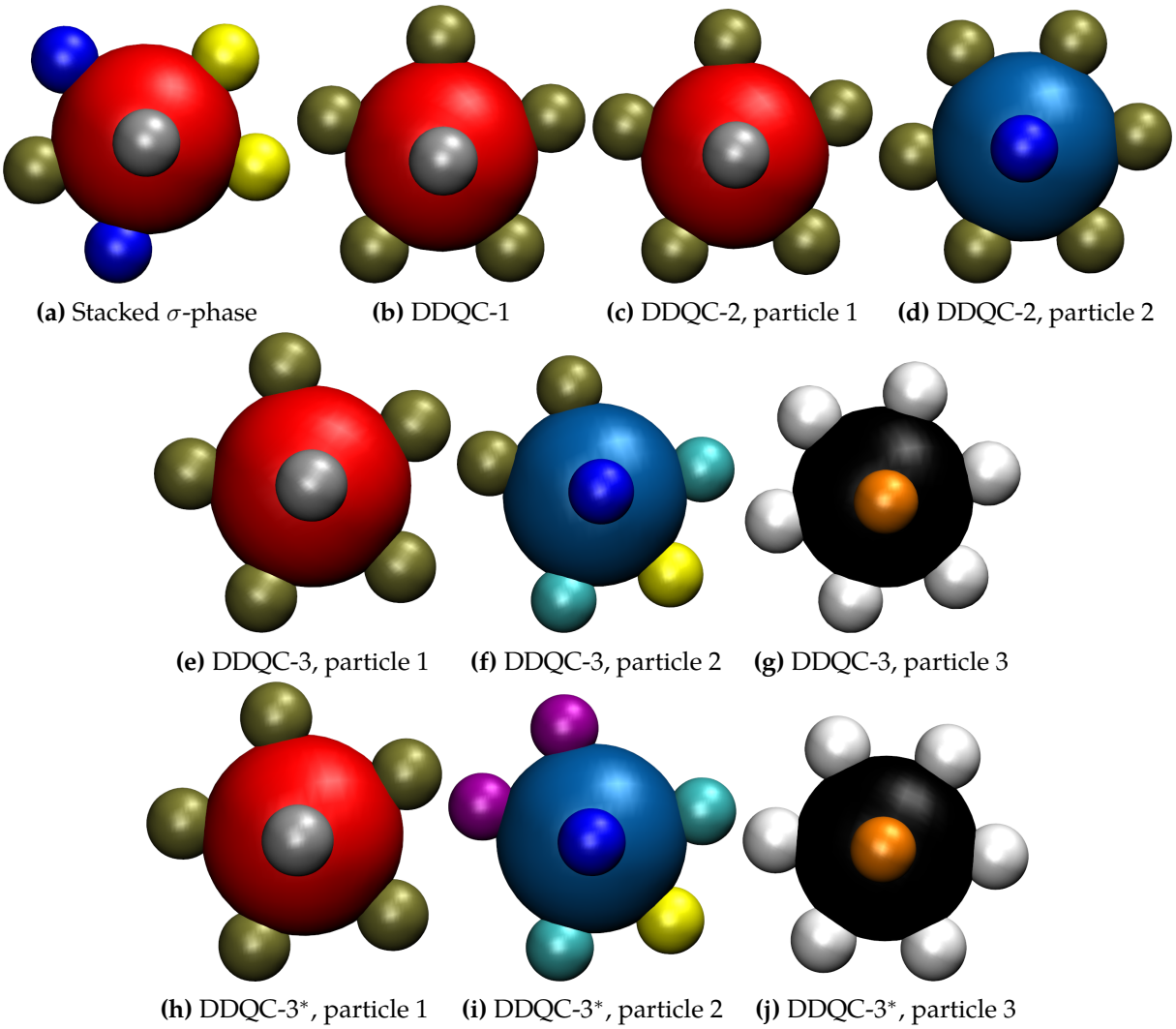

(a) Stacked σ-phase **(b)** DDQC-1 **(c)** DDQC-2, particle 1 **(d)** DDQC-2, particle 2

(e) DDQC-3, particle 1 **(f)** DDQC-3, particle 2 **(g)** DDQC-3, particle 3

(h) DDQC-3*, particle 1 **(i)** DDQC-3*, particle 2 **(j)** DDQC-3*, particle 3

Figure 4.2: Images of the patchy particles designed to form stacked σ or a DDQC, as specified in Table 4.3. For all particles, an unseen patch is directly opposite the patch pointing out of the page, and of the same type; these are the axial patches. The difference between designs DDQC-3 and -3* is subtle: for their respective type-2 particles **[(f)** and **(i)]**, the two in-plane patches opposite the yellow patch are of different types. In DDQC-3, they are of the same type as the in-plane patches of the type-1 particle **[(e)]**. In DDQC-3*, they are of a different type.

4.2 Stacked σ-phase

As a precursor to a DDQC, I targeted an approximant: a stacking of planes which each have a σ-phase square-triangle tiling arrangement [Fig. 4.1(a)], with planes stacked periodically, directly above one another. Note that although this is the same type of structure as the 3D Frank-Kasper σ-phase [246,247], it has a different arrangement of particles (which can be thought of as a different atomic decoration). Hence, for clarity, I call it 'stacked σ'. Individual σ-phase planes were

assembled in prior 2D patchy-particle studies [1,3].

My patchy-particle design for forming stacked σ is given in Table 4.3, following the design scheme in section 2.4, and pictured in Fig. 4.2(a). All particles occupy the same Wyckoff position, and lie on a mirror plane (each layer is a mirror). Therefore the one occupied Wyckoff position corresponds to only 1 particle type. 2 axial patches, on opposite sides of the particle and perpendicular to the in-plane patches, join particles to neighbouring layers; these are of the same type, because they map onto each other by the mirror plane coincident with the layer. 5 in-plane patches are spaced unequally, consecutively at $0, 2\pi/12, 5\pi/12, 7\pi/12, 10\pi/12$ rad, with 3 different patch types among them. The design is fully selective—each patch type interacts with only one patch type—and fully specifies the target structure. As usual, $\sigma_{\text{ang}} = 0.3$ rad and $\sigma_{\text{tor}} = 0.6$ rad.

I simulated $N = 864$ particles (6^3 sets of the primitive cell of 4 particles), for 7.575×10^6 MC cycles, in serial. I annealed, decreasing T^* stepwise by 2×10^{-4} every 7.5×10^4 MC cycles. I repeated this protocol eight times, beginning at temperatures in the range $T^*_{\text{init}} = [0.105, 0.14]$, and annealing over $\Delta T^* = 0.02$.[†]

Stacked σ assembled successfully, nucleating at $T^* \approx 0.1194$.[‡] A representative final configuration can be seen in Fig. 4.3. Although the structure is not perfect (with some defects, and not all layers growing to the same size), it is clear that stacked σ assembled correctly. This is all I wished to demonstrate; it paves the way for the DDQC structure.

[†] I established this simulation protocol, and the temperatures used, after numerous preliminary simulations; the same is true for all future simulations.

[‡] This temperature, as for later reported nucleation temperatures, is the *highest observed* nucleation temperature. Since nucleation is stochastic, in other simulations it occurred at lower temperatures, and it is likely that it could occur at higher temperatures.

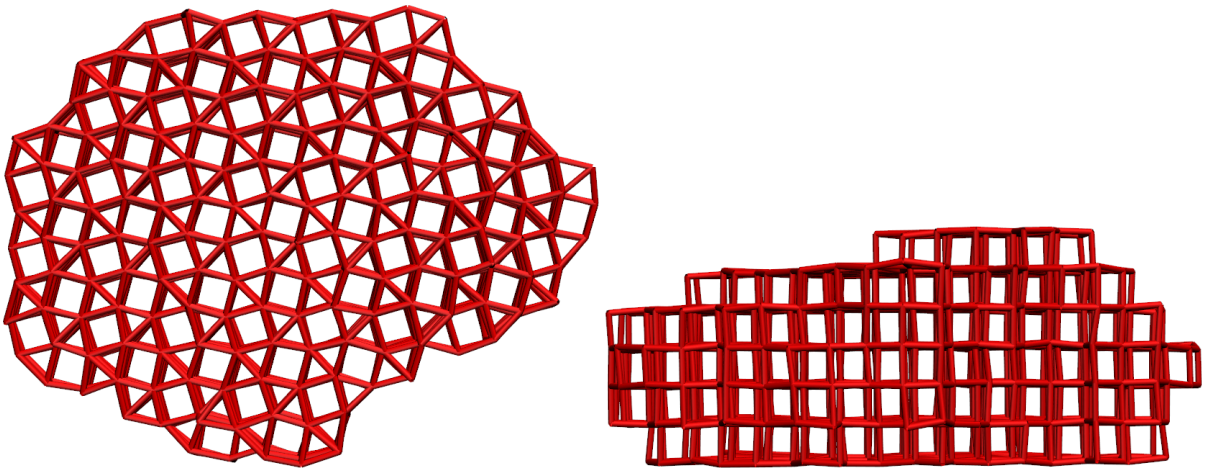

(a) Top view (patchy bonds)

(b) Side view (patchy bonds)

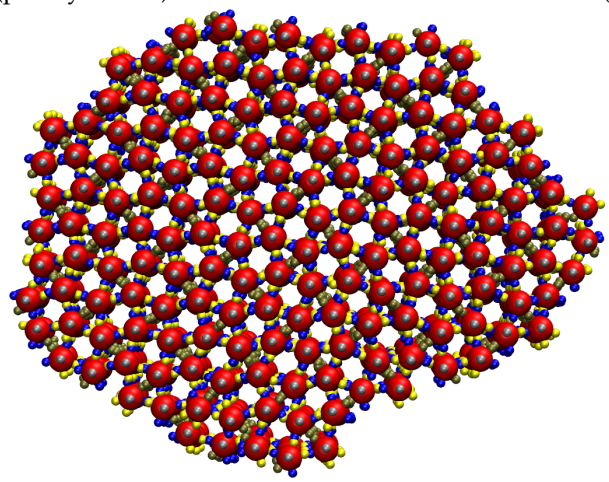

(c) Top view (patchy particles)

Figure 4.3: Final cluster assembled for stacked σ design, for $N = 864$ and $\sigma_{\text{ang}} = 0.3$ rad, at $T^* = 0.105$, for the simulation with $T^*_{\text{init}} = 0.125$. Structure is depicted in **(a)** and **(b)** by patchy bonds: bonds are shown for particle pairs within $1.3\sigma_{\text{LJ}}$. The same structure is depicted in **(c)** as patchy particles, as described in Fig. 3.1.

4.3 Dodecagonal quasicrystals

4.3.1 Unary design: Regularly-spaced, identical patches

4.3.1.1 Particle design

My first approach to forming a DDQC was the simplest—that of Refs. 1,2. Particles have 5 regularly-spaced, in-plane patches, and all in-plane patches are identical—they interact with all other in-plane patches, with equal strength. Reducing patch selectivity compared to my design for stacked σ (section 4.2) allows particles more freedom in their bonding arrangements—

Table 4.3: Design details for the sets of patchy particles designed to form stacked σ or a DDQC. Images of each particle are shown in Fig. 4.2. Note that QCs do not have (3D) crystallographic space groups and Wyckoff sites.

Structure	**Particle type**	**Patch details**					
		Number	Unit vector	Patch type	Interacts with (type)	Reference vector number	Offset angle(s) (rad)[a]
Stacked σ-phase	1	1	$(1.0, 0.0, 0.0)$	1	1	2	0.0
		2	$(0.0, 1.0, 0.0)$	2	2	1	$0.0, \pi$
		3	$(0.0, 0.5, -\sqrt{3}/2)$	3	4	1	$0.0, \pi$
		4	$(0.0, -\sqrt{3}/2, -0.5)$	4	3	1	$0.0, \pi$
		5	$(0.0, -\sqrt{3}/2, 0.5)$	4	3	1	$0.0, \pi$
		6	$(0.0, 0.5, \sqrt{3}/2)$	3	4	1	$0.0, \pi$
		7	$(-1.0, 0.0, 0.0)$	1	1	2	0.0
DDQC-1	1	1	$(1.0, 0.0, 0.0)$	1	1	2	$-4\pi/5, -2\pi/5, 0.0, 2\pi/5, 4\pi/5$
		2	$(0.0, 1.0, 0.0)$	2	2	1	$0.0, \pi$
		3	$(0.0, (\sqrt{5}-1)/4, -\sqrt{10+2\sqrt{5}}/4)$	2	2	1	$0.0, \pi$
		4	$(0.0, -(\sqrt{5}+1)/4, -\sqrt{10-2\sqrt{5}}/4)$	2	2	1	$0.0, \pi$
		5	$(0.0, -(\sqrt{5}+1)/4, \sqrt{10-2\sqrt{5}}/4)$	2	2	1	$0.0, \pi$
		6	$(0.0, (\sqrt{5}-1)/4, \sqrt{10+2\sqrt{5}}/4)$	2	2	1	$0.0, \pi$
		7	$(-1.0, 0.0, 0.0)$	1	1	2	$-4\pi/5, -2\pi/5, 0.0, 2\pi/5, 4\pi/5$
DDQC-2	1	1	$(1.0, 0.0, 0.0)$	1	1	2	n/a[b]
		2	$(0.0, 1.0, 0.0)$	2	2	1	$0.0, \pi$
		3	$(0.0, (\sqrt{5}-1)/4, -\sqrt{10+2\sqrt{5}}/4)$	2	2	1	$0.0, \pi$
		4	$(0.0, -(\sqrt{5}+1)/4, -\sqrt{10-2\sqrt{5}}/4)$	2	2	1	$0.0, \pi$
		5	$(0.0, -(\sqrt{5}+1)/4, \sqrt{10-2\sqrt{5}}/4)$	2	2	1	$0.0, \pi$
		6	$(0.0, (\sqrt{5}-1)/4, \sqrt{10+2\sqrt{5}}/4)$	2	2	1	$0.0, \pi$
		7	$(-1.0, 0.0, 0.0)$	1	1	2	n/a[b]
	2	1	$(1.0, 0.0, 0.0)$	3	3	2	n/a[b]
		2	$(0.0, 1.0, 0.0)$	2	2	1	$0.0, \pi$
		3	$(0.0, 0.5, -\sqrt{3}/2)$	2	2	1	$0.0, \pi$
		4	$(0.0, -0.5, -\sqrt{3}/2)$	2	2	1	$0.0, \pi$
		5	$(0.0, -1.0, 0.0)$	2	2	1	$0.0, \pi$
		6	$(0.0, -0.5, \sqrt{3}/2)$	2	2	1	$0.0, \pi$

Continued on next page

Table 4.3 (*Continued from previous page*)

Structure	Particle type	Patch details					
		Number	Unit vector	Patch type	Interacts with (type)	Reference vector number	Offset angle(s) (rad)[a]
DDQC-2 (*cont.*)	2	7	$(0.0, 0.5, \sqrt{3}/2)$	2	2	1	$0.0, \pi$
		8	$(-1.0, 0.0, 0.0)$	3	3	2	n/a[b]
DDQC-3	1	1	$(1.0, 0.0, 0.0)$	1	1	2	n/a[b]
		2	$(0.0, 1.0, 0.0)$	2	2	1	$0.0, \pi$
		3	$(0.0, (\sqrt{5}-1)/4, -\sqrt{10+2\sqrt{5}}/4)$	2	2	1	$0.0, \pi$
		4	$(0.0, -(\sqrt{5}+1)/4, -\sqrt{10-2\sqrt{5}}/4)$	2	2	1	$0.0, \pi$
		5	$(0.0, -(\sqrt{5}+1)/4, \sqrt{10-2\sqrt{5}}/4)$	2	2	1	$0.0, \pi$
		6	$(0.0, (\sqrt{5}-1)/4, \sqrt{10+2\sqrt{5}}/4)$	2	2	1	$0.0, \pi$
		7	$(-1.0, 0.0, 0.0)$	1	1	2	n/a[b]
	2	1	$(1.0, 0.0, 0.0)$	3	3	2	n/a[b]
		2	$(0.0, 1.0, 0.0)$	4	5	1	$0.0, \pi$
		3	$(0.0, 0.5, -\sqrt{3}/2)$	6	6	2	0.0
		4	$(0.0, -\sqrt{3}/2, -0.5)$	2	2	1	$0.0, \pi$
		5	$(0.0, -\sqrt{3}/2, 0.5)$	2	2	1	$0.0, \pi$
		6	$(0.0, 0.5, \sqrt{3}/2)$	6	6	2	0.0
		7	$(-1.0, 0.0, 0.0)$	3	3	2	n/a[b]
	3	1	$(1.0, 0.0, 0.0)$	7	7	2	n/a[b]
		2	$(0.0, 1.0, 0.0)$	5	4	1	$0.0, \pi$
		3	$(0.0, 0.5, -\sqrt{3}/2)$	5	4	1	$0.0, \pi$
		4	$(0.0, -0.5, -\sqrt{3}/2)$	5	4	1	$0.0, \pi$
		5	$(0.0, -1.0, 0.0)$	5	4	1	$0.0, \pi$
		6	$(0.0, -0.5, \sqrt{3}/2)$	5	4	1	$0.0, \pi$
		7	$(0.0, 0.5, \sqrt{3}/2)$	5	4	1	$0.0, \pi$
		8	$(-1.0, 0.0, 0.0)$	7	7	2	n/a[b]
DDQC-3*	1	1	$(1.0, 0.0, 0.0)$	1	1	2	n/a[b]
		2	$(0.0, 1.0, 0.0)$	2	2,8	1	$0.0, \pi$
		3	$(0.0, (\sqrt{5}-1)/4, -\sqrt{10+2\sqrt{5}}/4)$	2	2,8	1	$0.0, \pi$
		4	$(0.0, -(\sqrt{5}+1)/4, -\sqrt{10-2\sqrt{5}}/4)$	2	2,8	1	$0.0, \pi$
		5	$(0.0, -(\sqrt{5}+1)/4, \sqrt{10-2\sqrt{5}}/4)$	2	2,8	1	$0.0, \pi$

Continued on next page

Table 4.3 (*Continued from previous page*)

Structure	Particle type	Patch details					
		Number	Unit vector	Patch type	Interacts with (type)	Reference vector number	Offset angle(s) (rad)[a]
		6	$(0.0, (\sqrt{5}-1)/4, \sqrt{10+2\sqrt{5}}/4)$	2	2,8	1	$0.0, \pi$
		7	$(-1.0, 0.0, 0.0)$	1	1	2	n/a[b]
	2	1	$(1.0, 0.0, 0.0)$	3	3	2	n/a[b]
		2	$(0.0, 1.0, 0.0)$	4	5	1	$0.0, \pi$
		3	$(0.0, 0.5, -\sqrt{3}/2)$	6	6	2	0.0
		4	$(0.0, -\sqrt{3}/2, -0.5)$	8	2,8	1	$0.0, \pi$
		5	$(0.0, -\sqrt{3}/2, 0.5)$	8	2,8	1	$0.0, \pi$
		6	$(0.0, 0.5, \sqrt{3}/2)$	6	6	2	0.0
		7	$(-1.0, 0.0, 0.0)$	3	3	2	n/a[b]
	3	1	$(1.0, 0.0, 0.0)$	7	7	2	n/a[b]
		2	$(0.0, 1.0, 0.0)$	5	4	1	$0.0, \pi$
		3	$(0.0, 0.5, -\sqrt{3}/2)$	5	4	1	$0.0, \pi$
		4	$(0.0, -0.5, -\sqrt{3}/2)$	5	4	1	$0.0, \pi$
		5	$(0.0, -1.0, 0.0)$	5	4	1	$0.0, \pi$
		6	$(0.0, -0.5, \sqrt{3}/2)$	5	4	1	$0.0, \pi$
		7	$(0.0, 0.5, \sqrt{3}/2)$	5	4	1	$0.0, \pi$
		8	$(-1.0, 0.0, 0.0)$	7	7	2	n/a[b]

[a] For the interaction between patch α on particle i and patch β on particle j, offset angles are measured clockwise when looking along $\mathbf{r}_{ij}$ from i to j. They are in the range $[-\pi, \pi)$.

[b] I did not include torsional interactions for axial patches, *i.e.* $\sigma_{\mathrm{tor,axial}} \to \infty$.

particles can bond in more ways than if only one pair of their patches interacts. Freedom allows disorder (and gives greater entropy), which is essential to quasicrystallinity. By spacing in-plane patches regularly, I allowed particles to bond in arrangements other than the (3^2, 4, 3, 4) square-triangle tiling of the σ-phase, as required in DDQCs: not only in other square-triangle tilings, but also in arrangements with 6 in-plane neighbours (*i.e.* HCP environments). The only differences between my design and that of Refs. 1,2 are: the addition of two axial patches, whose type is distinct (they only interact with each other); and the inclusion of torsional interactions. The full design is given in Table 4.3, named 'DDQC-1', and the particle is pictured in Fig. 4.2(b).

4.3.1.2 Preliminary testing

To begin, I kept $\sigma_{\text{ang}} = 0.3$ rad and $\sigma_{\text{tor}} = 0.6$ rad. I simulated $N = 2000$ particles, for 1.212×10^7 MC cycles, in serial. I annealed, decreasing T^* by 1×10^{-4} every 1.2×10^5 MC cycles. I repeated this protocol five times, beginning at temperatures in the range $T^*_{\text{init}} = [0.136, 0.14]$, and simulating for $\Delta T^* = 0.01$. The system assembled into a 3D phase of layered square-triangle tilings, nucleating at $T^* \approx 0.1348$. A representative final configuration can be seen in Fig. 4.4(a,b). I found that σ environments [Fig. 4.1(a)] were very common, while some H environments [Fig. 4.1(f)] were present. However, I detected no particles in an HCP environment [Fig. 4.1(c)]—as required for dodecagons, and thus DDQCs. Hence, the results were promising, but further tuning was needed.

Interestingly, when I turned off torsional interactions for the axial patches ($\sigma_{\text{tor,axial}} \to \infty$)—allowing particles to freely rotate around their inter-plane axis—the same structure assembled with similar success.[†] A sample configuration is shown in Fig. 4.4(c,d). This indicates that axial-patch torsional interactions are not essential for the assembly of stacked square-triangle tilings. Moreover, an HCP environment formed, as marked in Fig. 4.4(c,d). (Nonetheless, I retained axial-patch torsional interactions for future DDQC-1 simulations.)

[†] I made a corresponding change to the starting temperature, $T^*_{\text{init}} = [0.14, 0.144]$, as the nucleation temperature increased to $T^* \approx 0.1355$.

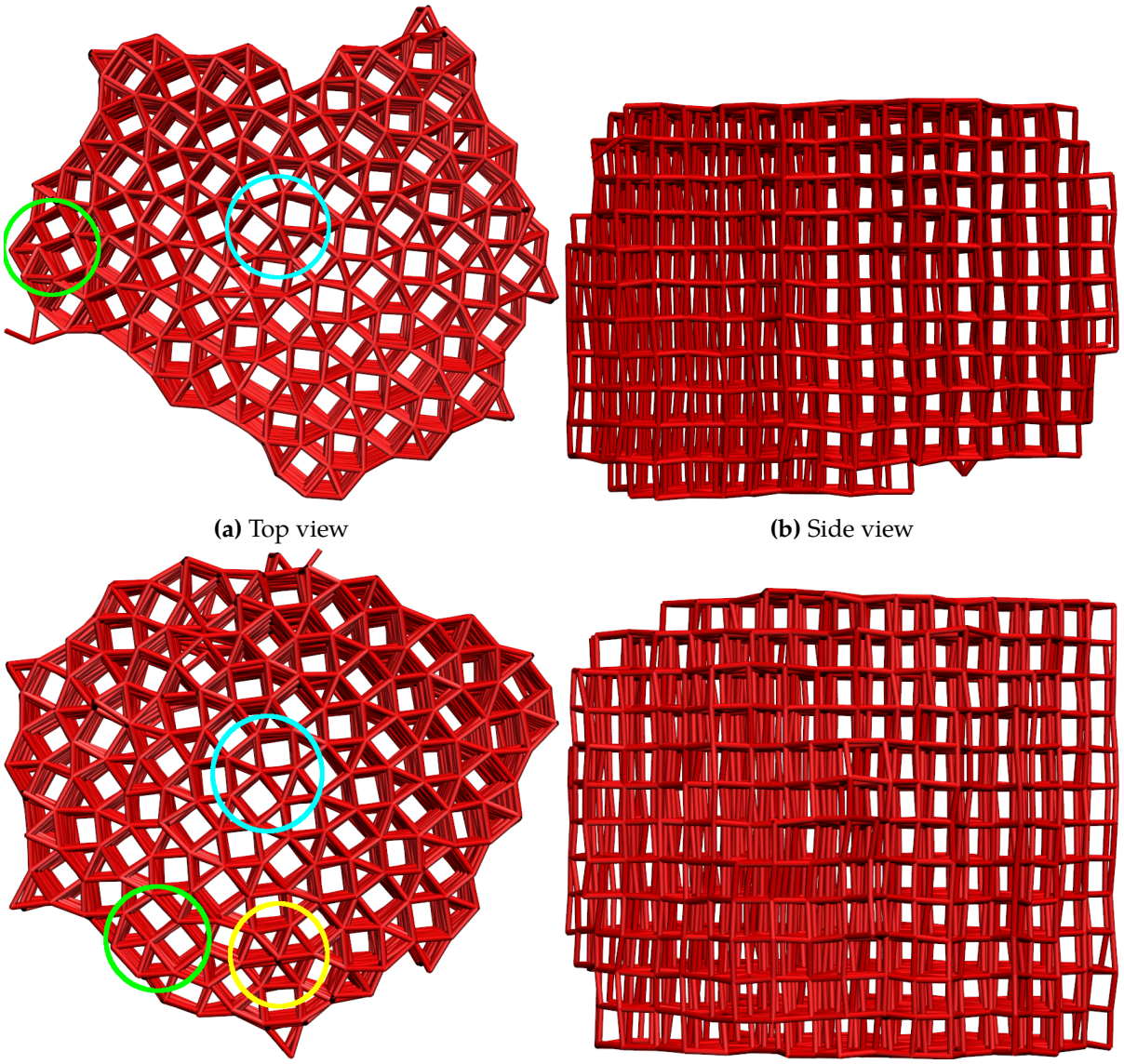

(a) Top view **(b)** Side view

(c) No axial-patch torsional interactions. Top view **(d)** No axial-patch torsional interactions. Side view

Figure 4.4: Final clusters assembled for DDQC-1 design, for $N = 2000$ and $\sigma_{\text{ang}} = 0.3$ rad, with **(a,b)** and without **(c,d)** torsional interactions (*i.e.* $\sigma_{\text{tor,axial}} \to \infty$). **(a,b)** Simulation began at $T^*_{\text{init}} = 0.137$, pictured at $T^* = 0.127$. **(c,d)** Simulation began at $T^*_{\text{init}} = 0.140$, pictured at $T^* = 0.130$. Example σ environments (dominant in all simulations) are circled in cyan, H environments in green, and an HCP environment in yellow [Figs. 4.1(a–c)].

4.3.1.3 Optimising angular patch width

The studies in Refs. 1,2 found stable DDQCs for angular patch widths greater than 0.3 rad: roughly in the range $0.4 \leq \sigma_{\text{ang}} \leq 0.6$ rad, and especially around $0.45 \leq \sigma_{\text{ang}} \leq 0.5$ rad (the precise values depend on thermodynamic parameters, among other things). Thus, I considered the same design with five angular patch widths: $\sigma_{\text{ang}} = 0.43, 0.46, 0.49, 0.52, 0.55$ rad. Prelimi-

nary simulations ($N = 2000$), revealed a number of basic, qualitative features of these systems. Increasing σ_{ang} (at least, for the widths I studied) has the following effects:

(i) It increases the melting temperature, T^*_{melt}. This is because wider patches can sustain larger thermal motion—worse patch alignment—with less energetic cost, and thus without breaking bonds. Entropic stabilisation, through vibrational and rotational entropy, is also greater. For $\sigma_{\text{ang}} = 0.43, 0.46, 0.49, 0.52, 0.55$ rad, $T^*_{\text{melt}} \approx 0.177, 0.189, 0.203, 0.217, 0.231$, respectively. Correspondingly, the value of T^*_{init} below which multiple nucleation occurred (as discussed for periodic structures in section 3.4.2) increased with σ_{ang}: $T^*_{\text{init}} \lesssim 0.16, 0.17, 0.18, 0.19, 0.196$ for the respective σ_{ang}.

(ii) It causes the structure to diverge from the defined patch vectors. Wider patches allow more flexible bonds; bond angles aren't adhered to as tightly. This effect multiplies over a series of patchy bonds. It is manifested in multiple ways:

a. Layers become less clear, even non-existent, through flexibility of axial bonds. For $\sigma_{\text{ang}} = 0.55$ rad (and somewhat for $\sigma_{\text{ang}} = 0.52$ rad), at higher T^* (but still below T^*_{melt}), I could not detect layers.

b. HCP environments become more common, because patches are wide enough to bond to patches on multiple particles. Thus, a 5-patch particle can bond to 6 other particles. Not all patches will be perfectly aligned, but the energetic cost is small because of the width of the patches, and is compensated by the additional bond.

c. Moreover, a particle with 5 wide, regularly-spaced in-plane patches has a quasi-isotropic potential. [Specifically, for $\sigma_{\text{ang}} = 0.55$ rad, the pair interaction is half as strong if one patch is 37° away from perfect alignment (the other patch being in perfect alignment). So for 5 regularly-spaced patches, at all in-plane angles the interaction strength of (at least) one patch is at least 63.6% of its maximum.] This means particles in the plane are free to arrange in any relative position, with little energetic cost. Thus I observed liquid-like behaviour in the plane (or sometimes liquid-solid coexistence) for wider

patches at higher temperatures. Liquid-like structure was more common at the edges of clusters rather than within clusters, presumably because not all bonds can be satisfied at the edges, so there is less energetic cost for an incorrect structure. (Particles at the edge of a cluster are in equilibrium between a gas and a condensed phase, since they are only weakly bonded, by at most a few patches.) The phase behaviour is like that of a LJ fluid. On cooling, the structures became more ordered.

(iii) The phase diagram changes. In particular, I observed that on lowering the temperature from the gas phase, at $\sigma_{\text{ang}} \lesssim 0.5$ rad, stacked σ becomes stable; but at $\sigma_{\text{ang}} \gtrsim 0.5$ rad, first stacked HCP becomes stable, with stacked σ only becoming stable at lower temperatures. This is consistent with the 2D results in Ref. 2 (and related to point b above), albeit with different values for the phase boundaries (temperature, pressure, *etc.*).

The above observations have implications for my attempt to successfully form DDQCs:

(i) The melting and multiple-nucleation temperatures give a window for the self-assembly of well-ordered clusters (different for each σ_{ang}). As for complex periodic structures (section 3.4.2), the temperature window for good assembly is fairly narrow. (I note again, though, that multiple nucleation is no failure of the correct structure to self-assemble, but only a problem for clearly observing the structure in a large cluster.)

(ii) HCP environments are essential for a DDQC; wider patches are thus preferable. However, wider patches also result in a lack of clear layers and liquid-like behaviour in the planes; no clear, ordered structure forms. Thus, an intermediate patch width is required.

(iii) In Ref. 2, the DDQC phase was positioned in the phase diagram, in two different cases: (1) at $0.45 \lesssim \sigma_{\text{ang}} \lesssim 0.52$ rad (narrower than the region of stability of the HCP-phase), the DDQC was favoured at temperatures between the *gas* phase and the σ-phase; and (2) at $0.52 \lesssim \sigma_{\text{ang}} \lesssim 0.6$ rad (the narrower end of the region of stability of the HCP-phase), the DDQC was favoured at temperatures between the *HCP* phase and the σ-phase. My observations thus far suggest that the 3D phase diagram is similarly shaped. Assembling

a DDQC is harder in case (2), for the following reason (see also section 2.3.1). In case (1), a DDQC may nucleate and grow on cooling from the gas. In case (2), this will not occur; instead, stacked HCP will nucleate from the gas. To form a DDQC, one could instead either: cool from the gas phase into stacked HCP, and then continue cooling to allow rearrangement into a DDQC; or, begin simulating at a temperature at which the DDQC is favoured. Some downsides of the first approach are that stacked HCP may not easily or quickly rearrange to the DDQC, and the computational cost is large as the simulation must cover a greater temperature range. Some downsides of the second approach are that multiple nucleation may occur (because $T^*_{\text{init}} < T^*_{\text{melt}}$), or other structural defects may arise. I attempted the first approach.

For the reasons given in points (ii) and (iii), I no longer considered patches with $\sigma_{\text{ang}} = 0.55$ rad.

Encouragingly, I observed dodecagon motifs [both edge-sharing and overlapping; Figs. 4.1(e,f)] in a number of simulations, suggesting a DDQC is possible from the DDQC-1 design. The size of these systems was of course, though, too small to analyse for quasicrystallinity.

The shape of the clusters formed in these simulations was not spherical (at least for systems without the liquid-like behaviour noted in point b). The clusters resembled more a cylinder, somewhat short and bulged. In-plane growth was fairly isotropic and seemingly random. Top and bottom layers were often smaller than middle layers. Overall, in-plane growth was faster than inter-plane growth. This is likely because particles have more (5) patches in the plane than out of it (2), so there is more energetic benefit to growth in a plane. (A gas-phase particle can form more patchy bonds in a plane, and can potentially form multiple bonds at once, by joining a cluster along a plane than by joining above or below a plane.) When multiple nucleation occurred, sometimes clusters later coalesced, forming composite clusters with irregular shapes. Alternatively, in a few cases, Ostwald ripening [436,439] occurred: surface particles on both clusters break off (in a gas-solid equilibrium), but gas-phase particles are more likely to join the larger of the two clusters. This is because larger clusters are energetically favoured, since they

have a smaller proportion of lower-energy surface particles.

4.3.1.4 Production runs

Methods. I simulated systems of $N = 20000$ particles with design DDQC-1 (Table 4.3), for $\sigma_{\text{ang}} = 0.43, 0.46, 0.49, 0.52$ rad, in parallel. I simulated over a larger temperature range for larger σ_{ang}, especially for σ_{ang} =0.52 rad—in order to cool from the gas phase, through stacked HCP, to the DDQC phase [as discussed in point (iii) immediately above]. Thus the annealing rate varied with σ_{ang}, in order to achieve results with reasonable computational cost. For the above respective σ_{ang}, the (continuous) annealing rates were 1.07, 1.07, 1.2, 3.87×10^{-4} per 10^5 MC cycles. (Note the much faster rate for $\sigma_{\text{ang}} = 0.52$ rad, due to the larger temperature range.) For each σ_{ang}, I repeated the protocol five times, each time beginning from a different random configuration. I began at slightly different temperatures in each repetition: $T^*_{\text{init}} = [0.176, 0.18]$, $[0.188, 0.192]$, $[0.203, 0.207]$, $[0.216, 0.220]$, for the respective σ_{ang}. I ended simulations once the structure (and total energy) was relatively constant. So the simulated temperature range not only varied between σ_{ang}, but also between individual repetitions. The ranges were within the following bounds, for the respective σ_{ang}: $0.0028 \leq \Delta T^* \leq 0.0039$, $0.0032 \leq \Delta T^* \leq 0.0056$, $0.0065 \leq \Delta T^* \leq 0.0091$, and $0.0228 \leq \Delta T^* \leq 0.0348$. The corresponding total numbers of MC cycles, for the respective σ_{ang} were in the following bounds: 2.63×10^6 to 3.66×10^6, 3.00×10^6 to 5.25×10^6, 4.06×10^6 to 5.69×10^6, and 2.95×10^6 to 4.50×10^6.[†‡]

System size. In order to simulate true QCs, one would require an infinite number of particles (and an infinitely large, *i.e.* non-periodic, simulation box, such that the structure does not extend from one side of the box to the other). Even to simulate a QC with a coherence length of the best experimental QCs (~ 10 μm), one would require $\sim 10^7$ particles [487]. $N = 20000$ particles (in

[†] In contrast to my NVT-ensemble simulations, the 2D DDQC patchy-particle simulations [1–3], were performed in the NPT ensemble. These studies also used volume change moves.

[‡] In the non-patchy, IQC study [349] (section 4.1.3.2), the authors selected the lowest-energy structures from a range of simulations, and tempered these at fixed, lower temperatures to remove defects and equilibrate. I did not do this in any simulations; it may have been useful, but it was not essential for my aim of simply demonstrating assembly of the target structure.

a finite cluster, within a large simulation box) is a reasonable approximation; this is the number of particles used to form the recent, non-patchy, IQC [349] (section 4.1.3.2).[†]

General observations. I observed nucleation at $T^* \approx 0.178, 0.191, 0.205, 0.219$ for $\sigma_{\text{ang}} = 0.43$, 0.46, 0.49, 0.52 rad, respectively. Well-ordered clusters grew quickly from this point, comparable to the periodic structures in Ch. 3. In the final configurations, some gas-phase particles remained in equilibrium with the cluster (as for the IQC study [349]). This is likely due to both the larger system sizes and slightly shorter simulation times. Clusters grew roughly equally in each direction, although with the short, bulged, cylinder shape noted above (section 4.3.1.3). During formation, however, the shapes were sometimes more faceted; they rounded over time. Multiple nucleation was rare, occurring only in one simulation for each of $\sigma_{\text{ang}} = 0.49, 0.52$ rad (that with the lowest T^*_{init}). Sample final configurations for each σ_{ang} are shown in Fig. 4.5.

As marked in the figures, for all σ_{ang} I observed σ, H, and HCP environments, as well as dodecagons in various arrangements. As noted earlier (section 4.3.1.3), for larger σ_{ang}, HCP environments were more common; correspondingly, dodecagon motifs were more common. More dodecagons are visible in Figs. 4.5(e,g) than (a,c). Further discussion of the structures formed, including characterisation using diffraction patterns, is given later in section 4.3.4.

As noted in earlier simulations (section 4.3.1.3), for larger σ_{ang}, layers were less ordered. This can be seen by comparing Figs. 4.5(b,d,f,h). In some cases, layers—and entire clusters—were bent (*i.e.* not flat), *e.g.* Fig. 4.5(b). This made it harder to identify the assembled structure. Nonetheless, overall the clusters had clear layers; the disorder was only significant for $\sigma_{\text{ang}} = 0.52$ rad at very high (condensed-phase) temperatures (*i.e.* upon nucleation from the gas, but not after further cooling). Moreover, the structures were similar and consistent between stacked layers, but not identical. This can be seen by viewing through the layers in Figs. 4.5(a,c,e,g): many square/triangle channels are clear, whereas some are not. Note, however, that even if

[†] The density of my systems, $\rho^* = 0.1\ \sigma_{\text{LJ}}^{-3}$, is also comparable to those in the same study, $\rho^* = 0.03$–$0.1\ \sigma_{\text{LJ}}^{-3}$ [349]. The three 2D studies on patchy-particle assembly of DDQCs [1–3] used $N \approx 2500$, which in 3D corresponds to $N \approx 125000$ ($= \sqrt{2500}^3$). However, to simulate this number of particles would be prohibitively expensive.

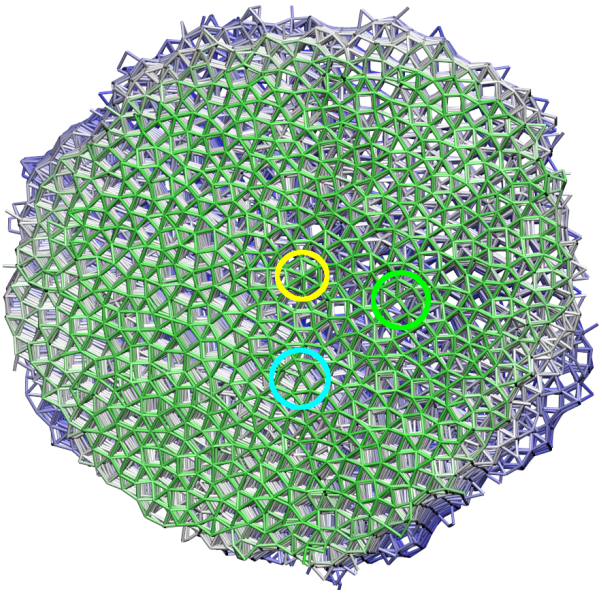

(a) $\sigma_{\text{ang}} = 0.43$ rad, top view

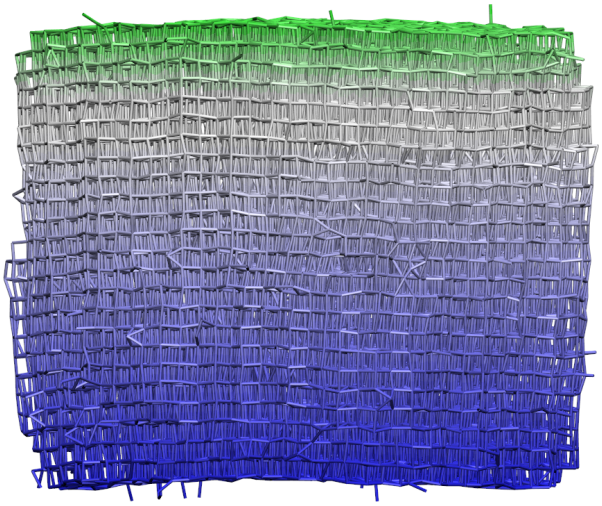

(b) $\sigma_{\text{ang}} = 0.43$ rad, side view

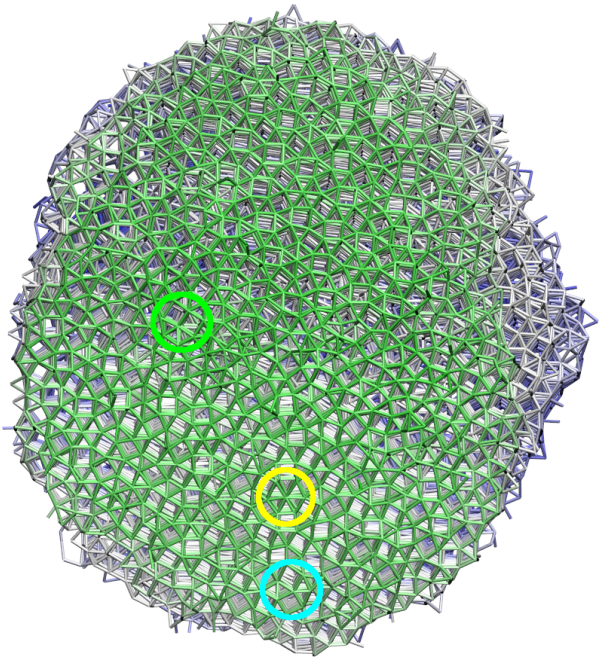

(c) $\sigma_{\text{ang}} = 0.46$ rad, top view

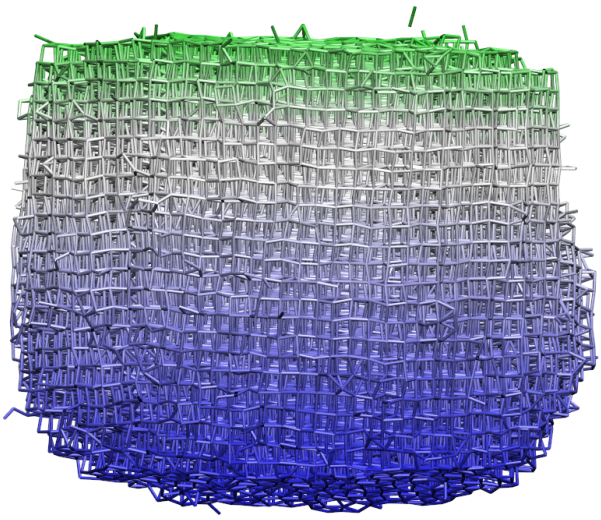

(d) $\sigma_{\text{ang}} = 0.46$ rad, side view

Figure 4.5: Final clusters assembled for DDQC-1 design, for $N = 20000$ and $\sigma_{\text{ang}} = 0.43$ rad **(a,b)**, or $\sigma_{\text{ang}} = 0.46$ rad **(c,d)**. Bonds are coloured by particle position, for viewing clarity: green in the foreground/on top, blue in the background/on the bottom. Gas-phase particles have been removed. Example σ environments are circled in cyan, H environments in green, and HCP environments in yellow. The simulation for $\sigma_{\text{ang}} = 0.43$ rad began at $T^*_{\text{init}} = 0.179$ and is shown at $T^* \approx 0.1754$; for $\sigma_{\text{ang}} = 0.46$ rad it began at $T^*_{\text{init}} = 0.189$ and is shown at $T^* \approx 0.1857$. *(Continued on next page.)*

the arrangement is not identical from layer to layer, this does not mean a 3D DDQC has not formed. The requirement for a 3D DDQC is simply a DDQC in each layer, even if the layers do not perfectly match each other.

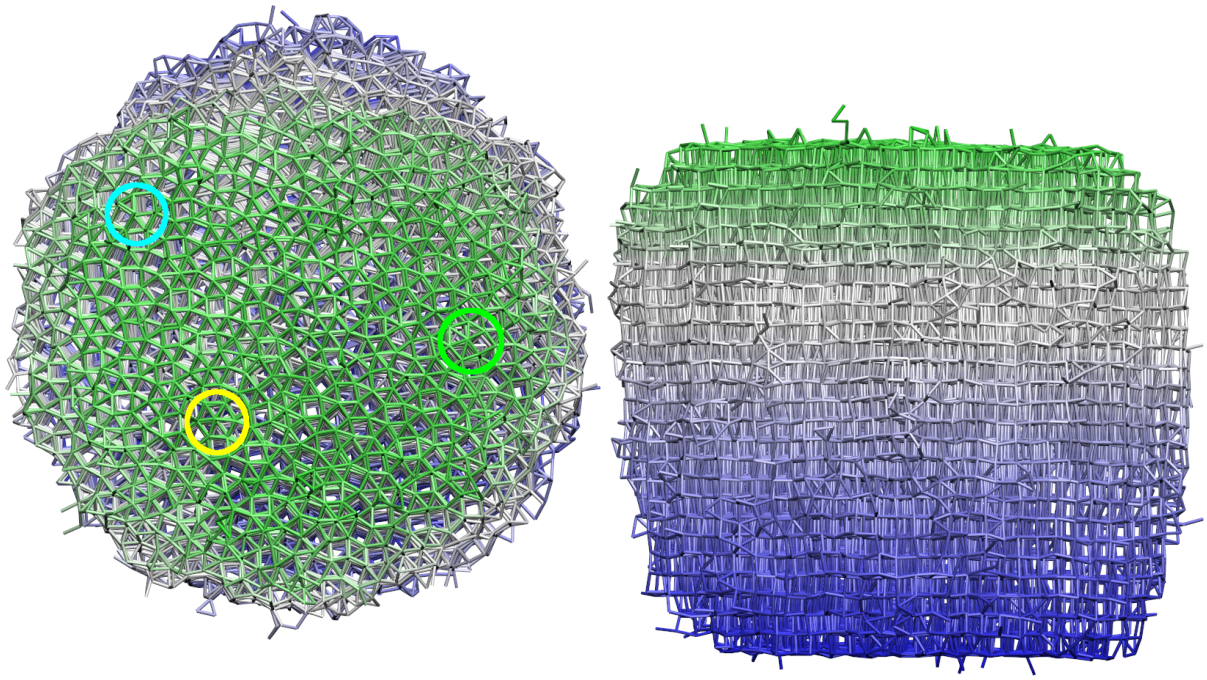

(e) $\sigma_{\text{ang}} = 0.49$ rad, top view

(f) $\sigma_{\text{ang}} = 0.49$ rad, side view

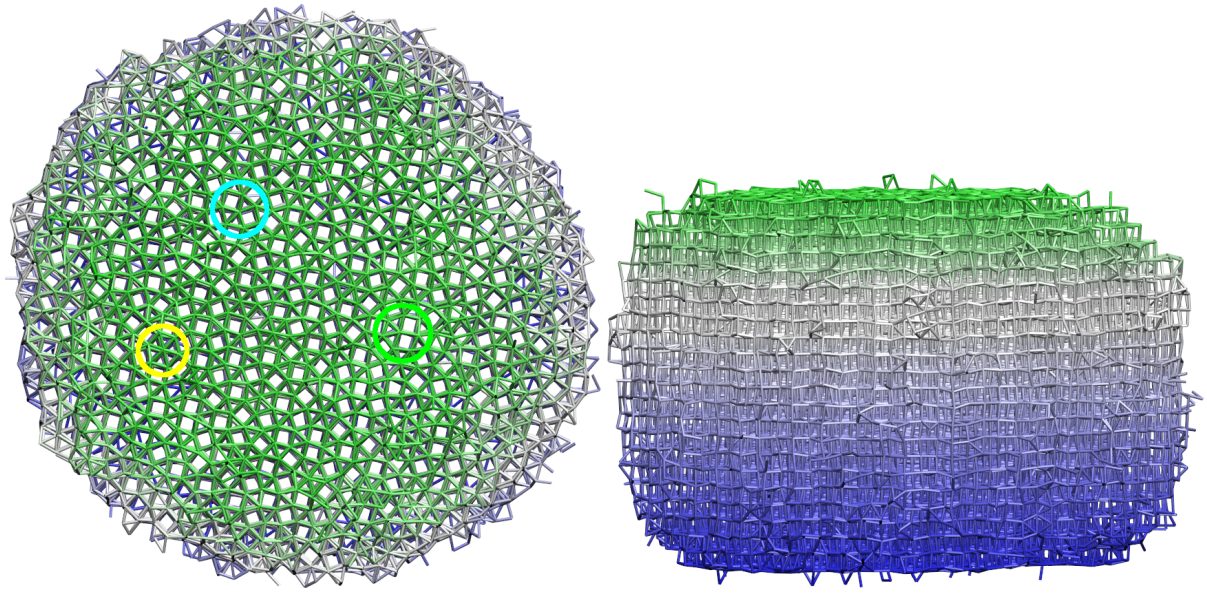

(g) $\sigma_{\text{ang}} = 0.52$ rad, top view

(h) $\sigma_{\text{ang}} = 0.52$ rad, side view

Figure 4.5: *(Continued from previous page.)* For $\sigma_{\text{ang}} = 0.49$ rad **(e,f)**, or $\sigma_{\text{ang}} = 0.52$ rad **(g,h)**. The simulation for $\sigma_{\text{ang}} = 0.49$ rad began at $T^*_{\text{init}} = 0.203$ and is shown at $T^* \approx 0.1955$; for $\sigma_{\text{ang}} = 0.52$ rad it began at $T^*_{\text{init}} = 0.218$ and is shown at $T^* \approx 0.1915$.

As also noted in earlier simulations (section 4.3.1.3), for $\sigma_{\text{ang}} = 0.49, 0.52$ rad and at higher (condensed-phase) temperatures, the structure was liquid-like or disordered. On cooling, the structure became more ordered—typically at around 0.003 and 0.016 below the respective nucleation temperatures. Examples of the disordered structures can be seen in Fig. 4.6 ($\sigma_{\text{ang}} = 0.49$ rad) and Figs. 4.7(a,b) ($\sigma_{\text{ang}} = 0.52$ rad). Layers were not clear, structures differed signifi-

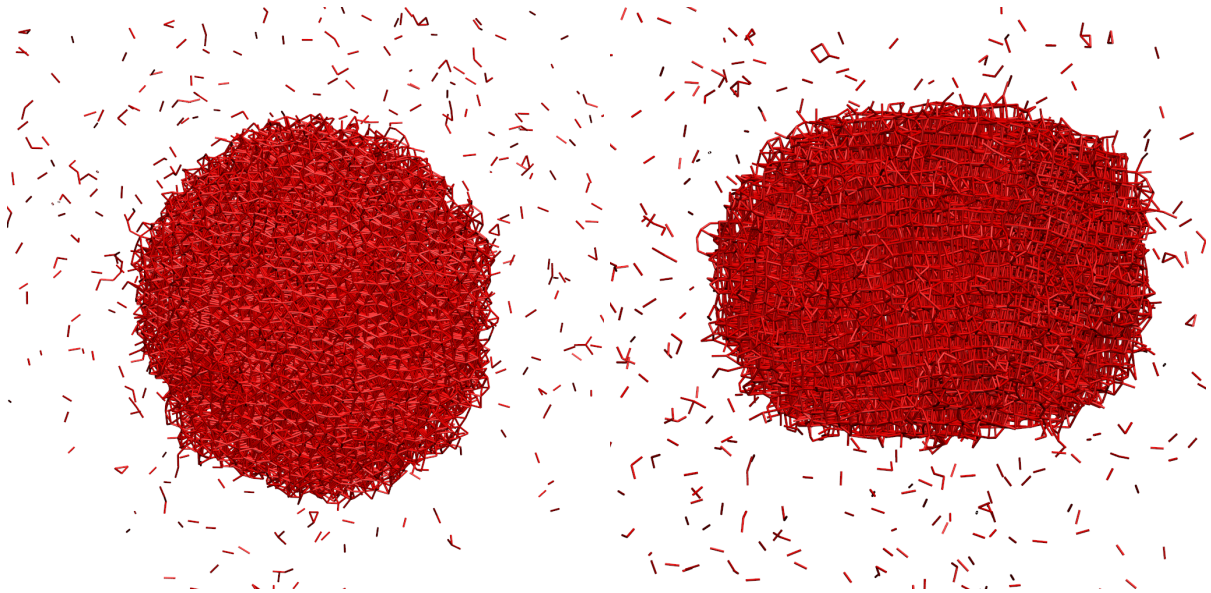

(a) Top view **(b)** Side view

Figure 4.6: Cluster assembled for the DDQC-1 design for $N = 20000$ and $\sigma_{\text{ang}} = 0.49$ rad, at an early stage of the simulation (soon after nucleation). The simulation began at $T^*_{\text{init}} = 0.205$ and is shown at $T^* \approx 0.2046$.

cantly between layers, and more particles were hexagonally coordinated. For $\sigma_{\text{ang}} = 0.52$ rad, the highest temperature ordered structure (or at least the dominant local environment) was stacked HCP; this rearranged to square-triangle tilings on further cooling. Fig. 4.7(c,d) is dominated by HCP environments, with some σ and H environments.

4.3.2 Binary design: 5- and 6-patch, selective patches

4.3.2.1 Particle design

My second approach at forming a DDQC was more complex than the DDQC-1 design; it was the first approach used in Ref. 3. The full design is given in Table 4.3, named 'DDQC-2', and the particles are pictured in Figs. 4.2(c,d). The system has two types of particles (a *binary* system), one with 5 in-plane patches and one with 6, in a ratio of 12:1 (see discussion in section 4.1.3.3). In-plane patches are equally spaced on both particle types. All in-plane patches—across both particles—are of the same type; all interact with each other, with equal strength. As for DDQC-1 (section 4.3.1.1): minimal patch selectivity gives particles more freedom when they arrange themselves, allowing disorder and giving greater entropy; regular patch spacing allows each

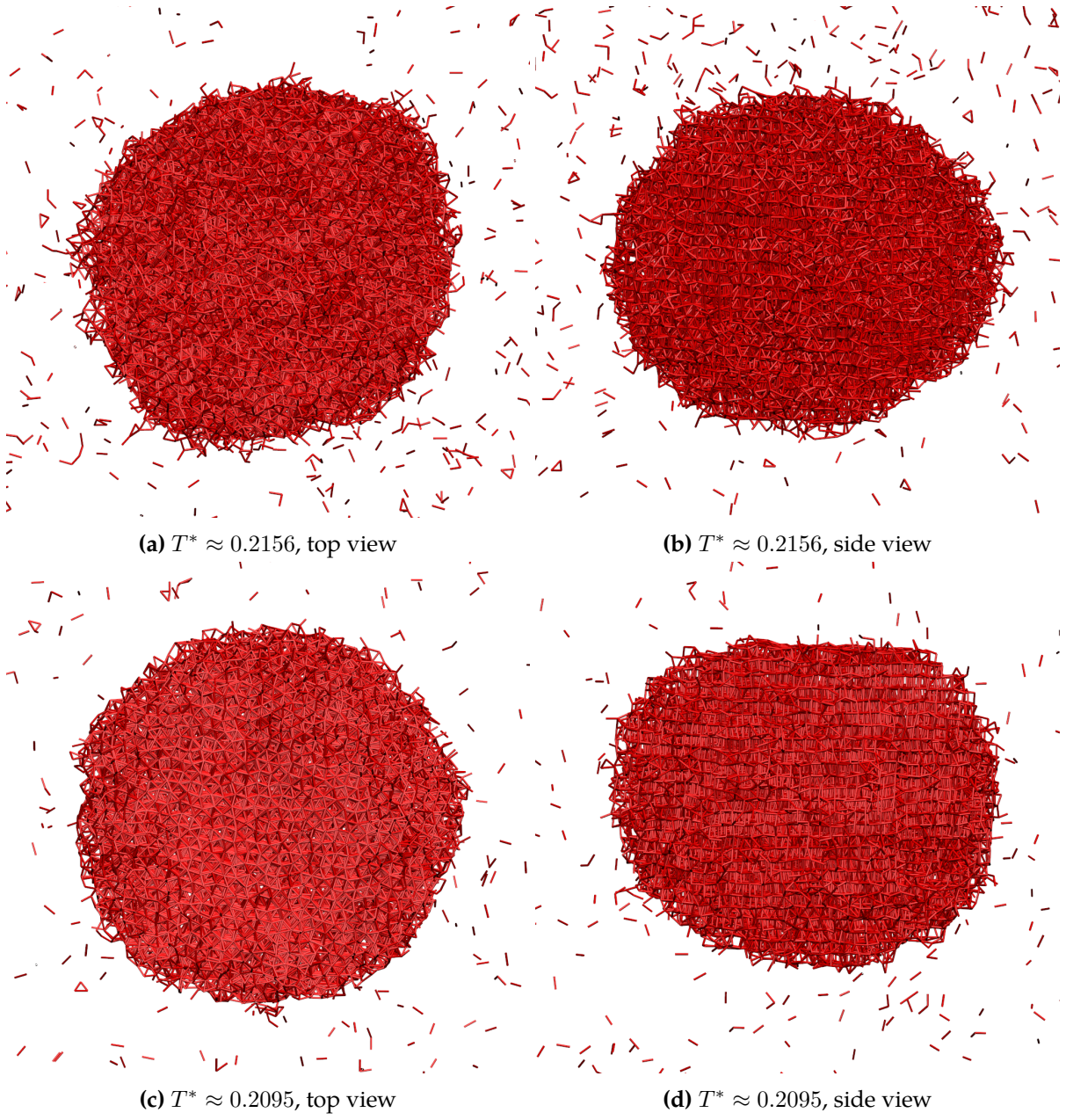

(a) $T^* \approx 0.2156$, top view

(b) $T^* \approx 0.2156$, side view

(c) $T^* \approx 0.2095$, top view

(d) $T^* \approx 0.2095$, side view

Figure 4.7: Clusters assembled for the DDQC-1 design for $N = 20000$ and $\sigma_{\mathrm{ang}} = 0.52$ rad, at early stages of the simulation (soon after nucleation). The simulation began at $T^*_{\mathrm{init}} = 0.218$ and is shown at two early stages: $T^* \approx 0.2156$ **(a,b)** and $T^* \approx 0.2095$ **(c,d)**.

particle to bond in various local arrangements. Unlike in DDQC-1, I deliberately included 6-patch particles (with an appropriate mole fraction) in order to form HCP local arrangements, and thus dodecagon motifs. Both types of particles have two axial patches, of distinct types from the in-plane patches and from the axial patches on the other particle type. I included torsional interactions, but not for axial patches (*i.e.* $\sigma_{\mathrm{tor,axial}} \to \infty$): I deemed (and found) these unnecessary, given the specificity already included in the design via patch positions; this also

allows greater freedom and disorder. As noted in section 4.3.1.2, axial-patch torsions did not seem essential for the DDQC-1 design, which is less specific than DDQC-2.

I set $\sigma_{\text{ang}} = 0.3$ rad and $\sigma_{\text{tor,lateral}} = 0.6$ rad, as usual. [The angular width is narrower than for DDQC-1 (section 4.3.1.3), since the design is already more specific, and 5-patch particles are not required in 6-coordinate environments.]

4.3.2.2 Preliminary testing

I simulated $N = 2002$ particles (154×13, the ratio of 5- to 6-patch particles being 12:1), for 1.212×10^7 MC cycles, in serial. I annealed over a range $\Delta T^* = 0.01$, decreasing T^* stepwise by 1×10^{-4} every 1.2×10^5 MC cycles. I repeated this protocol five times, beginning at a range of temperatures $T^*_{\text{init}} = [0.138, 0.142]$), given nucleation occurred at $T^* \approx 0.138$.

A sample configuration can be seen in Fig. 4.8. The assembled clusters showed elements of DDQC structure (alongside some defects): square-triangle tilings (including σ, H, and HCP environments), some dodecagon motifs, and some disorder. The main problem, however, was that hexagons (and dodecagons) were rare, and the dominant environment was σ; thus, visually, it did not seem that a DDQC formed. The 6-patch particles were often located at the edges of layers, and/or clumped together, and/or in 5-coordinate environments [as in Fig. 4.8(a)]. They were instead designed to form hexagons surrounded by 5-patch particles; and ideally they would spread throughout each layer. This suggests there was a lack of mixing between 5- and 6-patch particles, causing local de-mixing of σ- and HCP-environments, respectively; a large σ-phase region is circled in cyan in Fig. 4.8(a).[†]

Even when 6-patch particles did form a hexagon near the middle of a layer, these were seldom stacked correctly from layer to layer throughout the cluster. Rather, often 6-patch particles were stacked on 5-patch particles. An example is circled in magenta in Fig. 4.8(a). Three likely reasons for this stacking problem are: (1) 6-patch particles were rare (mole fraction $1/13$), and

[†] Note that some clumping of 6-patch particles also occurred for the corresponding 2D design in Ref. 3, as shown in Fig. 3(c) therein. Some such de-mixing is compatible with a DDQC, but not too much—otherwise insufficient dodecagons form.

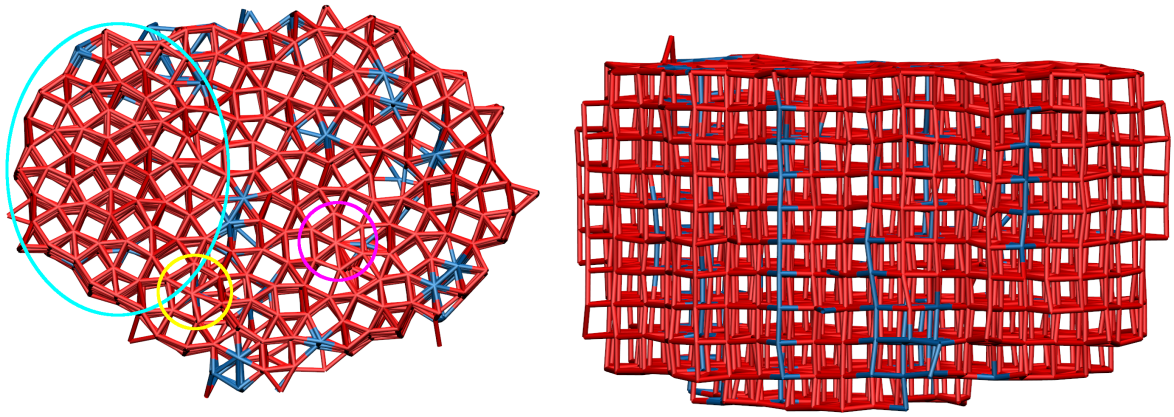

(a) Top view **(b)** Side view

Figure 4.8: Final cluster assembled for DDQC-2 design, for $N = 2002$ and $\sigma_{\text{ang}} = 0.3$ rad. Bonds are coloured by particle type [Table 4.3 and Figs. 4.2(c,d)]: red for particle type 1 (5 patches), blue for particle type 2 (6 patches). In **(a)**: a σ-phase region is circled in cyan; an example of incorrect stacking is circled in magenta [particle type varies down the axial chain, as can also be seen in **(b)**]; and an example of an HCP environment around a 5-patch rather than 6-patch particle is circled in yellow. The simulation began at $T^*_{\text{init}} = 0.142$ and is shown at $T^* = 0.132$.

so it was probabilistically difficult for them to find each other in order to stack correctly; (2) most 6-patch particles de-mixed towards the edge of layers, so were not available to stack above hexagons—thus intensifying reason (1); and (3) since there are 5 or 6 in-plane patches, but only 2 axial patches, the energetic cost of an incorrect axial bond (*i.e.* between a 5-patch and 6-patch particle) is less important than that of an incorrect in-plane bond, and particles can get stuck with incorrect axial bonds if their in-plane patches are correctly bonded. Sometimes, hexagons formed around 5-patch particles which were stacked on 6-patch particles; the structure in both layers was the same. (This is unfavourable for the central 5-patch particles, as its patches are misaligned.) An example is circled in yellow in Fig. 4.8(a). Nevertheless, incorrect stacking of patchy-particle types (or misaligned patchy bonds) is irrelevant for the cluster's structure. It is interesting—and promising, for the general goal of forming a 3D DDQC—that incorrect axial bonds are compatible with various DDQC-like planar structures. As noted in section 4.3.1.4 under 'General observations', it is not necessary that each layer of a DDQC be identical and correctly stacked.

Given the above results, I did not pursue further simulation of the DDQC-2 system. How-

ever, it still seems that this design may enable a 3D DDQC, as found in 2D [3]. The structures showed a promising degree of disorder—moreso than in many early design variations for DDQC-3 (section 4.3.3.2)—likely because of the limited patch selectivity. De-mixing of particle types was also less than in many early DDQC-3 designs: some 5- and 6-patch particles co-nucleated and so were joined from the start of cluster growth.

A further problem I observed in some simulations [not that shown in Fig. 4.8(b)] was the cluster shape: rather than the short cylinders observed for stacked σ and DDQC-1 designs, the cylinders were tall and narrow. This meant the layers were relatively small, making it more difficult to detect quasicrystalline structure within layers. A likely reason is that in-plane patches were poorly aligned (due to disorder and defects), so the energy of in-plane bonds was lower than its maximum; axial patches were better aligned. Thus growth was thermodynamically favoured in an axial direction. However, note that the problem is *not* that the design does not yield a DDQC, but rather only a practical problem of detecting DDQC structure. One solution, as discussed ahead for DDQC-3, is to weaken the strength of axial bonds.

4.3.3 Ternary design: 5-, 5-, and 6-patch particles, selective patches

4.3.3.1 Particle design

My third DDQC design was the most complex and specific: it followed the final approach in Ref. 3. The full design is given in Table 4.3, named 'DDQC-3'; the particles are pictured in Figs. 4.2(e–g). The different particle types are more specifically designed, so as to take different positions within the edge-sharing and overlapping dodecagon motifs, as signified by the colours in Figs. 4.1(e,f). Dodecagons are centred on type-3 particles. Type-2 particles are designed to form a hexagon around 6-patch particles. In edge-sharing dodecagon motifs, hexagons are joined by type-1 particles; in overlapping dodecagon motifs, hexagons are joined by additional type-2 particles.

The system has three types of particles (a *ternary* system), two with 5 in-plane patches (types

1 and 2) and one with 6 (type 3), in a ratio 6:6:1. In-plane patches are equally spaced on type-1 and -3 (6-patch) particles; but in type-2 particles they are spaced as in the stacked σ design (*i.e.* consecutively at $0, 2\pi/12, 5\pi/12, 7\pi/12, 10\pi/12$ rad). All 5 in-plane patches on type-1 particles are of the same type, and 2 in-plane patches on type-2 particles are also of that same type; all 7 of these patches attract each other equally (whether on a particle of the same or a different type). All 6 in-plane patches of type-3 particles are of the same type, and attract 1 patch on type-2 particles. These patches do *not* interact with patches on the *same* type of particle, so as to favour hetero-particle-type bonding and disfavour homo-particle-type bonding, thus promoting mixing of particle types. The remaining 2 in-plane patches of type-2 particles are of the same type and interact with each other only.[†] All types of particles have 2 additional axial patches, of distinct types from the in-plane patches and from the axial patches on other particle types.

Compared to DDQC-1 (section 4.3.1.1) and DDQC-2 (section 4.3.2.1), patch selectivity is greater, as is specificity in other ways (*e.g.* specific in-plane patch angles for particle type 2, rather than regular patch spacing). This gives greater control over particle positions in the assembled structure. However, it also risks reducing disorder (and entropy), because particles have less freedom in bonding arrangements.

As for DDQC-2, I set $\sigma_{\text{ang}} = 0.3$ rad and $\sigma_{\text{tor,lateral}} = 0.6$ rad throughout [*i.e.* I included torsional interactions, but not for axial patches ($\sigma_{\text{tor,axial}} \to \infty$)].

4.3.3.2 Preliminary testing: Tuning interaction strengths

I first simulated the DDQC-3 design with all interaction strengths equal, for $N = 832$ (since $832 = 4^3 \times 13$), in serial. Patches formed correct bonds as programmed by the design, and so particles arranged into their correct local environments (*e.g.* hexagons of type-2 particles formed around type-3 particles). Moreover, stacked layers matched each other better than for DDQC-2

[†] In the design of Ref. 3, these two patches have different types, and the different types attract each other but not themselves. Here, in a 3D system, particles are able to flip axially, meaning this distinction would be irrelevant.

(section 4.3.2.2; *i.e.* particles of the same type were almost always above and below each other in axial chains). Most likely, this is due to having *three* (rather than two) different axial patch types and greater overall selectivity: if one axial bond is incorrect, this has a knock-on effect of more incorrect in-plane bonds via the adjoined particles; so there is greater energetic incentive to ensure all axial bonds are correct.

However, as for DDQC-2 (section 4.3.2.2), HCP environments often grouped together (particle types 2 and 3), and were often at the edges of layers, leaving large areas of type-1 particles in the middle. The former formed a stacked HCP (mostly), and the latter a stacked σ-phase; thus there was de-mixing.[†]

On closer observation of the assembly kinetics, the mechanism behind this behaviour was clear: particles assembled in stages. Type-1 particles aggregated first, presumably due to entropic and kinetic reasons. Entropically, their in-plane patches are identical and all attract each other, so they have the greatest freedom (compared with any other pair of particle types) in joining with one another—the most number of possible ways of bonding. Kinetically, they are the (equal) most common particle, and have the largest number of interacting patches, so it is easier for two of their patches to find each other in simulation (than for any other pair of interacting patch types). Type-3 particles, although they also have identical in-plane patches, cannot bond with themselves; and patches on type-2 particles are highly selective. In the second assembly stage, type-2 particles gradually began to join on; as the concentration of gas-phase type-1 particles decreased, this type of bonding became more likely. Since they joined predominantly around type-1 particles, type-2 particles did not usually join in arrangements that allowed them to form hexagons around type-3 particles (*i.e.* type-2 particles were 'passivated'). In the third stage, once sufficient type-2 particles had joined, type-3 particles bonded to these; thus they were usually on the outside, and rarely found a good site to form a hexagon.

This mechanism suggests a solution: tune the interaction strengths between particles, so as

[†] Some de-mixing also occurred for the corresponding 2D design in Ref. 3, as shown in Fig. 7(c) therein. Some such de-mixing is compatible with a DDQC, but not too much—otherwise insufficient dodecagons form.

to compensate for these entropic and kinetic effects, and encourage structures to grow from the gas phase with all particle types involved. Ideally, an HCP environment of one 6-patch particle surrounded by six type-2 particles would form first. This cluster would grow by the addition of more 5-patch particles, and occasional hexagons (irregularly spaced). In what follows, I describe the effects of a range of adaptations to the interaction strength matrixs ε.[†] (Up until now, in this thesis $\varepsilon_{\alpha\beta} = 1$ for all interacting patch-type pairs α and β, and $\varepsilon_{\alpha\beta} = 0$ for all non-interacting patch-type pairs.) My goal was to tune these interaction strengths to find those that lead to successful formation of a DDQC. Most testing was performed for $N = 975 = 75 \times 13$, and some for $N = 2600 = 200 \times 13$, in serial.

General lessons. Firstly, a large difference in $\varepsilon_{\alpha\beta}$ between different patch pairs in a system is problematic. It makes assembly hierarchical: patch types with larger $\varepsilon_{\alpha\beta}$ join first, as this is more energetically favourable.[‡] While this in itself is not necessarily a problem, for the DDQC-3 design it causes poor mixing of particle types, because the stronger interactions are between an exclusive pair of particles. For example, increasing $\varepsilon_{2,2}$ (the indices '2,2' refer to the patch types in Table 4.3), favours particle type-1 to -1, type-1 to -2, and type-2 to -2 bonds, causing type-1 and -2 particles to join together first. This leaves type-3 particles to bond on the outside, unable to form hexagons. Moreover, if it is not possible to form a cluster with the same relative concentration of particle types as the system, while selectively satisfying the stronger bonds, then multiple clusters form. In practice, I found differences of $\gtrsim 20\%$ in $\varepsilon_{\alpha\beta}$ were problematic.

Secondly, more broadly speaking, adjusting $\varepsilon_{\alpha\beta}$ for particular patch pairs α, β can cause other disruptions to the assembly process and structures formed—sometimes unforeseen, sometimes unhelpful. In addition, the more complex and precise the design, the more difficult it would be to replicate experimentally. Thus, it is best to minimise the complexity and precision

[†] Note that I only adjust interaction strengths for patch types that already interact, *i.e.* I do not allow new patch interactions.

[‡] Relatedly, changing $\varepsilon_{\alpha\beta}$ also changes T^*_{melt} for patchy bonds between types α and β: T^*_{melt} is greater for stronger bonds. Thus when annealing, stronger bonds form first, and weaker bonds form at cooler temperatures.

of tuned interaction strengths.

Thirdly, the growth rate and shape and of the assembled cluster depends on the relative strengths of in-plane and axial patch interactions. If axial bonds are stronger (either due to increased axial interaction strengths, or decreased in-plane interaction strengths), the clusters grow more quickly axially than in-plane, and form taller, narrower cylinders; and vice versa. The larger the difference in $\varepsilon_{\alpha\beta}$, the stronger the effect.

Axial patches. I hoped to assemble clusters that formed cylinders wider than they were tall. Tall, narrow cylinders formed in some DDQC-2 simulations (section 4.3.2.2) and for some earlier DDQC-3 simulations. This made it harder to identify the in-plane structure—especially for an aperiodic structure like a DDQC. (But it is *not* a problem for the assembly of the correct structure.) To achiever wider cylinders, I decreased $\varepsilon_{1,1}$, $\varepsilon_{3,3}$, and $\varepsilon_{7,7}$ (*i.e.* the axial bond strengths for each particle type). This had the desired effect. A reduction in axial $\varepsilon_{\alpha\beta}$ of 5% was sufficient; significantly larger reductions led to wider cylinders, but had other effects too.

Strengthening and weakening type-2 patches. Type-2 patches (Table 4.3) join particle pairs type-1 to -1, type-1 to -2, and type-2 to -2. By *strengthening* their interaction (increasing $\varepsilon_{2,2}$), I hoped to increase the mixing of type-1 and -2 particles, and in turn to bring more 6-patch particles into the middle of each layer through their interaction with type-2 particles. However, while particle type-1 and -2 interactions were stronger, particle type-1 and -1 interactions *also* became stronger, so type-1 particles still aggregated by themselves first (perhaps even more markedly than before the interaction strength was adjusted).

Thus instead, I *weakened* $\varepsilon_{2,2}$. Type-1 particles no longer aggregated first, as desired. The relatively stronger interactions between type-2 and -3 particles meant that hexagons formed earlier, and became a part of the growing cluster (*i.e.* other particles joined around them), rather than type-3 particles bonding at a later stage on the outside. Thus, I observed less de-mixing of σ- and HCP-phases, and the presence of dodecagon motifs—both edge-sharing and overlap-

ping. I found that a reduction in $\varepsilon_{2,2}$ of roughly 10% was appropriate. Given the success of the design, I performed some preliminary tests for a much larger system, $N = 20007 = 1539 \times 13$, in parallel. Although this new design improved the structures compared to previous designs, there was room for further improvement. In particular, some de-mixing was still present, albeit to a smaller extent.

Distinguishing different type-2 patches. The above discussion suggests a further adjustment: distinguishing the patchy interactions between type-1 to -1, type-1 to -2, and type-2 to -2 particles. My goal was to increase the relative interaction strength and mixing between particle types-1 and -2, but *not* types-1 and -1 or types-2 and -2. This could only be achieved by introducing a new patch type. Thus, design DDQC-3* [Table 4.3, Figs. 4.2(h–j)] changes the two type-2 patches on type-2 particles to become type-8 patches; *both* types-2 and -8 patches attract *both* types-2 and -8 patches, but can now do this with *different* $\varepsilon_{\alpha\beta}$.[†] In this way, the strengths of the different interparticle bonds can be independently tuned.

I decreased $\varepsilon_{2,2}$ and $\varepsilon_{8,8}$ (*i.e.* between particle types-1 and -1, and types-2 and -2), but not $\varepsilon_{2,8} = \varepsilon_{8,2}$ (*i.e.* between particle types-1 and -2). This improved on the previous results: hexagons (still) formed first, and they were better spread throughout the structure—yet in a disordered manner—rather than σ-/HCP-phase de-mixing.

As an alternative with a similar effect, I kept all $\varepsilon_{\alpha\beta}$ the same except for *increasing* $\varepsilon_{2,8}$ (*i.e.* particle types-1 and -2). While this also produced a spread of hexagons through the structure, no longer did they form first. This is because, just as when I strengthened $\varepsilon_{2,2}$ for DDQC-3, the interactions between particle types-2 and -3 (*i.e.* those needed to form hexagons) were now weaker than another interaction in the system, namely between patch types 2 and 8. Thus, the latter bonds formed earlier than hexagon bonds; particles of type-2 prefer type-1 to type-3. So, fewer hexagons assembled, and this alternative approach was worse than the original.

In both approaches, a concern was that the more precisely-controlled the patchy interactions

[†] There are no further differences between designs DDQC-3 and -3*.

would lead to more regular and less disordered structures. This manifested in a prevalence of edge-sharing dodecagon motifs over overlapping motifs. For this reason, I only made a small change, $\varepsilon_{2,2} = \varepsilon_{8,8} = 0.9$.

Weakening type-6 patches. In the above adjustment, I weakened all interactions between particle types-1 and -1 (via $\varepsilon_{2,2}$). I also weakened some interactions between particle types-2 and -2 (via $\varepsilon_{8,8}$), but not all: particle types-2 and -2 are also joined by patch types-6 and -6. Thus, as a final test, I weakened $\varepsilon_{6,6}$. While this also yielded good structures, with mixing of particle types and disordered arrangements of hexagons, it also disfavoured overlapping dodecagon motifs [Fig. 4.1(f)], in which bonds between particle types-2 and -2 are more common. Therefore, I did not retain this adjustment.

Conclusions. There were promising signs for a DDQC in the initial DDQC-3 design with all interaction strengths equal. However, fine-tuning the interaction strengths gave greater control over the assembled structure. The most promising design was DDQC-3*, with $\varepsilon_{2,2} = \varepsilon_{8,8} = 0.9$ (*i.e.* bonds between particle types-1 and -1 and types-2 and -2 weakened), and $\varepsilon_{1,1} = \varepsilon_{3,3} = \varepsilon_{7,7} = 0.95$ (*i.e.* axial bonds weakened), and all other bond strengths unchanged ($\varepsilon_{2,8} = \varepsilon_{8,2} = \varepsilon_{4,5} = \varepsilon_{5,4} = \varepsilon_{6,6} = 1$, and $\varepsilon_{\alpha\beta} = 0$ for all other α, β).

4.3.3.3 Production runs

Methods. Using the DDQC-3* design just described (Table 4.3), I simulated systems of $N = 20007 = 1359 \times 13$ particles, in parallel. I repeated the protocol four times, each time beginning from a different random configuration, and at a slightly different temperature: $T^*_{\text{init}} = [0.127, 0.13]$. The (continuous) annealing rate was 5×10^{-5} per 10^5 MC cycles. I ended simulations once the structure (and total energy) was relatively constant, usually at $T^* \approx 0.125$. So the total number of MC cycles varied between simulations, from 2.5×10^6 to 5.5×10^6, as did the

temperature range, $0.0015 \lesssim \Delta T^* \lesssim 0.0035$.[†]

General observations. Self-assembly snapshots for one simulation can be seen in Fig. 4.9. I observed nucleation at $T^* \approx 0.127$. Nucleation typically began with the formation of a hexagon—a 6-patch particle surrounded by six type-2 particles—as in Fig. 4.9(a). Typically, this nucleus did not grow for a significant period; the snapshot in Fig. 4.9(b) shows an unchanged nucleus. (The hexagon nuclei were in equilibrium with the gas phase; sometimes they broke apart, and/or sometimes—but rarely—others formed.) Eventually, type-2 and -1 particles then grew from the hexagon, and more hexagons were incorporated [Fig. 4.9(c)]. Cluster growth was then rapid: the snapshots in Figs. 4.9(c–f) were taken at short intervals. During growth, layers extended outwards simultaneously with new layers forming. As for the DDQC-1 simulations (section 4.3.1.4), the final configurations [Fig. 4.9(f)] contained some gas-phase particles in equilibrium with the cluster.

Final clusters were typically quasi-cylindrical, relatively isotropic in the plane, but shaped randomly. They were wider than they were tall; clusters had around 20 layers (of 1000 particles), compared to around 25 layers for DDQC-1 (of 800 particles). This is due to the weaker axial bond strengths I used, to allow easier structural identification. Multiple nucleation was rare, and secondary nuclei were usually absorbed into the main cluster very early on, rather than forming distinct, large clusters themselves. Unlike for the DDQC-1 design with wider patches, layers were neatly stacked and hardly bent, allowing one to see down interstices through the whole structure [Fig. 4.9(f)]. De-mixing was minimal; in particular, type-2 and -3 particles were spread across the cluster, not concentrated at the edges of layers.

A final configuration is shown in Fig. 4.10, for the same simulation as in Fig. 4.9. Given the clear ordering, especially between layers, it is easy to see the prevalence of square-triangle

[†] The 2D DDQC patchy-particle simulations of multiple particle types [3] used exchange moves, to speed up equilibration between the different types. I did not; it was not necessary, because I formed clusters from a low-density gas, so particles were able to move around more easily (the aforementioned simulations were at higher density, forming an extended phase spanning the simulation box).

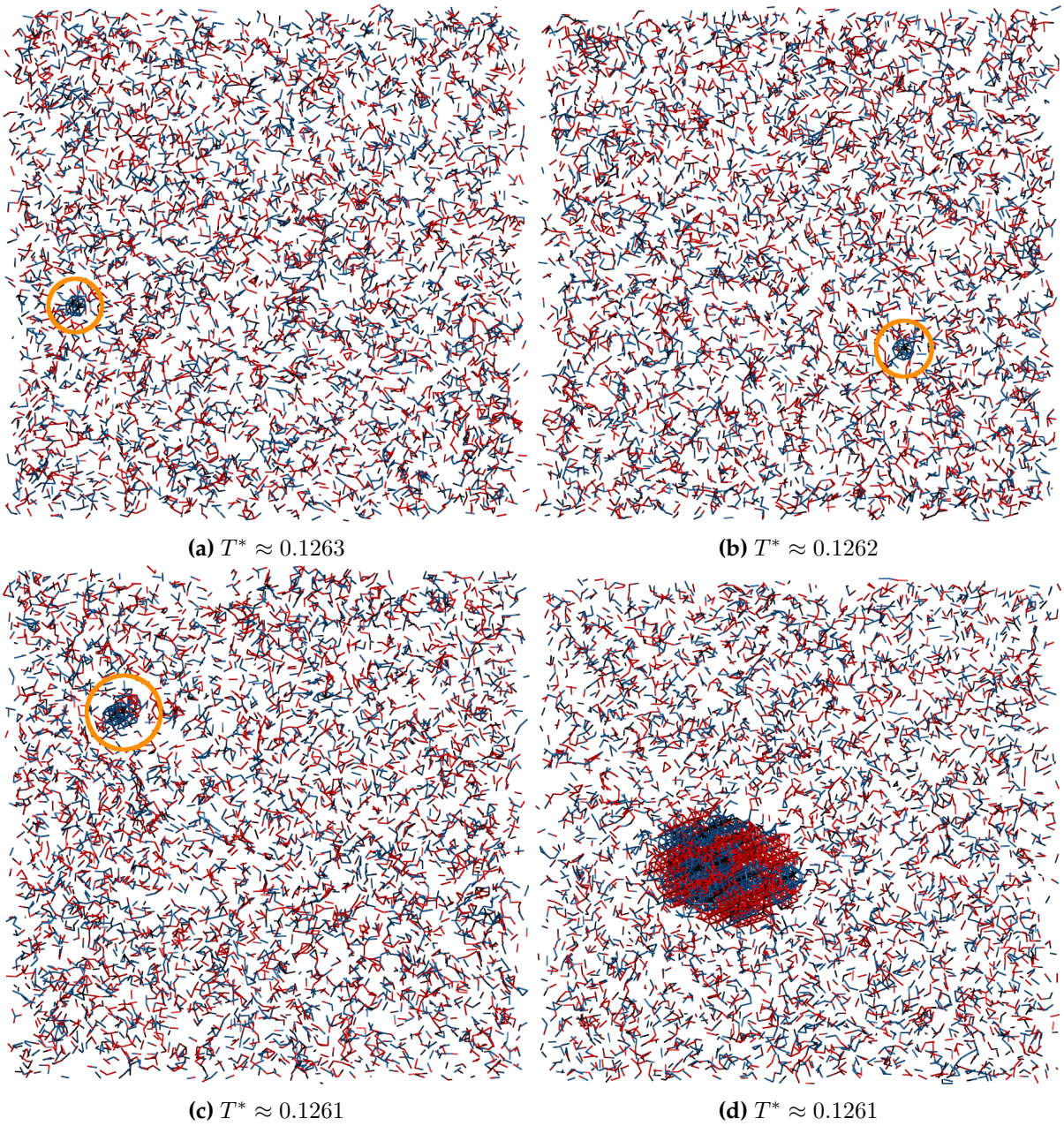

(a) $T^* \approx 0.1263$ **(b)** $T^* \approx 0.1262$

(c) $T^* \approx 0.1261$ **(d)** $T^* \approx 0.1261$

Figure 4.9: Simulation snapshots showing self-assembly for the DDQC-3* design, for $N = 20007$ and $\sigma_{\text{ang}} = 0.3$ rad, for simulation beginning at T^*_{init} 0.127. Bonds are coloured by particle type [Table 4.3 and Figs. 4.2(h–j)]: red for type 1 (5 patches), blue for type 2 (5 patches), black for type 3 (6 patches). **(a)** nucleation of a hexagon; **(b)** the nucleus has still not grown after a further 3.6×10^5 MC cycles ($\Delta T^* = 0.00018$); **(c)** cluster growth begins; and **(d)** growth proceeds rapidly, with hexagons incorporated into the cluster. *(Continued on next page.)*

patterns; σ, H, and HCP environments are all present. HCP environments were common, as were DDQC dodecagon motifs, both edge-sharing and overlapping. Nonetheless, there were signs of disorder essential to DDQCs, for example in the irregular spacing of the two dodecagon motifs. Further discussion of the structures formed, including characterisation via diffraction,

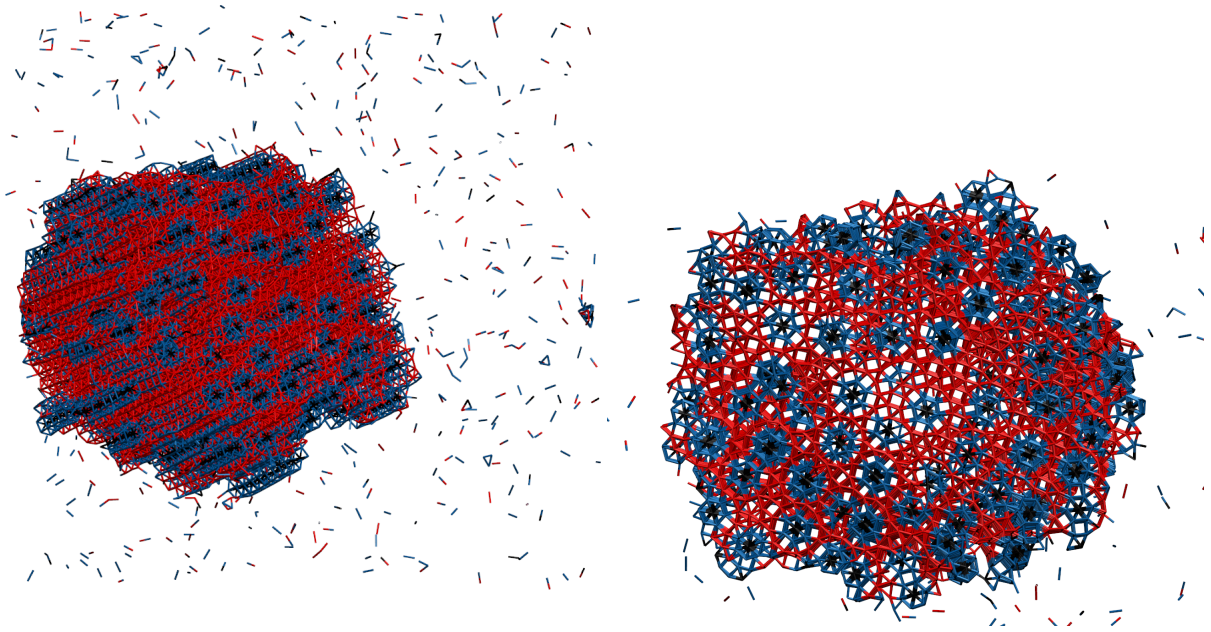

(e) $T^* \approx 0.1260$ **(f)** $T^* \approx 0.1259$

Figure 4.9: *(Continued from previous page.)* **(e)** Cluster growth continues rapidly [only 4.2×10^5 MC cycles ($\Delta T^* = 0.00021$) have passed since snapshot **(b)**], and **(f)** cluster is almost fully assembled (rotated for clear viewing of structure).

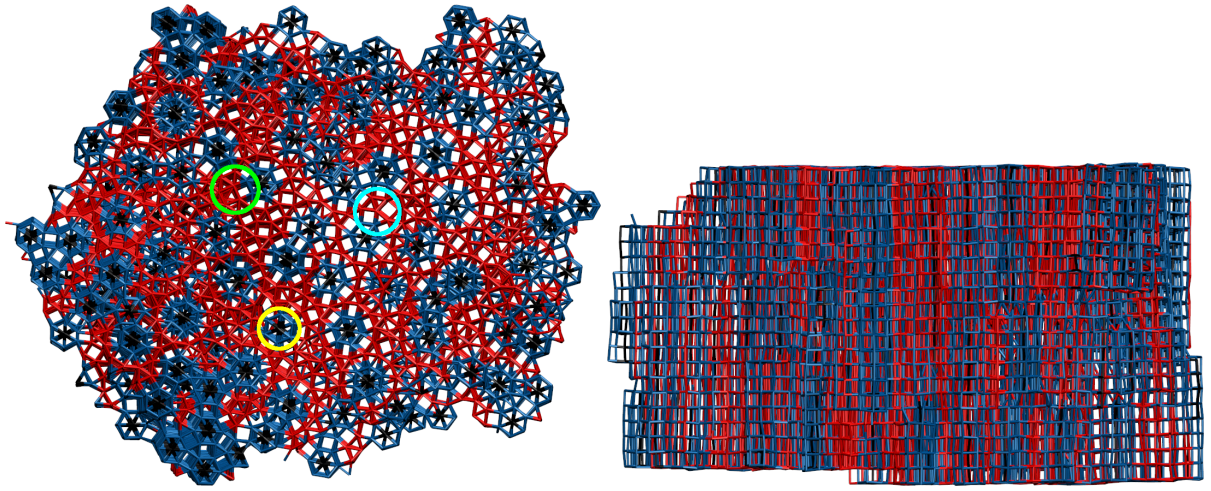

(a) Top view **(b)** Side view

Figure 4.10: Final cluster assembled for DDQC-3* design, for $N = 20007$ and $\sigma_{\text{ang}} = 0.3$ rad. Bonds are coloured by particle type [Table 4.3 and Figs. 4.2(h–j)]: red for type 1 (5 patches), blue for type 2 (5 patches), black for type 3 (6 patches). In **(a)**: an example σ environment is circled in cyan, an H environment in green, and an HCP environment in yellow. The simulation began at $T^*_{\text{init}} = 0.127$ and is shown at $T^* \approx 0.1255$. Gas-phase particles have been removed.

is immediately ahead in section 4.3.4.

4.3.4 Detecting quasicrystallinity: Diffraction patterns

The clusters I assembled were clearly periodic (approximately) in the axial direction, as shown by their distinct, regular layers. The structures of each layer were similar or identical, as seen by the alignment of particles and interstices when looking through the planes. Visually, the layers seemed to be arranged as DDQCs; at the least, they contained quasicrystalline motifs. However, quasicrystalline structure cannot be confirmed visually. QCs are not translationally periodic, and it is difficult to determine whether a structure repeats over long length scales. In addition, detecting orientational order—and thus distinguishing a QC from a random square-triangle tiling (which is orientationally disordered)—is difficult visually.[†] The most common way of detecting quasicrystallinity in a physical sample is measuring its Bragg diffraction pattern, which reveals orientational order. QCs are orientationally ordered, so display sharp Bragg peaks at particular angles. Yet they have rotational symmetries forbidden to periodic crystals (*i.e.* symmetries other than 2-, 3-, 4-, and 6-fold rotations; section 4.1.1), so can be distinguished from periodic crystals. The equivalent detection method in simulations is to calculate the structure factor.

In this section, I introduce the structure factor (section 4.3.4.1), explain how I calculated it (section 4.3.4.2), and then present and discuss the structure factors calculated for my systems (section 4.3.4.3).

4.3.4.1 Background

In *Bragg diffraction*, incident waves (electromagnetic or wave-particles, *e.g.* neutrons, of a sufficiently small wavelength) are scattered by the particles in a sample material [397]. The scattered waves interfere with each other (constructively or destructively) according to their phase differences, and are detected. The interference pattern depends on the relative positions of the parti-

[†] Indeed, both in experiment and simulation, many assembled structures have been thought to be QCs, but later discovered to simply have large unit cells, or to be random tilings.

cles as well as their relative scattering powers (*i.e.* the intensity of their scattered waves). Thus, the diffraction pattern reveals features of the structure. Ordered structures give sharp *Bragg peaks* in the pattern, whereas disordered structures give diffuse patterns, because scattering is essentially random.

The (static, or geometric) *structure factor*, $S(\mathbf{q})$, mathematically describes the amplitude and phase of wave scattering from a structure (via a Fourier transform of the radial distribution function) [397]:

$$S(\mathbf{q}) = \frac{1}{N_{\text{clu}}} \sum_{j}^{N_{\text{clu}}} \sum_{k}^{N_{\text{clu}}} \exp\left[-2\pi i \mathbf{q} \cdot (\mathbf{r}_j - \mathbf{r}_k)\right]. \tag{4.1}$$

$\mathbf{q} = (q_x, q_y, q_z)$ is the scattering wave vector (in units of inverse length),[†] N_{clu} is the number of particles in the cluster (so if not all N particles in the system joined the cluster, then $N_{\text{clu}} \neq N$), and $\mathbf{r}_j$ is the position of particle j. Equation 4.1 calculates the net scattered intensity at an angle given by $\mathbf{q}$, based on the relative positions of particles ($\mathbf{r}_j - \mathbf{r}_k$), by summing the contribution from each pair of particles (and dividing by the total number of particles) [397]. It assumes that particles are identical, that scattering is weak, and that absorption, refraction, and multiple scattering events are negligible. The structure factor is directly related to the diffraction pattern: specifically, the *positions* of peaks are the same, but the *amplitudes* (intensities) may not be.

For a 3D structure, a 2D structure factor is calculated by projecting the arrangement of particles onto a 2D plane, in a specified direction (typically of high symmetry) [398].

4.3.4.2 Methods

Before calculating the structure factor for a cluster assembled in my simulations, I first removed all gas-phase particles. I then rotated the cluster so that the average direction of all axial patches (which point in the periodic direction) is aligned in the z-direction. Note that the axial patches of the rotated particles are not all perfectly aligned, because of thermal noise: different particles have slightly different orientations, and the cluster has bent layers. Nonetheless it was sufficient

[†] Specifically, $\mathbf{q} \equiv \mathbf{k}_{\text{scat}} - \mathbf{k}_{\text{inc}}$, where $\mathbf{k}_{\text{scat}}$ and $\mathbf{k}_{\text{inc}}$ are respectively the scattered and incident wave vectors. Note that often $\mathbf{q}$ is defined with a factor 2π included, but I instead include the factor 2π explicitly in Eq. 4.1.

for my purposes. All layers are thus projected together onto the x, y-plane; *i.e.* I calculate $S(\mathbf{q})$ for $\mathbf{q} = (q_x, q_y, 0)$. I then shifted the cluster's centre of mass to the middle of the simulation box.

Rather than calculating $S(\mathbf{q})$ as in Eq. 4.1, it is sufficient to calculate only its real part:

$$\mathrm{Re}[S(\mathbf{q})] = \frac{1}{N_{\mathrm{clu}}} \sum_{i}^{N_{\mathrm{clu}}} \sum_{j}^{N_{\mathrm{clu}}} \cos\left[2\pi\mathbf{q} \cdot (\mathbf{r}_i - \mathbf{r}_j)\right]. \tag{4.2}$$

[The negative exponential operand in Eq. 4.1 has become positive within the cosine, because $\cos(x) = \cos(-x)$.] The calculation of $\mathrm{Re}[S(\mathbf{q})]$ can be simplified because: (1) if $i = j$, then $\mathbf{r}_i - \mathbf{r}_j = 0$ and thus $\cos\left[2\pi\mathbf{q} \cdot (\mathbf{r}_i - \mathbf{r}_j)\right] = 1$; (2) $\cos\left[2\pi\mathbf{q} \cdot (\mathbf{r}_i - \mathbf{r}_j)\right] = \cos\left[2\pi\mathbf{q} \cdot (\mathbf{r}_j - \mathbf{r}_i)\right]$; and (3) $\cos\left[2\pi(q_x, q_y) \cdot (\mathbf{r}_i - \mathbf{r}_j)\right] = \cos\left[2\pi(-q_x, -q_y) \cdot (\mathbf{r}_i - \mathbf{r}_j)\right]$. [(2) and (3) depend on the aforementioned symmetry of the cosine function.] I calculated a grid of values for $\mathrm{Re}[S(\mathbf{q})]$, spaced at $\Delta q_x = \Delta q_y = 0.02\ \sigma_{\mathrm{LJ}}^{-1}$ (and in some cases for $\Delta q_x = \Delta q_y = 0.01, 0.04, 0.08\ \sigma_{\mathrm{LJ}}^{-1}$).

Some other simulation studies (*e.g.* that on non-patchy, IQCs [349]) quench the system to $T \approx 0$ before calculating the structure factor. This removes thermal noise in particle vibrations, producing a more ordered structure and sharper diffraction peaks. Sometimes (*e.g.* [349]) structure factors are averaged over a number of configurations, again to produce clearer diffraction patterns by eliminating noise. But the phase of a QC can change during a simulation, and if so, the configurations will be uncorrelated; this would yield diffuse peaks or even a uniform pattern. I did not find either technique necessary; my diffraction patterns were clear enough for my purposes.

4.3.4.3 Results

Examples of the calculated structure factors are shown in Fig. 4.11. For both the DDQC-1 and -3* designs, the patterns have the distinctive 12-fold rotational symmetry of DDQCs, which is forbidden in periodic crystals and thus indicates quasicrystallinity (if it occurs along with sharp peaks, which indicate long-range order). However, pseudo-12-fold symmetry may arise from: the presence of approximants; multiple domains in different orientations, each with 3-, 4-, or 6-

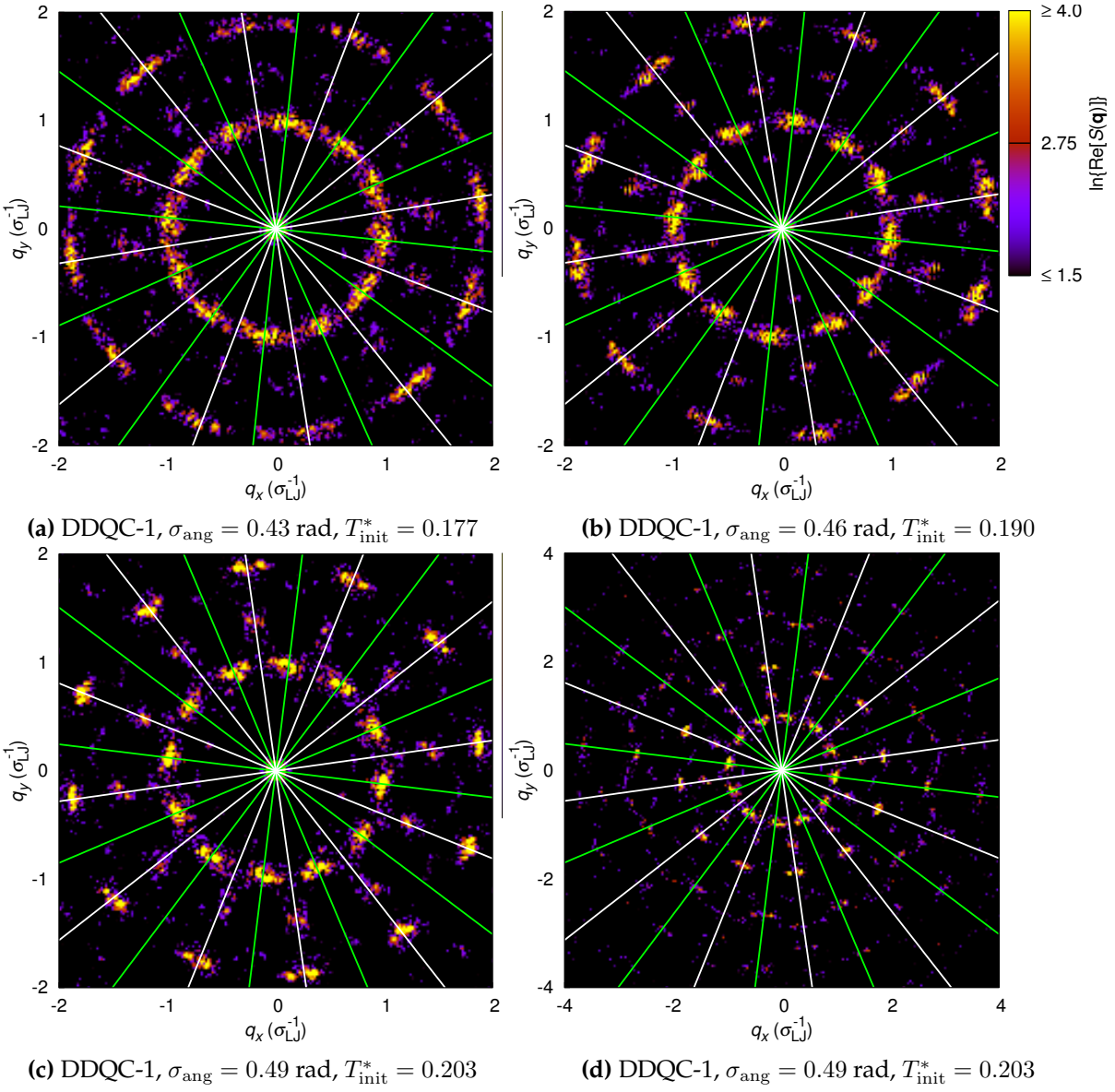

(a) DDQC-1, $\sigma_{\mathrm{ang}} = 0.43$ rad, $T^*_{\mathrm{init}} = 0.177$

(b) DDQC-1, $\sigma_{\mathrm{ang}} = 0.46$ rad, $T^*_{\mathrm{init}} = 0.190$

(c) DDQC-1, $\sigma_{\mathrm{ang}} = 0.49$ rad, $T^*_{\mathrm{init}} = 0.203$

(d) DDQC-1, $\sigma_{\mathrm{ang}} = 0.49$ rad, $T^*_{\mathrm{init}} = 0.203$

Figure 4.11: Diffraction patterns for final structures, calculated as described in text. **(c)** and **(d)** correspond to the cluster in Figs. 4.5(e,f), and show different ranges of $\mathbf{q}$ for the same system. Adjacent green lines are angled at $\pi/6$ rad, as are adjacent white lines; adjacent green and white lines are angled at $\pi/12$ rad. Green lines pass through peaks in the inner ring, and white lines through peaks in the second ring. The colour key for all plots is shown to the right of (b). *(Continued on next page.)*

fold symmetry; or random square-triangle tilings with most bonds in 12 symmetric directions. So it is important to carefully check these patterns [398]. While the Bragg peaks show some breadth, this is to be expected. It is due to: thermal noise (I did not quench my structures; section 4.3.4.2); screw dislocations (section 4.3.5) and other defects; small clusters (around 900 particles per layer); using one configuration rather than averaging over multiple (section 4.3.4.2); and disorder between layers. I overlaid the patterns with lines angled at $2\pi/12$ rad to each other

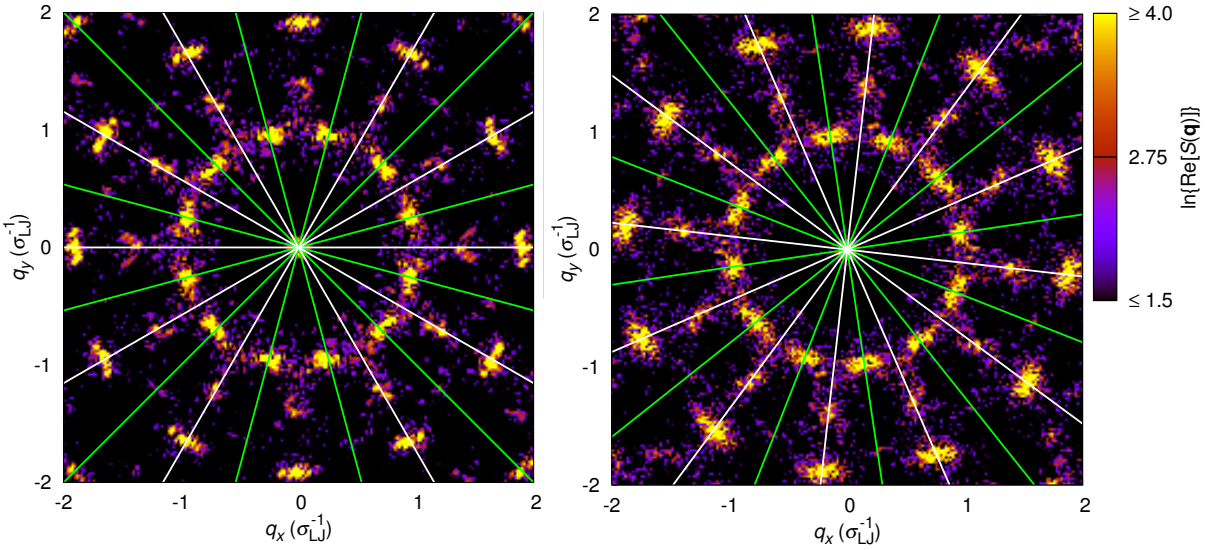

(e) DDQC-1, $\sigma_{\mathrm{ang}} = 0.52$ rad, $T^*_{\mathrm{init}} = 0.216$

(f) DDQC-3*, $\sigma_{\mathrm{ang}} = 0.3$ rad, $T^*_{\mathrm{init}} = 0.128$

Figure 4.11: *(Continued from previous page.)*

(green for inner ring, white for second ring), which demonstrates that the peaks are indeed aligned with 12-fold symmetry. The inner ring is positioned at $\|\mathbf{q}\| \approx 0.89\ \sigma_{\mathrm{LJ}}^{-1}$, corresponding to $r_{ij} \approx 1.122\sigma_{\mathrm{LJ}} \approx 2^{1/6}\sigma_{\mathrm{LJ}}$, *i.e.* the LJ minimum and nearest-neighbour bond length. The diffraction patterns are inflationary: *i.e.* peaks in the same direction are positioned at distances from the origin in reciprocal space of $d, dl, dl^2, \ldots$ for some constants d and l (here $d \approx 0.89\ \sigma_{\mathrm{LJ}}^{-1}$). [This is best seen in Fig. 4.11(d).] This is characteristic of a QC structure, which is inflationary and translationally aperiodic.

4.3.5 Screw dislocations

I observed an unexpected and interesting phenomenon in numerous simulations: screw dislocations. In this section, I first introduce screw dislocations (section 4.3.5.1), and then describe and discuss my observations (section 4.3.5.2).

4.3.5.1 Background

A *screw dislocation* is a type of crystallographic defect, specifically a *line defect* (or *dislocation*); the other type of line defect is an edge dislocation [397,398]. A screw dislocation is pictured in Fig. 4.12(a). One can imagine generating a screw dislocation as follows: (1) take a vertical cut,

perpendicular to the stacked layers of a crystal [the *slip plane*; shaded red in Fig. 4.12(a)]; (2) draw a line down the slip plane [again, perpendicular to the layers; this is the *dislocation line*; dashed red in Fig. 4.12(a)]; (3) on one side of the slip plane and one side of the dislocation line, slip the structure up by one layer (*i.e.* by the inter-layer lattice vector) to join with the next layer up on the other side of the plane (without breaking any bonds on the original side of the plane).[†] Thus, moving around the dislocation line (and perpendicular to it) between adjacent particles, one traces a helix rather than a closed loop. A screw dislocation is characterised by the *Burgers vector* [marked by a red arrow in Fig. 4.12(a)], which is the vector between the start and end of the trace as one completes a single circuit [the *Burgers circuit*; marked purple in Fig. 4.12(a)] of this helix around the dislocation line.[‡] In the simplest case, the Burgers vector is just the inter-layer lattice vector (parallel to the dislocation line), because one moves up one plane after tracing one Burgers circuit.

In a perfect screw dislocation, the dislocation line is single, straight, and persistent throughout the whole structure; but in real (imperfect) systems, it can bend (change direction and/or position within the structure), fork (split), and annihilate (end, when two opposite dislocations meet) [563]. Further, a screw dislocation can move over time through a cluster; if it moves to the edge of the cluster it is destroyed.

Screw dislocations (like all defects) are thermodynamically unfavourable in crystals, because they cause strain around the dislocation line (where the layers deform), break the regular structure, and prevent some particles from occupying their preferred local environments. They often arise because they are kinetically favourable during crystal growth [398,564–566]. A growing screw dislocation involves a step [or ledge; Fig. 4.12(a)], from the dislocation line outwards to the edge of the structure. Growth occurs from the ledge to cover the layer below. The ledge is always present—never destroyed, continually regenerating—because as each particle adds,

[†] The slip could in fact be two or more layers; I only describe the simplest case.

[‡] More precisely: in a crystal with no dislocation, trace a closed circuit on a plane around the position where the dislocation line will be introduced, noting the number of lattice points moved in each direction. Then, introduce the screw dislocation, and trace the same number of steps along the (distorted) lattice in each direction. The latter trace is not closed; the vector from the start to the end of the trace is the Burgers vector.

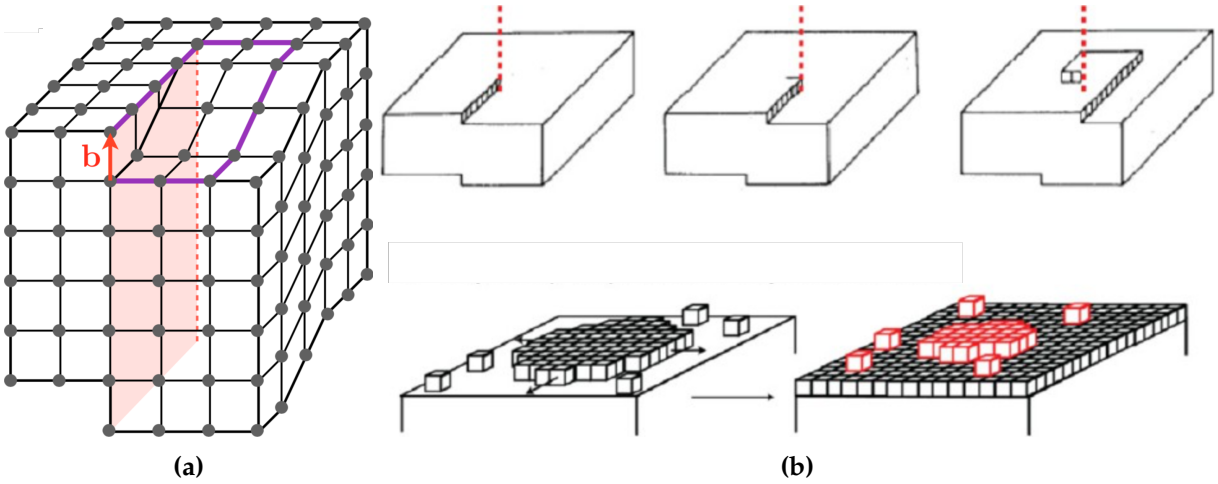

Figure 4.12: **(a)** Depiction of a screw dislocation in a periodic crystal. Grey circles are positioned at the lattice points. The dashed red line represents the screw dislocation line. The red arrow marked **b** shows the Burgers vector, obtained from the difference between the start and end points of the purple path (which would be closed if no dislocation were present). The coloured area (pale red) represents the slip plane; the layers on either side have slipped vertically from each other by one lattice vector. Growth occurs from the step/ledge on top (anticlockwise around the dislocation line, when viewed from above.) Reprinted with permission from Ref. 562, © of the author. **(b)** Comparison of growth from the ledge of a screw dislocation (top) with growth from the addition of a new layer to a defect-free periodic crystal (bottom). Reprinted with permission from Ref. 562, © American Chemical Society.

the ledge propagates around the dislocation line. Compare two scenarios [Fig. 4.12(b)]: (1) a particle adds to the flat surface of a crystal layer, nucleating a new layer; and (2) a particle adds to a screw dislocation ledge. The former is energetically costly and thus kinetically slow: the particle can form a bond in only one direction, so is therefore weakly bound and easily breaks off; it is unlikely to remain until further particles can join on and stabilise the new layer. The latter is less energetically costly and thus quicker: a particle can bond in at least two directions at a screw ledge, and so binds more strongly and is more likely to remain in place until further particles add. In this way, a screw ledge acts like a seed for growth. The structure grows from the ledge, proceeding in a helix [while also growing outwards from the dislocation line; Fig. 4.12(b)]. There is never a need to nucleate a new layer. Because screw dislocations catalyse crystal growth, they are especially common at low supersaturation, and in structures with slow growth rates.

Screw dislocations (like other defects) are not simply of theoretical interest; they affect es-

sentially all material properties, sometimes significantly. In particular, they may affect photonic properties [567–571]. Thus, the presence of screw dislocations in QCs (and other PBG structures) could be significant. To some extent, it is possible to control the presence and positions of dislocations, and thus to control material properties [563]. Dislocations have been studied in systems of colloids and NPs, and shown to play important roles such as to rationally drive crystal growth of desired materials [566,572,573].

Screw dislocations in quasicrystals. Since the definitions relating to dislocations, including those above, were originally made for periodic crystals, they do not all hold for QCs [398,563]. For example, while it is simple to define a Burgers circuit around a lattice plane for a periodic crystal, by following a series the lattice vectors, this is not possible for a QC, which does not have (3D) lattice vectors. Nonetheless, the definitions have been adapted for QCs, by making use of QC symmetry in higher dimensions [398,563].[†] The details of the definitions and characterisation of QC screw dislocations are not essential for my purposes.[‡] I seek only a qualitative understanding of the growth and structure of QCs. The appearance and behaviour of screw dislocations is similar in QCs to that in periodic crystals, so observation of the dislocations is sufficient, alongside the above definitions. Furthermore, in my DDQCs the Burgers vector is always in the crystalline direction. Thus, even though the Burgers circuit is not well-defined, the plane on which it is formed *is* well-defined. This makes the screw dislocations easy to observe.

As far as I am aware, there are no reports of screw dislocations in a QC, either in experiment or simulation. They have been studied analytically in only a few, simple cases [*e.g.* one-dimensional (1D) hexagonal QCs [578–581]]. I am also not aware of screw dislocations forming in any previous patchy-particle simulations; although this is unsurprising, given there have been limited 3D patchy-particle studies (section 1.3.2).

[†] For example, while the Burgers vector for periodic crystals is three-dimensional, for 8- or 12-fold QCs it is four-dimensional, and for IQCs it is six-dimensional.

[‡] See Refs. 560,561,568,569,574–576 for theoretical discussion, and Refs. 571,577 for experimental discussion, of dislocations in QCs. Unfortunately, most discussion is on edge dislocations rather than screws.

4.3.5.2 Observations and discussion

I observed screw dislocations in most simulations for the DDQC-1 design (including all for $\sigma_{\text{ang}} = 0.43, 0.46$ rad). To check the veracity of this phenomenon, I repeated some simulations from different starting configurations; screw dislocations still arose.[†] Given how consistent they were, they seemed to be a likely product of the DDQC-1 system, rather than occurring by chance only under specific conditions (the formation of defects is stochastic). Thus they may be physically favourable. However, I observed no screw dislocations for the DDQC-3 or -3* designs (or DDQC-2).

Usually, I easily detected screw dislocations visually, by their characteristic growth ledges [Fig. 4.12(a)]. For further clarity, I quenched the systems, to remove thermal noise and to allow particles to settle into a more ordered, favourable configuration (but without rearranging and removing the dislocation). To do this, I simulated at $T^* = 0.01$ for 5×10^5 MC cycles (without annealing); the configurations and energies were constant well before the end of these simulations. Furthermore, I coloured particles according to their energies, so as to identify those with higher energy (under more strain due to the dislocation). Finally, I cut through the interior of the structures (at various angles) so as to visualise the dislocation lines. Example screw dislocations for DDQC-1 systems are shown in Figs. 4.13, 4.14, 4.15, and 4.16.

Screw dislocations are visible by a ledge at the surface and a dislocation line. Characteristically, particles along the dislocation line have higher energy, because the layers have slipped and the particles on either side join at different (unfavourable) angles; there is strain in the system. Thus, patches are misaligned. Particles along the ledge have even higher energies: as well as having misaligned patches, they are bonded to fewer particles. Note, however, that other high-energy particles are present: (1) surface particles, especially those at facets, inherently have higher energies due to fewer patchy bonds; and (2) other defects are present in each

[†] Specifically, I simulated for $\sigma_{\text{ang}} = 0.43$ rad from $T^*_{\text{init}} = 0.178, 0.176$, and $\sigma_{\text{ang}} = 0.46$ rad from $T^*_{\text{init}} = 0.19, 0.189, 0.188$, over $\Delta T^* = 0.0016$ for 1.5×10^6 MC cycles at the original annealing rate (1.07×10^{-4} per 10^5 MC cycles).

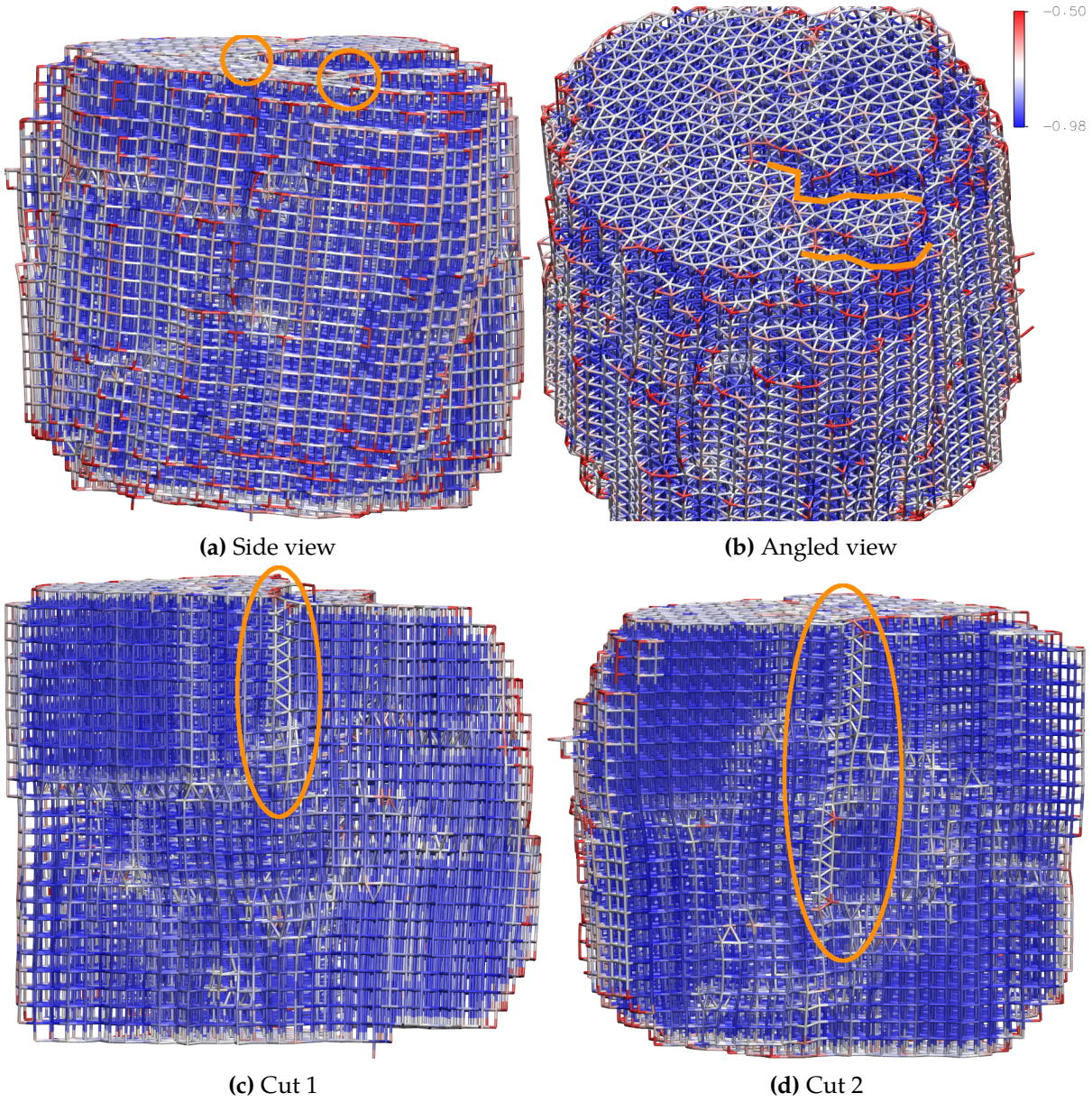

(a) Side view **(b)** Angled view

(c) Cut 1 **(d)** Cut 2

Figure 4.13: Screw dislocations in final cluster assembled for DDQC-1 design, for $N = 20000$, $\sigma_{\text{ang}} = 0.43$ rad, and $T^*_{\text{init}} = 0.177$. Bonds are coloured by particle energy. [Energy per particle is in reduced units, ϵ_{LJ}, and scaled (divided) by the number of patches (7) per particle, such that -1 is the lowest possible value.[a] The energy scale is shown as an inset above (b), with higher energy in red and lower energy in blue.] The system has been quenched, and (most) gas-phase particles have been removed. In **(a)**, two distinct dislocation lines at the surface are circled. In **(b)**, the paths of the screw ledges are marked—they are above the orange lines, as shown by the higher-energy particles. **(c,d)** show cuts through the cluster, from two directions, circling the (same) dislocation line in the interior of the cluster. Particles along the dislocation line have higher energy than those around them, because their in-plane bonds are misaligned due to the dislocation, as can be seen. The dislocation line is not straight throughout the structure, and thus cannot be seen from top to bottom in one cut.

[a] Scaling the energy is important for comparison between particles in systems that contain particles with different numbers of patches, such as for the DDQC-3 or -3* designs.

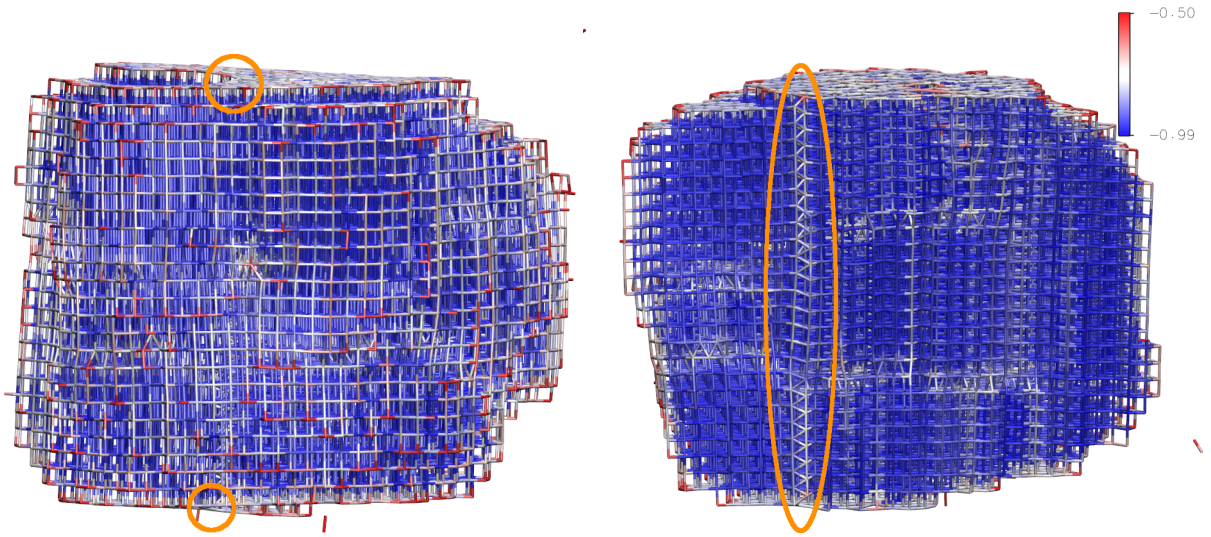

(a) Side view **(b)** Cut

Figure 4.14: Screw dislocation in final cluster assembled for DDQC-1 design, for $N = 20000$, $\sigma_{\text{ang}} = 0.46$ rad, and $T^*_{\text{init}} = 0.191$. Bonds are coloured by particle energy. [The energy scale is shown as an inset above (b).] **(a)** circles the dislocation line at the surface, on both ends. **(b)** shows a cut through the cluster, circling the dislocation line, which can be seen from top to bottom. For further details and comments, see the caption of Fig. 4.13.

structure.[†] Screw dislocations usually bend within the structure, so cannot be seen in entirety in one cut [Figs. 4.14(b) and 4.15(b) are exceptions]; sometimes they are destroyed by another defect (*e.g.* Fig. 4.17). In some cases (*e.g.* Fig. 4.13), two distinct screw dislocations are present. In some cases, the screw dislocation slips two rather than one crystal layer.

The presence of screw dislocations raises a number of questions and points of interest. In what follows, I address these one by one. The ultimate goal is to understand why and how screw dislocations form. Note that, alongside screw dislocations (and in simulations with no screw dislocations), I also observed other defects, such as vacancies (1D), edge dislocations (2D), and grain boundaries (3D); these are, however, more common and of less interest.

Why do screw dislocations form for DDQC-1 but not DDQC-3 or -3*? There are likely two reasons. Firstly, in my DDQC-3 and -3* designs, the patch width was far narrower ($\sigma_{\text{ang}} = 0.3$ rad) than in my DDQC-1 design ($\sigma_{\text{ang}} = 0.43, 0.46, 0.49, 0.52$ rad). Wider patches are compatible with greater structural strain (*i.e.* misalignment). Specifically, where the layers deform

[†] One could add that (3) there is still some thermal noise, so particles have vibrated from their preferred positions. However this is negligible for $T^* = 0.01$.

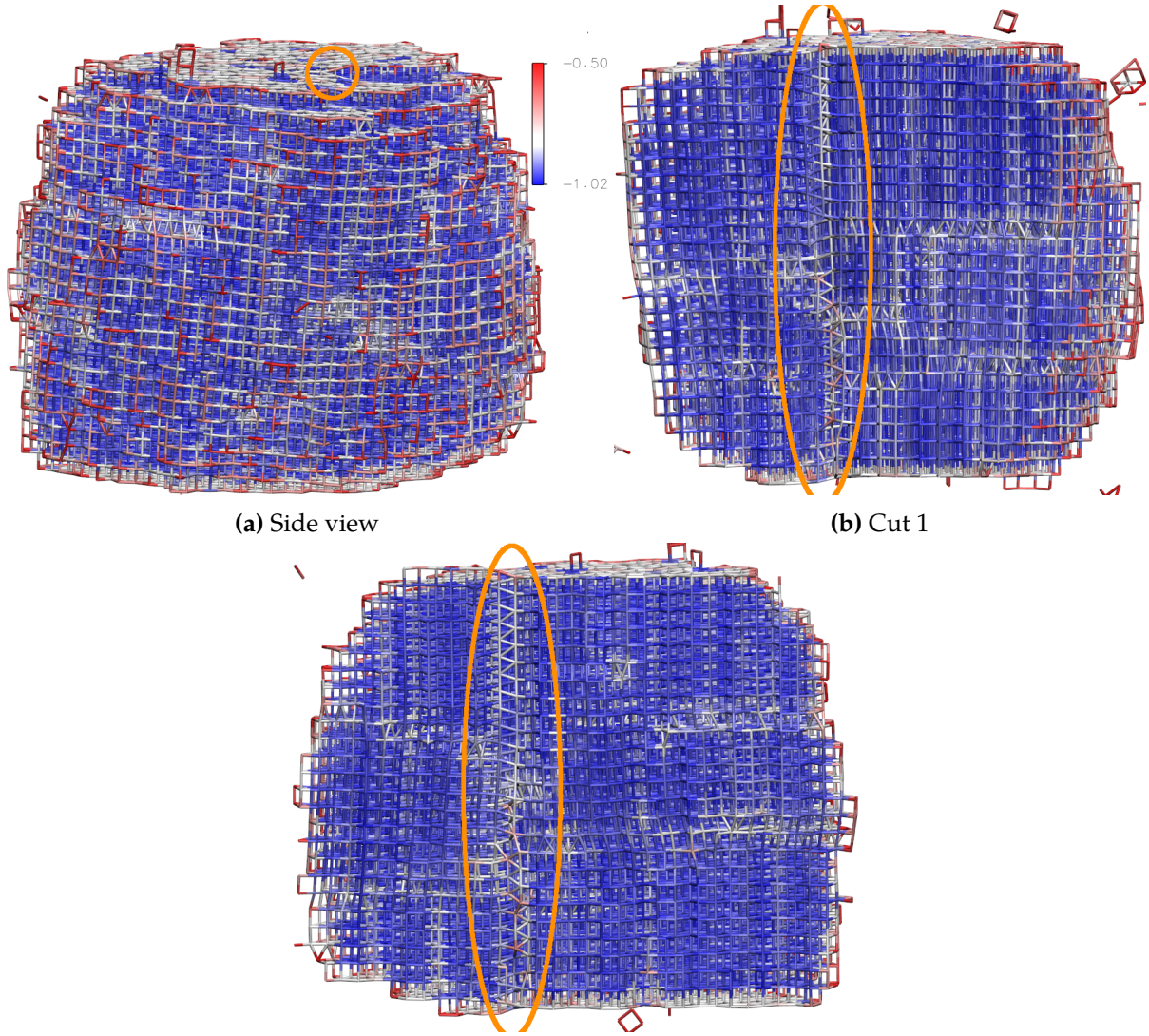

(a) Side view **(b)** Cut 1

(c) Cut 2

Figure 4.15: Screw dislocation in final cluster assembled for DDQC-1 design, for $N = 20000$, $\sigma_{\text{ang}} = 0.49$ rad, and $T^*_{\text{init}} = 0.204$. Bonds are coloured by particle energy. [The energy scale is shown as an inset above (a).] In **(a)**, a dislocation line at the surface is circled. **(b,c)** show cuts through the cluster, from two directions, circling the (same) dislocation line in the interior of the cluster. The dislocation line can be seen from top to bottom. For further details and comments, see the caption of Fig. 4.13.

(bend) around the screw dislocation line, the energetic cost is lower for wider patches. There is a trade-off between the dislocation's energetic cost and its kinetic benefit (faster formation), and it seems the preference changes between $\sigma_{\text{ang}} = 0.3$ rad and $\sigma_{\text{ang}} = 0.43$ rad. To confirm this reason, I performed simulations for large systems with my DDQC-1 design, but with $\sigma_{\text{ang}} = 0.3$ rad ($N = 20000$, in parallel, 7×10^6 MC cycles over the temperature range $\Delta T^* = 0.01$, beginning from $T^*_{\text{init}} = 0.135, 0.14, 0.145$, at an annealing rate 1.43×10^{-4} per 10^5 MC cycles). I observed no

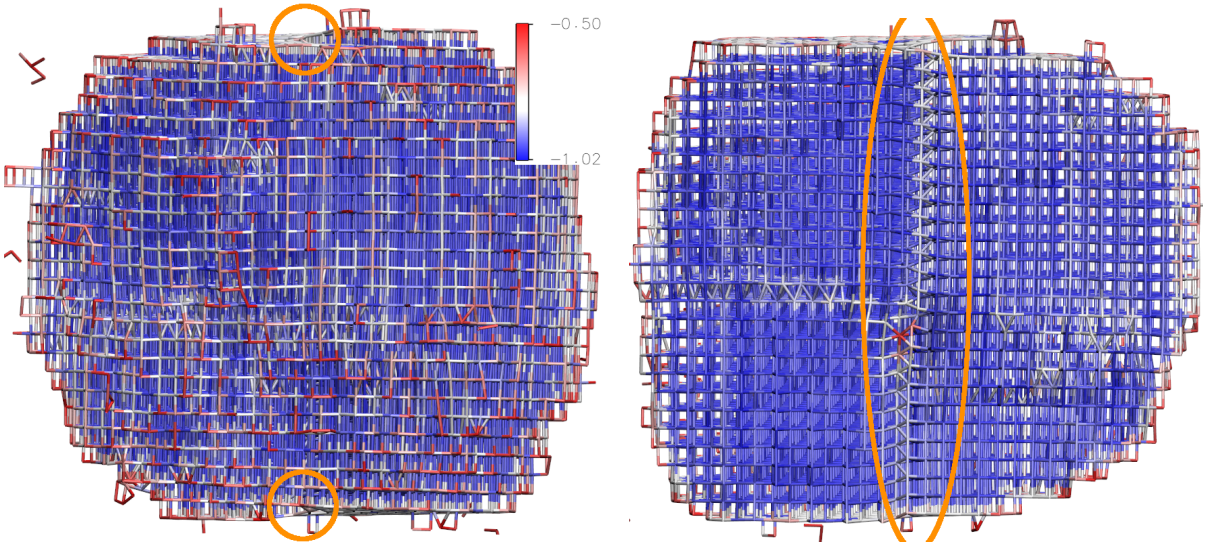

(a) Side view **(b)** Cut

Figure 4.16: Screw dislocation in final cluster assembled for DDQC-1 design, for $N = 20000$, $\sigma_{\text{ang}} = 0.49$ rad, and $T^*_{\text{init}} = 0.205$. Bonds are coloured by particle energy. [The energy scale is shown as an inset above (a).] **(a)** circles the dislocation line at the surface, at both ends. **(b)** shows a cut through the cluster, circling the dislocation line. For further details and comments, see the caption of Fig. 4.13.

screw dislocations.[†] Secondly, DDQC-3 and -3* are more specific designs than DDQC-1. They have more particle and patch types, which are more selective. Probably, this makes it more difficult for the particles to arrange correctly in a screw dislocation.

Why might screw dislocations not form for very wide patches? For the DDQC-1 design, I did not detect screw dislocations in a few simulations with $\sigma_{\text{ang}} = 0.49, 0.52$ rad. (These were the only conditions in which I did not detect a screw dislocation for DDQC-1.) In these cases, the large degree of disorder in the structures (*e.g.* incorrectly stacked layers) made it difficult to be sure no screw dislocation was present. However it may be that screw dislocations are less favourable at higher patch widths. As noted (section 4.3.1.4), at $\sigma_{\text{ang}} = 0.49, 0.52$ rad, often a cluster nucleated in a liquid-like disordered phase, then rearranged and ordered itself on further cooling. I thus hypothesise that screw dislocations are less likely to occur for QC growth from a liquid drop than from a vapour.

[†] Interestingly, however, I observed a greater occurrence of other defects, such as grain boundaries. It seems that such other defects cause less strain than screw dislocations.

Do screw dislocations form in other patchy-particle structures? Or do they only form for QCs? To test this, I simulated large systems ($N = 20000$, in parallel) for my stacked σ design (section 4.2). (I simulated for 7×10^6 MC cycles, across a temperature range $\Delta T^* = 0.01$, beginning at $T^*_{\text{init}} = 0.12, 0.125, 0.13, 0.135$, at an annealing rate 1.43×10^{-4} per 10^5 MC cycles.) Screw dislocations arose in this system also, and an example can be seen in Fig. 4.17.[†] This suggests that the reason for the occurrence of screw dislocations for DDQC-1 is less to do with the QC structure[‡]—which would have been a significant result—but more the layered structure and/or patchy-particle system. Interestingly, the screw dislocations formed here despite the lower patch width ($\sigma_{\text{ang}} = 0.3$ rad, at which DDQC-1 did *not* form screw dislocations); this suggests the energetic cost (strain) of the screw dislocation is less for the stacked σ design.

How did the screw dislocations evolve over time? To answer this, I carefully studied the cluster growth in systems that formed screw dislocations. In particular, I focussed on the early stages of growth after nucleation. I removed gas-phase particles and quenched the systems before visualisation, as described at the beginning of section 4.3.5.2. In all four screw-dislocation-forming DDQC-1 systems that I studied, I observed screw dislocations in the earliest recorded clusters which were large enough to show such defects ($500 \lesssim N_{\text{clu}} \lesssim 2000$). (For the system I studied with $\sigma_{\text{ang}} = 0.49$ rad, since the structure was quite disordered in its early stages, it was only possible to clearly observe the screw dislocation when $N_{\text{clu}} \approx 5000$.) Examples of these early-stage screw dislocations can be seen in Fig. 4.18. (These dislocations remained throughout their respective simulations, *i.e.* they did not rearrange over time.)

In stacked σ systems, I did not observe screw dislocations in the earliest few recorded stages

[†] These clusters formed very short, wide cylinders—only around 12–15 layers. Far more in-plane growth occurred than axial growth. The reason is likely the one noted earlier (section 4.3.1.3): there are more (5) patchy bonds possible in a plane than axially (2), so there is more energetic benefit to a particle extending a plane than forming a new plane. This is *especially* the case for my fully specific stacked σ design, in which patches can be perfectly aligned (whereas in the disordered DDQC, there is necessarily some imperfect bonding); stacked σ clusters show very good alignment of particles in and between layers.

[‡] This is supported by the absence of screw dislocations in other simulations that formed QCs, such as those in Table 4.2.

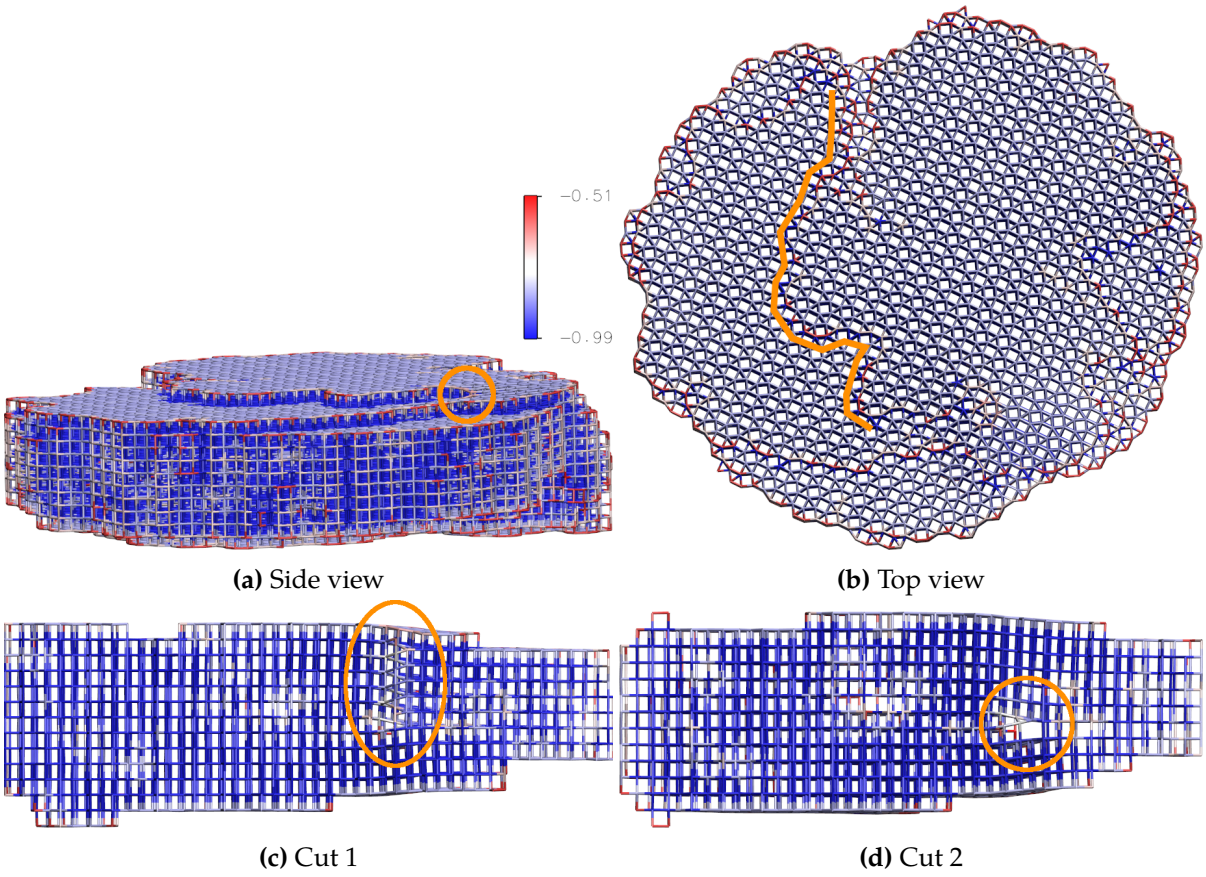

(a) Side view **(b)** Top view

(c) Cut 1 **(d)** Cut 2

Figure 4.17: Screw dislocation in final cluster assembled for stacked σ design, for $N = 20000$, $\sigma_{\text{ang}} = 0.3$ rad, and $T^*_{\text{init}} = 0.13$. Bonds are coloured by particle energy. [The energy scale is shown as an inset above (a).] **(a)** circles the dislocation line at the surface. In **(b)**, the path of the screw ledge is marked—it is to the right of the orange lines, as shown by the higher-energy particles. **(c,d)** show cuts through the cluster, from the same direction but at different positions, circling the (same) dislocation line in the interior of the cluster. The dislocation line is destroyed at another defect in (d), and thus does not run from top to bottom of the structure. For further details and comments, see the caption of Fig. 4.13.

of the cluster ($N_{\text{clu}} \lesssim 7000$).[†] But it is difficult to be sure they were not present, especially because these clusters only comprised 10 or fewer layers. Moreover, it is possible they annealed out during quenching of individual early-stage configurations. The early stages of growth for one such system are shown in Fig. 4.19, beginning before the screw dislocation is visible.

Thus, it seems that screw dislocations are favourable for cluster growth right from the beginning (at least in these systems). Unfortunately, it is difficult to be certain of their presence immediately after nucleation. Given the energetic cost of screw dislocations, it is unlikely that clusters nucleate with a screw dislocation, but they seem to arise very soon after. Whatever

[†] Cluster growth was rapid after nucleation, so I only recorded a few configurations between nucleation and clusters of this size.

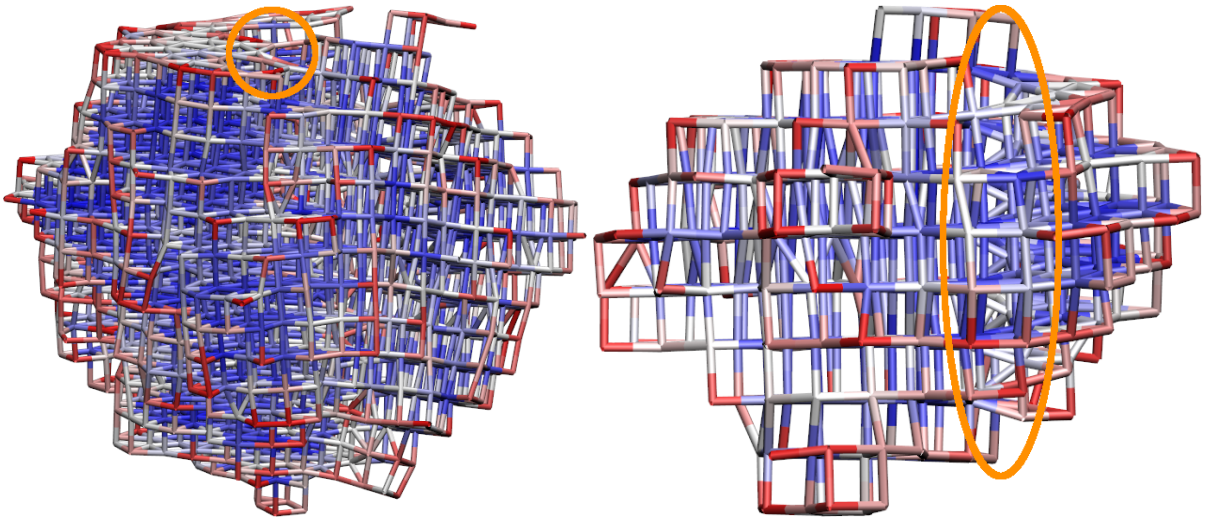

(a) $\sigma_{\mathrm{ang}} = 0.43$ rad

(b) $\sigma_{\mathrm{ang}} = 0.46$ rad

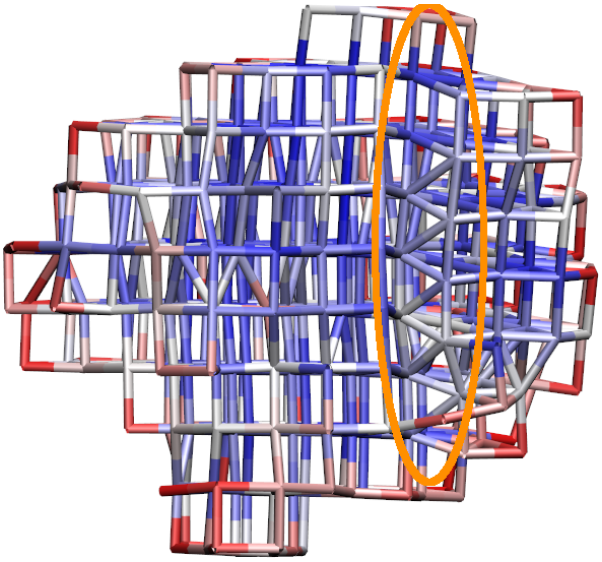

(c) $\sigma_{\mathrm{ang}} = 0.46$ rad, cut

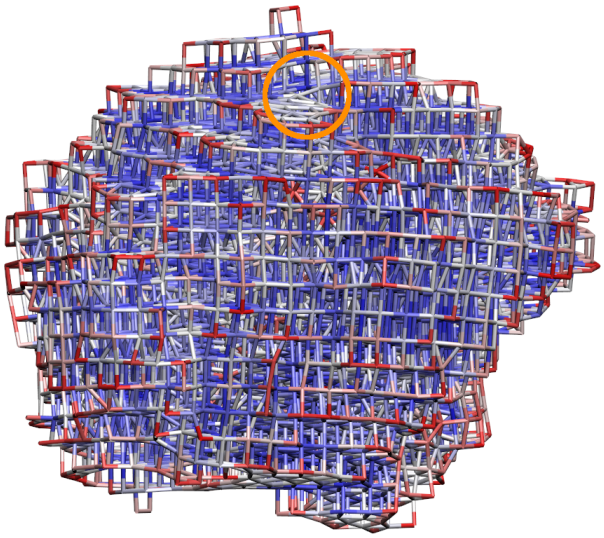

(d) $\sigma_{\mathrm{ang}} = 0.49$ rad

Figure 4.18: Screw dislocations in early-stage clusters (soon after nucleation) for DDQC-1 systems with $N = 20000$. Bonds are coloured by particle energy. **(a)** $\sigma_{\mathrm{ang}} = 0.43$ rad, $T^*_{\mathrm{init}} = 0.177$, shown at $T^* \approx 0.1765$, $N_{\mathrm{clu}} \approx 1990$ (cf. final cluster in Fig. 4.13). **(b,c)** $\sigma_{\mathrm{ang}} = 0.46$ rad, $T^*_{\mathrm{init}} = 0.191$, shown at $T^* \approx 0.1899$, $N_{\mathrm{clu}} \approx 540$ (cf. final cluster in Fig. 4.14). **(d)** $\sigma_{\mathrm{ang}} = 0.49$ rad, $T^*_{\mathrm{init}} = 0.204$, shown at $T^* \approx 0.2033$, $N_{\mathrm{clu}} \approx 5000$ (cf. final cluster in Fig. 4.15). In **(a,d)**, the dislocation line is circled at the surface; **(b)** circles the dislocation line through the cluster, seen by the higher-energy particles with bonds at an angle to the layers; **(c)** shows a cut through the cluster, revealing the dislocation line in the interior of the cluster. For further details and comments, see the caption of Fig. 4.13.

the case, they likely persist for the aforementioned kinetic reasons of catalysing growth (section 4.3.5.1).

After these early stages, as a cluster grew the screw ledge continued to advance around the dislocation line. Cluster growth seemed to be fastest at the screw ledge (but still occurred in

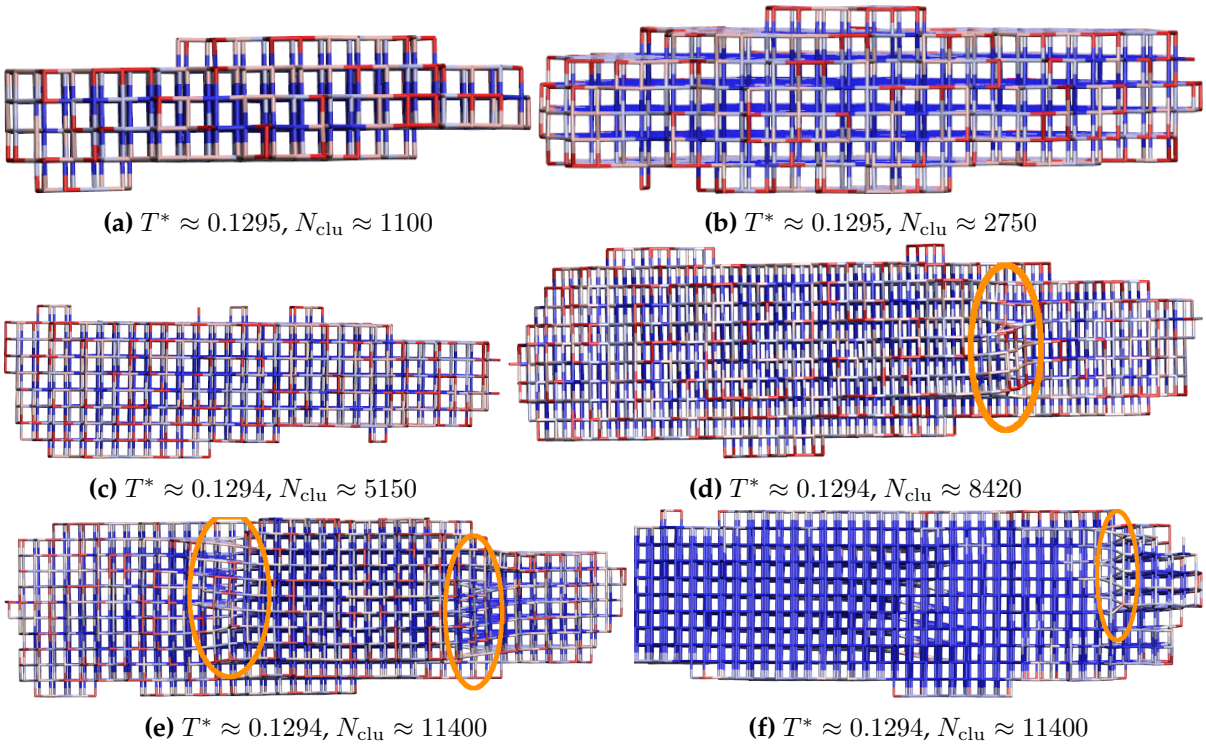

(a) $T^* \approx 0.1295$, $N_{\mathrm{clu}} \approx 1100$ **(b)** $T^* \approx 0.1295$, $N_{\mathrm{clu}} \approx 2750$

(c) $T^* \approx 0.1294$, $N_{\mathrm{clu}} \approx 5150$ **(d)** $T^* \approx 0.1294$, $N_{\mathrm{clu}} \approx 8420$

(e) $T^* \approx 0.1294$, $N_{\mathrm{clu}} \approx 11400$ **(f)** $T^* \approx 0.1294$, $N_{\mathrm{clu}} \approx 11400$

Figure 4.19: Screw dislocations in early-stage clusters (soon after nucleation) for stacked σ system with $N = 20000$, $\sigma_{\mathrm{ang}} = 0.3$ rad, and $T^*_{\mathrm{init}} = 0.130$ (cf. final cluster in Fig. 4.17). Bonds are coloured by particle energy. A screw dislocation cannot be seen in **(a–c)**, but only in **(d–f)**, as circled and seen by the higher-energy particles with bonds at an angle to the layers. **(e)** circles two dislocations, and **(f)** shows a cut through the same configuration, revealing one dislocation line in the interior of the cluster. For further details and comments, see the caption of Fig. 4.13.

other places). In some cases the dislocation line moved within the cluster over time, but in only a few cases was it lost to the edge of the cluster. This suggests that the thermodynamic driving force to remove dislocations was weak, or the kinetic process to remove it was slow (or both). (The thermodynamic driving force to remove a dislocation comes from both the structural strain, and the additional facets on the cluster due to the screw ledge. Particles at the ledge are more weakly bonded than on a smooth surface, and so break off more easily than other particles; over time, this causes the cluster to smooth off the ledge by shifting the dislocation line towards the edge of the cluster.) Nonetheless, it is likely that given more time, more screw dislocations would be destroyed. Qualitatively, the dislocation line was usually fairly straight, but small bends were common. The position of the dislocation line varied, sometimes at the centre of the cluster, sometimes towards the edge.

Why do screw dislocations arise in my patchy systems? They have not been observed in other simulations or experiments, so is there something distinct about my systems? I propose two possible features. Firstly, my structures are *layered*—stacked planes—and so have flat surfaces (on the top and bottom). This exaggerates the kinetic difference between nucleation of a new layer, and addition to a screw dislocation ledge [Fig. 4.12(b)]. For other structures without such well-defined layers, the surface is not entirely flat—some particles protrude, to varying extents—so particles can bond more strongly to a surface when forming a new layer; the surface continually has some seed sites for growth. Secondly, bonding by *patches* also exaggerates the kinetic difference between nucleation of a new layer and addition to a screw ledge. A patchy particle bonds at a well-defined number of well-defined points. In the case of nucleation of a new layer in my DDQC-1 and stacked σ systems, only one patchy bond (out of seven per particle) forms—a very weak bond. For addition at a screw ledge, three or four patchy bonds (one axial, plus two or three in-plane) may form—far stronger. This marked difference may greatly favour screw dislocations. In contrast, for a non-patchy particle with isotropic interactions, the difference between the two scenarios is not as strong. Such a particle may wedge in between a few others on a surface, forming a stronger bond than would a patchy particle.

4.4 Conclusions

I have demonstrated, for the first time, the self-assembly of 3D QCs from patchy particles (with torsional interactions), for the particular case of DDQCs. I assembled DDQCs from two distinct systems: a unary system with 5 regularly-spaced in-plane patches; and a ternary system, two particles having 5 in-plane patches, and one having 6 in-plane patches.[†] In the unary system, the patches are wide and non-selective, and the ability to form QCs seemingly depends on the flexibility of these particles to bond in different arrangements—specifically, in all the local motifs that are found in a DDQC. In the ternary system, by contrast, the patches are narrower and

[†] It is also possible that DDQCs may form from a binary system that I considered, one particle with 5 in-plane patches and one with 6. I did not fully explore this system.

selective, and the QC structure is *partially encoded* in the design; the designer has more control. Of course, it is not possible for a design (with a finite number of particle types) to fully specify a QC structure, as QCs are aperiodic and disordered; and besides, a fully specific design would have low configurational entropy, which is an important factor in QC stability [2,531]. Furthermore, the larger the number of particle types, the more difficult experimental realisation becomes. Thus, the ternary design guides the particles to a few local positions, but leaves particles some flexibility. Introducing more particle types brings complications—for example, particles did not properly mix, leading to separation between regions of different arrangements. I thus needed to carefully tune the design (via patchy interaction strengths) in order to observe successful assembly.

This work extends previous studies [1–3] that formed 2D DDQCs. The 3D approach and results were similar, although more complicated. It also extends the work in the previous chapter on periodic target structures, showing that a similar patchy-particle design approach can be used for aperiodic targets, even though they have no single uniquely determined structure. It is significant that patchy particles, which only control nearest-neighbour bonding, can achieve *global* quasicrystalline order; as in Ch. 3, a crucial factor is torsional interactions, which control next-nearest-neighbour arrangements (and by extension, all further neighbour shells). DDQCs were both thermodynamically favoured by the patches, and kinetically accessible. This bodes well for the use of patchy particles for applications in materials, devices, and (nano)technologies.

The complications and fine-tuning in this chapter should not put off future simulation or experimental work on assembling DDQCs from multiple particle types: they formed robustly, and the fine-tuning was mostly needed to make the assembled clusters easier to analyse. Given 2D DDQCs were recently assembled using DNA multi-arm tiles [4], following the patchy-particle simulations [1–3], it seems plausible for the same approach to achieve 3D DDQCs.

A more complex target than a DDQC is an IQC, which is aperiodic in all three dimensions. IQCs have a large variety of local environments—of the order of 100. To design a small number

of patchy particles with the flexibility to occupy each of these environments seems challenging (even though many of the environments are similar). Nonetheless, recently a collaborator, Dr. Eva González Noya,, has done so, following a similar approach to mine: rationally designing patchy particles based on periodic approximants, but allowing particles flexibility in bond angles and patch complementarity. This is a significant result, especially given the complex, finely tuned, empirical, long-range potentials used to form IQCs in a non-patchy study [349] are likely to be difficult to realise experimentally. Final simulations are ongoing, and Dr. Noya hopes to publish the results in 2019.

An interesting and unexpected observation was screw dislocations, which arose consistently in my stacked σ and unary DDQC systems (but not the ternary DDQC systems, which has narrower patches). Screw dislocations kinetically assist growth, and were present from the earliest stages of cluster growth. They may arise in my patchy systems due to the layered structures I studied, and the nature of patchy bonding. It is the first occurrence of a screw dislocation in a QC structure of which I am aware, either in experiment or simulation.

Possible further work includes:

(i) More precise characterisation of structures, including whether each structure is best considered as a random square-triangle tiling [531] or as a well-defined projection of a higher-dimensional periodic crystal. This will require larger systems.

(ii) More detailed analysis of the thermodynamics and kinetics of screw dislocations, in different structures. What is their energetic cost? What is their quantitative kinetic advantage? Are they destroyed/lost over time, once a cluster has formed? What are the required conditions (*e.g.* σ_{ang}) for their formation?

(iii) Assembly of QCs with other symmetries (*e.g.* decagonal, octagonal).

(iv) Preparing for the experimental realisation of 3D DDQCs, by for instance further tuning the design (*e.g.* σ_{ang}) and assembly conditions (*e.g.* temperature), and using a more accurate interaction model for colloids or NPs.

Chapter 5

Shape Fluctuations in Twisted Nanotubes: Mechanics from Internal Stress

In Ch. 3 I designed and simulated systems of patchy particles to form periodic target structures. The patches were all perfectly aligned and oriented in the targets (with no strain)—fully satisfied—and thus the patch design programmed the targets uniquely and specifically. In Ch. 4 I designed and simulated systems to form DDQCs. The patches were not all perfectly aligned—not fully satisfied—but flexibility in their interactions (through non-selective patches, and/or wide patches) allowed them to favour the target structure (despite strain). In this chapter, I design and simulate systems of patchy particles which form helical, nanotube-like structures (not 3D extended phases), and further explore 'imperfect' patchy interactions. I deliberately design patches that are not perfectly aligned in the structure, so as to apply stress to the patchy bonds (*i.e.* internal stress, not external). Unlike with the DDQCs, rather than finding the optimum strained arrangement, the structures respond to the stress by deforming in thermal shape fluctuations. I observe and analyse their mechanical behaviour. In particular, I examine whether the deformed conformations are chiral (helical).

In the previous two chapters, I designed patchy-particle systems to control material properties by targeting particular structures, since structure (partially) determines properties. In this chapter, I control material (especially mechanical) properties not just by favouring a structure, but also by applying internal stress to it and inducing strain. As in previous chapters, the systems studied here, although simple models, are designed to provide insight into experimental systems. In particular, chiral conformations of tube-like structures are relevant to the origins of

cholesteric ordering in liquid crystal phases.

In the introduction (section 5.1), I describe some relevant experimental systems, introduce important open questions concerning chiral liquid-crystalline phases, and review previous work in modelling these systems. I then describe my patchy-particle designs (section 5.2), with progressive adaptations and tests, and state my simulation methods (section 5.3). I discuss my results via a range of analyses (section 5.4). Finally, I draw conclusions and discuss possible future approaches (section 5.5).

5.1 Introduction and background

5.1.1 Helical structures and cholesteric phases

5.1.1.1 Definitions

The ultimate focus of this chapter is lyotropic liquid crystal (LC) phases with cholesteric ordering. By way of background [582], *lyotropic* LC phases are formed by mesogenic objects[†] when dissolved in a solvent (usually water, as is the case for biological systems). Their ordering depends on the concentration of the solvent, and they undergo phase transitions as the concentration changes.

Objects in *cholesteric* (or *chiral nematic*) LC phases [Fig. 5.1(a)] have nematic local order (*i.e.* the objects tend to be parallel, without short-range translational ordering), but the *nematic director* (the direction of alignment) rotates as one passes through the sample in a direction perpendicular to the objects' alignment. The *cholesteric pitch* [marked in Fig. 5.1(a)] is the spatial period (distance) of this rotation. A cholesteric arrangement has chiral long-range orientational ordering, as it cannot be superimposed on its mirror image. It is *axially* chiral, a special case of

[†] In this chapter, I use the term '*object*' to denote the particles which (may) assemble into cholesteric phases. Objects may be comprised of smaller building blocks, such as protein monomers or capsomere proteins in viruses (or in the case of my simulations, patchy particles), hence I avoid the term 'particle', which may be ambiguous. Objects may include DNA double helices, protein α-helices, virus filaments, or other polymers; or superstructures of smaller entities, whether biological or synthetic (*e.g.* DNA origami structures).

chirality, rather than chiral at stereocentre.[†] In *left-handed* cholesteric phases [as in Fig. 5.1(a)], the nematic director rotates anti-clockwise from near to far when viewed down the axis, and in *right-handed* phases it rotates clockwise.

5.1.1.2 Examples of structures and systems

Lyotropic cholesteric liquid crystals (LCLCs) are common in colloidal polymer systems, both natural (especially biological) and artificial [582,583,587–589]. They are often formed from helical (and thus chiral) polymers. Biological helical polymers which form LCLCs include protein α-helices, *i.e.* polypeptides (right-handed; *e.g.* filamentous actin [590], collagen, silk fibroin [591]), and DNA double helices [right-handed for B-DNA, the most common form in nature, with helical pitch of 10–10.5 base pairs (bp); [587,592–596]]. Other biological cholesteric phases are formed from polysaccharides or glycopolymers (*e.g.* cellulose [597,598], chitin [599], schizophyllan [600]). Thus, cholesteric phases can be found in, for instance [583]: bacterial nucleoids, chromosomes of single-cell dinoflagellates, sperm nuclei of many vertebrates; exoskeletons/cuticles of arthropods (*e.g.* crustaceans like crabs and lobsters, insects like beetles), bone, dentin, tendons, cornea (of *e.g.* fish, amphibians, reptiles, birds), fish scales, parts of cephalopods (*e.g.* cuttlebone, squid pen); mollusc nacres, silk (from *e.g.* spiders and silkworms); and plant cell walls (of *e.g.* fern leaves, berry-like fruits, wood, cotton). Suspensions of some rod-like viruses also show cholesteric phases, *e.g. fd* [601–603] [Fig. 5.1(c)] and M13 [604,605] filamentous bacteriophages. Synthetic helical objects which form cholesteric phases include polyisocyanates [606,607] and polysilanes [608].

5.1.1.3 Applications

LCLCs can have interesting optical (*e.g.* iridescence; tunable colour filtering; light polarisation; selective reflection of, or different refractive indices for, left- or right-handed circularly polarised light), photonic (*e.g.* photonic band-gaps), electronic, plasmonic, chemical (*e.g.* asym-

[†] In this chapter, only axial chirality is discussed, not stereogenic chirality (which is more familiar to most chemists).

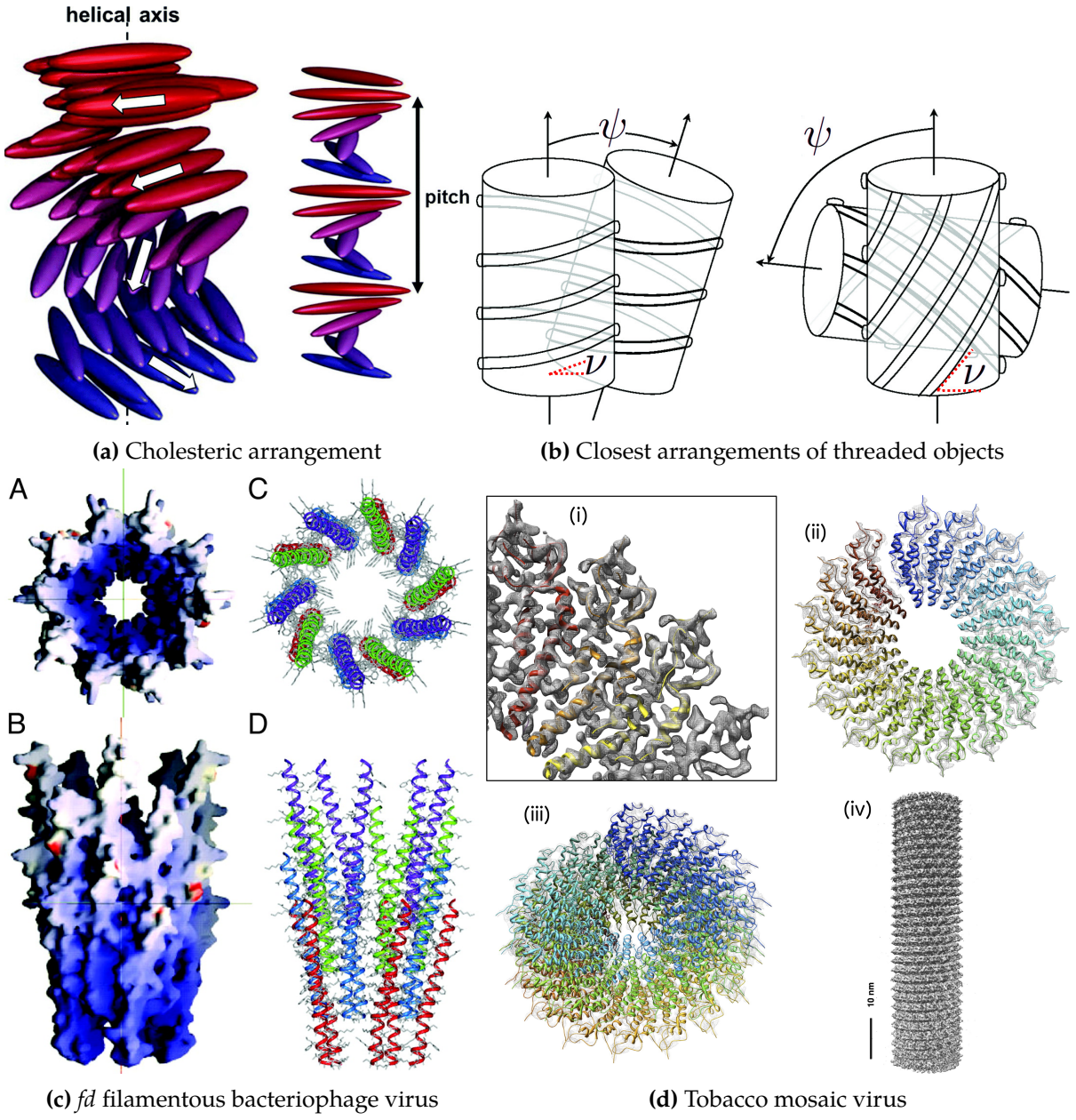

(a) Cholesteric arrangement

(b) Closest arrangements of threaded objects

(c) *fd* filamentous bacteriophage virus

(d) Tobacco mosaic virus

Figure 5.1: **(a)** Illustrations of cholesteric LC phase. Objects are coloured by their orientations. The left images marks the nematic director (white arrows) and helical axis; the right marks the cholesteric pitch. **(b)** Pairs of right-handed threaded (screw-like) objects, arranged in their closest—entropically favoured—configurations. The thread angles, ν, and the angles of relative twist of adjacent objects, ψ, are marked. Strongly twisted ($\nu \lesssim \pi/4$ rad, left image), right-handed objects can align their grooves and approach most closely when in a right-handed ($\psi > 0$) cholesteric arrangement (*i.e.* iso-chiral). Weakly twisted ($\nu \gtrsim \pi/4$ rad, right image), right-handed objects can align their grooves when in a left-handed ($\psi < 0$) cholesteric arrangement (*i.e.* anti-chiral). **(c)** Model of Y21M *fd* filamentous bacteriophage capsid, as shown from end (A,C) and side (B,D) of rod. The model was made from the coat protein subunit structure, as determined by solid-state NMR spectroscopy, with the symmetry obtained from fibre diffraction studies. A,B: electrostatic potential on the molecular surface. C,D: arrangement of the coat proteins in pentamers. **(d)** Tobacco mosaic virus density map: (i) quarter slice through three adjacent subunits; (ii) one turn (16 subunits); (iii) three turns (49 subunits) [(ii) and (iii) are end views with superimposed atomic coordinates]; (iv) 3D reconstruction of a rod segment from electron micrographs.
(a,b,c,d) Reprinted with permission from Refs. 583,584,585,586, respectively, © The Royal Society of Chemistry, American Chemical Society, National Academy of Sciences, and Elsevier, respectively.

metric catalysis), and mechanical or rheological (*e.g.* load-stabilisation, resistance) properties [589,609,610]. Many of these properties occur in nature; others can be engineered artificially. As such, LCLCs have been and may be applied in diverse areas [589,611,612] such as architecture, textiles (*e.g.* camouflage, reflective and/or flexible display materials), energy (*e.g.* electrolytes for batteries, photovoltaics), automobiles, optical sensors, and biomedical devices and materials [613] (*e.g.* implants, diagnostic materials, artificial muscles). Many potential applications are biologically inspired (*e.g.* [614]). Greater understanding of the origins of cholesteric phases is thus of significant interest. Synthesis of LCLCs is active and improving [589,615], to meet this goal.

5.1.2 Understanding cholesteric phases and their origins

While it has long been known that chiral objects *tend to* form chiral phases, the origin of this ordering is in many cases not understood, despite much research [602,609,615–618]. Moreover, general understanding is lacking of the factors that determine the handedness and cholesteric pitch. Cholesteric ordering may arise through both entropy and enthalpy; diverse physical and chemical interactions may be involved, along with shape fluctuations. Macroscopic ordering depends on the microscopic objects' structure and behaviour, but the (possibly hierarchical) mechanism(s) by which microscopic chirality is transferred to an assembly—known as *chiral amplification* (or *propagation*)—is unclear and non-trivial, in many systems. The diversity of systems displaying cholesteric phases, and their complexity, makes understanding and predicting cholesteric phases especially challenging. If one could understand and control cholesteric assembly, rational design of objects for bottom-up self-assembly could yield useful materials, devices and (nano)technologies [619–621]. As such, research probing these origins and mechanisms is active (*e.g.* general experimental and theoretical investigations [622–627], for DNA [594,596,628,629], for *fd* virus [601,602,630–632], for rod-like viruses in general [603,631], for cellulose [597,598], for chitin nanocrystals [599,633], and for collagen I assemblies [634]).

5.1.2.1 Steric argument

One important factor (among others) in chiral amplification is steric (shape) effects. All else equal, two objects prefer to minimise their pair excluded volume, and thus adopt configurations that allow better packing; this gives the objects in an arrangement more available room to move—and thus greater entropy. For two continuously threaded chiral objects, the arrangement that minimises their separation (at the closest point) has been studied [635]. For weakly twisted objects, it is an *anti-chiral* arrangement [*i.e.* the handedness of the pair is *opposite* to the handedness of an object's axial twist; objects with right- (left-)handed twist form left- (right-)handed phases], while for strongly twisted objects it is an *iso-chiral* arrangement (*i.e.* the handedness of the pair is the *same* as the handedness of the axial twist). Such arrangements locally align the helix grooves at the point of closest contact, as shown in Fig. 5.1(b). This geometric argument has been investigated and demonstrated in simulations of hard particles (*i.e.* with purely steric interactions)—helical chains of overlapping spheres [618,624], and twisted cuboids [636]. Increasing the level of twist from weak twisting caused a reduction in the chirality of the anti-chiral cholesteric phase (*i.e.* a larger cholesteric pitch) until the iso-chiral phase was stabilised. Thus, the cholesteric handedness depends on the level of twist.

The level of twist can be measured by the thread angle, ν, the angle between the normal to the object's long axis and the vector tracing the helical path [Fig. 5.1(b)].[†] The crossover level of twist has been empirically shown to be $\nu \approx \pi/4$ rad (*i.e.* anti-chiral arrangements for $\nu \gtrsim \pi/4$ rad, iso-chiral for $\nu \lesssim \pi/4$ rad).[‡]

Although this steric principle has predicted theoretical and simulation results for rigid objects with well-defined threads, it has less success predicting experimental behaviour, which is more complex. The origins of the cholesteric handedness in many experimental systems is still

[†] ν is sometimes denoted elsewhere as 'α' or 'ψ', and/or called the *helix inclination angle*.

[‡] Specifically: crossover inclination angle $\nu = 45°$ was theoretically conjectured for grooved cylinders [584]; $40° \lesssim \nu \lesssim 60°$ was found in simulations of hard twisted cuboids, depending on the geometry of the cuboids [636]; $\nu \approx 40°$ was found in simulations of helical chains of hard, overlapping spheres [624], and in similar systems, for shallow grooves ν was found to be up to $75°$ [618].

an open question, as is why certain chiral objects only exhibit nematic phases.

5.1.2.2 Problem cases

Two particular cases have attracted interest over a long period, including recently, yet are not understood.

1. B-DNA handedness. The B-DNA double helix is strongly twisted ($\nu \approx \pi/6$ rad) and right-handed. The steric argument predicts B-DNA double helices will form a right-handed, isochiral phase. Systems of hard B-DNA double helices have indeed been theoretically predicted to form right-handed phases [637,638]. However, in experiments B-DNA double helices form *left*-handed, *anti-chiral* phases [629].[†] Moreover, the chirality was significantly stronger (*i.e.* shorter pitch) in experiment than in simulation of hard particles [638]. (In addition, M13 virus, which is right-handed with $\nu \approx 41°$, also forms a left-handed cholesteric phase [604]. However, this result is less significant given the uncertainty in the crossover thread angle discussed in section 5.1.2.1.)

It has been argued, with evidence from numerical studies, that this discrepancy can be explained by electrostatic interactions between double helices [584,637]; the repulsive interactions between helical charge distributions potentially favour chiralities with the opposite handedness to the steric argument. (A similar argument was also made for the aforementioned M13 virus cholesteric phase [604].) However, later numerical studies ruled out this hypothesis [638,639]. One study [639] concluded that electrostatic interactions do not favour any particular handedness. Another [638] found they only reduce the level of chirality (cholesteric pitch), but do not change the handedness. Thus, it seems steric and electrostatic effects are insufficient to explain both the handedness and pitch of B-DNA double helix cholesteric phases.

[†] Systems of ultrashort B-DNA double helices were found to form *both* left- and right-handed cholesteric phases [596].

2. Rod-like (or filamentous) viruses. The rod-like capsids of filamentous viruses have a helical (and thus chiral) arrangement of capsid proteins on their surfaces. Some rod-like viruses, such as *fd* [601–603,630,640,641] [Fig. 5.1(c)], M13 [604,605], Pf3 [641], and tf-1 [641] filamentous bacteriophages, form cholesteric phases. But other rod-like viruses chiral capsids do not; chirality is not transferred from the micro- to macroscopic domains. For instance, tobacco mosaic virus [640,642] [Fig. 5.1(d)], Pf1[†] [601,640,641], IKe [641], $I_2$2 [641], and X-2 [641] instead form nematic phases (or at least the cholesteric pitch is too large to be observed in experiments).[‡] In addition, small changes in *fd* virus—a small mutation [631], or chemical surface modifications [632]—can cause a change in the handedness or pitch of its cholesteric phase.

Both the steric argument, and electrostatic interactions between surface charge distributions, have been considered as the cause of the disparate ordering in systems of different viruses. However, when *fd* is covered in a thick layer of (neutral) polyethylene glycol, obscuring the steric chirality of the capsid surface and weakening any short-range electrostatic interactions, it still shows cholesteric phase behaviour [602]. Long-range electrostatic interactions were also ruled out, since cholesteric ordering still arises when the system is at the virus' isoelectric point. As steric or electrostatic interactions are unable to explain this behaviour, the origin of the cholesteric ordering of *fd* is unclear.

5.1.2.3 Recent progress towards better understanding

Experimental. Recent experiments [36], applying self-assembling DNA origami technology, have enabled a clearer analysis of the origins and mechanisms involved in cholesteric ordering of helical objects. Bundles of tightly cross-linked,[§] parallel B-DNA double helices, with double helices in a honeycomb (open hexagonal) arrangement, serve as rod-like objects (with very sim-

[†] The structures of *fd* [643] and Pf1 [630,644] are similar, with only small differences in their surface protein arrangements.

[‡] Other objects with helical structures, besides rod-like viruses, also form nematic phases rather than cholesteric, *e.g.* microtubules (polymers of tubulin) [645].

[§] A pair of double helices is cross-linked by a bond between a pair of single DNA strands (*staple strands*), one from each of the double helices.

ilar properties to the virus filaments). By inserting or deleting base pairs at targeted positions along a double helix [646], internal mechanical stress is introduced in the double helix: the helix is forced to rotate less or more (respectively) than it would prefer to. The stress is transferred between double helices via the cross-links. This can cause the bundle to both twist (helically) along the bundle axis, and bend. Quantitative control over the shape is possible by carefully determining base pair insertions and deletions. Specifically, cross-links are positioned every 7 or 14 bp (on average every 10.5 bp); over 7 bp, B-DNA twists $2\pi/3$ rad (the helical pitch is ~ 10.5 bp). With double helices in a honeycomb arrangement, a double helix bonds to each of its neighbours once every 4π rad rotation. *Inserting* (*deleting*) a base pair in a section between cross-links causes under- (over-)winding of the double helix in that section, generating a right- (left-)hand torque which causes right- (left-)handed bundle twisting (as compensation).[†]

This control over twist was applied [36] in fixed and tight honeycomb bundles of six double helices (6DHs). Four bundle designs were engineered (each described here in its equilibrium ground state), as shown in Fig. 5.2(a):

(i) '*s*' (for 'straight'): no twist (no strain), due to no insertions or deletions.

(ii) '*rh*' (right-handed): $\sim 2\pi$ rad right-handed bundle twist along the filament, compensating for under-winding strain from insertions.

(iii) '*lh*' (left-handed): $\sim 2\pi$ rad left-handed bundle twist along the filament, compensating for over-winding strain from deletions.

(iv) '*2lh*' (double left-handed): $\sim 4\pi$ rad left-handed bundle twist along the filament, compensating for over-winding strain from deletions.

Colloidal systems of each type of bundle assembled into cholesteric LC phases. In all cases, the bundle twist is weak ($\nu_{\text{bundle}} \gg \pi/4$ rad), so the steric argument (section 5.1.2.1) predicts bundles to form anti-chiral phases (*i.e.* rh in a left-handed phase, lh and 2lh in right-handed phases).

[†] Alongside the torque, tensile stress or compression is introduced because the altered double helix section is constrained axially by the cross-links at either end: insertions (deletions) cause a push (pull) to lengthen (shorten) that section of the double helix.

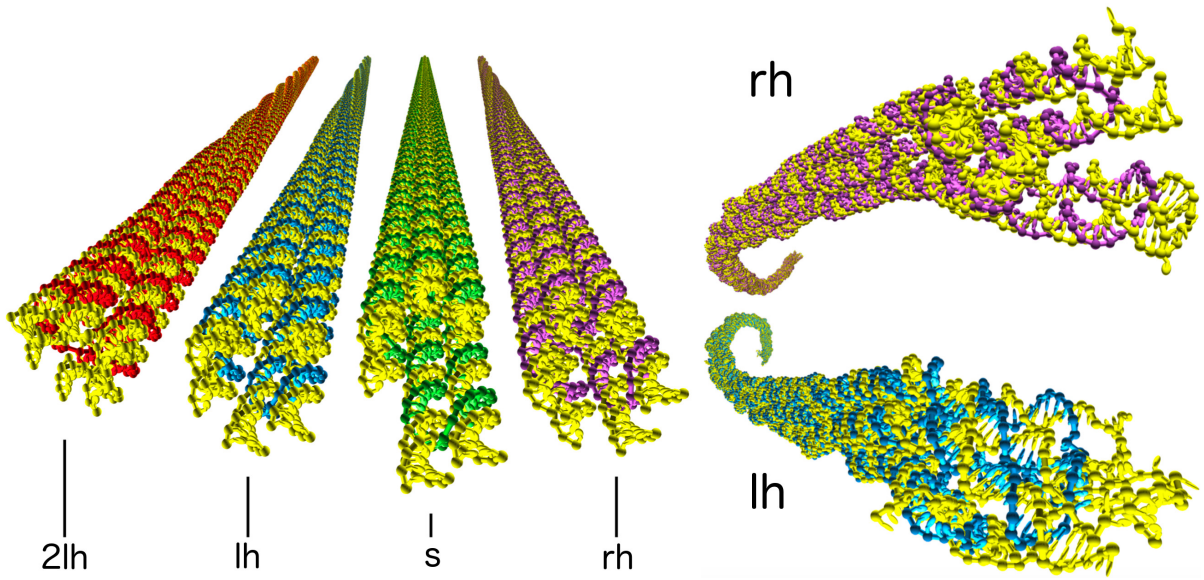

(a) 6DH bundles **(b)** Sample 6DH bundle conformations

Figure 5.2: (a) Bundles of six tightly cross-linked, parallel B-DNA double helices, arranged in a honeycomb formation (each double helix has one yellow strand, and one other-coloured strand). Each has a different (or no) axial twist, as described in the main text: '2lh' = double left-handed, 'lh' = left-handed, 's' = straight, 'rh' = right-handed. **(b)** Example solenoidal conformations of rh and lh 6DH bundles, due to thermal shape fluctuations, showing their typical left- and right-handed backbone chiralities, respectively. Colours as in (a). Reprinted with permission from Ref. 5, © of the authors.

However this was not observed: 2lh formed a left-handed phase, lh a weakly right-handed phase, and rh a right-handed phase (*i.e.* iso-chiral in most cases).[‡] Thus, although cholesteric pitch and handedness could be tuned by controlling (nanoscale) DNA structure, the mechanism was still unclear.

Numerical. The experimental 6DH systems were analysed in-depth numerically [5], revealing the underlying mechanism. The 6DH bundles were first treated as hard objects (*i.e.* with only steric interactions) with rigid shapes—twisted but straight. Their cholesteric phases followed the predictions of the steric argument (section 5.1.2.1): as weakly twisted objects ($\nu_{\text{bundle}} \gg \pi/4$ rad), they formed anti-chiral phases (*i.e.* the cholesteric handedness was opposite to the axial twist of an individual bundle; rh formed a left-handed phase, lh and 2lh formed right-handed phases, and s formed a weak right-handed phases[†]). This does not match the experimental

[‡] s formed a weakly right-handed phase (with cholesteric pitch in between that of lh and rh).

[†] The reason the s bundles formed a right-handed phase is because, although the bundles are not twisted, their six individual DNA double helices are. B-DNA twist is strong ($\nu_{\text{B-DNA}} < \pi/4$ rad), so it causes an iso-chiral (*i.e.* left-

results just discussed; moreover, the predicted cholesteric pitch is much larger than in experiment. Introducing electrostatics into the simulations only reduced the chirality (increased the cholesteric pitch)—as for assemblies of individual B-DNA double helices (section 5.1.2.2).

Since steric and electrostatic effects could not explain the cholesteric pitch or handedness, a new factor was considered: shape fluctuations (*i.e.* the objects were considered as flexible, not rigid and straight, with intra-object mechanics) [5,638].[†] These occur in solution through thermal energy. To analyse the nature of these thermal fluctuations, a long, coarse-grained oxDNA simulation [6] was run for each 6DH bundle.[‡] Fourier analysis of the resulting conformations found long-wavelength deformation modes along the bundle backbones. As the 6DH bundles (other than s) fluctuate, they writhe, adopting helical (or solenoidal), and thus chiral, conformations. On average they each exhibited a stable particular net handedness. Specifically, lh and 2lh adopted right-handed solenoidal conformations, while rh adopted a left-handed solenoidal conformation—that is, 6DH bundles adopted conformations with opposite handedness to their axial twist. Representative conformations are shown in Fig. 5.2(b). This is because, in the 6DH systems, anti-chiral conformations relieve some of the internal mechanical stress which gave rise to the bundle twist; the cost of writhing in an anti-chiral solenoid is partially offset by a reduction in the cost of under- or over-winding within the DNA double helices. The resulting solenoidal shapes were weakly twisted (*i.e.* the helical pitch was large; $\nu_{\text{solenoid}} \gg \pi/4$ rad).

To predict the cholesteric behaviour, accounting for this flexibility, a theoretical approach [5] was applied to ensembles of 6DH bundle configurations generated by oxDNA simulations (rather than to ensembles of straight, ground-state bundles). The results confirmed that the 6DH bundles formed cholesteric phases with handedness opposite to their net solenoidal chirality (in line with the steric argument). Thus, the cholesteric handedness was the same as the (weak)

handed) phase by the steric argument, just as predicted for individual B-DNA double helices (section 5.1.2.2).

[†] Previous models seeking to predict cholesteric handedness and pitch using factors besides steric and electrostatic effects, also usually neglected shape fluctuations [604,647].

[‡] Considering objects individually is a reasonable approximation for DNA origami, given the low packing fractions of their LCLC phases and their long, stiff nature (or large persistence length—the ratio of the persistence length to the contour length is greater than around 5 [36]). The contour length and persistence length are defined in sections 5.4.1 and 5.4.4, respectively.

axial twist: lh and 2lh formed left-handed phases, while rh formed a right-handed phase. (s, as when shape fluctuations were neglected, formed a weakly right-handed phase.) These numerical results match those in experiments [36], not only in handedness, but also in cholesteric pitch. (While lh formed a weakly right-handed cholesteric phase in experiment, but a weakly left-handed phase in simulation, the difference (as measured by cholesteric pitch) is small, and might be explained by minor errors in the numerical model [5].) Shape fluctuations dominate the steric and electrostatic factors previously considered; the results differed little when electrostatic interactions were included or excluded.

Thus the mechanism of chiral amplification is hierarchical: the chirality of the bundle axial twist is reversed in the chirality of a bundle's solenoidal shape conformation, which in turn is reversed in the chirality of the bulk cholesteric phase. Instead of the cholesteric phase being anti-chiral to the twist, it is anti-chiral to the solenoidal shape. Although this analysis only considered the specific case of 6DH bundles, the new chiral amplification mechanism it uncovered seems potentially quite general, and has been suggested to apply more widely. Filament bundles are a common motif in both biological and synthetic contexts, and their arrangement is known to be influenced by geometric frustration and mechanical mechanisms [648]. In particular, the mechanism may apply to rod-like viruses; flexible, solenoidal conformations were previously proposed to explain the cholesteric phase behaviour of *fd* virus [602]. Recently [649], researchers demonstrated the ability to rationally design and self-assemble helical tubes from protein monomers, with great control over structure and mechanics. This raises the possibility of creating and controlling cholesteric phases of proteins.

5.1.3 Aims and approach

In the above case of 6DH bundles (section 5.1.2.3), internally stressed helical objects adopt solenoidal shapes in their thermal fluctuations, and then these solenoids order in cholesteric phases. The chiral handedness and pitch is controllable: (weakly twisted) bundles form opposite-

handed solenoids, which arrange in opposite-handed cholesteric phases. Is this hierarchical mechanism more general—does it apply beyond 6DH bundles? If so, then it is of significant interest. Chiral objects and their cholesteric phases are abundant in nature (section 5.1.1.2), and it is likely that helical objects will also be able to fulfil a variety of functions in artificial contexts. Thus, not only will understanding chiral shape fluctuations potentially improve our understanding of nature, for example why certain rod-like viruses form cholesteric phases but others do not (section 5.1.2.2), it may also lead to a range of applications.

It seems likely that the second hierarchical stage—in which solenoidal shapes arrange in anti-chiral cholesteric phases—*is* general; it agrees with the steric argument. Therefore here I focus on the first stage—stressed chiral tubes adopting solenoidal conformations. The questions I aim to address are as follows. Is the anti-chiral conformation of an internally, mechanically stressed chiral tube a general phenomenon—does it occur for other tube-like helical objects, such as rod-like viruses (*e.g. fd*, tobacco mosaic virus)? (In viruses, internal stress could come from protein-protein interactions, rather than under- or over-wound DNA double helices.) Is it possible to *design* certain internal stress into a simple tube-like helical object, so that the resulting fluctuation-stabilised conformation(s) is solenoidal? If so, is it possible to control the handedness and pitch of the solenoidal conformation—can opposite handedness to the (weak) twist in the tube be programmed? If not, what effects *does* the internal stress have on helical objects?

I use patchy particles to form tube-like objects, and build the stress into their patchy interactions to cause twisting. Although chiral tubes have previously been assembled from and modelled by patchy particles, patchy particles have not been used to deliberately introduce internal stress and study its effects. As in previous chapters, patchy particles are a very simple model, but they are therefore able to provide insight into a range of real systems, and identify the crucial factors that cause observed behaviour.

5.2 Design

In this section I describe the tube-like helical structure I studied, and the patchy particles I designed to form it. I then describe the design alterations I made to apply internal stress to the tube. I emphasise that I did *not* try to replicate (or even coarse-grain) the 6DH bundle systems discussed above. My helical system is similar—I *did* try to replicate the mechanical behaviour—but different in important ways; it is simpler, and the network of interactions between the elements making up the tubes is different. I aim to apply forces that generate a net torque, hence causing the tubes to twist, as in the 6DH bundle systems. [Note that, when I speak of a tube 'twisting', I do not refer to a helical arrangement of particles as one progresses in the direction of the axis. Rather, I refer to a twisting of the tube as a whole, like that shown for 6DH bundles (other than s) in Fig. 5.2(a).] I want the helical structure—periodic loops down the long axis—to remain, but the patchy bonds to not be entirely satisfied, and thus for there to be strain.

5.2.1 Basic tube structure

There are many suitable helical structures I could have studied; while I provide some rationale for my choice, a full explanation is not possible. The undistorted 1-start helix I study, labelled 'u6' ('u' for undistorted), is tube-like, tight (*i.e.* particles are packed densely and there are no gaps in the helix wall), straight, and has particles aligned parallel with the axis, as shown in Fig. 5.3. I arbitrarily chose a right-handed helix.

The number of particles within each 2π rad loop of the (undistorted) helix, N_{loop}, is 6 (hence the '6' in 'u6'). (Undistorted helices with arbitrary N_{loop} are analogously labelled 'uN_{loop}'.) As N_{loop} increases, the structure becomes more like a cylinder (the axial rise per particle is small). As N_{loop} decreases, the helix diameter becomes smaller, and the stress per patchy bond (if introduced) will be large. $N_{\text{loop}} = 6$ seems a good balance. Every seventh particle is aligned parallel to the axis, forming six parallel *axial chains* (as seen in the end-on view in Fig. 5.4(a)); these

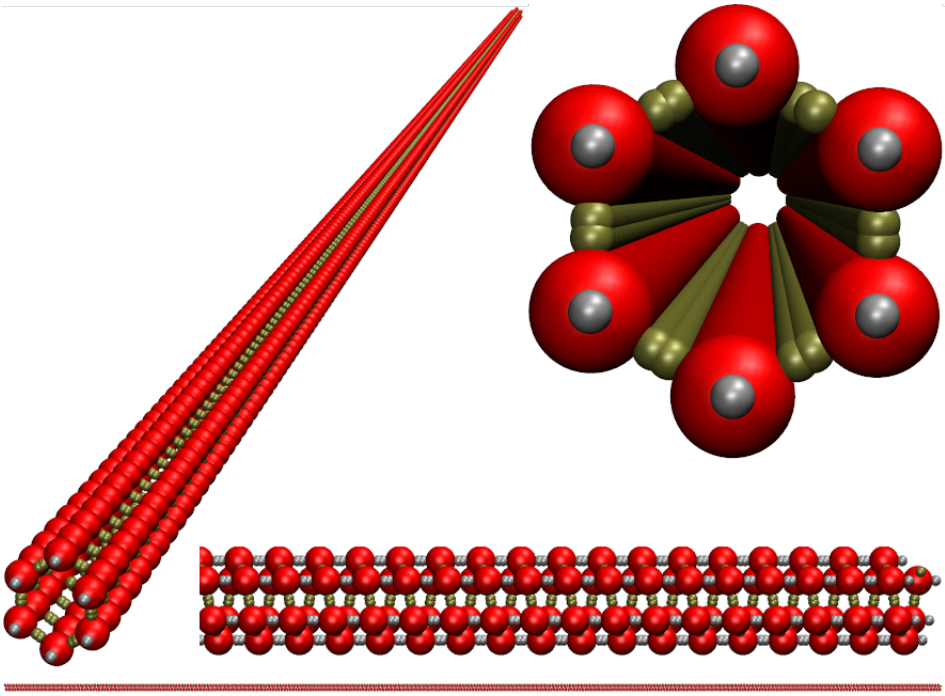

Figure 5.3: Undistorted helix with 6 particles within each 2π rad loop of the helix, formed from $N = 1998$ patchy particles. Four different views, clockwise from left: angled (perspective projection); end-on (perspective), showing six parallel axial chains; side, close-up (orthographic); side, full helix (orthographic). Particles are as in Fig. 5.4(a).

chains are similar to the six double helices in a 6DH bundle.

I use 4 patches per particle: 2 axial, and 2 lateral (the former are coloured silver in Figs. 5.3 and 5.4, the latter gold). Axial patches are directly opposite each other, and maintain the helix structure. In the distorted designs, it is through distorting the lateral patches that I apply stress: the preferences of the two types of patches are in competition (neither can be fully satisfied), causing shape deformations.

The u6 patchy-particle design is given in Table 5.1. It was derived using a helix with inter-particle bond lengths of the LJ minimum energy ($2^{1/6}\sigma_{\mathrm{LJ}}$), for both lateral and axial bonds. So the helical pitch is $2^{1/6}\sigma_{\mathrm{LJ}}$. The particles are all of the same type, and there are 2 patch types (axial and lateral). They have C_2 point symmetry. An image of the particle is shown in Fig. 5.4(a). The (undistorted) structure as a whole has 6-fold helical symmetry. I derived the design (patch vectors and offset angles) from the helical geometry.

5.2.2 Stressed helices

As for the 6DH bundle systems, I apply internal stresses—generating a net torque—to the basic helix structure, to cause it to twist. These stresses are generated by a deviation in patch directions. There are many possible ways of defining such a deviation; as long as it causes a net torque in the correct direction, there is no *a priori* reason to prefer one definition over another.

My definition is as follows: for the distorted helix labelled 'd6,$N_{\mathrm{loop}}^{\mathrm{dis}}$' ($N_{\mathrm{loop}}^{\mathrm{dis}} \neq 6$; 'd' for distorted), the lateral patches are positioned relative to each other as they would be in the undistorted helix u$N_{\mathrm{loop}}^{\mathrm{dis}}$. In other words, from the u$N_{\mathrm{loop}}^{\mathrm{dis}}$ helix, which is as described above for u6 (section 5.2.1),[†] I take the angle between lateral patches and use it in my distorted d6,$N_{\mathrm{loop}}^{\mathrm{dis}}$ structure. All other patch properties in d6,$N_{\mathrm{loop}}^{\mathrm{dis}}$ remain the same as for u6 (*i.e.* the u$N_{\mathrm{loop}}^{\mathrm{dis}}$ system has no relevance other than for calculating the lateral bond angle). Thus, unchanged details include: the angle between axial patches (π rad), the angles between axial and lateral patches (and therefore the design favours an axial rise of one bond length, $2^{1/6}\sigma_{\mathrm{LJ}}$, every six particles around the loop), and all offset (torsional) angles.

Maintaining offset angles[‡] in d6,$N_{\mathrm{loop}}^{\mathrm{dis}}$ at the same values as for u6 means the torsional component of the potential favours a u6 helix, whereas the lateral patches favour a helix with $N_{\mathrm{loop}} \neq 6$. They are in competition (just as the lateral and axial patches are), and thus the structure is stressed—fully satisfied neither in a u6 arrangement nor a u$N_{\mathrm{loop}}^{\mathrm{dis}}$ arrangement. In any case, since I used a relatively wide torsional angle, this is not the main source of stress (as in previous chapters, $\sigma_{\mathrm{tor}} = 0.6$ rad). Preliminary simulations in which the offset angle matched the geometry of the u$N_{\mathrm{loop}}^{\mathrm{dis}}$ helix (and so matched the lateral patch angle) showed no significant difference.

[†] That is, u$N_{\mathrm{loop}}^{\mathrm{dis}}$ is the helix in which: axial and lateral bond lengths remain at $2^{1/6}\sigma_{\mathrm{LJ}}$, so the axial rise per particle is $2^{1/6}/N_{\mathrm{loop}}^{\mathrm{dis}}\sigma_{\mathrm{LJ}}$; a 2π rad loop is divided into $N_{\mathrm{loop}}^{\mathrm{dis}}$ points, so the projected lateral bond angle when viewing down the axis is $\pi - 2\pi/N_{\mathrm{loop}}^{\mathrm{dis}}$ rad; and the helical radius is more or less than for $N_{\mathrm{loop}} = 6$. Note that if $N_{\mathrm{loop}}^{\mathrm{dis}}$ is not an integer, then in u$N_{\mathrm{loop}}^{\mathrm{dis}}$, axial chains are not defined as particles in adjacent rows are not aligned parallel with the axis; for example, in u6.5, particles in every second row are aligned parallel with the axis.

[‡] Specifically, the offset angles for the two axial patches.

The primary effect of changing the lateral bond angle is to introduce a torque into the system. In d6,$N_{\mathrm{loop}}^{\mathrm{dis}}$, for $N_{\mathrm{loop}}^{\mathrm{dis}} > 6$ ($N_{\mathrm{loop}}^{\mathrm{dis}} < 6$), the lateral bond angle is wider (narrower) than in u6, so the helix wants a smaller (larger) helical turn per particle. However the axial patchy bonds and torsional offset angles oppose this torque. The structure is stressed, and finds a compromise whereby it turns somewhat less (more), until the cost of the imperfect axial bonds and torsional interactions is balanced by that of the imperfect lateral bonds. Consequently, particles in adjacent rows are no longer aligned parallel with the axis; there is an incremental rotation from row to row. Looking down an axial chain, the helix is twisted: left-handed (anticlockwise) for $N_{\mathrm{loop}}^{\mathrm{dis}} > 6$, right-handed (clockwise) for $N_{\mathrm{loop}}^{\mathrm{dis}} < 6$.[†] For $N_{\mathrm{loop}}^{\mathrm{dis}} > 6$ ($N_{\mathrm{loop}}^{\mathrm{dis}} < 6$), a component of the force on each particle pushes outwards from (inwards to) the helix axis, favouring the helix radius to increase (decrease).

The force applied in the d6,$N_{\mathrm{loop}}^{\mathrm{dis}}$ structures is similar to that in the 6DH bundle systems, but not the same. Important differences include the following:

(i) Stress is applied at smaller axial intervals in my structures than the 6DH bundles. This is because along my axial chains, every particle is bonded to both its lateral neighbours; stress is applied at each bond. In 6DH bundles, cross-links to one other double helix only occur every 7 or 14 bp, so stress is only applied at these points. Nonetheless, if the twist of my objects is similar to that of the 6DH bundles, the net stresses are likely also similar.

(ii) In a related point, a particle's two lateral patchy bonds, at which the stress is applied in my structures, are roughly at the same point along the helix axis. However in 6DH bundles, the cross-links to neighbouring double helices are not at the same point; they alternate from side to side.

(iii) There are differences in the origins of the stresses. The stress in 6DH bundles comes from under- or over-winding of each double helix, which then causes the bundle as a whole to twist. In my structures, the origin is preferred bond angles (via patches).

[†] This applies for a right-handed helix, as in my structures; the handedness is opposite for a left-handed helix.

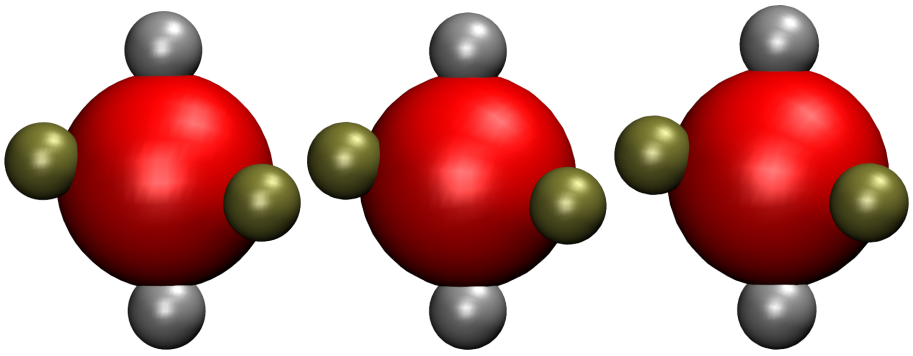

(a) u6 **(b)** d6,6.4 **(c)** d6,5.6

Figure 5.4: Images of the patchy particle designed for each helical design, as specified in Table 5.1. Axial patches (in silver) are exactly opposite each other; lateral patches (gold) are angled at roughly $2\pi/3$ rad, but the precise value varies between designs. The difference between designs is small, and hard to see visually. **(a)** Undistorted helix with 6 particles within each 2π rad loop of the helix (full structure shown in Fig. 5.3). **(b)** Distorted helix, as for (a) but lateral patches are positioned relative to each other as they are in an undistorted helix with 6.4 particles per 2π rad loop. **(c)** As for (b), but 5.6 particles per distorted loop.

The d6,$N_{\text{loop}}^{\text{dis}}$ patchy-particle design is given in Table 5.1 for the particular cases of $N_{\text{loop}}^{\text{dis}} = 6.4, 5.6$. Images of the corresponding particles are shown in Figs. 5.4(b,c).

5.2.3 Design tuning

I primarily needed to fine-tune two variables: $N_{\text{loop}}^{\text{dis}}$ for distorted structures d6,$N_{\text{loop}}^{\text{dis}}$; and the angular patch width σ_{ang}. The output I needed to maximise was the amount of stress, as manifest in twisting and writhing of the helix; but I was limited by the need for the helical structure with $N_{\text{loop}} \approx 6$ to hold together. I thus tested extreme values of $N_{\text{loop}}^{\text{dis}}$ and σ_{ang}, finding the most extreme values for which the $N_{\text{loop}} \approx 6$-helix was stable. (The temperature also must be optimised alongside $N_{\text{loop}}^{\text{dis}}$ and σ_{ang}, but I simulated at a range of temperatures for each set of parameters.) I typically simulated $N = 1998$ particles (333 loops of 6 particles) in the temperature range $0.061 \leq T^* \leq 0.07$, for 2×10^7 MC cycles.

$N_{\text{loop}}^{\text{dis}}$. Given the axial patches are opposite each other, they favour a helix with an integer value of N_{loop} (so that particles are aligned parallel with the axis). Thus, if $N_{\text{loop}}^{\text{dis}} > 6.5$ or $N_{\text{loop}}^{\text{dis}} < 5.5$, the patchy particles I designed would likely favour a helix with $N_{\text{loop}} = n \neq 6$ for some integer n, rather than a twisted helix with $N_{\text{loop}} \approx 6$. (The offset angles of the axial patches, in

Table 5.1: Design details for the patchy particles used to form the undistorted helix with $N_{\text{loop}} = 6$, u6, and two distorted helices, d6,6.4 and d6,5.6. Images of each particle are shown in Fig. 5.4. The design procedure is discussed in section 5.2.

Structure	**Particle type**	**Patch details**					
		Number	Unit vector	Patch type	Interacts with (type)[a]	Reference vector number	Offset angle(s) (rad)[b]
u6	1	1	$(1.0, 0.0, 0.0)$	1	1	2	$2\pi/3$
		2	$(1/6, \sqrt{35}/6, 0.0)$	2	2	1	π
		3	$(-1/6, -\sqrt{35}/12 \approx -0.493007, \sqrt{(35/3)}/4 \approx 0.853913)$	2	2	4	π
		4	$(-1.0, 0.0, 0.0)$	1	1	3	$2\pi/3$
d6,6.4	1	1	$(1.0, 0.0, 0.0)$	1	1	2	$2\pi/3$
		2	$(1/6, \sqrt{35}/6, 0.0)$	2	2	1	π
		3	$(-1/6, -0.546284, 0.820851)$	2	2	4	π
		4	$(-1.0, 0.0, 0.0)$	1	1	3	$2\pi/3$
d6,5.6	1	1	$(1.0, 0.0, 0.0)$	1	1	2	$2\pi/3$
		2	$(1/6, \sqrt{35}/6, 0.0)$	2	2	1	π
		3	$(-1/6, -0.430175, 0.887227)$	2	2	4	π
		4	$(-1.0, 0.0, 0.0)$	1	1	3	$2\pi/3$

[a] Patches of each type selectively interact with patches of only one patch type (which here is the same type).

[b] For the interaction between patch α on particle i and patch β on particle j, offset angles are measured clockwise when looking along $\mathbf{r}_{ij}$ from i to j. They are in the range $[-\pi, \pi)$.

competition with the lateral patches, would still favour $N_{\text{loop}} = 6$; but as discussed, these are more flexible—apply a weaker force—than the lateral patches, since $\sigma_{\text{tor}} > \sigma_{\text{ang}}$.) Tests with $N_{\text{loop}}^{\text{dis}} = 5, 7$ verified this hypothesis: the helix either broke apart, or contracted (respectively, expanded) to form a helix with $N_{\text{loop}} \approx 5, 7$ in certain segments (but not in entirety).

Next, I tested $N_{\text{loop}}^{\text{dis}} = 5.5, 6.5$. In these cases, one may expect the helix to arrange with *either* $N_{\text{loop}} \approx 5, 7$ (respectively) *or* $N_{\text{loop}} \approx 6$, so as to satisfy the axial patches—*i.e.* to choose one or the other nearby integer values of N_{loop}. It is also possible that the arrangement may vary along the helix, perhaps alternating between $N_{\text{loop}} \approx 5, 7$ and $N_{\text{loop}} \approx 6$. While I did not observe such behaviour, there was a significant degree of stress in the helices. The helices twisted, but the integrity of the $N_{\text{loop}} \approx 6$-helix was reduced—even at relatively low temperatures, particles broke off. (In general, the stress seemed greater for $N_{\text{loop}}^{\text{dis}} = 5.5$ than for $N_{\text{loop}}^{\text{dis}} = 6.5$. Most likely this is because the relative change in bond angle is greater in the former case.)

I therefore tested $N_{\text{loop}}^{\text{dis}} = 5.6, 6.4$. The helical structure with $N_{\text{loop}} \approx 6$ was stable, and there was still significant twist. While I also tested $N_{\text{loop}}^{\text{dis}} = 5.7, 6.3$, these values gave reduced stress and twist; see for example Fig. 5.5. So $N_{\text{loop}}^{\text{dis}} = 5.6, 6.4$ seemed most promising; the design is specified in Table 5.1 and particles shown in Figs. 5.4(b,c).

σ_{ang}. Wider patch widths give more flexible bonds, enabling greater twist for a given stress; however they also apply less stress, which is the cause of the twist. In initial simulations I tested $\sigma_{\text{ang}} = 0.2, 0.3, 0.4$ rad (in each case, I used the same value for all patches). Not only was the stress and resulting twist small (see Fig. 5.5 for $\sigma_{\text{ang}} = 0.3$ rad), but it did not change much between these σ_{ang} values (it was slightly greater for larger σ_{ang}). Presumably, this is due to the aforementioned opposing effects of varying σ_{ang}.

The dilemma can be resolved by differentiating the angular patch width of the two patch types. Flexibility in *axial* patchy bonds is primarily what allows twisting. The stress, on the other hand, is applied through the distorted *lateral* patches. Therefore, decreasing the lateral patch

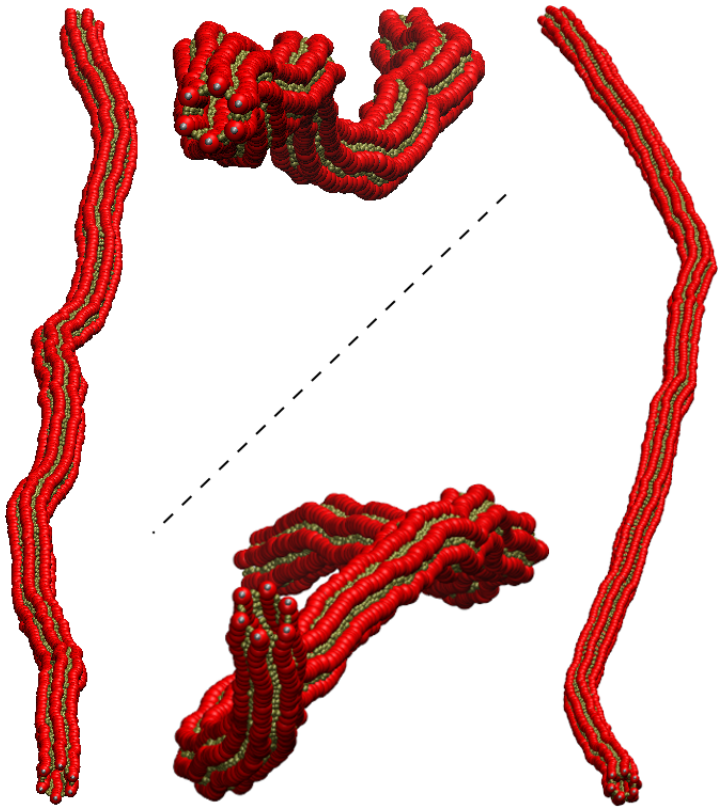

Figure 5.5: Sample conformations for distorted helices, from particle designs d6,6.3 (left/top) and d6,5.7 (right/bottom), each shown from two angles. Note the lack of twist in both structures, and the relatively small writhing for d6,6.3 (the greater writhing for d6,5.7 was uncommon in simulations for $N_{\mathrm{loop}}^{\mathrm{dis}} = 6.3, 5.7$ and/or σ_{ang} 0.3). $N = 1998$, $T^* = 0.07$, $\sigma_{\mathrm{ang}} = 0.3$ rad (for all patches).

width should apply greater stress, and increasing the axial patch width should allow a greater twist response. I tested $\sigma_{\mathrm{ang,lateral}} = 0.1$ rad (*i.e.* for lateral patches) and $\sigma_{\mathrm{ang,axial}} = 0.5$ rad (*i.e.* for axial patches), and this increased the amount of helical twist. [$\sigma_{\mathrm{ang}} = 0.1$ rad means that the interaction is half as strong if one patch angle is 6.7° away from perfect alignment (the other patch being at perfect alignment). For $\sigma_{\mathrm{ang}} = 0.5$ rad, the corresponding angle is 34°.] I therefore used these values for all future simulations.

5.3 Methods

Systems simulated. I simulated particles of the d6,6.4 and d6,5.6 design, in systems of $N = 4998$ particles (833 loops of 6 particles). I also simulated particles of the u6 design as a con-

trol, in systems of $N = 1998$ particles (333 loops of 6 particles).[†] It was important to simulate large systems, because the pitch of the solenoidal shapes is expected to be large (see ahead, section 5.4.1).

Initial configurations. I began simulations with the particles already arranged as in the u6 structure—tube-like, straight, perfectly aligned—rather than from a random, fluid-phase configuration. My interest in this project is the mechanical properties of the assembled structure, rather than its assembly.

Moreover, in simulations for distorted (d6,$N_{\mathrm{loop}}^{\mathrm{dis}}$) helices, I further reduced the simulation time by beginning with particles arranged as in a *twisted* (but still straight, not bent) helix. The appropriate amount of twist was determined from the results of preliminary simulations for smaller systems: 2π rad per 1000 particles (roughly $187\ \sigma_{\mathrm{LJ}}$), left-handed for d6,6.4 and right-handed for d6,5.6. This meant the helices did not have to gradually adopt their twisted configurations—a slow process, as the twist propagate along the axis incrementally.

Helix capping. In initial simulations, I observed that when helices broke apart (because the temperature was too high), this mostly occurred at either end. This is because the end particles have fewer satisfied patchy bonds, so are more weakly bound to the helix. To enable simulation at higher temperatures and thus larger thermal fluctuations, I artificially prevented the end particles breaking off. I did this by increasing (doubling) the strength of all patchy bonds for the final 12 particles ('caps') at each end of the helix. I emphasise that this is purely a simulation technique, not a representation of any real system; but it has no problematic effects (other than reducing the twisting and writhing at the ends of the helix). Capping the helices in this way enabled a simulation temperature increase of roughly 33%. However, due to the harmonic nature of the potential energy close to the equilibrium geometry, this does not correspond to an equal increase in the size of thermal shape fluctuations; rather, the size of shape fluctuations

[†] Although particles in the control system are able to have all their patches perfectly satisfied, their shapes still fluctuate due to thermal energy. But the average conformation should be random.

increases by a smaller amount.

Temperature. Given I was not self-assembling helices, I did not anneal; instead, I simulated at a constant temperature. For each system, I simulated at temperatures just below that at which patchy bonds broke and the helix broke apart (which I refer to as T^*_{melt} for simplicity). The higher the temperature, the larger the thermal shape fluctuations, and the easier to analyse them. So I carefully optimised the temperature for each system. For the d6,6.4 and d6,5.6 systems, I simulated at four temperatures: $T^* = 0.061, 0.066, 0.071, 0.076$ (at $T^* > 0.08$, some particles broke off the helices, over very long time-scales). Higher temperatures were possible for the control system (u6), because its patchy bonds were not stressed; I simulated at $T^* = 0.076$, 0.078, 0.08, 0.082, 0.084, 0.086, 0.088, 0.09.

Other details. I simulated using oxDNA (section 2.2.3.2); $N = 4998$ is around the crossover size when parallel simulations become faster than serial (section 2.2.4.2). For both stressed designs with $N = 4998$, I simulated for $\sim 1.9 \times 10^7$ MC cycles; for the unstressed design with $N = 1998$, I simulated for $\sim 1.2 \times 10^7$ MC cycles.

5.4 Results, analysis, and discussion

I first describe the geometry of my helices, in comparison to that of the 6DH bundles (5.4.1). I begin by measuring some basic mechanical properties of the helices—the amount of twist (section 5.4.2) and the persistence length (5.4.4)—and then perform a more complex analysis of the solenoidal shape fluctuations (5.4.5). [An intermediate computation, of the helix backbone (section 5.4.3), is also required.] I qualitatively compare some results between 6DH bundles and my patchy-particle systems. But as noted these are significantly different systems, and not directly comparable. Representative final configurations for each system are shown in Fig. 5.6.

To analyse solenoidal conformations (other than for measuring the twist), I took a sequence of 150–240 configurations from my simulations (a similar number for each system), spaced at $4\times$

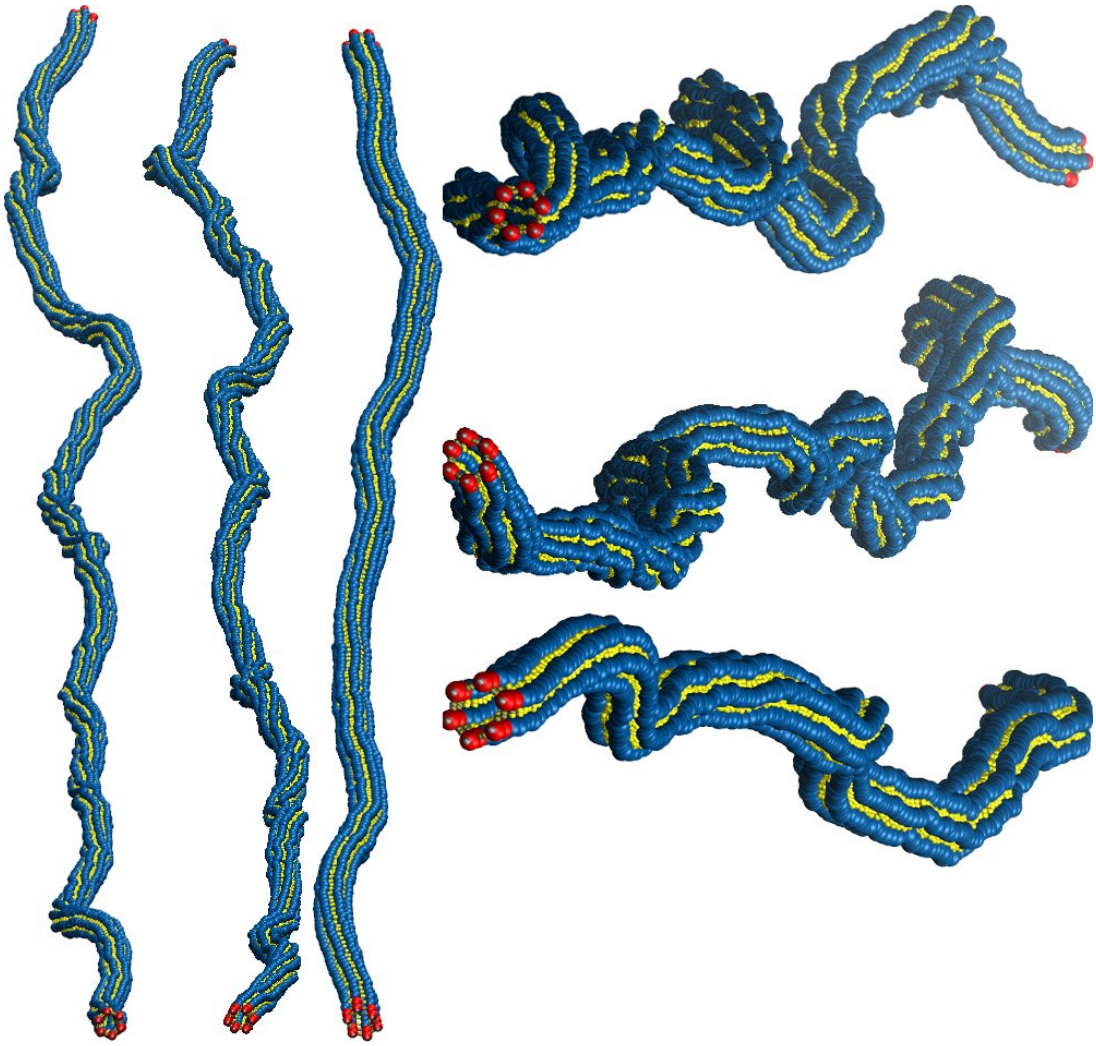

Figure 5.6: Sample conformations showing thermal shape fluctuations of helices. Left- and right-hand images are two angles of the same conformation. Left to right (on left-hand side) and top to bottom (right side): stressed design d6,6.4, stressed design d6,5.6, and unstressed design u6. Note the axial twist in the stressed structures (left-handed for d6,6.4, right-handed for d6,5.6) but negligible twist for u6. $N = 4998$ (d6,6.4 and d6,5.6) and $N = 1998$ (u6), $T^* = 0.076$, $\sigma_{\text{ang,lateral}} = 0.1$ rad and $\sigma_{\text{ang,axial}} = 0.5$ rad.

10^4 MC cycles. I took configurations beginning after relaxation (*i.e.* once the amounts of twisting and writhing were constant).[†] I averaged each of my measurements over these conformations, to give statistically significant results. Thermal fluctuations mean individual conformations may not be representative, but since thermal fluctuations are random, the average of a measurement over a sufficient number of distinct conformations *is* representative.

[†] I gauged this directly by visual inspection. At the start of simulations, helices were straight; they began bending immediately, and at a certain point the amount of writhing was fairly constant (but the shape of individual conformations still varied).

5.4.1 System geometry

The following values are estimates to allow qualitative comparison. The *contour length*, l_c, of a polymer chain is the distance from one end to the other in the chain's longest (physically possible) conformation [89]. For a 6DH bundle or one of my helices, this is the distance when the chain is perfectly straight (or when bent, the length as measured along the backbone).

6DH bundles. The 6DH bundles have experimental contour length $l_c \approx 420$ nm [36]. I estimate the diameter, D, of the bundle (measured to the 'outsides', *i.e.* based on its excluded volume) to be $D_{6\mathrm{DH}} \approx 8$ nm.[†] This gives a filament aspect ratio of $l_c/D \approx 52.5$—high for experiments, and similar to that for *fd* virus. For the 6DH bundles, the solenoidal pitch was of the order of 25–125 nm ≈ 76–378 bp ≈ 3.1–16 $D_{6\mathrm{DH}}$; thus, a similar (or larger) aspect ratio should be suitable to observe solenoidal fluctuations in a similar system.

Given there is a cross-link on average every 10.5 bp, and each double helix within a bundle has 1268–1270 bp [36], there are ~ 121 cross-links per double-helix; thus, each double helix is bonded to *one of* its neighbours on average every $\sim 0.434\ D_{6\mathrm{DH}}$.

Patchy-particle helices. The diameter of my (unstressed) patchy particle (labelled 'PP') helices, again measured to the outside, is $D_{\mathrm{PP}} \approx 3.34\sigma_{\mathrm{LJ}}$ (treating each patchy particle as having a diameter of the LJ minimum, $2^{1/6}\sigma_{\mathrm{LJ}}$). For untwisted helices in their ground state, with $N = 4998$, $l_c \approx 935\sigma_{\mathrm{LJ}}$; for $N = 1998$, $l_c \approx 374\ \sigma_{\mathrm{LJ}}$. (The average contour length of the relaxed helices increases only slightly, moreso at higher temperature: for $N = 4998$ and d6,6.4, $l_c \approx 941\sigma_{\mathrm{LJ}}$; for $N = 4998$ and d6,5.6, $l_c \approx 939\sigma_{\mathrm{LJ}}$; for $N = 1998$ and u6, $l_c \approx 376\sigma_{\mathrm{LJ}}$.[†]) Thus, for $N = 4998$, the aspect ratio $l_c/D_{\mathrm{PP}} \approx 285$; for $N = 1998$, $l_c/D_{\mathrm{PP}} \approx 112$. These values are significantly greater than those for the 6DH bundles; my systems should be large enough to observe any potential solenoidal shape fluctuations.

[†] In 2D origami, the average separation between double helices is ~ 3 nm [650,651], and the diameter of a B-DNA double helix is ~ 2 nm [650,652]. Thus, the bundle diameter can be estimated as $D_{6\mathrm{DH}} \approx 3 \times 2 + 2 = 8$ nm.

[†] These values are averages over all temperatures simulated, for each system, and over all relaxed configurations.

Each axial chain is bonded to *both* its neighbours at every particle in the chain, *i.e.* every $\sim 0.336\ D_{\mathrm{PP}}$—a much higher frequency of 'cross-linking' than for the 6DH bundles.

5.4.2 Twist

The amount a helix twists is easily measured. The average twist in the stressed helices after relaxation is similar to that in their initial twisted configurations, as expected (because the twist used in the initial configurations was obtained from the twist in stressed, bent helices). That is, the stressed helices twisted approximately 2π rad per 1000 helical particles, or 0.112 rad per D_{PP}, left-handed for d6,6.4 and right-handed for d6,5.6. The unstressed helix, u6, had negligible twist, as expected. The respective twists can be seen in Fig. 5.6. For comparison, for the lh and rh 6DH bundles (those with one complete twist), the ground-state twist (*i.e.* before shape deformations) is 0.120 rad per D_{6DH}. (The twist is expected to decrease somewhat during relaxation.) The presence of a significant amount of twist in my systems confirms that my stressed designs do indeed apply a torque and induce twisting, in the correct directions.

5.4.3 Helix backbone

To calculate the persistence length and analyse shape fluctuations, I require the contour of the helix backbone, rather than the helical path defined by the sequence of patchy particles. The helix *backbone* is a sequence of points through the centre of the helix. I define each backbone point as the average position of 6 consecutive particles, with one backbone point defined for each particle (except the first 2 and final 3 particles).[†]

This definition is imperfect, because in twisted helices (with $N_{\mathrm{loop}} \approx 6$), 6 particles do not complete a loop of exactly 2π rad; the rotation is slightly more or less due to the twist. Thus, the average position of 6 particles is not exactly at the centre of the helical path; it is biased to one side, and the direction of bias oscillates along the helix contour. The size of this variation is neg-

[†] Formally, the points of the backbone, $\mathbf{b}_i$, are defined as $\mathbf{b}_i = \sum_{i-2}^{i+3} \mathbf{r}_i/6$. Thus for a helix of N particles, the backbone has $N-5$ points.

ligible when analysing conformations (5.4.5), because the bias is dominated by the writhing of the whole helix. However, the bias is noticeable when measuring the persistence length (5.4.4).

5.4.4 Persistence length

5.4.4.1 Definition and calculation method

The *persistence length*, l_p, measures the stiffness (the inverse of flexibility) of a rod-like object. It is the length scale below which the object behaves as a flexible rod (*i.e.* with some consistency in direction along its contour), and above which its conformation must instead be treated statistically. More formally, l_p is the length over which correlations in the tangential direction of the rod are lost. Consider the exponential decay given by

$$\langle \cos\omega \rangle_s = \exp(-L/l_p), \tag{5.1}$$

where '$\langle\rangle_s$' denotes an average (expectation value) over both all points s along the rod's contour, and over an ensemble of configurations. ω is the angle between the tangent at s and that at $s+L$[†] (which is distance L along the contour from s). l_p is the characteristic length scale of this decay. From Eq. 5.1, l_p is given directly by

$$l_p = \frac{-L}{\ln\langle \cos\omega \rangle_s}. \tag{5.2}$$

I calculated the (discretised) tangent at each point along the backbone, and then calculated the persistence length following Eq. 5.2. I calculated l_p for a discrete set of values of L: $\{1, 2, \ldots, M\}\ \Delta s$, where $M = 4000$ for $N = 4998$ (and $M = 1350$ for $N = 1998$), and Δs is the distance between consecutive points on the helix backbone (which is equivalent to the axial distance between consecutive particles along the helical path).[‡] For each value of L, in calculating l_p I averaged over all backbone points s except the first 12 and final $12 + L$ backbone points,

[†] Thus, $\cos\omega = \hat{\mathbf{t}}(s) \cdot \hat{\mathbf{t}}(s+L)$, where $\hat{\mathbf{t}}(s)$ is the unit vector in the direction of the tangent to the contour at point s.

[‡] Calculating l_p for larger values of L would give reduced statistical reliability, since too few pairs of backbone points are spaced more than $M\Delta s$ apart. In any case, I tested various M, and my values were suitable.

as the mechanical behaviour may differ somewhat at the ends of the backbone from the rest of the backbone—generally the ends are less constrained, but in this instance the cap particles also have stronger bonds. I averaged over all relaxed configurations of a simulation at the same time as averaging over backbone points s.

5.4.4.2 Results

The persistence length is plotted as a function of the backbone separation which it was measured, L, in Fig. 5.7. To discuss the shape of the curves, I first compare my helices to a *worm-like chain* (WLC) [653]. A WLC is a model polymer that is semi-flexible (stiff; rigid at small length scales, *i.e.* neighbouring segments point in very similar directions, but flexible at large length scales) and continuously flexible (*i.e.* the flexibility is constant—and the bending modulus well-defined—over all length scales). The corresponding plot for a WLC is a horizontal line—l_p is the same when measured at any L. However, my helices are *not* continuously flexible, because they are granular—they are defined by discrete particles. On small length scales, flexibility is affected—increased—by individual patchy bonds, and the bending modulus is poorly defined. At larger length scales, when the granularity becomes negligible, the flexibility is constant. This explains the shape of the curves in Fig. 5.7. At short length scales ($L \lesssim 550\sigma_{\mathrm{LJ}}$, for d6,6.4 and d6,5.6, or $L \lesssim 200\sigma_{\mathrm{LJ}}$, for u6), l_p is not constant, rather it increases fairly steadily (*i.e.* the helices are flexible, and the tangents are poorly correlated). But at longer length scales, l_p is more constant, and higher (*i.e.* the helices are stiffer, and the tangents are better correlated). The value of interest is that in the long length-scale limit; measuring l_p at a range of L helps confirm whether it was measured at sufficiently large L.

The second feature of interest is the high-frequency, periodic oscillation in l_p for the d6,6.4 and d6,5.6 designs [only visible on close inspection of Fig. 5.7(a,b), but manifested in the breadth of the curves]. This is due to the imperfect definition of the helix backbone for twisted helices (section 5.4.3). The position of each backbone point is biased; the direction of bias varies peri-

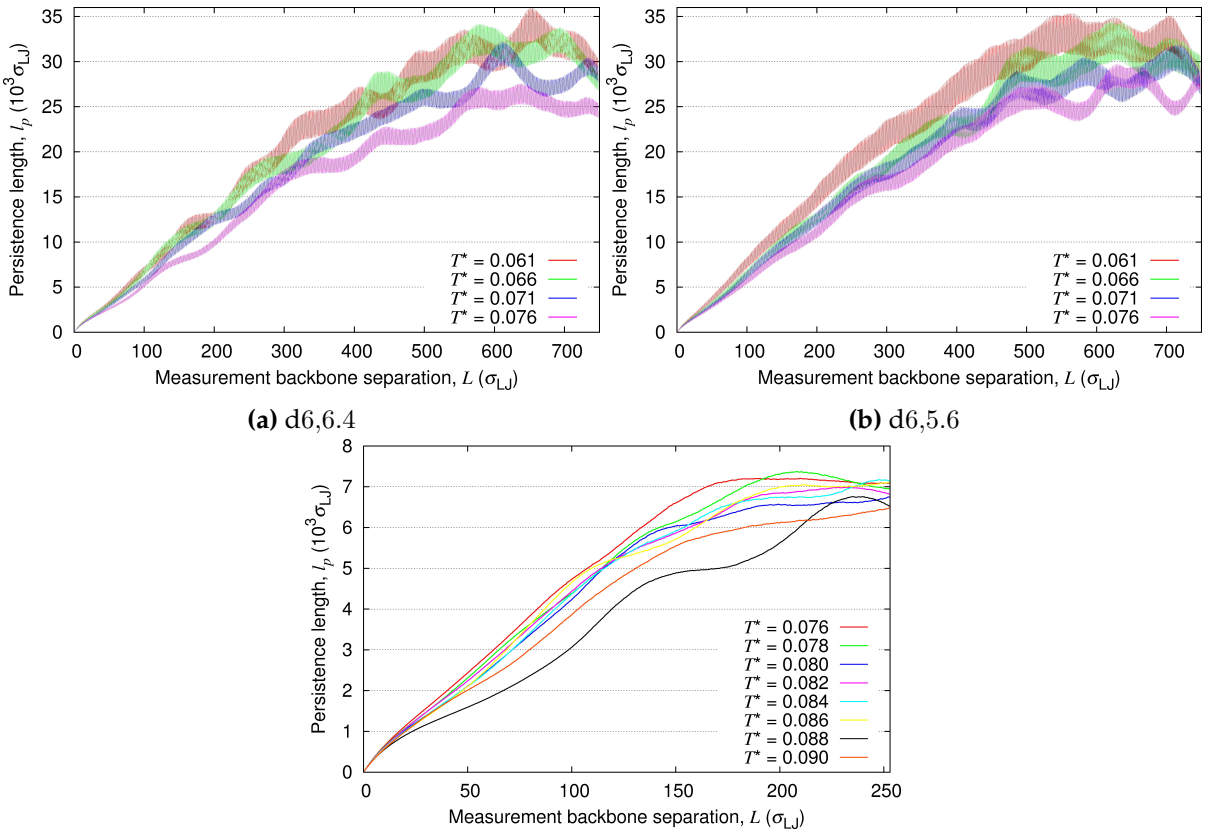

(a) d6,6.4 **(b)** d6,5.6

(c) u6

Figure 5.7: Persistence lengths, l_p, of patchy particle helices, as measured at backbone separation L (along the helix backbone contour) according to Eq. 5.2, for d6,6.4, d6,5.6, and u6 systems. $N = 4998$ (d6,6.4 and d6,5.6) and $N = 1998$ (u6).

odically along the backbone. Any bias causes a weakening (as opposed to strengthening) in the correlation between the direction of two tangents, because the bias is always perpendicular to the direction of the true backbone. The weakening of the correlation is greater for some values of L than for others, depending on the periodicity of the bias. In fact, the period of oscillation in l_p in Fig. 5.7 is roughly $2^{1/6}\sigma_{\mathrm{LJ}}$. This is the same period as of the oscillation in the bias of the backbone (*i.e.* the backbone distance covered by 6 particles around the helical path). Those values of L with the least weakened correlation correspond to the most accurate measurement of l_p. Therefore, the best measurement of l_p is the *largest* (*i.e.* measured at the peaks of the oscillations, in the asymptotic region).

I also note that there is some larger-scale fluctuation in the curves in Fig. 5.7; this is presumably statistical.

In any case, my measurement of l_p is only approximate, for better understanding of the mechanical behaviour of my helices, and for comparison with the 6DH bundles. Considering a temperature of $T^* = 0.076$ for comparison across each design, from Fig. 5.7: for the unstressed u6 systems, $l_p \approx 7500\sigma_{\mathrm{LJ}} \approx 2250\ D_{\mathrm{PP}}$; for d6,6.4, $l_p \approx 26000\sigma_{\mathrm{LJ}} \approx 7800\ D_{\mathrm{PP}}$; for d6,5.6, $l_p \approx 30000\sigma_{\mathrm{LJ}} \approx 9000\ D_{\mathrm{PP}}$. These values correspond to $l_p/l_c \approx 20$, 28, 32, respectively. For the 6DH bundles, $l_p \approx 2400$ nm $\approx 300\ D_{\mathrm{6DH}}$ and so $l_p/l_c \approx 5.7$ [36]. Thus, my helical objects are far stiffer than the 6DH bundles; most likely this relates (at least partly) to their higher frequency of bonds between axial chains (section 5.4.1). The stiffness can also be seen by the small shape fluctuations in Fig. 5.6.

One possible source of error in these measurements is that the range of L is not great enough to confirm that the measured values have reached their limiting values at large L. (This is not helped by the greater statistical noise in the data for larger L.) It is unusual that l_p is smaller for u6 than for d6,6.4 or d6,5.6—the absence of stress should not increase flexibility. Moreover, the gradients of the u6 plots (Fig. 5.7) roughly match those for d6,6.4 and d6,5.6, until they flatten at larger L. Perhaps if the system size for u6 was the same as for d6,6.4 and d6,5.6, the measured l_p values would continue increasing at larger L, to similar values as for d6,6.4 and d6,5.6. By the same argument, the values for d6,6.4 and d6,5.6 may be slight under-estimates.

5.4.5 Solenoidal shape fluctuations

5.4.5.1 Background

To analyse solenoidal shape conformations, I followed the approach introduced in Ref. 5; full explanations and derivations are provided therein. I quantified how much a deformation mode of a helical object (about its long axes) matched a solenoid. More specifically, I measured the extent to which the helical tubes adopted a circular solenoidal conformation, either left- or right-handed, for a given solenoidal pitch; I repeated for a range of pitches. The measure of circular helicity (of the solenoidal conformation backbone, not the particles within the helix), $\mathcal{H}$, takes

values in the range $[-1, 1]$. The sign gives the handedness, $\mathcal{H} < 0$ for left-handed and $\mathcal{H} > 0$ for right-handed; the magnitude gives the degree of helicity. Thus, $\mathcal{H} = -1$ for a perfect left-handed circular solenoid, and $\mathcal{H} = 1$ for a perfect right-handed solenoid. A Fourier analysis calculates $\mathcal{H}$ at discrete wavenumbers, $k > 0$, corresponding to the reciprocal of the pitch of a solenoidal deformation mode. So this analysis measures helicity (or its absence), and the handedness, at different values of the pitch; it reveals the pitch and handedness of the most strongly adopted solenoidal deformation mode.

By way of further explanation, consider a *perfect*, circular solenoid with its solenoidal axis in the z direction. A *transverse position vector*, $\mathbf{r}_\perp$, is the vector from the solenoidal axis, in the xy-plane (*i.e.* perpendicular to the axis), to a point along the solenoid. Moving in the z direction (along the axis), the x- and y-components of $\mathbf{r}_\perp$ oscillate periodically with equal amplitude and frequency and a $\pi/2$ rad phase offset. For an *arbitrary* (imperfect) conformation with its long axis aligned with z, the x- and y-components of $\mathbf{r}_\perp$ are taken with respect to the curvilinear abscissa of the backbone. By measuring the cross-correlation between the x- and y-components, one quantifies their coherence and so quantifies the helicity of that conformation. This measurement is repeated for many Fourier modes of the x- and y-components of $\mathbf{r}_\perp$. Because the more general solenoidal cross-section shape is elliptical, not circular, the complete analysis is more complicated; Ref. 5 gives further details.

In addition to the net backbone helicity, I quantified the average geometrical shapes of the helical deformation modes. I calculated the elliptical semi-major and semi-minor axes, r_+ and r_-, respectively, to determine how circular or elliptical is the cross-section of a solenoidal deformation mode (for various Fourier modes). I also calculated $||\tilde{\mathbf{r}}_\perp||^2$, the square of the magnitude of the Fourier components of the transverse position vector (*i.e.* the size of deformations perpendicular to the axis).[†]

In calculating all these values, I again averaged over all relaxed configurations. Only long-

[†] '$||\tilde{\mathbf{r}}_\perp||$' denotes the Euclidean norm of $\tilde{\mathbf{r}}_\perp$, *i.e.* $||\tilde{\mathbf{r}}_\perp|| = \sqrt{\tilde{\mathbf{r}}_\perp \cdot \tilde{\mathbf{r}}_\perp^*} = \sqrt{|\tilde{r}_{\perp x}|^2 + |\tilde{r}_{\perp y}|^2}$. $\tilde{\mathbf{r}}_\perp^*$ is the complex conjugate of $\tilde{\mathbf{r}}_\perp$. $\tilde{\mathbf{r}}_\perp$ is the Fourier transform of $\mathbf{r}_\perp$.

wavelength deformation modes are of interest—$k \lesssim 0.05\ \sigma_{\mathrm{LJ}}^{-1}$. The distance over which a stressed patchy-particle system twists 2π rad corresponds to $k \approx 0.0053\ \sigma_{\mathrm{LJ}}^{-1} \approx 0.018\ D_{\mathrm{PP}}^{-1}$ (section 5.4.2), and this is roughly the length scale over which solenoidal conformations are expected. The 6DH bundle systems have a similar amount of twist to mine (section 5.4.2), so one may expect similar wavelength solenoidal deformation modes. In the 6DH bundle systems, the strongest solenoidal conformation was at $k \approx 0.015\ \mathrm{nm}^{-1} \approx 0.12\ D_{\mathrm{6DH}}^{-1}$. This corresponds in my systems to $k \approx 0.12\ D_{\mathrm{PP}}^{-1} \approx 0.036\ \sigma_{\mathrm{LJ}}^{-1}$. Given my systems are stiffer than the 6DH bundles (section 5.4.4.2), one might expect longer-wavelength (smaller-k) solenoidal conformations.

5.4.5.2 Results and discussion

Helicity. The helicity analysis is presented in Figs. 5.8(a–c). The measured helicity is clearly very noisy, across all wavenumbers. There is no obvious pattern, either within or between the u6, d6,6.4, and d6,5.6 systems. Certainly, one cannot discern anti-chiral shape deformations (*i.e.* opposite handedness of the solenoidal conformations and the helical twists)—the handedness of the conformations at different k fluctuates frequently, seemingly randomly. It is not clear what, if any, is the strongest solenoidal deformation (either its pitch or handedness), for each simulation. At small length scales (large k), $\langle \mathcal{H}(k) \rangle$ is expected to converge towards zero—or at least be much closer to zero than for small k. This is because short-length fluctuations are expected to be entirely random, so should cancel when averaged over many configurations. However, this is not the case in my systems—the magnitude of $\langle \mathcal{H}(k) \rangle$ is still large at $k \gg 0.05\ \sigma_{\mathrm{LJ}}^{-1}$. The noise is greater at large length scales (small k), presumably because fluctuations take longer to equilibrate at these length scales.

In order to reduce the noise, for each system (d6,6.4, d6,5.6, and u6), I averaged over configurations at *all* temperatures (*i.e.* for different simulations), and performed the same anaysis; the results are in Figs. 5.8(d). This is physically reasonable because I do not expect $\langle \mathcal{H}(k) \rangle$ to be strongly temperature-dependent: if there is a signal, it should be the same at different tem-

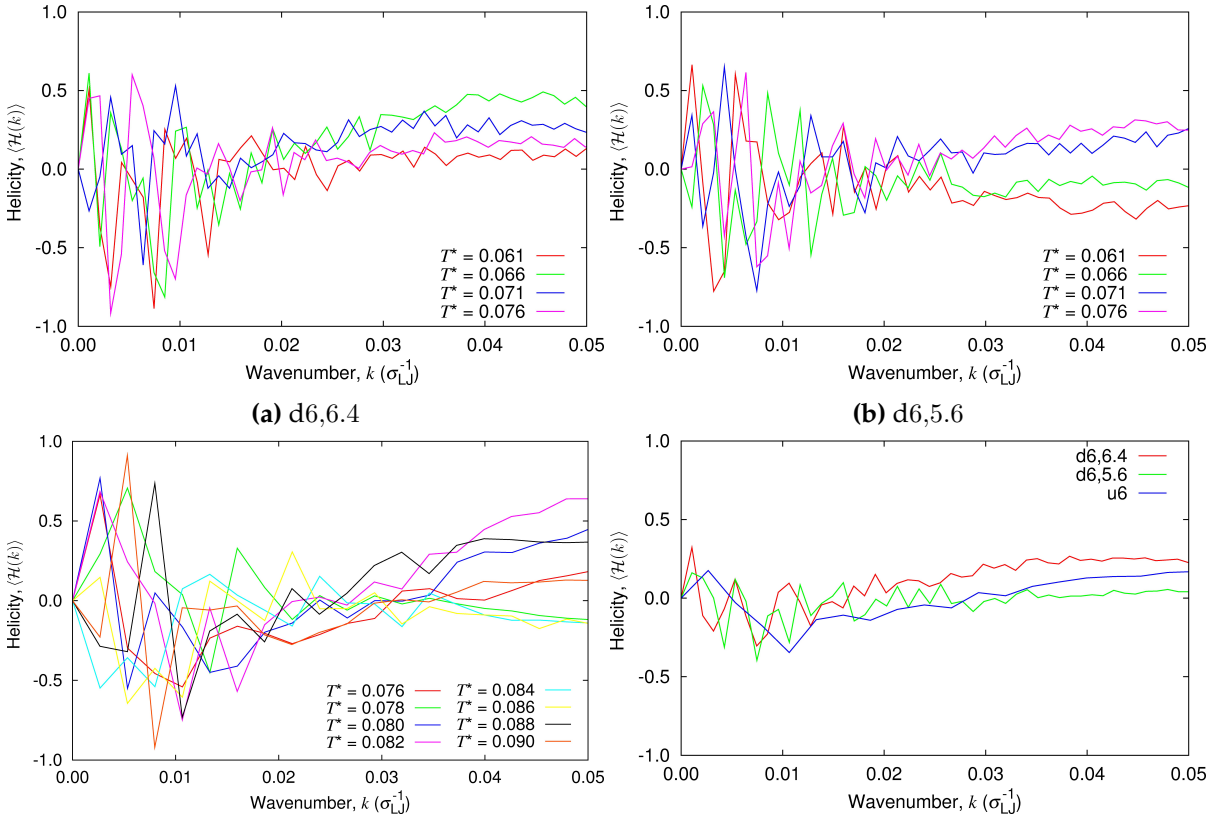

(a) d6,6.4 **(b)** d6,5.6

(c) u6 **(d)** Averages over different temperatures

Figure 5.8: Average (across all relaxed conformations) backbone helicity of solenoidal deformation modes, $\langle\mathcal{H}(k)\rangle$, as a function of wavenumber k, for d6,6.4, d6,5.6, and u6 systems. In **(d)**, I averaged all configurations used to calculate (a), (b), and (c). $N = 4998$ (d6,6.4 and d6,5.6) and $N = 1998$ (u6).

peratures (only slightly weaker or stronger). Although the results are less noisy, there is still no clear trend within or between the systems; the magnitudes are smaller, suggesting no significant signal.

Perhaps the shape fluctuations of the helices are not at equilibrium (despite long simulation times), or the sampling is insufficient. But equilibration time is faster at small length scales than at large length scales, and as noted noise is still present at shorter length scales. Moreover, the results changed little when I analysed configurations from earlier in the simulations, suggesting the simulations were not further converging. Thus, I do not think the problem is simply that the systems have not equilibrated.

The solution to the high signal-to-noise ratio in the results is probably simply to run the simulations for longer in order to obtain a greater number of uncorrelated configurations over

which to average. That no clear trends have emerged so far may be due both to (1) the high stiffness of the helical tubes (as noted in section 5.4.4.2), and (2) the complexity of the network of axial and lateral interactions within the tubes. Regarding (1), the stiffness is a result of the narrowness of the patch widths that were needed to induce significant twists in the tubes. The stiffness may reduce the signal as the potential energetic advantage of chiral over achiral fluctuations is likely to be smaller when the fluctuations are smaller. Regarding (2), although the initial expectation was that solenoidal writhing of the appropriate handedness would be favoured as it would reduce the internal stress in the *axial* interactions, it is less clear what effects it has on the energetically-as-important *lateral* interactions. The stiffness and complex network of interactions are ultimately due to the design of the system; thus, a possible approach to reduce the noise is to improve the design. I discuss this in section 5.5.

In any case, I obtained a null result, which neither supports nor opposes the observation of anti-chiral shape deformations in 6DH bundles [5].

Fluctuation shape and size. Given the null result, the geometric details of the helices are of less interest; but I present them to help better understand my results. Fig. 5.9 shows the average semi-major and -minor elliptical axes across a range of solenoidal deformation modes. Notice first that $\langle r_+ \rangle$ and $\langle r_- \rangle$ are both very small, of the order of 1 $\sigma_{\mathrm{LJ}}^{-1}$ or less. This is consistent with the high stiffness of the tubes. Clear solenoidal shape fluctuations are unlikely when the fluctuations are so small. Secondly, notice that $\langle r_+ \rangle$ and $\langle r_- \rangle$ both decrease as the length scale decreases (*i.e.* k increases), as expected; fluctuations can be (and are) larger at larger length scales. Thirdly, the conformations have a significant degree of ellipticity (rather than circularity): $\langle r_+ \rangle / \langle r_- \rangle$ is typically of the order of 4. Fourthly, as for $\langle \mathcal{H}(k) \rangle$, the results are similar for all three systems studied. Finally, a significant amount of noise is present (especially at small k, for which equilibration of fluctuations takes longer), although in this case the trend is clearer.

The transverse fluctuation spectrum is shown in Fig. 5.10. This presents the average values

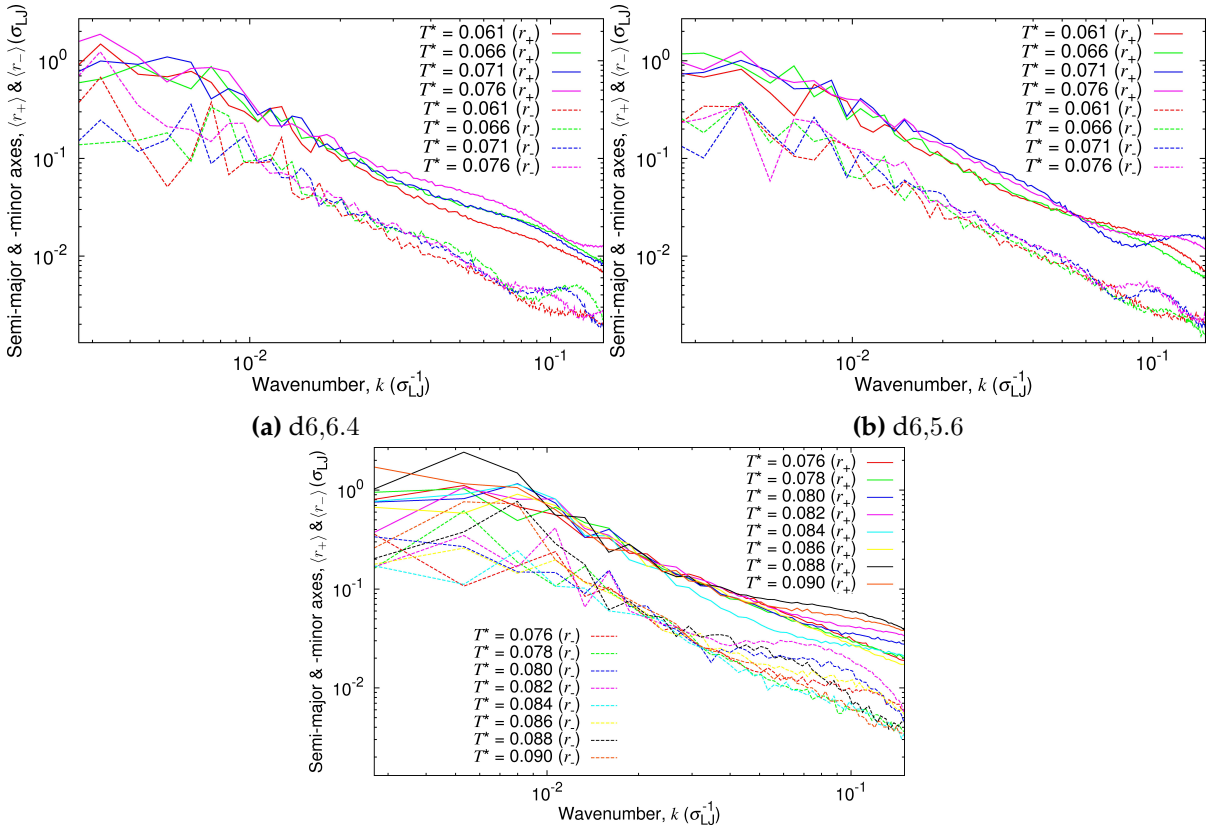

(a) d6,6.4 **(b)** d6,5.6

(c) u6

Figure 5.9: Average (across all relaxed conformations) semi-major and -minor axes, $\langle r_+ \rangle$ and $\langle r_- \rangle$, of elliptical shapes of solenoidal deformation modes, as a function of wavenumber, k, for d6,6.4, d6,5.6, and u6 systems. Both axes are scaled logarithmically. $N = 4998$ (d6,6.4 and d6,5.6) and $N = 1998$ (u6).

of $||\tilde{\mathbf{r}}_\perp||^2$ as a function of k—indicating the size of the solenoidal deformation modes. While the results are similar for all three systems studied, $\langle ||\tilde{\mathbf{r}}_\perp||^2 \rangle$ is slightly greater for the stressed designs than for the unstressed control, as expected. The stressed patchy bonds cause a strain which is offset by writhing. As for $\langle r_+ \rangle$ and $\langle r_- \rangle$, $\langle ||\tilde{\mathbf{r}}_\perp||^2 \rangle$ decreases (*i.e.* fluctuations become smaller) as the length scale decreases, and some noise is present (especially at small k). The scaling of $\langle ||\tilde{\mathbf{r}}_\perp||^2 \rangle$ with k is similar to that observed for 6DH bundles [5].[†]

5.5 Conclusions

I have demonstrated the design and simulation of patchy particles which apply internal mechanical stress to a structure, through imperfectly aligned patches; such a project is unique. I

[†] $\langle ||\tilde{\mathbf{r}}_\perp||^2 \rangle$ scales roughly as k^{-3}, at larger k. The ideal scaling at small k is k^{-4} [5].

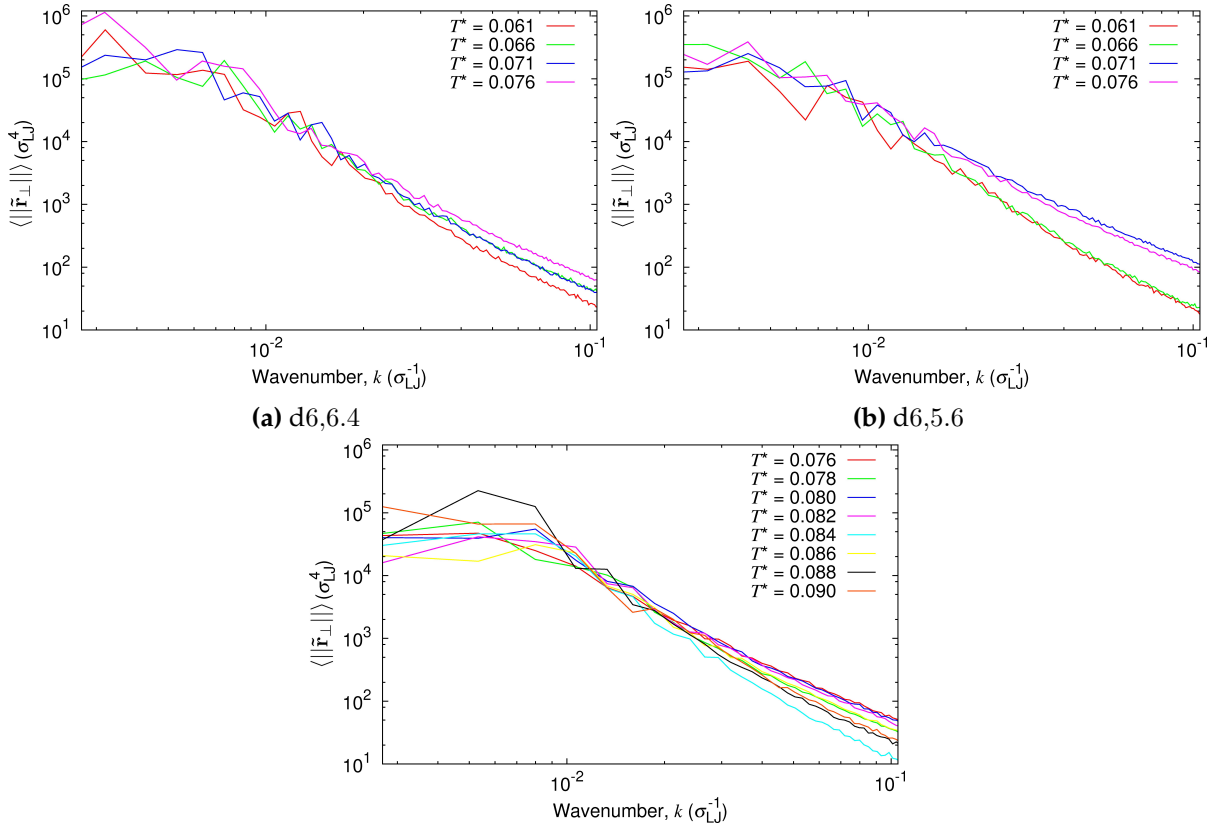

(a) d6,6.4 **(b)** d6,5.6

(c) u6

Figure 5.10: Transverse fluctuation spectrum of elliptical shapes of solenoidal deformation modes, as a function of wavenumber, k, for d6,6.4, d6,5.6, and u6 systems. Vertical axes represent the average (across all relaxed conformations) of $||\tilde{\mathbf{r}}_\perp||^2$. Both axes are scaled logarithmically. $N = 4998$ (d6,6.4 and d6,5.6) and $N = 1998$ (u6).

studied the example of helical, tube-like objects. The stress caused the helices to deform by twisting; a control system, without stress, had no average twist and smaller average shape fluctuations. However, I did not demonstrate the phenomenon of anti-chiral shape deformations recently observed in DNA origami systems of bundles of six double helices [5]. I observed no clear trend in shape deformations; my systems showed a null result, neither supporting or opposing this previous result. Thus, the main question raised is how solenoidal shape deformations can be better observed in patchy-particle systems—*i.e.* what can be done differently.

As noted (section 5.4.5.2), longer simulations may be required to better equilibrate the systems and to increase the number of uncorrelated configurations over which to average. Other algorithms which are more efficient for clusters may be useful, such as virtual move MC (section 2.2.5.2) or molecular dynamics (section 2.2.5.1), which allow collective motion. Parallel MC

simulations may also be useful. Alternatively, simulating larger systems may be worthwhile, in case solenoidal fluctuations occur on a larger length scale, but this will further increase the equilibration times.

That no clear trend was yet apparent from the results may be due to the stiffness of the helices, and/or the complex interplay between axial and lateral interactions. In this case, the best means of observing them may be a change to the helical (and patchy particle) design.[†] Regarding stiffness, the difficulty is achieving a balance: stiff individual patchy interactions (*i.e.* small σ_{ang}) apply more stress, which is the cause of shape fluctuations; but they also oppose bending, and thus reduce thermal fluctuations. In the 6DH bundles, stress comes from twisting an individual double helix; these can be twisted more or less. Flexibility for shape fluctuations is controlled by cross-links between double helices; more cross-links make the bundles stiffer. Thus, the amount of stress and the bending flexibility are uncoupled in 6DH bundles, and can be separately tuned; no balancing act is required.

Perhaps no solution is possible within similar patchy-particle systems. I tested larger distortions in the bond angle (section 5.2.3), but this was unsuccessful; in any case, the distortions I did use were already large enough to generate significant helical twisting. I also tried changing the offset angles and angular patch widths (the torsional patch width does not seem relevant).

However, I offer one alternative design suggestion. It attempts to more closely model the 6DH bundle systems, in order to replicate their behaviour. The design is as follows: retain all axial patches, but use fewer lateral patches (for example, lateral patches could be placed only on every third particle in an axial chain); use the offset angles of the axial patches to induce twisting down each axial chain; thus, each lateral bond will be stressed by the relative twist of neighbouring axial chains. (Lateral patch angles may no longer need to be distorted.) This design treats each axial chain of patchy particles more like a double helix in a 6DH bundle, and lateral patches more like cross-links. It will increase bending flexibility, and if carefully de-

[†] One could instead focus on increasing the size of the fluctuations (as I did by capping my helices), for example by tuning the bond strengths and temperature.

signed, the lateral stress may still be significant. However, the design is more complicated, with more parameters. But if such a design shows solenoidal—and anti-chiral—shape fluctuations, it may help clarify the origins of cholesteric ordering in rod-like, chiral mesogens.

Finally, I note an intriguing similarity between the structures of my systems and the tobacco mosaic virus [Fig. 5.1(d)]—both are (weakly-inclined) helices, with both axial and lateral interactions. My systems as yet did not show chiral shape deformations, and so if this is the mechanism for cholesteric ordering, as argued in Ref. 5, they may not form a cholesteric phase. Tobacco mosaic virus also does not form a cholesteric phase. In contrast, the 6DH bundles and *fd* virus [Fig. 5.1(c)] are structured as parallel, long filaments. Both these systems form cholesteric phases, in the former case (at least) due to chiral shape fluctuations. I speculate that the reason for the different behaviour of the systems—and concerning the viruses, this is an unsolved problem—may be these different kinds of structures.

Chapter 6

Conclusion

6.1 Overview of topics

In this thesis, I explored the rational use of patchy particles to control material properties, by designing particles to either *assemble into* a target structure, or to *apply internal stress to* a structure. Patchy particles, usually colloids or NPs, are actively researched and generate broad interest. The ability to synthesise them has improved greatly over the past 15 years, with precision (*e.g.* to give monodisperse products), variety, and customisation. As such, we are seeing increasingly complex structures assembled from patchy particles, both finite clusters and extended phases. Simulations continue to pioneer our understanding of their behaviour and possible assemblies.

The many possible applications of colloidal particle or NP assemblies centre on materials, devices, and technologies, in diverse fields, at the nano- and micro-scales. These assemblies can have a range of interesting properties (*e.g.* photonic, electronic, optical, mechanical, magnetic, plasmonic)—and undoubtedly, more will be discovered, allowing unforeseen uses. Often the proposed applications of colloidal or NP assemblies require complex, extended, 3D structures; thus I pursued such structures in this thesis. Patchy particles are especially promising for these structures because they can be rationally designed and tuned. They are thus suitable for self-assembly (which has greater potential than top-down approaches), and for applying internal stress. Since my research is general and theoretical, it is difficult to predict specific applications; but it may be of value in unexpected ways. In addition, understanding the behaviour of systems of patchy particles is useful for understanding similar natural systems, such as proteins (*e.g.* viruses) and condensed matter systems.

I addressed the fundamental question of how to design a system that forms a given (ordered)

structure, here by the design of self-assembling patchy particles. I used—and extended—one of two main patchy-particle models from prior simulations. Using both a serial and a newly-developed parallel MC algorithm (for the former, I implemented the patchy-particle model; for the latter, I analysed its speedup), I performed simulations of particle assembly and behaviour. I observed successful—and failed—self-assembly of target structures, and analysed the assembly kinetics and the structures formed. I pursued more complicated (3D, extended phases, large unit cells or quasicrystalline) structures than in previous research. I also explored the design of patchy particles to invoke internal mechanical stress in a structure, specifically a helical tube-like object; and I used such stressed structures to study physical behaviour, specifically chiral shape fluctuations. This example is relevant to the origins of cholesteric ordering in rod-like, chiral mesogens. Furthermore, this is the first study I am aware of in which internal stress was deliberately introduced and studied in a patchy-particle system. All the above pursuits touch on another fundamental question, that of how individual particle interactions determine collective structure and behaviour.

6.2 Summary of results

I carried out three distinct but related projects, and here I briefly review the outcomes of each.

6.2.1 Periodic crystals

In Ch. 3, I demonstrated a systematic design scheme for a set of patchy particles to form a unique and specific periodic target structure. In the resulting designs, the target structure is the free-energy global minimum structure (below some cutoff temperature), due to the specificity encoded by precise patch positions, patch-interaction selectivity, and restrictions on the torsional orientations of bonded particles (a fairly novel feature of my designs). The scheme can be applied to any periodic structure, using that structure's crystallographic symmetry. As a proof-of-concept, I demonstrated the correctness of the designs, and the ability of the sets

of patchy particles to self-assemble into their respective target structures, for five complex, extended, 3D structures: clathrate types I and II, BC8, cP4, and A15. These structures extend those previously assembled from patchy particles, which are mostly simple, 2D structures, and often finite. The sets of patchy particles I used were correspondingly more complex than in other studies—though they are not out of the realm of experimental possibility. Moreover, the design scheme is entirely *rational*; many previous studies simply observed and analysed the structures formed from given particles, or designed particles more intuitively.

All structures assembled successfully and robustly in reasonable simulation times; they were thermodynamically favoured, and kinetically accessible. (Structures with more complex and specific designs generally formed more slowly.) Notably, the model's ignorance of different nearest-neighbour bond distances within a structure did not matter. Torsional interactions kinetically assisted formation, by controlling *next*-nearest neighbour bonding and thus disfavouring disordered aggregates which often form without them. I observed they were essential for the formation of one structure (BC8), but not for another (clathrate I); the difference is presumably due to the greater specificity of the clathrate I design (due to its greater complexity). The assembly of sets of particles with significantly different numbers of patches may be problematic, as the particles' binding energies can then be quite different, but it did not prevent A15 assembling. It is possible to simplify my patchy-particle designs—*i.e.* reduce the encoded information—which would be valuable for their experimental realisation. I probed this by removing some patches from the A15 particles, and torsional interactions for clathrate I (as noted above), and demonstrating successful assembly. However there is room for more systematic work down this avenue. Given my success with a variety of complex, open, tetrahedrally-coordinated structures,[†] it seems the design scheme could be applied to any periodic structure.

[†] Open structures are usually harder to form, because of their low density; there are many competing tetrahedrally-coordinated structures.

6.2.2 Dodecagonal quasicrystals

To further increase the complexity of the structures formed by rationally designed particles, I next (Ch. 4) assembled 3D DDQCs, which are of great theoretical and practical interest. This project extended earlier work [1–3] which formed 2D DDQCs, and is the first demonstration of the self-assembly of any 3D QC from patchy particles. Following the earlier work, I first assembled a stacked σ-phase, a periodic approximant of DDQCs, using the design scheme of the previous chapter. I then demonstrated the assembly of DDQCs from two distinct systems: a unary system with 5 evenly-spaced, non-selective, in-plane patches; and a ternary system with selective patchy interactions, 2 particles having 5 in-plane patches, and 1 having 6 in-plane patches.[†] While I did not apply a systematic design scheme to achieve these designs, and some intuition was involved, the designs were still rational—a similar approach could be applied to other QCs.

The methods and outcomes were similar to those for 2D DDQCs, although more complicated. In the unary system, the DDQC was stabilised by wide and non-selective patches; a particle was able to form different bonding arrangements, and thus occupy different local environments (both 5- and 6-coordinate), including all those found in DDQCs. By contrast, in the ternary system (with narrower patches), the design more specifically programmed the DDQC structure. The two systems represent different routes to rationally assembling QCs. A more specific design gives more control, such as greater ability to fine-tune interaction parameters and to distinguish different interactions in a structure. However, if the design is too specific, the structure loses its disorder (indeed, a QC structure—which is aperiodic—cannot be fully specified by a finite number of patchy particles, unlike periodic structures) and has low configurational entropy. (In addition, overly specific designs make experimental realisation more difficult.) Thus, my ternary design balanced specificity—different particle types occupy different

[†] It is possible that DDQCs may also form from a binary system (as in the earlier 2D work [3]), 1 particle having 5 in-plane patches and 1 having 6. But I did not fully explore this system.

positions in the DDQC—with flexibility and disorder. The ternary design was more problematic than the unary design—specifically, particle types de-mixed—and in fine-tuning interaction parameters to resolve such problems, sometimes other problems were introduced. Nonetheless, DDQCs seemed to assemble robustly for both the unary and ternary designs; as for the periodic structures, they were both thermodynamically favoured, and kinetically accessible. Torsional interactions are seemingly important for QCs, enabling global order to arise from local interactions. I analysed the structures via their diffraction patterns, which although of limited quality, seemed to confirm dodecagonal symmetry. (Improving the structural characterisation is an area of possible future work.)

However there were differences to the 2D systems. In particular, I observed screw dislocations in almost all simulations for the stacked σ-phase and unary DDQC systems (but not for the ternary DDQC systems, whose narrower patches disfavoured such defects). Screw dislocations presumably assisted cluster growth; they arose in the earliest stages of growth. I am not aware of screw dislocations arising in other QC structures, either in experiment or simulation, nor of screw dislocations arising in other patchy-particle systems. I discussed how their presence in my systems may be due to the layered structures, and the nature of patchy bonding.

6.2.3 Chiral shape fluctuations in twisted nanotubes

In the first two projects, I designed sets of patchy particles to assemble into complex structures, first with perfectly aligned patches (for periodic structures), and then with imperfectly aligned patches (for dodecagonal quasicrystals, which can form because of the flexibility of the patchy interactions). In the latter case, some stress was present in the target structure. In the third project, I focussed on this idea, and deliberately introduced internal stress into a structure via imperfectly aligned patches in order to understand its mechanical effects. The systems I studied were helical, nanotube-like structures, and I analysed their shape deformations (under thermal fluctuations) as a result of the stress. I studied such systems because they are relevant

to understanding the origins of cholesteric phases in liquid crystals. Recently, a new hierarchical mechanism of cholesteric ordering was found [5], in which mechanically stressed, twisted DNA origami filaments adopt solenoidal (and thus chiral) shape conformations, and in turn arrange into a cholesteric phase. In particular, the solenoidal conformations are anti-chiral (*i.e.* of opposite handedness) to the chirality of the origamis' twist.

Thus, I demonstrated the design and simulation of stressed patchy-particle helical systems, with the stress causing the helices to deform by twisting. However, I observed no clear trend in solenoidal shape deformations; the fluctuations were noisy. So regarding anti-chiral shape deformations, my systems gave a null result. To resolve this would require longer simulations to generate larger samples of uncorrelated, relaxed configurations. However, the high stiffness of the tubes and/or the complex network of axial and lateral patchy interactions made observation of any potential anti-chiral effects more difficult. I discussed a possible different patchy-particle design approach, modelled more closely on the DNA origami filaments, that may lead to solenoidal shape deformations. Nonetheless, for the first time I showed the possibility of controlling material (in this case, mechanical) properties in patchy-particle systems by imperfect patch alignment. More broadly speaking, I demonstrated the potential of simple patchy-particle models to model the behaviour and properties of complex systems.

6.3 Outlook

I have provided a proof-of-concept, rather than an in-depth study, of the design and self-assembly of patchy particles into complex, ordered structures. I have demonstrated this approach for a range of structures, and qualitatively analysed design principles, self-assembly kinetics, and thermodynamics. Since I used a simple patchy-particle model, my results reveal general behaviour and principles, rather than those specific to a particular system. I have also provided a proof-of-concept of the use of patchy-particle models to study the behaviour of complex systems. My results give encouragement for future work in these fields, including more rigorous

and detailed studies. Specific suggestions for future modelling work were discussed in each chapter; I also noted the exciting recent (unpublished) assembly of icosahedral QCs from patchy particles. Further modelling could also, in general, expand the scope of my work. I considered only: spherical particles; small (so not, *e.g.*, Janus particles), attractive patches on repulsive particles; non-hierarchical assembly; monodisperse particles; and uniform particle sizes. Outside each of these limitations is space for further research. For example, the formation of QCs may be aided by repulsive patches, hierarchical pathways, polydisperse particles, and/or different particle sizes.

I hope each project of this thesis will also contribute to *experimental* advances, as an inspiration and a guide. Scientific developments, especially those in which experiments proceed from modelling, can sometimes seem slow. Almost 20 years ago, my research group observed signs of quasicrystalline order in 2D systems of patchy particles. A few years later, preliminary simulation observations were published [198]. Seven years ago, rigorous and thorough patchy-particle simulations demonstrated the formation of 2D DDQCs [1]. Two years ago, further simulations, combined with coarse-grained simulations of experimental (DNA origami) systems, suggested a route to realisation [3]. This year, an experimental group realised the assembly of 2D DDQCs [4] from DNA multi-arm tiles, following guidance from the previous modelling results. (Of course, other developments were made in between, both from the same group and others.) Now, this thesis has shown the assembly of *3D* DDQCs in simulations. I hope the current results can be another link in the chain of scientific development—and this applies to all current results, not only those concerning QCs.

Experimental approaches. It presently appears that DNA origami is the most promising approach for future experimental developments. In principle, it seems plausible that the complex periodic structures assembled here (or others), as well as the DDQC, could be formed from DNA origami or multi-arm tiles. As yet, the control over and complexity of 3D, extended phases

formed by origamis is limited, but not because of any known logical barrier.

Design scheme. The design scheme I demonstrated lays the groundwork for the assembly of essentially any periodic structure. It could be useful for researchers targeting a particular structure, due to the properties they predict it possessing. Simulators could study the relevant design with a more physically realistic model, optimising and simplifying the scheme (*e.g.* patch selectivity) and the assembly conditions; experimentalists could follow from there. The design scheme could potentially even be used algorithmically: take as input the crystallographic data of the structure, and produce as output a set of patchy particles to form it. It could perhaps also be made more powerful, for example in identifying redundant features of a design in order to make it simpler.

Cholesteric phases. I am optimistic that further refining and testing of patchy-particle systems can find a system which displays chiral shape fluctuations, similar to those in DNA origami bundles [5]. There is a wide space of possible systems to study; but the behaviour in DNA systems seems relatively general. If patchy-particle systems can help generalise the mechanism of chiral shape fluctuations, this mechanism could be investigated in various systems, both in modelling and experiment, as a potential cause of cholesteric ordering.

Bibliography

[1] M. N. van der Linden, J. P. K. Doye & A. A. Louis, 'Formation of dodecagonal quasicrystals in two-dimensional systems of patchy particles,' *J. Chem. Phys.*, **136**, 054904, 2012.

[2] A. Reinhardt, F. Romano & J. P. K. Doye, 'Computing phase diagrams for a quasicrystal-forming patchy-particle system,' *Phys. Rev. Lett.*, **110**, 25503, 2013.

[3] A. Reinhardt, J. S. Schreck, F. Romano & J. P. K. Doye, 'Self-assembly of two-dimensional binary quasicrystals: a possible route to a DNA quasicrystal,' *J. Phys.: Condens. Matter*, **29**, 014006, 2017.

[4] L. Liu, Z. Li, Y. Li & C. Mao, 'Rational design and self-assembly of two-dimensional, dodecagonal DNA quasicrystals,' *J. Am. Chem. Soc.*, 2019.

[5] M. M. C. Tortora, G. Mishra, D. Prešern & J. P. K. Doye, 'Chiral shape fluctuations and the origin of chirality in cholesteric phases of DNA origamis,' .

[6] P. Šulc, F. Romano, T. E. Ouldridge, L. Rovigatti, J. P. K. Doye & A. A. Louis, 'Sequence-dependent thermodynamics of a coarse-grained DNA model,' *J. Chem. Phys.*, **137**, 135101, 2012.

[7] J. A. Anderson, E. Jankowski, T. L. Grubb, M. Engel & S. C. Glotzer, 'Massively parallel Monte Carlo for many-particle simulations on GPUs,' *J. Comput. Phys.*, **254**, 27, 2013.

[8] H. Wondratschek, 'Part 8. Introduction to space-group symmetry,' in T. Hahn (editor), *International Tables for Crystallography, Vol. A*, chapter 8, pp. 720–740 (Kluver Academic Publisher, London), 5th edition, 2006.

[9] C. Hammond, 'Crystal Symmetry,' in *Basics Crystallogr. Diffr.*, chapter 4, pp. 99–134 (Oxford University Press, Oxford), 4th edition, 2015.

[10] S. C. Glotzer, M. J. Solomon & N. A. Kotov, 'Self-assembly: From nanoscale to microscale colloids,' *AIChE J.*, **50**, 2978, 2004.

[11] G. M. Whitesides & B. Grzybowski, 'Self-assembly at all scales,' *Science*, **295**, 2418, 2002.

[12] G. M. Whitesides & M. Boncheva, 'Beyond molecules: self-assembly of mesoscopic and macroscopic components,' *Proc. Natl. Acad. Sci. U.S.A.*, **99**, 4769, 2002.

[13] G. A. Ozin, K. Hou, B. V. Lotsch, L. Cademartiri, D. P. Puzzo, F. Scotognella, A. Ghadimi & J. Thomson, 'Nanofabrication by self-assembly,' *Mater. Today*, **12**, 12, 2009.

[14] R. F. Service, 'How far can we push chemical self-assembly?' *Science*, **309**, 95, 2005.

[15] A. B. Pawar & I. Kretzschmar, 'Fabrication, assembly, and application of patchy particles,' *Macromol. Rapid Commun.*, **31**, 150, 2010.

[16] M. A. Boles, M. Engel & D. V. Talapin, 'Self-assembly of colloidal nanocrystals: from intricate structures to functional materials,' *Chem. Rev.*, **116**, 11220, 2016.

[17] E. Bianchi, B. Capone, I. Coluzza, L. Rovigatti & P. D. J. van Oostrum, 'Limiting the valence: advancements and new perspectives on patchy colloids, soft functionalized nanoparticles and biomolecules,' *Phys. Chem. Chem. Phys.*, **19**, 19847, 2017.

[18] A. Courty, J. Richardi, P. A. Albouy & M.-P. Pileni, 'How to control the crystalline structure of supracrystals of 5-nm silver nanocrystals,' *Chem. Mater.*, **23**, 4186, 2011.

[19] N. A. Mahynski, L. Rovigatti, C. N. Likos & A. Z. Panagiotopoulos, 'Bottom-up colloidal crystal assembly with a twist,' *ACS Nano*, **10**, 5459, 2016.

[20] C. L. Porter & J. C. Crocker, 'Directed assembly of particles using directional DNA interactions,' *Curr. Opin. Colloid Interface Sci.*, **30**, 34, 2017.

[21] K. Zhao & T. G. Mason, 'Directing colloidal self-assembly through roughness-controlled depletion attractions,' *Phys. Rev. Lett.*, **99**, 268301, 2007.

[22] D. S. Goodsell, *Bionanotechnology: Lessons from Nature* (Wiley-Liss, Hoboken), 1st edition, 2004.

[23] P. J. G. Buttler, 'The current picture of the structure and assembly of tobacco mosaic virus,' *J. Gen. Virol.*, **65**, 253, 1984.

[24] A. Zlotnick, 'Theoretical aspects of virus capsid assembly,' *J. Mol. Recognit.*, **18**, 479, 2005.

[25] L. A. Amos, 'Microtubule structure and its stabilisation,' *Org. Biomol. Chem.*, **2**, 2153, 2004.

[26] D. J. Lunn, J. R. Finnegan & I. Manners, 'Self-assembly of "patchy" nanoparticles: a versatile approach to functional hierarchical materials,' *Chem. Sci.*, **6**, 3663, 2015.

[27] V. Grantcharova, E. J. Alm, D. Baker & A. L. Horwich, 'Mechanisms of protein folding,' *Curr. Opin. Struct. Biol.*, **11**, 70, 2001.

[28] N. C. Seeman, 'DNA in a material world,' *Nature*, **421**, 427, 2003.

[29] J. Bath & A. J. Turberfield, 'DNA nanomachines,' *Nat. Nanotechnol.*, **2**, 275, 2007.

[30] T. Tørring, N. V. Voigt, J. Nangreave, H. Yan & K. V. Gothelf, 'DNA origami: A quantum leap for self-assembly of complex structures,' *Chem. Soc. Rev.*, **40**, 5636, 2011.

[31] L. Di Michele & E. Eiser, 'Developments in understanding and controlling self assembly of DNA-functionalized colloids,' *Phys. Chem. Chem. Phys.*, **15**, 3115, 2013.

[32] I. Saaem & T. H. Labean, 'Overview of DNA origami for molecular self-assembly,' *Wiley Interdiscip. Rev.: Nanomed. Nanobiotechnol*, **5**, 150, 2013.

[33] P. E. Theodorakis, N. G. Fytas, G. Kahl & C. Dellago, 'Self-assembly of DNA-functionalized colloids,' *Condens. Matter Phys.*, **18**, 228101, 2015.

[34] W. B. Rogers, W. M. Shih & V. N. Manoharan, 'Using DNA to program the self-assembly of colloidal nanoparticles and microparticles,' *Nat. Rev. Mater.*, **1**, 16008, 2016.

[35] S. Angioletti-Uberti, B. M. Mognetti & D. Frenkel, 'Theory and simulation of DNA-coated colloids: a guide for rational design,' *Phys. Chem. Chem. Phys.*, **18**, 6373, 2016.

[36] M. Siavashpouri, C. H. Wachauf, M. J. Zakhary, F. Praetorius, H. Dietz & Z. Dogic, 'Molecular engineering of chiral colloidal liquid crystals using DNA origami,' *Nat. Mater.*, **16**, 849, 2017.

[37] M. Antonietti & S. Förster, 'Vesicles and liposomes: A self-assembly principle beyond lipids,' *Adv. Mater.*, **15**, 1323, 2003.

[38] H. N. Miras, G. J. T. Cooper, D.-L. Long, H. Bögge, A. Müller, C. Streb & L. Cronin, 'Unveiling the transient template in the self-assembly of a molecular oxide nanowheel,' *Science*, **327**, 72, 2010.

[39] L. Schmidt-Mende, A. Fechtenkötter, K. Müllen, E. Moons, R. H. Friend & J. D. MacKenzie, 'Self-organized discotic liquid crystals for high-efficiency organic photovoltaics,' *Science*, **293**, 1119, 2001.

[40] A. Kumar, N. L. Abbott, E. Kim, H. A. Biebuyck & G. M. Whitesides, 'Patterned self-assembled monolayers and meso-scale phenomena,' *Acc. Chem. Res.*, **28**, 219, 1995.

[41] Z. Nie, A. Petukhova & E. Kumacheva, 'Properties and emerging applications of self-assembled structures made from inorganic nanoparticles,' *Nat. Nanotechnol.*, **5**, 15, 2010.

[42] W. Liu, J. Halverson, Y. Tian, A. V. Tkachenko & O. Gang, 'Self-organized architectures from assorted DNA-framed nanoparticles,' *Nat. Chem.*, **8**, 867, 2016.

[43] A. Jain, J. A. Bollinger & T. M. Truskett, 'Inverse methods for material design,' *AIChE J.*, **60**, 2732, 2014.

[44] É. Duguet, A. Perro & S. Ravaine, 'Design and elaboration of colloidal molecules: an overview,' *Chem. Soc. Rev.*, **40**, 941, 2011.

[45] L. Cademartiri, K. J. M. Bishop, P. W. Snyder & G. A. Ozin, 'Using shape for self-assembly,' *Philos. Trans. R. Soc. A*, **370**, 2824, 2012.

[46] G. van Anders, D. Klotsa, A. S. Karas, P. M. Dodd & S. C. Glotzer, 'Digital alchemy for materials design: colloids and beyond,' *ACS Nano*, **9**, 9542, 2015.

[47] F. Zhang, S. Jiang, S. Wu, Y. Li, C. Mao, Y. Liu & H. Yan, 'Complex wireframe DNA origami nanostructures with multi-arm junction vertices,' *Nat. Nanotechnol.*, **10**, 779, 2015.

[48] J. P. K. Doye, A. A. Louis & M. Vendruscolo, 'Inhibition of protein crystallization by evolutionary negative design,' *Phys. Biol.*, **1**, P9, 2004.

[49] S. C. Glotzer & M. J. Solomon, 'Anisotropy of building blocks and their assembly into complex structures,' *Nat. Mater.*, **6**, 557, 2007.

[50] S. M. Woodley & R. Catlow, 'Crystal structure prediction from first principles,' *Nat. Mater.*, **7**, 937, 2008.

[51] L. Filion, M. Marechal, B. van Oorschot, D. Pelt, F. Smallenburg & M. Dijkstra, 'Efficient Method for Predicting Crystal Structures at Finite Temperature: Variable Box Shape Simulations,' *Phys. Rev. Lett.*, **103**, 188302, 2009.

[52] S. M. Rupich & D. V. Talapin, 'Colloidal self-assembly: Interlocked octapods,' *Nat. Mater.*, **10**, 815, 2011.

[53] E. Jankowski & S. C. Glotzer, 'Screening and designing patchy particles for optimized self-assembly propensity through assembly pathway engineering,' *Soft Matter*, **8**, 2852, 2012.

[54] G. Doppelbauer, E. G. Noya, E. Bianchi & G. Kahl, 'Self-assembly scenarios of patchy colloidal particles,' *Soft Matter*, **8**, 7768, 2012.

[55] P. F. Damasceno, M. Engel & S. C. Glotzer, 'Predictive self-assembly of polyhedra into complex structures,' *Science*, **337**, 453, 2012.

[56] J. Zhang, E. Luijten & S. Granick, 'Toward design rules of directional Janus colloidal assembly,' *Annu. Rev. Phys. Chem.*, **66**, 581, 2015.

[57] J. A. Millan, D. Ortiz & S. C. Glotzer, 'Effect of shape on the self-assembly of faceted patchy nanoplates with irregular shape into tiling patterns,' *Soft Matter*, **11**, 1386, 2015.

[58] C. De Michele, T. Bellini & F. Sciortino, 'Self-assembly of bifunctional patchy particles with anisotropic shape into polymers chains: Theory, simulations, and experiments,' *Macromolecules*, **45**, 1090, 2012.

[59] F. Sciortino, 'Gel-forming patchy colloids and network glass formers: Thermodynamic and dynamic analogies,' *Eur. Phys. J. B*, **64**, 505, 2008.

[60] S. Whitelam, I. Tamblyn, J. P. Garrahan & P. H. Beton, 'Emergent rhombus tilings from molecular interactions with M-fold rotational symmetry,' *Phys. Rev. Lett.*, **114**, 115702, 2015.

[61] Z. Zhang & S. C. Glotzer, 'Self-assembly of patchy particles,' *Nano Lett.*, **4**, 1407, 2004.

[62] S. C. Glotzer, 'Some assembly required,' *Science*, **306**, 419, 2004.

[63] E. Bianchi, R. Blaak & C. N. Likos, 'Patchy colloids: state of the art and perspectives,' *Phys. Chem. Chem. Phys.*, **13**, 6397, 2011.

[64] G.-R. Yi, D. J. Pine & S. Sacanna, 'Recent progress on patchy colloids and their self-assembly,' *J. Phys.: Condens. Matter*, **25**, 193101, 2013.

[65] S. Ravaine & E. Duguet, 'Synthesis and assembly of patchy particles: Recent progress and future prospects,' *Curr. Opin. Colloid Interface Sci.*, **30**, 45, 2017.

[66] É. Duguet, C. Hubert, C. Chomette, A. Perro & S. Ravaine, 'Patchy colloidal particles for programmed self-assembly,' *Comptes Rendus Chim.*, **19**, 173, 2016.

[67] K. Thorkelsson, P. Bai & T. Xu, 'Self-assembly and applications of anisotropic nanomaterials: A review,' *Nano Today*, **10**, 48, 2015.

[68] Y.-S. Cho, G.-R. Yi, J.-M. Lim, S.-H. Kim, V. N. Manoharan, D. J. Pine & S.-M. Yang, 'Self-organization of bidisperse colloids in water droplets,' *J. Am. Chem. Soc.*, **127**, 15968, 2005.

[69] J. K. Kummerfeld, T. S. Hudson & P. Harrowell, 'The densest packing of AB binary hard-sphere homogeneous compounds across all size ratios,' *J. Phys. Chem. B*, **112**, 10773, 2008.

[70] L. Onsager, 'The effects of shape on the interaction of colloidal particles,' *Ann. N.Y. Acad. Sci.*, **51**, 627, 1949.

[71] D. C. Rapaport, 'Self-assembly of polyhedral shells: A molecular dynamics study,' *Phys. Rev. E*, **20**, 051905, 2004.

[72] Y. Yin & A. P. Alivisatos, 'Colloidal nanocrystal synthesis and the organic-inorganic interface,' *Nature*, **437**, 664, 2005.

[73] D. C. Rapaport, 'Role of reversibility in viral capsid growth: A paradigm for self-assembly,' *Phys. Rev. Lett.*, **101**, 186101, 2008.

[74] Z. Quan & J. Fang, 'Superlattices with non-spherical building blocks,' *Nano Today*, **5**, 390, 2010.

[75] D. V. Talapin, J.-S. Lee, M. V. Kovalenko & E. V. Shevchenko, 'Prospects of colloidal nanocrystals for electronic and optoelectronic applications,' *Chem. Rev.*, **110**, 389, 2010.

[76] J. de Graaf, R. van Roij & M. Dijkstra, 'Dense regular packings of irregular nonconvex particles,' *Phys. Rev. Lett.*, **107**, 155501, 2011.

[77] J. de Graaf, L. Filion, M. Marechal, R. van Roij & M. Dijkstra, 'Crystal-structure prediction via the Floppy-Box Monte Carlo algorithm: Method and application to hard (non)convex particles,' *J. Chem. Phys.*, **137**, 214101, 2012.

[78] S. Torquato & Y. Jiao, 'Organizing principles for dense packings of nonspherical hard particles: Not all shapes are created equal,' *Phys. Rev. E*, **86**, 011102, 2012.

[79] P. F. Damasceno, M. Engel & S. C. Glotzer, 'Crystalline assemblies and densest packings of a family of truncated tetrahedra and the role of directional entropic forces,' *ACS Nano*, **6**, 609, 2012.

[80] A. A. Shah, B. Schultz, K. L. Kohlstedt, S. C. Glotzer & M. J. Solomon, 'Synthesis, assembly, and image analysis of spheroidal patchy particles,' *Langmuir*, **29**, 4688, 2013.

[81] G. van Anders, N. K. Ahmed, R. Smith, M. Engel & S. C. Glotzer, 'Entropically patchy particles: Engineering valence through shape entropy,' *ACS Nano*, **8**, 931, 2014.

[82] N. D. Burrows, A. M. Vartanian, N. S. Abadeer, E. M. Grzincic, L. M. Jacob, W. Lin, J. Li, J. M. Dennison, J. G. Hinman & C. J. Murphy, 'Anisotropic nanoparticles and anisotropic surface chemistry,' *J. Phys. Chem. Lett.*, **7**, 632, 2016.

[83] Y. Geng, G. van Anders, P. M. Dodd, J. Dshemuchadse & S. C. Glotzer, 'Engineering entropy for the inverse design of colloidal crystals from hard shapes,' .

[84] R. Cersonsky, G. van Anders, P. M. Dodd & S. C. Glotzer, 'Relevance of packing to colloidal self-assembly,' *Proc. Natl. Acad. Sci. U.S.A.*, **115**, 1439, 2018.

[85] A. van Blaaderen, 'Colloidal molecules and beyond,' *Science*, **301**, 470, 2003.

[86] N. Dorsaz, L. Filion, F. Smallenburg & D. Frenkel, 'Spiers Memorial Lecture: Effect of interaction specificity on the phase behaviour of patchy particles,' *Faraday Discuss.*, **159**, 9, 2012.

[87] V. N. Manoharan, 'Colloidal matter: packing, geometry, and entropy,' *Science*, **349**, 1253751, 2015.

[88] Z. Mao, H. Xu & D. Wang, 'Molecular mimetic self-assembly of colloidal particles,' *Adv. Funct. Mater.*, **20**, 1053, 2010.

[89] A. D. McNaught & A. Wilkinson (editors), *Compendium of Chemical Terminology (the "Gold Book")* (Blackwell Scientific Publications, Oxford), 2nd edition, 2014.

[90] Y. Xia, B. Gates, Y. Yin & Y. Lu, 'Monodispersed colloidal spheres: old materials with new applications,' *Adv. Mater.*, **12**, 693, 2000.

[91] M. Asai, A. Cacciuto & S. K. Kumar, 'Quantitative analogy between polymer-grafted nanoparticles and patchy particles,' *Soft Matter*, **11**, 793, 2015.

[92] N. A. Mahynski & A. Z. Panagiotopoulos, 'Grafted nanoparticles as soft patchy colloids: Self-assembly versus phase separation,' *J. Chem. Phys.*, **142**, 074901, 2015.

[93] E. Bianchi, G. Kahl, C. N. Likos & F. Sciortino, 'Patchy particles,' *J. Phys.: Condens. Matter*, **27**, 230301, 2015.

[94] O. Cayre, V. N. Paunov & O. D. Velev, 'Fabrication of asymmetrically coated colloid particles by microcontact printing techniques,' *J. Mater. Chem.*, **13**, 2445, 2003.

[95] A. M. Jackson, J. W. Myerson & F. Stellacci, 'Spontaneous assembly of subnanometre-ordered domains in the ligand shell of monolayer-protected nanoparticles,' *Nat. Mater.*, **3**, 330, 2004.

[96] M. G. Moffitt, 'Self-assembly of polymer brush-functionalized inorganic nanoparticles: From hairy balls to smart molecular mimics,' *J. Phys. Chem. Lett.*, **4**, 3654, 2013.

[97] C. Bao, S. Tang, R. A. E. Wright, P. Tang, F. Qiu, L. Zhu & B. Zhao, 'Effect of molecular weight on lateral microphase separation of mixed homopolymer brushes grafted on silica particles,' *Macromolecules*, **47**, 6824, 2014.

[98] R. M. Choueiri, E. Galati, H. Thérien-Aubin, A. Klinkova, E. M. Larin, A. Querejeta-Fernández, L. Han, H. L. Xin, O. Gang, E. B. Zhulina, M. Rubinstein & E. Kumacheva, 'Surface patterning of nanoparticles with polymer patches,' *Nature*, **538**, 79, 2016.

[99] M. M. Maye, D. Nykypanchuk, M. Cuisinier, D. van der Lelie & O. Gang, 'Stepwise surface encoding for high-throughput assembly of nanoclusters,' *Nat. Mater.*, **8**, 388, 2009.

[100] L. Feng, R. Dreyfus, R. Sha, N. C. Seeman & P. M. Chaikin, 'DNA patchy particles,' *Adv. Mater.*, **25**, 2779, 2013.

[101] H. Lin, S. Lee, L. Sun, M. Spellings, M. Engel, S. C. Glotzer & C. A. Mirkin, 'Clathrate colloidal crystals,' *Science*, **355**, 931, 2017.

[102] T. Trinh, C. Liao, V. Toader, M. Barłóg, H. S. Bazzi, J. Li & H. F. Sleiman, 'DNA-imprinted polymer nanoparticles with monodispersity and prescribed DNA-strand patterns,' *Nat. Chem.*, **10**, 184, 2018.

[103] I. A. Banerjee, L. Yu & H. Matsui, 'Location-specific biological functionalization on nanotubes: attachment of proteins at the ends of nanotubes using Au nanocrystal masks,' *Nano Lett.*, **3**, 283, 2003.

[104] K. K. Caswell, J. N. Wilson, U. H. F. Bunz & C. J. Murphy, 'Preferential end-to-end assembly of gold nanorods by biotin-streptavidin connectors,' *J. Am. Chem. Soc.*, **125**, 13914, 2003.

[105] T. Tigges, D. Hoenders & A. Walther, 'Preparation of highly monodisperse monopatch particles with orthogonal click-type functionalization and biorecognition,' *Small*, **11**, 4540, 2015.

[106] G. Zhang, D. Wang & H. Möhwald, 'Patterning microsphere surfaces by templating colloidal crystals,' *Nano Lett.*, **5**, 143, 2005.

[107] G. Zhang, D. Wang & H. Möhwald, 'Decoration of microspheres with gold nanodots—Giving colloidal spheres valences,' *Angew. Chemie - Int. Ed.*, **44**, 7767, 2005.

[108] G. Zhang, D. Wang & H. Möhwald, 'Nanoembossment of Au patterns on microspheres,' *Chem. Mater.*, **18**, 3985, 2006.

[109] A. B. Pawar & I. Kretzschmar, 'Patchy particles by glancing angle deposition,' *Langmuir*, **24**, 355, 2008.

[110] A. B. Pawar & I. Kretzschmar, 'Multifunctional patchy particles by glancing angle deposition,' *Langmuir*, **25**, 9057, 2009.

[111] C. E. Snyder, A. M. Yake, J. D. Feick & D. Velegol, 'Nanoscale functionalization and site-specific assembly of colloids by particle lithography,' *Langmuir*, **21**, 4813, 2005.

[112] A. M. Yake, C. E. Snyder & D. Velegol, 'Site-specific functionalization on individual colloids: Size control, stability, and multilayers,' *Langmuir*, **23**, 9069, 2007.

[113] T. T. Chastek, S. D. Hudson & V. A. Hackley, 'Preparation and characterization of patchy particles,' *Langmuir*, **24**, 13897, 2008.

[114] L. Wang, L. Xia, G. Li, S. Ravaine & X. S. Zhao, 'Patterning the surface of colloidal microspheres and fabrication of nonspherical particles,' *Angew. Chemie - Int. Ed.*, **47**, 4725, 2008.

[115] S. Jiang & S. Granick, 'Controlling the geometry (Janus balance) of amphiphilic colloidal particles,' *Langmuir*, **24**, 2438, 2008.

[116] P. D. J. van Oostrum, M. Hejazifar, C. Niedermayer & E. Reimhult, 'Simple method for the synthesis of inverse patchy colloids,' *J. Phys.: Condens. Matter*, **27**, 234105, 2015.

[117] M. Sabapathy, R. A. Mathews K & E. Mani, 'Self-assembly of inverse patchy colloids with tunable patch coverage,' *Phys. Chem. Chem. Phys.*, **19**, 13122, 2017.

[118] D. J. Kraft, R. Ni, F. Smallenburg, M. Hermes, K. Yoon, D. A. Weitz, A. van Blaaderen, J. Groenewold, M. Dijkstra & W. K. Kegel, 'Surface roughness directed self-assembly of patchy particles into colloidal micelles,' *Proc. Natl. Acad. Sci. U.S.A.*, **109**, 10787, 2012.

[119] S. Sacanna, W. T. M. Irvine, P. M. Chaikin & D. J. Pine, 'Lock and key colloids,' *Nature*, **464**, 575, 2010.

[120] S.-H. Kim, A. D. Hollingsworth, S. Sacanna, S.-J. Chang, G. Lee, D. J. Pine & G.-R. Yi, 'Synthesis and assembly of colloidal particles with sticky dimples,' *J. Am. Chem. Soc.*, **134**, 16115, 2012.

[121] Y. Wang, Y. Wang, X. Zheng, G.-R. Yi, S. Sacanna, D. J. Pine & M. Weck, 'Three-dimensional lock and key colloids,' *J. Am. Chem. Soc.*, **136**, 6866, 2014.

[122] Y. Yin, Y. Lu, B. Gates & Y. Xia, 'Template-assisted self-assembly: a practical route to complex aggregates of monodispersed colloids with well-defined sizes, shapes, and structures,' *J. Am. Chem. Soc.*, **123**, 8718, 2001.

[123] V. N. Manoharan, M. T. Elsesser & D. J. Pine, 'Dense packing and symmetry in small clusters of microspheres,' *Science*, **301**, 483, 2003.

[124] V. N. Manoharan & D. J. Pine, 'Building materials by packing spheres,' *Mater. Res. Soc. Bull.*, **29**, 91, 2004.

[125] Y.-S. Cho, G.-R. Yi, S.-H. Kim, S.-J. Jeon, M. T. Elsesser, H. K. Yu, S.-M. Yang & D. J. Pine, 'Particles with coordinated patches or windows from oil-in-water emulsions,' *Chem. Mater.*, **19**, 3183, 2007.

[126] D. J. Kraft, W. S. Vlug, C. M. van Kats, A. van Blaaderen, A. Imhof & W. K. Kegel, 'Self-assembly of colloids with liquid protrusions,' *J. Am. Chem. Soc.*, **131**, 1182, 2009.

[127] D. J. Kraft, J. Groenewold & W. K. Kegel, 'Colloidal molecules with well-controlled bond angles,' *Soft Matter*, **5**, 3823, 2009.

[128] A. Perro, E. Duguet, O. Lambert, J.-C. Taveau, E. Bourgeat-Lami & S. Ravaine, 'A chemical synthetic route towards "colloidal molecules",' *Angew. Chemie - Int. Ed.*, **48**, 361, 2009.

[129] A. Perro & V. N. Manoharan, 'Bulk synthesis of polymer-inorganic colloidal clusters,' *Langmuir*, **26**, 18669, 2010.

[130] Y.-S. Cho, G.-R. Yi, S.-H. Kim, M. T. Elsesser, D. R. Breed & S.-M. Yang, 'Homogeneous and heterogeneous binary colloidal clusters formed by evaporation-induced self-assembly inside droplets,' *J. Colloid Interface Sci.*, **318**, 124, 2008.

[131] Y. Wang, Y. Wang, D. R. Breed, V. N. Manoharan, L. Feng, A. D. Hollingsworth, M. Weck & D. J. Pine, 'Colloids with valence and specific directional bonding,' *Nature*, **491**, 51, 2012.

[132] K.-H. Roh, D. C. Martin & J. Lahann, 'Biphasic Janus particles with nanoscale anisotropy,' *Nat. Mater.*, **4**, 759, 2005.

[133] K.-H. Roh, D. C. Martin & J. Lahann, 'Triphasic nanocolloids,' *J. Am. Chem. Soc.*, **128**, 6796, 2006.

[134] D. J. Kraft, J. Hilhorst, M. A. P. Heinen, M. J. Hoogenraad, B. Luigjes & W. K. Kegel, 'Patchy polymer colloids with tunable anisotropy dimensions,' *J. Phys. Chem. B*, **115**, 7175, 2011.

[135] A. H. Gröschel, F. H. Schacher, H. Schmalz, O. V. Borisov, E. B. Zhulina, A. Walther & A. H. E. Müller, 'Precise hierarchical self-assembly of multicompartment micelles,' *Nat. Commun.*, **3**, 710, 2012.

[136] F. Lo Verso & C. N. Likos, 'End-functionalized polymers: Versatile building blocks for soft materials,' *Polymer*, **49**, 1425, 2008.

[137] H. Yan, S. H. Park, G. Finkelstein, J. H. Reif & T. H. LaBean, 'DNA-templated self-assembly of protein arrays and highly conductive nanowires,' *Science*, **301**, 1882, 2003.

[138] Y. He, Y. Chen, H. Liu, A. E. Ribbe & C. Mao, 'Self-assembly of hexagonal DNA two-dimensional (2D) arrays,' *J. Am. Chem. Soc.*, **127**, 12202, 2005.

[139] Y. He, Y. Tian, A. E. Ribbe & C. Mao, 'Highly connected two-dimensional crystals of DNA six-point-stars,' *J. Am. Chem. Soc.*, **128**, 15978, 2006.

[140] Y. He, T. Ye, M. Su, C. Zhang, A. E. Ribbe, W. Jiang & C. Mao, 'Hierarchical self-assembly of DNA into symmetric supramolecular polyhedra,' *Nature*, **452**, 198, 2008.

[141] C. Zhang, M. Su, Y. He, X. Zhao, P.-a. Fang, A. E. Ribbe, W. Jiang & C. Mao, 'Conformational flexibility facilitates self-assembly of complex DNA nanostructures,' *Proc. Natl. Acad. Sci. U.S.A.*, **105**, 10665, 2008.

[142] C. Zhang, S. H. Ko, M. Su, Y. Leng, A. E. Ribbe, W. Jiang & C. Mao, 'Symmetry controls the face geometry of DNA polyhedra,' *J. Am. Chem. Soc.*, **131**, 1413, 2009.

[143] F. Zhang, Y. Liu & H. Yan, 'Complex Archimedean tiling self-assembled from DNA nanostructures,' *J. Am. Chem. Soc.*, **135**, 7458, 2013.

[144] F. Zhang, S. Jiang, W. Li, A. Hunt, Y. Liu & H. Yan, 'Self-assembly of complex DNA tessellations by using low-symmetry multi-arm DNA tiles,' *Angew. Chemie - Int. Ed.*, **55**, 8860, 2016.

[145] Y. Li, Z. Liu, G. Yu, W. Jiang & C. Mao, 'Self-assembly of molecule-like nanoparticle clusters directed by DNA nanocages,' *J. Am. Chem. Soc.*, **137**, 4320, 2015.

[146] W. Liu, M. Tagawa, H. L. Xin, T. Wang, H. Emamy, H. Li, K. G. Yager, F. W. Starr, A. V. Tkachenko & O. Gang, 'Diamond family of nanoparticle superlattices,' *Science*, **351**, 582, 2016.

[147] Y. Tian, Y. Zhang, T. Wang, H. L. Xin, H. Li & O. Gang, 'Lattice engineering through nanoparticle-DNA frameworks,' *Nat. Mater.*, **15**, 654, 2016.

[148] Y. Wang, A. D. Hollingsworth, S. K. Yang, S. Patel, D. J. Pine & M. Weck, 'Patchy particle self-assembly via metal coordination,' *J. Am. Chem. Soc.*, **135**, 14064, 2013.

[149] C. N. Likos, 'Soft matter with soft particles,' *Soft Matter*, **2**, 478, 2006.

[150] R. P. Sear & G. Jackson, 'Thermodynamic perturbation theory for association with bond cooperativity,' *J. Chem. Phys.*, **105**, 1113, 1996.

[151] R. P. Sear, 'Phase behavior of a simple model of globular proteins,' *J. Chem. Phys.*, **111**, 4800, 1999.

[152] P. R. ten Wolde & D. Frenkel, 'Enhancement of protein crystal nucleation by critical density fluctuations,' *Science*, **277**, 1975, 1997.

[153] N. Kern & D. Frenkel, 'Fluid-fluid coexistence in colloidal systems with short-ranged strongly directional attraction,' *J. Chem. Phys.*, **118**, 9882, 2003.

[154] J. M. Berg, J. L. Tymoczko & L. Stryer, *Biochemistry* (W. H. Freeman, New York City), 5th edition, 2002.

[155] M. Jones & G. Jones, *Advanced Biology* (Cambridge University Press, Cambridge), 1st edition, 1997.

[156] S. Jones & J. M. Thornton, 'Protein-protein interactions: A review of protein dimer structures,' *Prog. Biophys. Mol. Biol.*, **63**, 31, 1995.

[157] C. N. Likos, N. Hoffmann, H. Löwen & A. A. Louis, 'Exotic fluids and crystals of soft polymeric colloids,' *J. Phys.: Condens. Matter*, **14**, 7681, 2002.

[158] M. E. Leunissen, C. G. Christova, A.-P. Hynninen, C. P. Royall, A. I. Campbell, A. Imhof, M. Dijkstra, R. van Roij & A. van Blaaderen, 'Ionic colloidal crystals of oppositely charged particles,' *Nature*, **437**, 235, 2005.

[159] M. R. Jones & C. A. Mirkin, 'Self-assembly gets new direction,' *Nature*, **491**, 42, 2012.

[160] M.-H. Wu & G. M. Whitesides, 'Fabrication of arrays of two-dimensional micropatterns using microspheres as lenses for projection photolithography,' *Appl. Phys. Lett.*, **78**, 2273, 2001.

[161] J. A. Champion, Y. K. Katare & S. Mitragotri, 'Making polymeric micro- and nanoparticles of complex shapes,' *Proc. Natl. Acad. Sci. U.S.A.*, **104**, 11901, 2007.

[162] S. Mitragotri & J. Lahann, 'Physical approaches to biomaterial design,' *Nat. Mater.*, **8**, 15, 2009.

[163] R. Roux, C. Ladavière, A. Montembault & T. Delair, 'Particle assemblies: Toward new tools for regenerative medicine,' *Mater. Sci. Eng. C*, **33**, 997, 2013.

[164] E. Dickinson & M. E. Leser (editors), *Food Colloids: Self-Assembly and Material Science* (The Royal Society of Chemistry, Cambridge), 2007.

[165] E. Dickinson, 'Use of nanoparticles and microparticles in the formation and stabilization of food emulsions,' *Trends Food Sci. Technol.*, **24**, 4, 2012.

[166] C. López, 'Materials aspects of photonic crystals,' *Adv. Mater.*, **15**, 1679, 2003.

[167] S. Furumi, H. Fudouzi & T. Sawada, 'Self-organized colloidal crystals for photonics and laser applications,' *Laser Photonics Rev.*, **4**, 205, 2010.

[168] J. Xu & Z. Guo, 'Biomimetic photonic materials with tunable structural colors,' *J. Colloid Interface Sci.*, **406**, 1, 2013.

[169] S. Noda, K. Tomoda, N. Yamamoto & A. Chutinan, 'Full three-dimensional photonic bandgap crystals at near-infrared wavelengths,' *Science*, **289**, 604, 2000.

[170] D. Cassagne, C. Jouanin & D. Bertho, 'Hexagonal photonic-band-gap structures,' *Phys. Rev. B*, **53**, 7134, 1996.

[171] T.-I. Weng & G. Y. Guo, 'Band structure of honeycomb photonic crystal slabs,' *J. Appl. Phys.*, **99**, 093102, 2006.

[172] O. Sigmund & K. Hougaard, 'Geometric properties of optimal photonic crystals,' *Phys. Rev. Lett.*, **100**, 153904, 2008.

[173] A. J. Garcia-Adeva, 'Band gap atlas for photonic crystals having the symmetry of the kagomé and pyrochlore lattices,' *New J. Phys.*, **8**, 1, 2006.

[174] A.-P. Hynninen, J. H. J. Thijssen, E. C. M. Vermolen, M. Dijkstra & A. van Blaaderen, 'Self-assembly route for photonic crystals with a bandgap in the visible region,' *Nat. Mater.*, **6**, 202, 2007.

[175] K. M. Ho, C. T. Chan & C. M. Soukoulis, 'Existence of a photonic gap in periodic dielectric structures,' *Phys. Rev. Lett.*, **65**, 3152, 1990.

[176] M. Maldovan, C. K. Ullal, W. C. Carter & E. L. Thomas, 'Exploring for 3D photonic bandgap structures in the 11 f.c.c. space groups,' *Nat. Mater.*, **2**, 664, 2003.

[177] M. Maldovan & E. L. Thomas, 'Diamond-structured photonic crystals,' *Nat. Mater.*, **3**, 593, 2004.

[178] T. T. Ngo, C. M. Liddell, M. Ghebrebrhan & J. D. Joannopoulos, 'Tetrastack: Colloidal diamond-inspired structure with omnidirectional photonic band gap for low refractive index contrast,' *Appl. Phys. Lett.*, **88**, 241920, 2006.

[179] M. E. Zoorob, M. D. B. Charlton, G. J. Parker, J. J. Baumberg & M. C. Netti, 'Complete photonic bandgaps in 12-fold symmetric quasicrystals,' *Nature*, **404**, 740, 2000.

[180] X. Zhang, Z.-Q. Zhang & C. T. Chan, 'Absolute photonic band gaps in 12-fold symmetric photonic quasicrystals,' *Phys. Rev. B*, **63**, 081105(R), 2001.

[181] W. Man, M. Megens, P. J. Steinhardt & P. M. Chaikin, 'Experimental measurement of the photonic properties of icosahedral quasicrystals,' *Nature*, **436**, 993, 2005.

[182] X. Zeng, 'Liquid quasicrystals,' *Curr. Opin. Colloid Interface Sci.*, **9**, 384, 2005.

[183] A. Della Villa, S. Enoch, G. Tayeb, V. Pierro, V. Galdi & F. Capolino, 'Band gap formation and multiple scattering in photonic quasicrystals with a Penrose-type lattice,' *Phys. Rev. Lett.*, **94**, 183903, 2005.

[184] A. Ledermann, L. Cademartiri, M. Hermatschweiler, C. Toninelli, G. A. Ozin, D. S. Wiersma, M. Wegener & G. von Freymann, 'Three-dimensional silicon inverse photonic quasicrystals for infrared wavelengths,' *Nat. Mater.*, **5**, 942, 2006.

[185] K. Ueda, T. Dotera & T. Gemma, 'Photonic band structure calculations of two-dimensional Archimedean tiling patterns,' *Phys. Rev. B*, **75**, 195122, 2007.

[186] J. Xu, R. Ma, X. Wang & W. Y. Tam, 'Icosahedral quasicrystals for visible wavelengths by optical interference holography,' *Opt. Express*, **15**, 4287, 2007.

[187] M. Florescu, S. Torquato & P. J. Steinhardt, 'Complete band gaps in two-dimensional photonic quasicrystals,' *Phys. Rev. B*, **80**, 155112, 2009.

[188] S. M. Thon, W. T. M. Irvine, D. Kleckner & D. Bouwmeester, 'Polychromatic photonic quasicrystal cavities,' *Phys. Rev. Lett.*, **104**, 243901, 2010.

[189] D. S. Wiersma, 'Disordered photonics,' *Nat. Photonics*, **7**, 188, 2013.

[190] D. H. Gracias, J. Tien, T. L. Breen, C. Hsu & G. M. Whitesides, 'Forming electrical networks in three dimensions by self-assembly,' *Science*, **289**, 1170, 2000.

[191] M. Boncheva, D. H. Gracias, H. O. Jacobs & G. M. Whitesides, 'Biomimetic self-assembly of a functional asymmetrical electronic device,' *Proc. Natl. Acad. Sci. U.S.A.*, **99**, 4937, 2002.

[192] M. I. Hussein, M. J. Leamy & M. Ruzzene, 'Dynamics of phononic materials and structures: Historical origins, recent progress, and future outlook,' *Appl. Mech. Rev.*, **66**, 040802, 2014.

[193] S. Zhang, 'Fabrication of novel biomaterials through molecular self-assembly,' *Nat. Biotechnol.*, **21**, 1171, 2003.

[194] X. Song, 'Role of anisotropic interactions in protein crystallization,' *Phys. Rev. E*, **66**, 011909, 2002.

[195] N. M. Dixit & C. F. Zukoski, 'Crystal nucleation rates for particles experiencing short-range attractions,' *J. Chem. Phys.*, **117**, 8540, 2002.

[196] A. Shiryayev, X. Li & J. D. Gunton, 'Simple model of sickle hemogloblin,' *J. Chem. Phys.*, **125**, 024902, 2006.

[197] A. W. Wilber, J. P. K. Doye, A. A. Louis, E. G. Noya, M. A. Miller & P. Wong, 'Reversible self-assembly of patchy particles into monodisperse icosahedral clusters,' *J. Chem. Phys.*, **127**, 085106, 2007.

[198] J. P. K. Doye, A. A. Louis, I.-C. Lin, L. R. Allen, E. G. Noya, A. W. Wilber, H. C. Kok & R. Lyus, 'Controlling crystallization and its absence: proteins, colloids and patchy models,' *Phys. Chem. Chem. Phys.*, **9**, 2197, 2007.

[199] J. K. Cheung, V. K. Shen, J. R. Errington & T. M. Truskett, 'Coarse-grained strategy for modeling protein stability in concentrated solutions. III: Directional protein interactions,' *Biophys. J.*, **92**, 4316, 2007.

[200] C. Gögelein, G. Nägele, R. Tuinier, T. Gibaud, A. Stradner & P. Schurtenberger, 'A simple patchy colloid model for the phase behavior of lysozyme dispersions,' *J. Chem. Phys.*, **129**, 085102, 2008.

[201] N. Wentzel & J. D. Gunton, 'Effect of solvent on the phase diagram of a simple anisotropic model of globular proteins,' *J. Phys. Chem. B*, **112**, 7803, 2008.

[202] A. W. Wilber, J. P. K. Doye, A. A. Louis & A. C. F. Lewis, 'Monodisperse self-assembly in a model with protein-like interactions,' *J. Chem. Phys.*, **131**, 175102, 2009.

[203] G. Villar, A. W. Wilber, A. J. Williamson, P. Thiara, J. P. K. Doye, A. A. Louis, M. N. Jochum, A. C. F. Lewis & E. D. Levy, 'Self-assembly and evolution of homomeric protein complexes,' *Phys. Rev. Lett.*, **102**, 118106, 2009.

[204] I. Coluzza, 'Transferable coarse-grained potential for de novo protein folding and design,' *PLoS One*, **9**, 1, 2014.

[205] J. J. McManus, P. Charbonneau, E. Zaccarelli & N. Asherie, 'The physics of protein self-assembly,' *Curr. Opin. Colloid Interface Sci.*, **22**, 73, 2016.

[206] J. Cai, J. P. Townsend, T. C. Dodson, P. A. Heiney & A. M. Sweeney, 'Eye patches: Protein assembly of index-gradient squid lenses,' *Science*, **357**, 564, 2017.

[207] E. G. Noya, C. Vega, J. P. K. Doye & A. A. Louis, 'The stability of a crystal with diamond structure for patchy particles with tetrahedral symmetry,' *J. Chem. Phys.*, **132**, 234511, 2010.

[208] B. W. Matthews, 'Solvent content of protein crystals,' *J. Mol. Biol.*, **33**, 491, 1968.

[209] J. Chang, A. M. Lenhoff & S. I. Sandler, 'Determination of fluid-solid transitions in model protein solutions using the histogram reweighting method and expanded ensemble simulations,' *J. Chem. Phys.*, **120**, 3003, 2004.

[210] M. F. Hagan & D. Chandler, 'Dynamic pathways for viral capsid assembly,' *Biophys. J.*, **91**, 42, 2006.

[211] A. W. Wilber, J. P. K. Doye & A. A. Louis, 'Self-assembly of monodisperse clusters: dependence on target geometry,' *J. Chem. Phys.*, **131**, 175101, 2009.

[212] L. Rovigatti, J. Russo & F. Romano, 'How to simulate patchy particles,' *Eur. Phys. J. E*, **41**, 59, 2018.

[213] P. J. Lu & D. A. Weitz, 'Colloidal particles: Crystals, glasses, and gels,' *Annu. Rev. Condens. Matter Phys.*, **4**, 217, 2013.

[214] B. Li, D. Zhou & Y. Han, 'Assembly and phase transitions of colloidal crystals,' *Nat. Rev. Mater.*, **1**, 15011, 2016.

[215] E. Bianchi, J. Largo, P. Tartaglia, E. Zaccarelli & F. Sciortino, 'Phase diagram of patchy colloids: towards empty liquids,' *Phys. Rev. Lett.*, **97**, 168301, 2006.

[216] C. De Michele, S. Gabrielli, P. Tartaglia & F. Sciortino, 'Dynamics in the presence of attractive patchy interactions,' *J. Phys. Chem. B*, **110**, 8064, 2006.

[217] F. Sciortino, E. Bianchi, J. F. Douglas & P. Tartaglia, 'Self-assembly of patchy particles into polymer chains: A parameter-free comparison between Wertheim theory and Monte Carlo simulation,' *J. Chem. Phys.*, **126**, 194903, 2007.

[218] F. Romano, P. Tartaglia & F. Sciortino, 'Gas-liquid phase coexistence in a tetrahedral patchy particle model,' *J. Phys.: Condens. Matter*, **19**, 321101, 2007.

[219] E. Zaccarelli, 'Colloidal gels: Equilibrium and non-equilibrium routes,' *J. Phys.: Condens. Matter*, **19**, 323101, 2007.

[220] P. Tartaglia & F. Sciortino, 'Association of limited valence patchy particles in two dimensions,' *J. Phys.: Condens. Matter*, **22**, 104108, 2010.

[221] F. Smallenburg & F. Sciortino, 'Liquids more stable than crystals in particles with limited valence and flexible bonds,' *Nat. Phys.*, **9**, 554, 2013.

[222] J. M. Tavares, P. I. C. Teixeira & M. M. Telo da Gama, 'How patchy can one get and still condense? The role of dissimilar patches in the interactions of colloidal particles,' *Mol. Phys.*, **107**, 453, 2009.

[223] R. Fantoni, D. Gazzillo, A. Giacometti, M. A. Miller & G. Pastore, 'Patchy sticky hard spheres: Analytical study and Monte Carlo simulations,' *J. Chem. Phys.*, **127**, 234507, 2007.

[224] B. A. H. Huisman, P. G. Bolhuis & A. Fasolino, 'Phase transition to bundles of flexible supramolecular polymers,' *Phys. Rev. Lett.*, **100**, 188301, 2008.

[225] F. Romano & F. Sciortino, 'Patchy from the bottom up,' *Nat. Mater.*, **10**, 171, 2011.

[226] F. Romano & F. Sciortino, 'Two dimensional assembly of triblock Janus particles into crystal phases in the two bond per patch limit,' *Soft Matter*, **7**, 5799, 2011.

[227] Q. Chen, S. C. Bae & S. Granick, 'Directed self-assembly of a colloidal kagome lattice,' *Nature*, **469**, 381, 2011.

[228] A. Perro, S. Reculusa, S. Ravaine, E. Bourgeat-Lami & E. Duguet, 'Design and synthesis of Janus micro- and nanoparticles,' *J. Mater. Chem.*, **15**, 3745, 2005.

[229] S. Jiang, Q. Chen, M. Tripathy, E. Luijten, K. S. Schweizer & S. Granick, 'Janus particle synthesis and assembly,' *Adv. Mater.*, **22**, 1060, 2010.

[230] M. Lattuada & T. A. Hatton, 'Synthesis, properties and applications of Janus nanoparticles,' *Nano Today*, **6**, 286, 2011.

[231] Q. Chen, J. Yan, J. Zhang, S. C. Bae & S. Granick, 'Janus and multiblock colloidal particles,' *Langmuir*, **28**, 13555, 2012.

[232] J. Hu, S. Zhou, Y. Sun, X. Fang & L. Wu, 'Fabrication, properties and applications of Janus particles,' *Chem. Soc. Rev.*, **41**, 4356, 2012.

[233] A. Walther & A. H. E. Müller, 'Janus particles: Synthesis, self-assembly, physical properties, and applications,' *Chem. Rev.*, **113**, 5194, 2013.

[234] J. Zhang, B. A. Grzybowski & S. Granick, 'Janus particle synthesis, assembly, and application,' *Langmuir*, **33**, 6964, 2017.

[235] S. C. Glotzer, M. A. Horsch, C. R. Iacovella, Z. Zhang, E. R. Chan & X. Zhang, 'Self-assembly of anisotropic tethered nanoparticle shape amphiphiles,' *Curr. Opin. Colloid Interface Sci.*, **10**, 287, 2005.

[236] C. R. Iacovella & S. C. Glotzer, 'Phase behavior of ditethered nanospheres,' *Soft Matter*, **5**, 4492, 2009.

[237] C. R. Iacovella & S. C. Glotzer, 'Complex crystal structures formed by the self-assembly of ditethered nanospheres,' *Nano Lett.*, **9**, 1206, 2009.

[238] T. Lafitte, S. K. Kumar & A. Z. Panagiotopoulos, 'Self-assembly of polymer-grafted nanoparticles in thin films,' *Soft Matter*, **10**, 786, 2014.

[239] B. Capone, I. Coluzza, F. LoVerso, C. N. Likos & R. Blaak, 'Telechelic star polymers as self-assembling units from the molecular to the macroscopic scale,' *Phys. Rev. Lett.*, **109**, 238301, 2012.

[240] L. Rovigatti, D. de las Heras, J. M. Tavares, M. M. Telo da Gama & F. Sciortino, 'Computing the phase diagram of binary mixtures: A patchy particle case study,' *J. Chem. Phys.*, **138**, 164904, 2013.

[241] A. J. Williamson, A. W. Wilber, J. P. K. Doye & A. A. Louis, 'Templated self-assembly of patchy particles,' *Soft Matter*, **7**, 3423, 2011.

[242] F. Romano & F. Sciortino, 'Patterning symmetry in the rational design of colloidal crystals,' *Nat. Commun.*, **3**, 975, 2012.

[243] F. Romano, E. Sanz & F. Sciortino, 'Phase diagram of a tetrahedral patchy particle model for different interaction ranges,' *J. Chem. Phys.*, **132**, 184501, 2010.

[244] A. Reinhardt & D. Frenkel, 'DNA brick self-assembly with an off-lattice potential,' *Soft Matter*, **12**, 6253, 2016.

[245] B. Grünbaum & G. C. Shephard, *Tilings and Patterns* (W. H. Freeman, New York City), 1st edition, 1987.

[246] F. C. Frank & J. S. Kasper, 'Complex alloy structures regarded as sphere packings. I. Definitions and basic principles,' *Acta Crystallogr.*, **11**, 184, 1958.

[247] F. C. Frank & J. S. Kasper, 'Complex alloy structures regarded as sphere packings. II. Analysis and classification of representative structures,' *Acta Crystallogr.*, **12**, 483, 1959.

[248] D. P. Shoemaker & C. B. Shoemaker, 'Icosahedral Coordination in Metallic Crystals,' in M. V. Jaric (editor), *Introduction to Quasicrystals*, chapter 1, pp. 1–57 (Academic Press, London), 1st edition, 1988.

[249] Z. Zhang, A. S. Keys, T. Chen & S. C. Glotzer, 'Self-assembly of patchy particles into diamond structures through molecular mimicry,' *Langmuir*, **21**, 11547, 2005.

[250] M. S. Wertheim, 'Fluids with highly directional attractive forces. I. Statistical thermodynamics,' *J. Stat. Phys.*, **35**, 19, 1984.

[251] M. S. Wertheim, 'Fluids with highly directional attractive forces. II. Thermodynamic perturbation theory and integral equations,' *J. Stat. Phys.*, **35**, 35, 1984.

[252] M. S. Wertheim, 'Fluids with highly directional attractive forces. III. Multiple attraction sites,' *J. Stat. Phys.*, **42**, 459, 1986.

[253] M. S. Wertheim, 'Fluids with highly directional attractive forces. IV. Equilibrium polymerization,' *J. Stat. Phys.*, **42**, 477, 1986.

[254] E. Bianchi, P. Tartaglia, E. Zaccarelli & F. Sciortino, 'Theoretical and numerical study of the phase diagram of patchy colloids: Ordered and disordered patch arrangements,' *J. Chem. Phys.*, **128**, 144504, 2008.

[255] P. J. Flory, *Principles of Polymer Chemistry* (Cornell University Press, Ithaca), 1st edition, 1953.

[256] E. Bianchi, P. Tartaglia, E. La Nave & F. Sciortino, 'Fully solvable equilibrium self-assembly process: Fine-tuning the clusters size and the connectivity in patchy particle systems,' *J. Phys. Chem. B*, **111**, 11765, 2007.

[257] J. Russo, P. Tartaglia & F. Sciortino, 'Reversible gels of patchy particles: role of the valence,' *J. Chem. Phys.*, **131**, 014504, 2009.

[258] E. G. Noya, C. Vega, J. P. K. Doye & A. A. Louis, 'Phase diagram of model anisotropic particles with octahedral symmetry,' *J. Chem. Phys.*, **127**, 054501, 2007.

[259] J. M. Tavares, P. I. C. Teixeira & M. M. Telo da Gama, 'Criticality of colloids with distinct interaction patches: The limits of linear chains, hyperbranched polymers, and dimers,' *Phys. Rev. E*, **80**, 021506, 2009.

[260] L. Hong, A. Cacciuto, E. Luijter & S. Granick, 'Clusters of charged Janus spheres,' *Nano Lett.*, **6**, 2510, 2006.

[261] L. Hong, A. Cacciuto, E. Luijten & S. Granick, 'Clusters of amphiphilic colloidal spheres,' *Langmuir*, **24**, 621, 2008.

[262] L. Nie, S. Liu, W. Shen, D. Chen & M. Jiang, 'One-pot synthesis of amphiphilic polymeric Janus particles and their self-assembly into supermicelles with a narrow size distribution,' *Angew. Chemie - Int. Ed.*, **46**, 6321, 2007.

[263] Q. Chen, J. K. Whitmer, S. Jiang, S. C. Bae, E. Luijten & S. Granick, 'Supracolloidal reaction kinetics of Janus spheres,' *Science*, **331**, 199, 2011.

[264] F. Sciortino, A. Giacometti & G. Pastore, 'Phase diagram of Janus particles,' *Phys. Rev. Lett.*, **103**, 237801, 2009.

[265] F. Sciortino, A. Giacometti & G. Pastore, 'A numerical study of one-patch colloidal particles: From square-well to Janus,' *Phys. Chem. Chem. Phys.*, **12**, 11869, 2010.

[266] F. Romano, E. Sanz & F. Sciortino, 'Role of the range in the fluid-crystal coexistence for a patchy particle model,' *J. Phys. Chem. B*, **113**, 15133, 2009.

[267] F. Romano, E. Sanz & F. Sciortino, 'Crystallization of tetrahedral patchy particles in silico,' *J. Chem. Phys.*, **134**, 174502, 2011.

[268] I. Saika-Voivod, F. Romano & F. Sciortino, 'Nucleation barriers in tetrahedral liquids spanning glassy and crystallizing regimes,' *J. Chem. Phys.*, **135**, 124506, 2011.

[269] F. Romano, J. Russo & H. Tanaka, 'Influence of patch-size variability on the crystallization of tetrahedral patchy particles,' *Phys. Rev. Lett.*, **113**, 138303, 2014.

[270] A. Giacometti, F. Lado, J. Largo, G. Pastore & F. Sciortino, 'Effects of patch size and number within a simple model of patchy colloids,' *J. Chem. Phys.*, **132**, 174110, 2010.

[271] G. Doppelbauer, E. Bianchi & G. Kahl, 'Self-assembly scenarios of patchy colloidal particles in two dimensions,' *J. Phys.: Condens. Matter*, **22**, 104105, 2010.

[272] M. Antlanger, G. Doppelbauer & G. Kahl, 'On the stability of Archimedean tilings formed by patchy particles,' *J. Phys.: Condens. Matter*, **23**, 404206, 2011.

[273] J. M. Tavares, L. Rovigatti & F. Sciortino, 'Quantitative description of the self-assembly of patchy particles into chains and rings,' *J. Chem. Phys.*, **137**, 044901, 2012.

[274] G. Doppelbauer, E. G. Noya, E. Bianchi & G. Kahl, 'Competing ordered structures formed by particles with a regular tetrahedral patch decoration,' *J. Phys.: Condens. Matter*, **24**, 284124, 2012.

[275] F. Romano, E. Sanz, P. Tartaglia & F. Sciortino, 'Phase diagram of trivalent and pentavalent patchy particles,' *J. Phys.: Condens. Matter*, **24**, 064113, 2012.

[276] E. Bianchi, C. N. Likos & G. Kahl, 'Self-assembly of heterogeneously charged particles under confinement,' *ACS Nano*, **7**, 4657, 2013.

[277] E. Bianchi, C. N. Likos & G. Kahl, 'Tunable assembly of heterogeneously charged colloids,' *Nano Lett.*, **14**, 3412, 2014.

[278] D. Z. Rocklin & X. Mao, 'Self-assembly of three-dimensional open structures using patchy colloidal particles,' *Soft Matter*, **10**, 7569, 2014.

[279] S. Whitelam, 'Minimal positive design for self-assembly of the Archimedean tilings,' *Phys. Rev. Lett.*, **117**, 228003, 2016.

[280] Z.-W. Li, Y.-L. Zhu, Z.-Y. Lu & Z.-Y. Sun, 'A versatile model for soft patchy particles with various patch arrangements,' *Soft Matter*, **12**, 741, 2016.

[281] A. Gemeinhardt, M. Martinsons & M. Schmiedeberg, 'Growth of two-dimensional dodecagonal colloidal quasicrystals: Particles with isotropic pair interactions with two length scales vs. patchy colloids with preferred binding angles,' *Eur. Phys. J. E*, **41**, 126, 2018.

[282] A. Gemeinhardt, M. Martinsons & M. Schmiedeberg, 'Stabilizing quasicrystals composed of patchy colloids by narrowing the patch width,' .

[283] S.-M. Yang, S.-H. Kim, J.-M. Lim & G.-R. Yi, 'Synthesis and assembly of structured colloidal particles,' *J. Mater. Chem.*, **18**, 2177, 2008.

[284] F. Li, D. P. Josephson & A. Stein, 'Colloidal assembly: The road from particles to colloidal molecules and crystals,' *Angew. Chemie - Int. Ed.*, **50**, 360, 2011.

[285] C.-C. Lin, C.-W. Liao, Y.-C. Chao & C. Kuo, 'Fabrication and characterization of asymmetric Janus and ternary particles,' *ACS Appl. Mater. Interfaces*, **2**, 3185, 2010.

[286] S. Jiang & S. Granick, 'A simple method to produce trivalent colloidal particles,' *Langmuir*, **25**, 8915, 2009.

[287] Y. Yu, B. Ai, H. Möhwald, Z. Zhou, G. Zhang & B. Yang, 'Fabrication of binary and ternary hybrid particles based on colloidal lithography,' *Chem. Mater.*, **24**, 4549, 2012.

[288] H. Bao, W. Peukert & R. N. Klupp Taylor, 'One-pot colloidal synthesis of plasmonic patchy particles,' *Adv. Mater.*, **23**, 2644, 2011.

[289] H. Bao, T. Bihr, A.-S. Smith & R. N. Klupp Taylor, 'Facile colloidal coating of polystyrene nanospheres with tunable gold dendritic patches,' *Nanoscale*, **6**, 3954, 2014.

[290] S.-H. Kim, G.-R. Yi, K. H. Kim & S.-M. Yang, 'Photocurable Pickering emulsion for colloidal particles with structural complexity,' *Langmuir*, **24**, 2365, 2008.

[291] V. Meester, R. W. Verweij, C. van der Wel & D. J. Kraft, 'Colloidal recycling: reconfiguration of random aggregates into patchy particles,' *ACS Nano*, **10**, 4322, 2016.

[292] Z. Nie, W. Li, M. Seo, S. Xu & E. Kumacheva, 'Janus and ternary particles generated by microfluidic synthesis: Design, synthesis, and self-assembly,' *J. Am. Chem. Soc.*, **128**, 9408, 2006.

[293] C.-H. Chen, R. K. Shah, A. R. Abate & D. A. Weitz, 'Janus particles templated from double emulsion droplets generated using microfluidics,' *Langmuir*, **25**, 4320, 2009.

[294] C. Sosa, R. Liu, C. Tang, F. Qu, S. Niu, M. Z. Bazant, R. K. Prud'homme & R. D. Priestley, 'Soft multifaced and patchy colloids by constrained volume self-assembly,' *Macromolecules*, **49**, 3580, 2016.

[295] A. Désert, C. Hubert, Z. Fu, L. Moulet, J. Majimel, P. Barboteau, A. Thill, M. Lansalot, E. Bourgeat-Lami, E. Duguet & S. Ravaine, 'Synthesis and site-specific functionalization of tetravalent, hexavalent, and dodecavalent silica particles,' *Angew. Chemie - Int. Ed.*, **52**, 11068, 2013.

[296] C. Hubert, C. Chomette, A. Désert, M. Sun, M. Treguer-Delapierre, S. Mornet, A. Perro, E. Duguet & S. Ravaine, 'Synthesis of multivalent silica nanoparticles combining both enthalpic and entropic patchiness,' *Faraday Discuss.*, **181**, 139, 2015.

[297] Z. Gong, T. Hueckel, G.-R. Yi & S. Sacanna, 'Patchy particles made by colloidal fusion,' *Nature*, **550**, 234, 2017.

[298] D. Zerrouki, J. Baudry, D. Pine, P. Chaikin & J. Bibette, 'Chiral colloidal clusters,' *Nature*, **455**, 380, 2008.

[299] S. Sacanna, L. Rossi & D. J. Pine, 'Magnetic click colloidal assembly,' *J. Am. Chem. Soc.*, **134**, 6112, 2012.

[300] Q. Chen, E. Diesel, J. K. Whitmer, S. C. Bae, E. Luijten & S. Granick, 'Triblock colloids for directed self-assembly,' *J. Am. Chem. Soc.*, **133**, 7725, 2011.

[301] X. Zheng, Y. Wang, Y. Wang, D. J. Pine & M. Weck, 'Thermal regulation of colloidal materials architecture through orthogonal functionalizable patchy particles,' *Chem. Mater.*, **28**, 3984, 2016.

[302] G. A. DeVries, M. Brunnbauer, Y. Hu, A. M. Jackson, B. Long, B. T. Neltner, O. Uzun, B. H. Wunsch & F. Stellacci, 'Divalent metal nanoparticles,' *Science*, **315**, 358, 2007.

[303] J.-W. Kim, J.-H. Kim & R. Deaton, 'DNA-linked nanoparticle building blocks for programmable matter,' *Angew. Chemie - Int. Ed.*, **50**, 9185, 2011.

[304] G. Chen, K. J. Gibson, D. Liu, H. C. Rees, J.-H. Lee, W. Xia, R. Lin, H. L. Xin, O. Gang & Y. Weizmann, 'Regioselective surface encoding of nanoparticles for programmable self-assembly,' *Nat. Mater.*, **18**, 169, 2019.

[305] C. A. Mirkin, R. L. Letsinger, R. C. Mucic & J. J. Storhoff, 'A DNA-based method for rationally assembling nanoparticles into macroscopic materials,' *Nature*, **382**, 607, 1996.

[306] A. P. Alivisatos, K. P. Johnsson, X. Peng, T. E. Wilson, C. J. Loweth, M. P. Bruchez, Jr. & P. G. Schultz, 'Organization of 'nanocrystal molecules' using DNA,' *Nature*, **382**, 609, 1996.

[307] W. J. Parak, T. Pellegrino, C. M. Micheel, D. Gerion, S. C. Williams & A. P. Alivisatos, 'Conformation of oligonucleotides attached to gold nanocrystals probed by gel electrophoresis,' *Nano Lett.*, **3**, 33, 2003.

[308] E. Auyeung, T. I. N. G. Li, A. J. Senesi, A. L. Schmucker, B. C. Pals, M. O. de la Cruz & C. A. Mirkin, 'DNA-mediated nanoparticle crystallization into Wulff polyhedra,' *Nature*, **505**, 73, 2014.

[309] D. Nykypanchuk, M. M. Maye, D. van der Lelie & O. Gang, 'DNA-guided crystallization of colloidal nanoparticles,' *Nature*, **451**, 549, 2008.

[310] S. Y. Park, A. K. R. Lytton-Jean, B. Lee, S. Weigand, G. C. Schatz & C. A. Mirkin, 'DNA-programmable nanoparticle crystallization,' *Nature*, **451**, 553, 2008.

[311] Y. Kim, R. J. Macfarlane, M. R. Jones & C. A. Mirkin, 'Transmutable nanoparticles with reconfigurable surface ligands,' *Science*, **351**, 579, 2016.

[312] H. Xing, Z. Wang, Z. Xu, N. Y. Wong, Y. Xiang, G. L. Liu & Y. Lu, 'DNA-directed assembly of asymmetric nanoclusters using Janus nanoparticles,' *ACS Nano*, **6**, 802, 2012.

[313] R. Schreiber, I. Santiago, A. Ardavan & A. J. Turberfield, 'Ordering gold nanoparticles with DNA origami nanoflowers,' *ACS Nano*, **10**, 7303, 2016.

[314] C. Zhang, R. J. Macfarlane, K. L. Young, C. H. J. Choi, L. Hao, E. Auyeung, G. Liu, X. Zhou & C. A. Mirkin, 'A general approach to DNA-programmable atom equivalents,' *Nat. Mater.*, **12**, 741, 2013.

[315] M. Y. Ben Zion, X. He, C. C. Maass, R. Sha, N. C. Seeman & P. M. Chaikin, 'Self-assembled three-dimensional chiral colloidal architecture,' *Science*, **358**, 633, 2017.

[316] L. Feng, L. L. Pontani, R. Dreyfus, P. Chaikin & J. Brujic, 'Specificity, flexibility and valence of DNA bonds guide emulsion architecture,' *Soft Matter*, **9**, 9816, 2013.

[317] E. V. Shevchenko, D. V. Talapin, N. A. Kotov, S. O'Brien & C. B. Murray, 'Structural diversity in binary nanoparticle superlattices,' *Nature*, **439**, 55, 2006.

[318] A. H. Gröschel, A. Walther, T. I. Löbling, F. H. Schacher, H. Schmalz & A. H. E. Müller, 'Guided hierarchical co-assembly of soft patchy nanoparticles,' *Nature*, **503**, 247, 2013.

[319] C. H. J. Evers, J. A. Luiken, P. G. Bolhuis & W. K. Kegel, 'Self-assembly of microcapsules via colloidal bond hybridization and anisotropy,' *Nature*, **534**, 364, 2016.

[320] X. Mao, Q. Chen & S. Granick, 'Entropy favours open colloidal lattices,' *Nat. Mater.*, **12**, 217, 2013.

[321] X. Mao, 'Entropic effects in the self-assembly of open lattices from patchy particles,' *Phys. Rev. E*, **87**, 062319, 2013.

[322] R. J. Macfarlane, B. Lee, M. R. Jones, N. Harris, G. C. Schatz & C. A. Mirkin, 'Nanoparticle superlattice engineering with DNA,' *Science*, **334**, 204, 2011.

[323] R. J. Macfarlane, M. N. O'Brien, S. H. Petrosko & C. A. Mirkin, 'Nucleic acid-modified nanostructures as programmable atom equivalents: forging a new "table of elements",' *Angew. Chemie - Int. Ed.*, **52**, 5688, 2013.

[324] M. Grünwald & P. L. Geissler, 'Patterns without patches: hierarchical self-assembly of complex structures from simple building blocks,' *ACS Nano*, **8**, 5891, 2014.

[325] F. H. M. Zetterling, M. Dzugutov & S. Lidin, 'γ-brass crystallization in a simple monotomic liquid,' *Mater. Res. Soc. Symp. Proc.*, **643**, K9.5.1, 2000.

[326] M. C. Rechtsman, F. H. Stillinger & S. Torquato, 'Optimized interactions for targeted self-assembly: application to a honeycomb lattice,' *Phys. Rev. Lett.*, **95**, 228301, 2005.

[327] M. C. Rechtsman, F. H. Stillinger & S. Torquato, 'Self-assembly of the simple cubic lattice with an isotropic potential,' *Phys. Rev. E*, **74**, 021404, 2006.

[328] M. Rechtsman, F. Stillinger & S. Torquato, 'Designed interaction potentials via inverse methods for self-assembly,' *Phys. Rev. E*, **73**, 011406, 2006.

[329] M. C. Rechtsman, F. H. Stillinger & S. Torquato, 'Synthetic diamond and wurtzite structures self-assemble with isotropic pair interactions,' *Phys. Rev. E*, **75**, 031403, 2007.

[330] E. Edlund, O. Lindgren & M. N. Jacobi, 'Using the uncertainty principle to design simple interactions for targeted self-assembly,' *J. Chem. Phys.*, **139**, 024107, 2013.

[331] É. Marcotte, F. H. Stillinger & S. Torquato, 'Communication: Designed diamond ground state via optimized isotropic monotonic pair potentials,' *J. Chem. Phys.*, **138**, 061101, 2013.

[332] A. Jain, J. R. Errington & T. M. Truskett, 'Inverse design of simple pairwise interactions with low-coordinated 3D lattice ground states,' *Soft Matter*, **9**, 3866, 2013.

[333] A. Jain, J. R. Errington & T. M. Truskett, 'Communication: phase behavior of materials with isotropic interactions designed by inverse strategies to favor diamond and simple cubic lattice ground states,' *J. Chem. Phys.*, **139**, 141102, 2013.

[334] G. Zhang, F. H. Stillinger & S. Torquato, 'Probing the limitations of isotropic pair potentials to produce ground-state structural extremes via inverse statistical mechanics,' *Phys. Rev. E*, **88**, 042309, 2013.

[335] B. A. Lindquist, R. B. Jadrich & T. M. Truskett, 'Communication: Inverse design for self-assembly via on-the-fly optimization,' *J. Chem. Phys.*, **145**, 111101, 2016.

[336] R. B. Jadrich, B. A. Lindquist & T. M. Truskett, 'Probabilistic inverse design for self-assembling materials,' *J. Chem. Phys.*, **146**, 184103, 2017.

[337] B. A. Lindquist, R. B. Jadrich, W. D. Piñeros & T. M. Truskett, 'Inverse design of self-assembling Frank-Kasper phases and insights into emergent quasicrystals,' *J. Phys. Chem. B*, **122**, 5547, 2017.

[338] W. D. Piñeros & T. M. Truskett, 'Designing pairwise interactions that stabilize open crystals: Truncated square and truncated hexagonal lattices,' *J. Chem. Phys.*, **146**, 144501, 2017.

[339] S. Torquato, 'Inverse optimization techniques for targeted self-assembly,' *Soft Matter*, **5**, 1157, 2009.

[340] M. Dzugutov, 'Glass formation in a simple monatomic liquid with icosahedral inherent local order,' *Phys. Rev. A*, **46**, R2984, 1992.

[341] M. Dzugutov, 'Monatomic model of icosahedrally ordered metallic glass formers,' *J. Non. Cryst. Solids*, **156-158**, 173, 1993.

[342] F. H. M. Zetterling, M. Dzugutov & S. I. Simdyankin, 'Formation of large-scale icosahedral clusters in a simple liquid approaching the glass transition,' *J. Non. Cryst. Solids*, **293-295**, 39, 2001.

[343] J. P. K. Doye, D. J. Wales, F. H. M. Zetterling & M. Dzugutov, 'The favored cluster structures of model glass formers,' *J. Chem. Phys.*, **118**, 2792, 2003.

[344] M. Dzugutov, 'Formation of a dodecagonal quasicrystalline phase in a simple monatomic liquid,' *Phys. Rev. Lett.*, **70**, 2924, 1993.

[345] A. Quandt & M. P. Teter, 'Formation of quasiperiodic patterns within a simple two-dimensional model system,' *Phys. Rev. B*, **59**, 8586, 1999.

[346] M. Engel & H.-R. Trebin, 'Self-assembly of monatomic complex crystals and quasicrystals with a double-well interaction potential,' *Phys. Rev. Lett.*, **98**, 225505, 2007.

[347] A. J. Archer, A. M. Rucklidge & E. Knobloch, 'Quasicrystalline order and a crystal-liquid state in a soft-core fluid,' *Phys. Rev. Lett.*, **111**, 165501, 2013.

[348] A. J. Archer, A. M. Rucklidge & E. Knobloch, 'Soft-core particles freezing to form a quasicrystal and a crystal-liquid phase,' *Phys. Rev. E*, **92**, 012324, 2015.

[349] M. Engel, P. F. Damasceno, C. L. Phillips & S. C. Glotzer, 'Computational self-assembly of a one-component icosahedral quasicrystal,' *Nat. Mater.*, **14**, 109, 2015.

[350] P. Subramanian, A. J. Archer, E. Knobloch & A. M. Rucklidge, 'Three-dimensional icosahedral phase field quasicrystal,' *Phys. Rev. Lett.*, **117**, 075501, 2016.

[351] P. F. Damasceno, S. C. Glotzer & M. Engel, 'Non-close-packed three-dimensional quasicrystals,' *J. Phys.: Condens. Matter*, **29**, 234005, 2017.

[352] T. Dotera, T. Oshiro & P. Ziherl, 'Mosaic two-lengthscale quasicrystals,' *Nature*, **506**, 208, 2014.

[353] M. Engel & H.-R. Trebin, 'Structural complexity in monodisperse systems of isotropic particles,' *Z. Kristallogr.*, **223**, 721, 2008.

[354] J. A. A. W. Elemans, A. E. Rowan & R. J. M. Nolte, 'Mastering molecular matter. Supramolecular architectures by hierarchical self-assembly,' *J. Mater. Chem.*, **13**, 2661, 2003.

[355] C. A. Silvera Batista, R. G. Larson & N. A. Kotov, 'Nonadditivity of nanoparticle interactions,' *Science*, **350**, 1242477, 2015.

[356] P. Schapotschnikow, R. Pool & T. J. H. Vlugt, 'Molecular simulations of interacting nanocrystals,' *Nano Lett.*, **8**, 2930, 2008.

[357] D. Frenkel & B. Smit, *Understanding Molecular Simulation: From Algorithms to Applications* (Academic Press, London), 2nd edition, 2001.

[358] M. P. Allen & D. J. Tildesley, *Computer Simulation of Liquids* (Oxford University Press, Oxford), 2nd edition, 2017.

[359] D. Rosenbaum, P. C. Zamora & C. F. Zukoski, 'Phase behavior of small attractive colloidal particles,' *Phys. Rev. Lett.*, **76**, 150, 1996.

[360] M. A. Miller, J. P. Doye & D. J. Wales, 'Structural relaxation in Morse clusters: energy landscapes,' *J. Chem. Phys.*, **110**, 328, 1999.

[361] H. Liu, S. K. Kumar & F. Sciortino, 'Vapor-liquid coexistence of patchy models: Relevance to protein phase behavior,' *J. Chem. Phys.*, **127**, 084902, 2007.

[362] H. Liu, S. K. Kumar, F. Sciortino & G. T. Evans, 'Vapor-liquid coexistence of fluids with attractive patches: An application of Wertheim's theory of association,' *J. Chem. Phys.*, **130**, 044902, 2009.

[363] J. Kolafa & I. Nezbeda, 'Monte Carlo simulations on primitive models of water and methanol,' *Mol. Phys.*, **61**, 161, 1987.

[364] M. H. Ford, S. M. Auerbach & P. A. Monson, 'On the mechanical properties and phase behavior of silica: A simple model based on low coordination and strong association,' *J. Chem. Phys.*, **121**, 8415, 2004.

[365] E. Del Gado, 'Aggregation of model gels with directional interactions,' *J. Phys.: Condens. Matter*, **22**, 104117, 2010.

[366] E. Del Gado & W. Kob, 'A microscopic model for colloidal gels with directional effective interactions: network induced glassy dynamics,' *Soft Matter*, **6**, 1547, 2010.

[367] X. Li, J. D. Gunton & A. Chakrabarti, 'A simple model of directional interactions for proteins,' *J. Chem. Phys.*, **131**, 115101, 2009.

[368] N. Metropolis, A. W. Rosenbluth, M. N. Rosenbluth, A. H. Teller & E. Teller, 'Equation of State Calculations by Fast Computing Machines,' *J. Chem. Phys.*, **21**, 1087, 1953.

[369] V. I. Manousiouthakis & M. W. Deem, 'Strict detailed balance is unnecessary in Monte Carlo simulation,' *J. Chem. Phys.*, **110**, 2753, 1999.

[370] D. J. Wales, *Energy Landscapes* (Cambridge University Press, Cambridge), 1st edition, 2003.

[371] J. E. Stone, D. J. Hardy, I. S. Ufimtsev & K. Schulten, 'GPU-accelerated molecular modeling coming of age,' *J. Mol. Graph. Model.*, **29**, 116, 2010.

[372] G. S. Pawley, K. C. Bowler, R. D. Kenway & D. J. Wallace, 'Concurrency and parallelism in MC and MD simulations in physics,' *Comput. Phys. Commun.*, **37**, 251, 1985.

[373] G. S. Heffelfinger & M. E. Lewitt, 'A comparison between two massively parallel algorithms for Monte Carlo computer simulation: An investigation in the grand canonical ensemble,' *J. Comput. Chem.*, **17**, 250, 1996.

[374] L. Verlet, 'Computer "experiments" on classical fluids. I. Thermodynamical properties of Lennard-Jones molecules,' *Phys. Rev.*, **159**, 98, 1967.

[375] D. Metcalfe, 'DRAND48(3),' 2017.

[376] NVIDIA, 'CUDA Toolkit Documentation—v10.0.130,' 2018.

[377] J. Nickolls, I. Buck, M. Garland & K. Skadron, 'Scalable parallel programming with CUDA,' *ACM Queue*, **6**, 40, 2008.

[378] K. Kikuchi, M. Yoshida, T. Maekawa & H. Watanabe, 'Metropolis Monte Carlo method as a numerical technique to solve the Fokker-Planck equation,' *Chem. Phys. Lett.*, **185**, 335, 1991.

[379] D. M. Heyes & A. C. Brańka, 'Monte Carlo as Brownian dynamics,' *Mol. Phys.*, **94**, 447, 1998.

[380] E. Sanz & D. Marenduzzo, 'Dynamic Monte Carlo versus Brownian dynamics: A comparison for self-diffusion and crystallization in colloidal fluids,' *J. Chem. Phys.*, **132**, 194102, 2010.

[381] F. Romano, C. De Michele, D. Marenduzzo & E. Sanz, 'Monte Carlo and event-driven dynamics of Brownian particles with orientational degrees of freedom,' *J. Chem. Phys.*, **135**, 124106, 2011.

[382] S. Whitelam, 'Approximating the dynamical evolution of systems of strongly interacting overdamped particles,' *Mol. Simul.*, **37**, 606, 2011.

[383] G. Tiana, L. Sutto & R. A. Broglia, 'Use of the Metropolis algorithm to simulate the dynamics of protein chains,' *Phys. A*, **380**, 241, 2007.

[384] R. T. Scarlett, J. C. Crocker & T. Sinno, 'Computational analysis of binary segregation during colloidal crystallization with DNA-mediated interactions,' *J. Chem. Phys.*, **132**, 234705, 2010.

[385] H. E. A. Huitema & J. P. van der Eerden, 'Can Monte Carlo simulation describe dynamics? A test on Lennard-Jones systems,' *J. Chem. Phys.*, **110**, 3267, 1999.

[386] L. Berthier & W. Kob, 'The Monte Carlo dynamics of a binary Lennard-Jones glass-forming mixture,' *J. Phys.: Condens. Matter*, **19**, 205130, 2007.

[387] L. Berthier, 'Revisiting the slow dynamics of a silica melt using Monte Carlo simulations,' *Phys. Rev. E*, **76**, 011507, 2007.

[388] B. Cichocki & K. Hinsen, 'Dynamic computer simulation of concentrated hard sphere suspensions. I. Simulation Technique and mean square displacement data,' *Phys. A*, **166**, 473, 1990.

[389] S. Whitelam & P. L. Geissler, 'Avoiding unphysical kinetic traps in Monte Carlo simulations of strongly attractive particles,' *J. Chem. Phys.*, **127**, 154101, 2007.

[390] S. Whitelam, E. H. Feng, M. F. Hagan & P. L. Geissler, 'The role of collective motion in examples of coarsening and self-assembly,' *Soft Matter*, **5**, 1251, 2009.

[391] Š. Růžička & M. P. Allen, 'Collective translational and rotational Monte Carlo cluster move for general pairwise interaction,' *Phys. Rev. E*, **90**, 033302, 2014.

[392] B. Chen & J. I. Siepmann, 'A novel Monte Carlo algorithm for simulating strongly associating fluids: applications to water, hydrogen fluoride, and acetic acid,' *J. Phys. Chem. B*, **104**, 8725, 2000.

[393] B. Chen & J. I. Siepmann, 'Improving the efficiency of the aggregation-volume-bias Monte Carlo algorithm,' *J. Phys. Chem. B*, **105**, 11275, 2001.

[394] A. J. Williamson, *Methods, rules and limits of successful self-assembly*, Ph.D. thesis, University of Oxford, 2011.

[395] W. M. Jacobs & D. Frenkel, 'Self-assembly of structures with addressable complexity,' *J. Am. Chem. Soc.*, **138**, 2457, 2016.

[396] K. Urban & M. Feuerbacher, 'Structurally complex alloy phases,' *J. Non. Cryst. Solids*, **334-335**, 143, 2004.

[397] N. W. Ashcroft & N. D. Mermin, *Solid State Physics* (Holt, Rinehart and Winston, London), 1st edition, 1976.

[398] C. Janot, *Quasicrystals: A Primer* (Oxford University Press, Oxford), 2nd edition, 1994.

[399] International Union of Crystallography, 'Report of the Executive Committee for 1991,' *Acta Crystallogr. A*, **48**, 922, 1992.

[400] G. B. Adams, M. O'Keeffe, A. A. Demkov, O. F. Sankey & Y.-M. Huang, 'Wide-band-gap Si in open fourfold-coordinated clathrate structures,' *Phys. Rev. B*, **49**, 8048, 1994.

[401] J. Gryko, P. F. McMillan, R. F. Marzke, G. K. Ramachandran, D. Patton, S. K. Deb & O. F. Sankey, 'Low-density framework form of crystalline silicon with a wide optical band gap,' *Phys. Rev. B*, **62**, R7707, 2000.

[402] L. C. Jacobson, W. Hujo & V. Molinero, 'Thermodynamic stability and growth of guest-free clathrate hydrates: a low-density crystal phase of water,' *J. Phys. Chem. B*, **113**, 10298, 2009.

[403] D. Samanta & R. Klajn, 'Clathrates grow up,' *Science*, **355**, 912, 2017.

[404] A. I. Goldman & R. F. Kelton, 'Quasicrystals and crystalline approximants,' *Rev. Mod. Phys.*, **65**, 213, 1993.

[405] C. S. Adorf, J. Antonaglia, J. Dshemuchadse & S. C. Glotzer, 'Inverse design of simple pair potentials for the self-assembly of complex structures,' *J. Chem. Phys.*, **149**, 204102, 2018.

[406] J. Crain, S. J. Clark, G. J. Ackland, M. C. Payne, V. Milman, P. D. Hatton & B. J. Reid, 'Theoretical study of high-density phases of covalent semiconductors. I. Ab initio treatment,' *Phys. Rev. B*, **49**, 5329, 1994.

[407] A. Mujica, A. Rubio, A. Muñoz & R. J. Needs, 'High-pressure phases of group-IV, III-V, and II-VI compounds,' *Rev. Mod. Phys.*, **75**, 863, 2003.

[408] R. H. Wentorf, Jr. & J. S. Kasper, 'Two new forms of silicon,' *Science*, **139**, 338, 1963.

[409] J. S. Kasper & S. M. Richards, 'The crystal structures of new forms of silicon and germanium,' *Acta Crystallogr.*, **17**, 752, 1964.

[410] J. Z. Hu, L. D. Merkle, C. S. Menoni & I. L. Spain, 'Crystal data for high-pressure phases of silicon,' *Phys. Rev. B*, **34**, 4679, 1986.

[411] Y.-X. Zhao, F. Buehler, J. R. Sites & I. L. Spain, 'New metastable phases of silicon,' *Solid State Commun.*, **59**, 679, 1986.

[412] G. Weill, J. L. Mansot, G. Sagon, C. Carlone & J. M. Besson, 'Characterisation of Si III and Si IV, metastable forms of silicon at ambient pressure,' *Semicond. Sci. Technol.*, **4**, 280, 1989.

[413] M. Imai, K. Yaoita, Y. Katayama, J.-Q. Chen & K. Tsuji, 'Amorphization from the quenched high-pressure phase of silicon and germanium,' *J. Non. Cryst. Solids*, **150**, 49, 1992.

[414] S. Ganguly, N. Kazem, D. Carter & S. M. Kauzlarich, 'Colloidal synthesis of an exotic phase of silicon: the BC8 structure,' *J. Am. Chem. Soc.*, **136**, 1296, 2014.

[415] R. J. Nelmes, M. I. McMahon, N. G. Wright, D. R. Allan & J. S. Loveday, 'Stability and crystal structure of BC8 germanium,' *Phys. Rev. B*, **48**, 9883, 1993.

[416] A. A. Correa, S. A. Bonev & G. Galli, 'Carbon under extreme conditions: Phase boundaries and electronic properties from first-principles theory,' *Proc. Natl. Acad. Sci. U.S.A.*, **103**, 1204, 2006.

[417] Y. Ma, A. R. Oganov & Y. Xie, 'High-pressure structures of lithium, potassium, and rubidium predicted by an ab initio evolutionary algorithm,' *Phys. Rev. B*, **78**, 014102, 2008.

[418] M. V. Nevitt, 'Miscellaneous structures of fixed stoichiometry,' in J. H. Westbrook (editor), *Intermetallic Compounds*, chapter 13, p. 663 (John Wiley & Sons, New York City), 1967.

[419] R. Vargas, P. Mariani, A. Gulik & V. Luzzati, 'Cubic phases of lipid-containing systems: The structure of phase Q223 (space group Pm3n). An X-ray scattering study,' *J. Mol. Biol.*, **225**, 137, 1992.

[420] V. S. Balagurusamy, G. Ungar, V. Percec & G. Johansson, 'Rational design of the first spherical supramolecular dendrimers self-organized in a novel thermotropic cubic liquid-crystalline phase and the determination of their shape by X-ray analysis,' *J. Am. Chem. Soc.*, **119**, 1539, 1997.

[421] P. Ziherl & R. D. Kamien, 'Soap froths and crystal structures,' *Phys. Rev. Lett.*, **85**, 3528, 2000.

[422] P. Ziherl & R. D. Kamien, 'Maximizing entropy by minimizing area: Towards a new principle of self-organization,' *J. Phys. Chem. B*, **105**, 10147, 2001.

[423] X. Zeng, G. Ungar, Y. Liu, V. Percec, A. E. Dulcey & J. K. Hobbs, 'Supramolecular dendritic liquid quasicrystals,' *Nature*, **428**, 157, 2004.

[424] V. Percec, M. Peterca, Y. Tsuda, B. M. Rosen, S. Uchida, M. R. Imam, G. Ungar & P. A. Heiney, 'Elucidating the structure of the $Pm\bar{3}n$ cubic phase of supramolecular dendrimers through the modification of their aliphatic to aromatic volume ratio,' *Chem. - Eur. J.*, **15**, 8994, 2009.

[425] D. Marsh, *Handbook of Lipid Bilayers* (CRC Press, Boca Raton), 2nd edition, 2013.

[426] K. Yue, M. Huang, R. L. Marson, J. He, J. Huang, Z. Zhou, J. Wang, C. Liu, X. Yan, K. Wu, Z. Guo, H. Liu, W. Zhang, P. Ni, C. Wesdemiotis, W.-B. Zhang, S. C. Glotzer & S. Z. D. Cheng, 'Geometry induced sequence of nanoscale Frank-Kasper and quasicrystal mesophases in giant surfactants,' *Proc. Natl. Acad. Sci. U.S.A.*, **113**, 14195, 2016.

[427] S. A. Kim, K.-J. Jeong, A. Yethiraj & M. K. Mahanthappa, 'Low-symmetry sphere packings of simple surfactant micelles induced by ionic sphericity,' *Proc. Natl. Acad. Sci. U.S.A.*, **114**, 4072, 2017.

[428] M. Volmer & A. Weber, 'Keimbildung in übersättigten gebilden,' *Z. Phys. Chem.*, **119**, 277, 1926.

[429] R. Becker & W. Döring, 'Kinetische behandlung der keimbildung in übersättigten dämpfen,' *Ann. Phys.*, **416**, 719, 1935.

[430] J. Frenkel, 'A general theory of heterophase fluctuations and pretransition phenomena,' *J. Chem. Phys.*, **7**, 538, 1939.

[431] D. W. Oxtoby, 'Homogeneous nucleation: theory and experiment,' *J. Phys.: Condens. Matter*, **4**, 7627, 1992.

[432] P. M. Chaikin & T. C. Lubensky, *Principles of Condensed Matter Physics* (Cambridge University Press, Cambridge), 1st edition, 1995.

[433] R. P. Sear, 'Nucleation: Theory and applications to protein solutions and colloidal suspensions,' *J. Phys.: Condens. Matter*, **19**, 033101, 2007.

[434] V. G. Dubrovskii, *Nucleation Theory and Growth of Nanostructures* (Springer-Verlag, Berlin), 1st edition, 2014.

[435] S. Karthika, T. K. Radhakrishnan & P. Kalaichelvi, 'A review of classical and nonclassical nucleation theories,' *Cryst. Growth Des.*, **16**, 6663, 2016.

[436] W. Ostwald, 'Studien über die bildung und umwandlung fester körper. 1. Abhandlung: Übersättigung und überkaltung,' *Z. Phys. Chem.*, **22**, 289, 1897.

[437] I. N. Stranski & D. Totomanow, 'Keimbildungsgeschwindigkeit und Ostwaldsche stufenregel,' *Z. Phys. Chem.*, **163**, 399, 1933.

[438] P. R. ten Wolde & D. Frenkel, 'Homogeneous nucleation and the Ostwald step rule,' *Phys. Chem. Chem. Phys.*, **1**, 2191, 1999.

[439] W. Ostwald, *Lehrbuch der Allgemeinen Chemie (Volume 2)* (Wilhelm Engelmann, Leipzig), 1896.

[440] T. Janssen, G. Chapuis & M. de Boissieu, *Aperiodic Crystals: From Modulated Phases to Quasicrystals* (Oxford University Press, Oxford), 1st edition, 2007.

[441] T. Dotera, 'Toward the discovery of new soft quasicrystals: from a numerical study viewpoint,' *J. Polym. Sci. B*, **50**, 155, 2012.

[442] W. Steurer, 'Why are quasicrystals quasiperiodic?' *Chem. Soc. Rev.*, **41**, 6719, 2012.

[443] H. S. M. Coxeter, *Introduction to Geometry* (Wiley, New York City), 2nd edition, 1989.

[444] P. J. Steinhardt, 'Quasicrystals: A brief history of the impossible,' *Rend. Lincei Sci. Fis. Nat.*, **24**, S85, 2013.

[445] D. Shechtman, I. Blech, D. Gratias & J. W. Cahn, 'Metallic phase with long-range orientational order and no translational symmetry,' *Phys. Rev. Lett.*, **53**, 1951, 1984.

[446] D. Levine & P. J. Steinhardt, 'Quasicrystals: a new class of ordered structures,' *Phys. Rev. Lett.*, **53**, 2477, 1984.

[447] A.-P. Tsai, '"Back to the future"—An account discovery of stable quasicrystals,' *Acc. Chem. Res.*, **36**, 31, 2003.

[448] W. Steurer, 'Twenty years of structure research on quasicrystals. Part I. Pentagonal, octagonal, decagonal and dodecagonal quasicrystals,' *Z. Kristallogr.*, **219**, 391, 2004.

[449] A.-P. Tsai, 'Icosahedral clusters, icosaheral order and stability of quasicrystals—a view of metallurgy,' *Sci. Technol. Adv. Mater.*, **9**, 013008, 2008.

[450] A.-P. Tsai, 'Discovery of stable icosahedral quasicrystals: progress in understanding structure and properties,' *Chem. Soc. Rev.*, **42**, 5352, 2013.

[451] M. Conrad & F. Krumeich, 'A dodecagonal quasicrystalline chalcogenide,' *Angew. Chemie - Int. Ed.*, **37**, 1383, 1998.

[452] S. Förster, K. Meinel, R. Hammer, M. Trautmann & W. Widdra, 'Quasicrystalline structure formation in a classical crystalline thin-film system,' *Nature*, **502**, 215, 2013.

[453] S. Förster, J. I. Flege, E. M. Zollner, F. O. Schumann, R. Hammer, A. Bayat, K.-M. Schindler, J. Falta & W. Widdra, 'Growth and decay of a two-dimensional oxide quasicrystal: High-temperature in situ microscopy,' *Ann. Phys.*, **529**, 1, 2017.

[454] L. Bindi, P. J. Steinhardt, N. Yao & P. J. Lu, 'Natural quasicrystals,' *Science*, **324**, 1306, 2009.

[455] P. J. Steinhardt & L. Bindi, 'In search of natural quasicrystals,' *Reports Prog. Phys.*, **75**, 092601, 2012.

[456] L. Bindi, N. Yao, C. Lin, L. S. Hollister, C. L. Andronicos, V. V. Distler, M. P. Eddy, A. Kostin, V. Kryachko, G. J. MacPherson, W. M. Steinhardt, M. Yudovskaya & P. J. Steinhardt, 'Natural quasicrystal with decagonal symmetry,' *Sci. Rep.*, **5**, 1, 2015.

[457] M. de Boissieu, 'Stability of quasicrystals: Energy, entropy and phason modes,' *Philos. Mag.*, **86**, 1115, 2006.

[458] K. Jiang, J. Tong, P. Zhang & A.-C. Shi, 'Stability of two-dimensional soft quasicrystals in systems with two length scales,' *Phys. Rev. E*, **92**, 042159, 2015.

[459] A. R. Denton & J. Hafner, 'Thermodynamically stable one-component quasicrystals: A density-functional survey of relative stabilities,' *Phys. Rev. B*, **56**, 2469, 1997.

[460] M. C. Rechtsman, H.-C. Jeong, P. M. Chaikin, S. Torquato & P. J. Steinhardt, 'Optimized structures for photonic quasicrystals,' *Phys. Rev. Lett.*, **101**, 073902, 2008.

[461] Y. S. Chan, C. T. Chan & Z. Y. Liu, 'Photonic band gaps in two dimensional photonic quasicrystals,' *Phys. Rev. Lett.*, **80**, 956, 1998.

[462] R. McGrath, U. Grimm & R. D. Diehl, 'The forbidden beauty of quasicrystals,' *Phys. World*, **17**, 23, 2004.

[463] T. Dotera, 'Quasicrystals in soft matter,' *Isr. J. Chem.*, **51**, 1197, 2011.

[464] Z. V. Vardeny, A. Nahata & A. Agrawal, 'Optics of photonic quasicrystals,' *Nat. Photonics*, **7**, 177, 2013.

[465] L. Levi, M. Rechtsman, B. Freedman, T. Schwartz, O. Manela & M. Segev, 'Disorder-enhanced transport in photonic quasicrystals,' *Science*, **332**, 1541, 2011.

[466] W. Steurer & D. Sutter-Widmer, 'Photonic and phononic quasicrystals,' *J. Phys. D.: Appl. Phys.*, **40**, R229, 2007.

[467] E. Maciá, 'The role of aperiodic order in science and technology,' *Reports Prog. Phys.*, **69**, 397, 2006.

[468] R. Lifshitz & H. Diamant, 'Soft quasicrystals – Why are they stable?' *Philos. Mag.*, **87**, 3021, 2007.

[469] J.-M. Dubois, 'Properties- and applications of quasicrystals and complex metallic alloys,' *Chem. Soc. Rev.*, **41**, 6760, 2012.

[470] N. Rivier, 'Non-stick quasicrystalline coatings,' *J. Non. Cryst. Solids*, **153-154**, 458, 1993.

[471] 'Sputtering technique forms versatile quasicrystalline coatings,' *Mater. Res. Soc. Bull.*, **36**, 581, 2011.

[472] S. Glotzer, 'The hunt for quasicrystals,' *Nature*, **565**, 156, 2019.

[473] S. J. Poon, 'Electronic properties of quasicrystals: An experimental review,' *Adv. Phys.*, **41**, 303, 1992.

[474] D. Oberhaus, 'Quasicrystals are nature's impossible matter,' 2015.

[475] S. Fischer, A. Exner, K. Zielske, J. Perlich, S. Deloudi, W. Steurer, P. Lindner & S. Förster, 'Colloidal quasicrystals with 12-fold and 18-fold diffraction symmetry,' *Proc. Natl. Acad. Sci. U.S.A.*, **108**, 1810, 2011.

[476] G. Ungar & X. Zeng, 'Frank-Kasper, quasicrystalline and related phases in liquid crystals,' *Soft Matter*, **1**, 95, 2005.

[477] G. Ungar, V. Percec, X. Zeng & P. Leowanawat, 'Liquid quasicrystals,' *Isr. J. Chem.*, **51**, 1206, 2011.

[478] Y. Roichman & D. G. Grier, 'Holographic assembly of quasicrystalline photonic heterostructures,' *Opt. Express*, **13**, 5434, 2005.

[479] S. P. Gorkhali, J. Qi & G. P. Crawford, 'Switchable quasi-crystal structures with five-, seven-, and ninefold symmetries,' *J. Opt. Soc. Am. B*, **23**, 149, 2006.

[480] J. Mikhael, J. Roth, L. Helden & C. Bechinger, 'Archimedean-like tiling on decagonal quasicrystalline surfaces,' *Nature*, **454**, 501, 2008.

[481] J. Mikhael, M. Schmiedeberg, S. Rausch, J. Roth, H. Stark & C. Bechinger, 'Proliferation of anomalous symmetries in colloidal monolayers subjected to quasiperiodic light fields,' *Proc. Natl. Acad. Sci. U.S.A.*, **107**, 7214, 2010.

[482] J. Mikhael, G. Gera, T. Bohlein & C. Bechinger, 'Phase behavior of colloidal monolayers in quasiperiodic light fields,' *Soft Matter*, **7**, 1352, 2011.

[483] N. A. Wasio, R. C. Quardokus, R. P. Forrest, C. S. Lent, S. A. Corcelli, J. A. Christie, K. W. Henderson & S. A. Kandel, 'Self-assembly of hydrogen-bonded two-dimensional quasicrystals,' *Nature*, **507**, 86, 2014.

[484] V. Fournée, É. Gaudry, J. Ledieu, M.-C. de Weerd, D. Wu & T. Lograsso, 'Self-organized molecular films with long-range quasiperiodic order,' *ACS Nano*, **8**, 3646, 2014.

[485] J. A. Smerdon, K. M. Young, M. Lowe, S. S. Hars, T. P. Yadav, D. Hesp, V. R. Dhanak, A. P. Tsai, H. R. Sharma & R. McGrath, 'Templated quasicrystalline molecular ordering,' *Nano Lett.*, **14**, 1184, 2014.

[486] L. Zaidouny, T. Bohlein, J. Roth & C. Bechinger, 'Periodic average structures of colloidal quasicrystals,' *Soft Matter*, **10**, 8705, 2014.

[487] M. de Boissieu, 'Icosahedral quasicrystals: assembled with one component,' *Nat. Mater.*, **14**, 18, 2015.

[488] D. V. Talapin, E. V. Shevchenko, M. I. Bodnarchuk, X. Ye, J. Chen & C. B. Murray, 'Quasicrystalline order in self-assembled binary nanoparticle superlattices,' *Nature*, **461**, 964, 2009.

[489] S. Narasimhan & T.-L. Ho, 'Mean-field-theory study of the energetics of icosahedral, decagonal, and dodecagonal quasicrystals,' *Phys. Rev. B*, **37**, 800, 1988.

[490] A. Takano, W. Kawashima, A. Noro, Y. Isono, N. Tanaka, T. Dotera & Y. Matsushita, 'A mesoscopic Archimedean tiling having a new complexity in an ABC star polymer,' *J. Polym. Sci. B*, **43**, 2427, 2005.

[491] G. H. Mehl, 'Quasi-periodic organization in soft self-assembling matter,' *Angew. Chemie - Int. Ed.*, **44**, 672, 2005.

[492] K. Hayashida, T. Dotera, A. Takano & Y. Matsushita, 'Polymeric quasicrystal: Mesoscopic quasicrystalline tiling in ABC star polymers,' *Phys. Rev. Lett.*, **98**, 195502, 2007.

[493] V. Percec, M. R. Imam, M. Peterca, D. A. Wilson, R. Graf, H. W. Spiess, V. S. K. Balagurusamy & P. A. Heiney, 'Self-assembly of dendronized triphenylenes into helical pyramidal columns and chiral spheres,' *J. Am. Chem. Soc.*, **131**, 7662, 2009.

[494] M. I. Bodnarchuk, E. V. Shevchenko & D. V. Talapin, 'Structural defects in periodic and quasicrystalline binary nanocrystal superlattices,' *J. Am. Chem. Soc.*, **133**, 20837, 2011.

[495] C. Xiao, N. Fujita, K. Miyasaka, Y. Sakamoto & O. Terasaki, 'Dodecagonal tiling in mesoporous silica,' *Nature*, **487**, 349, 2012.

[496] J. Zhang & F. S. Bates, 'Dodecagonal quasicrystalline morphology in a poly(styrene-b-isoprene-b-styrene-b-ethylene oxide) tetrablock terpolymer,' *J. Am. Chem. Soc.*, **134**, 7636, 2012.

[497] M. I. Bodnarchuk, R. Erni, F. Krumeich & M. V. Kovalenko, 'Binary superlattices from colloidal nanocrystals and giant polyoxometalate clusters,' *Nano Lett.*, **13**, 1699, 2013.

[498] Z. Yang, J. Wei, P. Bonville & M.-P. Pileni, 'Beyond entropy: Magnetic forces induce formation of quasicrystalline structure in binary nanocrystal superlattices,' *J. Am. Chem. Soc.*, **137**, 4487, 2015.

[499] J. Wei, N. Schaeffer & M.-P. Pileni, 'Ligand exchange governs the crystal structures in binary nanocrystal superlattices,' *J. Am. Chem. Soc.*, **137**, 14773, 2015.

[500] T. M. Gillard, S. Lee & F. S. Bates, 'Dodecagonal quasicrystalline order in a diblock copolymer melt,' *Proc. Natl. Acad. Sci. U.S.A.*, **113**, 5167, 2016.

[501] J. I. Urgel, D. Écija, G. Lyu, R. Zhang, C.-A. Palma, W. Auwärter, N. Lin & J. V. Barth, 'Quasicrystallinity expressed in two-dimensional coordination networks,' *Nat. Chem.*, **8**, 657, 2016.

[502] X. Ye, J. Chen, M. E. Irrgang, M. Engel, A. Dong, S. C. Glotzer & C. B. Murray, 'Quasicrystalline nanocrystal superlattice with partial matching rules,' *Nat. Mater.*, **16**, 214, 2017.

[503] M. Paßens, V. Caciuc, N. Atodiresei, M. Feuerbacher, M. Moors, R. E. Dunin-Borkowski, S. Blügel, R. Waser & S. Karthäuser, 'Interface-driven formation of a two-dimensional dodecagonal fullerene quasicrystal,' *Nat. Commun.*, **8**, 15367, 2017.

[504] M. Zu, P. Tan & N. Xu, 'Forming quasicrystals by monodisperse soft core particles,' *Nat. Commun.*, **8**, 2089, 2017.

[505] H. G. Schoberth, H. Emmerich, M. Holzinger, M. Dulle, S. Förster & T. Gruhn, 'Molecular dynamics study of colloidal quasicrystals,' *Soft Matter*, **12**, 7644, 2016.

[506] R. Ryltsev, B. Klumov & N. Chtchelkatchev, 'Self-assembly of the decagonal quasicrystalline order in simple three-dimensional systems,' *Soft Matter*, **11**, 6991, 2015.

[507] A. P. Smith, 'Stable one-component quasicrystals,' *Phys. Rev. B*, **43**, 11635, 1991.

[508] A. R. Denton & H. Löwen, 'Stability of colloidal quasicrystals,' *Phys. Rev. Lett.*, **81**, 469, 1998.

[509] V. E. Dmitrienko & S. B. Astaf'ev, 'Oscillating interatomic potentials and growth of icosahedral quasicrystals,' *Phys. Rev. Lett.*, **75**, 1538, 1995.

[510] V. E. Dmitrienko, S. B. Astaf'ev & M. Kléman, 'Monte Carlo simulations of icosahedral quasicrystal growth and melting,' *Phys. Rev. B*, **59**, 286, 1999.

[511] M. Elenius, F. H. M. Zetterling, M. Dzugutov, D. C. Fredrickson & S. Lidin, 'Structural model for octagonal quasicrystals derived from octagonal symmetry elements arising in β-Mn crystallization of a simple monatomic liquid,' *Phys. Rev. B*, **79**, 144201, 2009.

[512] J. W. Roth, R. Schilling & H.-R. Trebin, 'Nucleation of quasicrystals by rapid cooling of a binary melt: A molecular-dynamics study,' *Phys. Rev. B*, **51**, 15833, 1995.

[513] J. Roth & C. L. Henley, 'A new binary decagonal Frank-Kasper quasicrystal phase,' *Philos. Mag. A*, **75**, 861, 1997.

[514] G. Y. Onoda, P. J. Steinhardt, D. P. DiVincenzo & J. E. S. Socolar, 'Growing perfect quasicrystals,' *Phys. Rev. Lett.*, **60**, 2653, 1988.

[515] K. Ingersent & P. J. Steinhardt, 'Matching rules and growth rules for pentagonal quasicrystal tilings,' *Phys. Rev. Lett.*, **64**, 2034, 1990.

[516] C. T. Hann, J. E. S. Socolar & P. J. Steinhardt, 'Local growth of icosahedral quasicrystalline tilings,' *Phys. Rev. B*, **94**, 014113, 2016.

[517] M. Schmiedeberg & H. Stark, 'Colloidal ordering on a 2D quasicrystalline substrate,' *Phys. Rev. Lett.*, **101**, 218302, 2008.

[518] R. Penrose, 'The role of aesthetics in pure and applied mathematical research,' *Bull. Inst. Math. Appl.*, **10**, 266, 1974.

[519] M. Gardner, 'Mathematical games: Extraordinary nonperiodic tiling that enriches the theory of tiles,' *Sci. Am.*, **236**, 110, 1977.

[520] R. Penrose, 'Pentaplexity: A class of non-periodic tilings of the plane,' *Math. Intell.*, **2**, 32, 1979.

[521] N. G. de Bruijn, 'Algebraic theory of Penrose's non-periodic tilings of the plane. II,' *Indag. Math.*, **84**, 53, 1981.

[522] N. G. de Bruijn, 'Algebraic theory of Penrose's non-periodic tilings of the plane. I,' *Indag. Math.*, **84**, 39, 1981.

[523] D. Levine & P. J. Steinhardt, 'Quasicrystals. I. Definition and structure,' *Phys. Rev. B*, **34**, 596, 1986.

[524] F. Lançon, L. Billard & P. Chaudhari, 'Thermodynamical properties of a two-dimensional quasicrystal from molecular dynamics calculations,' *Europhys. Lett.*, **2**, 625, 1986.

[525] F. Lançon & L. Billard, 'Two-dimensional system with a quasi-crystalline ground state,' *J. Phys.*, **49**, 249, 1988.

[526] M. Widom, K. J. Strandburg & R. H. Swendsen, 'Quasicrystal equilibrium state,' *Phys. Rev. Lett.*, **58**, 706, 1987.

[527] K. J. Strandburg, 'Random-tiling quasicrystal,' *Phys. Rev. B*, **40**, 6071, 1989.

[528] P. W. Leung, C. L. Henley & G. V. Chester, 'Dodecagonal order in a two-dimensional Lennard-Jones system,' *Phys. Rev. B*, **39**, 446, 1989.

[529] L. H. Tang & M. V. Jarić, 'Equilibrium quasicrystal phase of a Penrose tiling model,' *Phys. Rev. B*, **41**, 4524, 1990.

[530] J. Roth & A. R. Denton, 'Solid-phase structures of the Dzugutov pair potential,' *Phys. Rev. E*, **61**, 6845, 2000.

[531] M. Oxborrow & C. L. Henley, 'Random square-triangle tilings: A model for twelvefold-symmetric quasicrystals,' *Phys. Rev. B*, **48**, 6966, 1993.

[532] E. A. Jagla, 'Phase behavior of a system of particles with core collapse,' *Phys. Rev. E*, **58**, 1478, 1998.

[533] A. Skibinsky, S. V. Buldyrev, A. Scala, S. Havlin & H. E. Stanley, 'Quasicrystals in a monodisperse system,' *Phys. Rev. E*, **60**, 2664, 1999.

[534] T. Dotera & T. Gemma, 'Dodecagonal quasicrystal in a polymeric alloy,' *Philos. Mag.*, **86**, 1085, 2006.

[535] M. Engel, M. Umezaki, H.-R. Trebin & T. Odagaki, 'Dynamics of particle flips in two-dimensional quasicrystals,' *Phys. Rev. B*, **82**, 134206, 2010.

[536] A. S. Keys & S. C. Glotzer, 'How do quasicrystals grow?' *Phys. Rev. Lett.*, **99**, 235503, 2007.

[537] M. Schmiedeberg & H. Stark, 'Comparing light-induced colloidal quasicrystals with different rotational symmetries,' *J. Phys.: Condens. Matter*, **24**, 284101, 2012.

[538] A. Haji-Akbari, M. Engel, A. S. Keys, X. Zheng, R. G. Petschek, P. Palffy-Muhoray & S. C. Glotzer, 'Disordered, quasicrystalline and crystalline phases of densely packed tetrahedra,' *Nature*, **462**, 773, 2009.

[539] A. Haji-Akbari, M. Engel & S. C. Glotzer, 'Phase diagram of hard tetrahedra,' *J. Chem. Phys.*, **135**, 194101, 2011.

[540] A. Haji-Akbari, M. Engel & S. C. Glotzer, 'Degenerate quasicrystal of hard triangular bipyramids,' *Phys. Rev. Lett.*, **107**, 215702, 2011.

[541] A. Haji-Akbari, E. R. Chen, M. Engel & S. C. Glotzer, 'Packing and self-assembly of truncated triangular bipyramids,' *Phys. Rev. E*, **88**, 012127, 2013.

[542] J. C. Johnston, N. Kastelowitz & V. Molinero, 'Liquid to quasicrystal transition in bilayer water,' *J. Chem. Phys.*, **133**, 154516, 2010.

[543] J. C. Johnston, S. Phippen & V. Molinero, 'A single-component silicon quasicrystal,' *J. Phys. Chem. Lett.*, **2**, 384, 2011.

[544] C. R. Iacovella, A. S. Keys & S. C. Glotzer, 'Self-assembly of soft-matter quasicrystals and their approximants,' *Proc. Natl. Acad. Sci. U.S.A.*, **108**, 20935, 2011.

[545] Z.-W. Chen & X.-J. Fu, 'Quasicrystalline phase with eighteen-fold diffraction symmetry in molecular dynamics simulations,' *Chinese Phys. Lett.*, **29**, 050204, 2012.

[546] K. Barkan, H. Diamant & R. Lifshitz, 'Stability of quasicrystals composed of soft isotropic particles,' *Phys. Rev. B*, **83**, 172201, 2011.

[547] K. Barkan, M. Engel & R. Lifshitz, 'Controlled self-assembly of periodic and aperiodic cluster crystals,' *Phys. Rev. Lett.*, **113**, 098304, 2014.

[548] L. Q. Costa Campos, C. C. de Souza Silva & S. W. S. Apolinario, 'Structural phases of colloids interacting via a flat-well potential,' *Phys. Rev. E*, **86**, 051402, 2012.

[549] C. V. Achim, M. Schmiedeberg & H. Löwen, 'Growth modes of quasicrystals,' *Phys. Rev. Lett.*, **112**, 255501, 2014.

[550] M. Schmiedeberg, C. V. Achim, J. Hielscher, S. C. Kapfer & H. Löwen, 'Dislocation-free growth of quasicrystals from two seeds due to additional phasonic degrees of freedom,' *Phys. Rev. E*, **96**, 012602, 2017.

[551] H. Pattabhiraman, A. P. Gantapara & M. Dijkstra, 'On the stability of a quasicrystal and its crystalline approximant in a system of hard disks with a soft corona,' *J. Chem. Phys.*, **143**, 164905, 2015.

[552] H. Pattabhiraman & M. Dijkstra, 'Phase behaviour of quasicrystal forming systems of core-corona particles,' *J. Chem. Phys.*, **146**, 114901, 2017.

[553] J. Dontabhaktuni, M. Ravnik & S. Žumer, 'Quasicrystalline tilings with nematic colloidal platelets,' *Proc. Natl. Acad. Sci. U.S.A.*, **111**, 2464, 2014.

[554] D. Salgado-Blanco & C. I. Mendoza, 'Non-additive simple potentials for pre-programmed self-assembly,' *Soft Matter*, **11**, 889, 2015.

[555] M. Mihalkovič & C. L. Henley, 'Empirical oscillating potentials for alloys from ab initio fits and the prediction of quasicrystal-related structures in the Al-Cu-Sc system,' *Phys. Rev. B*, **85**, 092102, 2012.

[556] A. Metere, P. Oleynikov, M. Dzugutov & S. Lidin, 'A smectic dodecagonal quasicrystal,' *Soft Matter*, **12**, 8869, 2016.

[557] R. Ryltsev & N. Chtchelkatchev, 'Universal self-assembly of one-component three-dimensional dodecagonal quasicrystals,' *Soft Matter*, **13**, 5076, 2017.

[558] M. Martinsons & M. Schmiedeberg, 'Growth of two-dimensional decagonal colloidal quasicrystals,' *J. Phys.: Condens. Matter*, **30**, 255403, 2018.

[559] S. Savitz, M. Babadi & R. Lifshitz, 'Multiple-scale structures: from Faraday waves to soft-matter quasicrystals,' *IUCrJ*, **5**, 247, 2018.

[560] D. Levine, T. C. Lubensky, S. Ostlund, S. Ramaswamy, P. J. Steinhardt & J. Toner, 'Elasticity and dislocations in pentagonal and icosahedral quasicrystals,' *Phys. Rev. Lett.*, **54**, 1520, 1985.

[561] J. E. S. Socolar, T. C. Lubensky & P. J. Steinhardt, 'Phonons, phasons, and dislocations in quasicrystals,' *Phys. Rev. B*, **34**, 3345, 1986.

[562] E. Dontsova, *Understanding of edge and screw dislocations in nanostructures by modeling and simulations*, Ph.d. dissertation, University of Minnesota, 2013.

[563] M. Sandbrink & M. Schmiedeberg, 'Course of dislocation lines in templated three-dimensional colloidal quasicrystals,' *Phys. Rev. B*, **90**, 064108, 2014.

[564] W. K. Burton, N. Cabrera & F. C. Frank, 'Role of dislocations in crystal growth,' *Nature*, **163**, 398, 1949.

[565] W. K. Burton, N. Cabrera & F. C. Frank, 'The growth of crystals and the equilibrium structure of their surfaces,' *Philos. Trans. R. Soc. A*, **243**, 299, 1951.

[566] F. Meng, S. A. Morin, A. Forticaux & S. Jin, 'Screw dislocation driven growth of nanomaterials,' *Acc. Chem. Res.*, **46**, 1616, 2013.

[567] M. Kléman, *Points, Lines, and Walls in Liquid Crystals, Magnetic Systems, and Various Ordered Media* (John Wiley & Sons, New York City), 1st edition, 1983.

[568] P. De & R. A. Pelcovits, 'Linear elasticity theory of pentagonal quasicrystals,' *Phys. Rev. B*, **35**, 8609, 1987.

[569] P. De & R. A. Pelcovits, 'Defect-mediated melting of pentagonal quasicrystals,' *J. Phys. A.: Math. Gen.*, **22**, 1167, 1989.

[570] D. R. Nelson, 'Toward a tetravalent chemistry of colloids,' *Nano Lett.*, **2**, 1125, 2002.

[571] M. Feuerbacher, 'Dislocations in icosahedral quasicrystals,' *Chem. Soc. Rev.*, **41**, 6745, 2012.

[572] A. Leonardi, S. Ryu, N. M. Pugno & P. Scardi, 'Eshelby twist and correlation effects in diffraction from nanocrystals,' *J. Appl. Phys.*, **117**, 163404, 2015.

[573] A. Repula & E. Grelet, 'Elementary edge and screw dislocations visualized at the lattice periodicity level in the smectic phase of colloidal rods,' *Phys. Rev. Lett.*, **121**, 097801, 2018.

[574] M. Kléman, Y. Gefen & A. Pavlovitch, 'Topological defects in non-Haüyan crystallography: The two-dimensional case,' *Europhys. Lett.*, **1**, 61, 1986.

[575] P. De & R. A. Pelcovits, 'Interaction energy of disclinations in pentagonal quasicrystals,' *Phys. Rev. B*, **38**, 5042, 1988.

[576] C. Dilger, R. Mikulla, J. Roth & H.-R. Trebin, 'Simulation of shear stress in icosahedral quasicrystals,' *Philos. Mag. A*, **75**, 425, 1997.

[577] W. Yang, R. Wang, M. Feuerbacher, P. Schall & K. Urban, 'Determination of the Burgers vector of dislocations in icosahedral quasicrystals by a high-resolution lattice-fringe technique,' *Philos. Mag. Lett.*, **80**, 281, 2010.

[578] T.-Y. Fan, X.-F. Li & Y.-F. Sun, 'A moving screw dislocation in a one-dimensional hexagonal quasicrystal,' *Acta Phys. Sin. (Overseas Ed.)*, **8**, 288, 1999.

[579] M. Li, H. Schnablegger & S. Mann, 'Coupled synthesis and self-assembly of nanoparticles to give structures with controlled organization,' *Nature*, **402**, 393, 1999.

[580] W.-M. Zhou & Y.-H. Song, 'Moving screw dislocation in cubic quasicrystal,' *Applied Mathematics and Mechanics (English Edition)*, **26**, 1611, 2005.

[581] L.-J. Jiang & G.-T. Liu, 'The interaction between a screw dislocation and a wedge-shaped crack in one-dimensional hexagonal piezoelectric quasicrystals,' *Chinese Phys. B*, **26**, 044601, 2017.

[582] P. G. de Gennes & J. Prost, *The Physics of Liquid Crystals* (Oxford University Press, Oxford), 2nd edition, 1993.

[583] M. Mitov, 'Cholesteric liquid crystals in living matter,' *Soft Matter*, **13**, 4176, 2017.

[584] A. G. Cherstvy, 'DNA cholesteric phases: The role of DNA molecular chirality and DNA-DNA electrostatic interactions,' *J. Phys. Chem. B*, **112**, 12585, 2008.

[585] A. C. Zeri, M. F. Mesleh, A. A. Nevzorov & S. J. Opella, 'Structure of the coat protein in fd filamentous bacteriophage particles determined by solid-state NMR spectroscopy,' *Proc. Natl. Acad. Sci. U.S.A.*, **100**, 6458, 2003.

[586] C. Sachse, J. Z. Chen, P.-D. Coureux, M. E. Stroupe, M. Fändrich & N. Grigorieff, 'High-resolution electron microscopy of helical specimens: A fresh look at tobacco mosaic virus,' *J. Mol. Biol.*, **371**, 812, 2007.

[587] F. Livolant, 'Ordered phases of DNA in vivo and in vitro,' *Phys. A*, **176**, 117, 1991.

[588] I. W. Hamley, 'Liquid crystal phase formation by biopolymers,' *Soft Matter*, **6**, 1863, 2010.

[589] L. Wang, A. M. Urbas & Q. Li, 'Nature-inspired emerging chiral liquid crystal nanostructures: From molecular self-assembly to DNA mesophase and nanocolloids,' *Adv. Mater.*, p. 1801335, 2018.

[590] P. Das, J. Xu, J. Roy & N. Chakrabarti, 'Liquid crystal polymorphism in F-actin: Optical microscopic and rotatory dispersion studies,' *J. Chem. Phys.*, **111**, 8240, 1999.

[591] I. Uematsu & Y. Uematsu, 'Polypeptide Liquid Crystals,' in N. A. Platé & M. Gordon (editors), *Liquid Crystal Polymers I (Advances in Polymer Science Volume 59)*, chapter 2, pp. 37–73 (Springer-Verlag, Berlin), 1st edition, 1984.

[592] C. Robinson, 'Liquid-crystalline structures in polypeptide solutions,' *Tetrahedron*, **13**, 219, 1961.

[593] F. Livolant, A. M. Levelut, J. Doucet & J. P. Benoit, 'The highly concentrated liquid-crystalline phase of DNA is columnar hexagonal,' *Nature*, **339**, 724, 1989.

[594] F. Livolant & A. Leforestier, 'Condensed phases of DNA: Structures and phase transitions,' *Prog. Polym. Sci.*, **21**, 1115, 1996.

[595] R. Podgornik, H. H. Strey & V. A. Parsegian, 'Colloidal DNA,' *Curr. Opin. Colloid Interface Sci.*, **3**, 534, 1998.

[596] G. Zanchetta, F. Giavazzi, M. Nakata, M. Buscaglia, R. Cerbino, N. A. Clark & T. Bellini, 'Right-handed double-helix ultrashort DNA yields chiral nematic phases with both right- and left-handed director twist,' *Proc. Natl. Acad. Sci. U.S.A.*, **107**, 17497, 2010.

[597] R. S. Werbowyj & D. G. Gray, 'Liquid crystalline structure in aqueous hydroxypropyl cellulose solutions,' *Mol. Cryst. Liq. Cryst.*, **34**, 97, 1976.

[598] J.-F. Revol, H. Bradford, J. Giasson, R. H. Marchessault & D. G. Gray, 'Helicoidal self-ordering of cellulose microfibrils in aqueous suspension,' *Int. J. Biol. Macromol.*, **14**, 170, 1992.

[599] J.-F. Revol & R. H. Marchessault, 'In vitro nematic ordering of chitin crystallites,' *Int. J. Biol. Macromol.*, **15**, 329, 1993.

[600] K. Yoshiba, A. Teramoto, N. Nakamura & T. Sato, 'Chiral interactions in polymer liquid crystals reflecting polymer conformations: Triple-helical polysaccharide schizophyllan and poly(γ-benzyl L-glutamate),' *Macromolecules*, **36**, 2108, 2003.

[601] Z. Dogic & S. Fraden, 'Cholesteric phase in virus suspensions,' *Langmuir*, **16**, 7820, 2000.

[602] E. Grelet & S. Fraden, 'What is the origin of chirality in the cholesteric phase of virus suspensions?' *Phys. Rev. Lett.*, **90**, 198302, 2003.

[603] Z. Dogic & S. Fraden, 'Ordered phases of filamentous viruses,' *Curr. Opin. Colloid Interface Sci.*, **11**, 47, 2006.

[604] F. Tombolato, A. Ferrarini & E. Grelet, 'Chiral nematic phase of suspensions of rodlike viruses: Left-handed phase helicity from a right-handed molecular helix,' *Phys. Rev. Lett.*, **96**, 258302, 2006.

[605] J. Cao, S. Liu, J. Xiong, Y. Chen & Z. Zhang, 'Stimuli responsive chiral liquid crystal phases of phenylboronic acid functionalized rodlike viruses and their interaction with biologically important diols,' *Chem. Commun.*, **50**, 10402, 2014.

[606] S. M. Aharoni, 'Rigid backbone polymers. 2. Polyisocyanates and their liquid-crystal behavior,' *Macromolecules*, **12**, 94, 1979.

[607] T. Sato, Y. Sato, Y. Umemura, A. Teramoto, Y. Nagamura, J. Wagner, D. Weng, Y. Okamoto, K. Hatada & M. M. Green, 'Polyisocyanates and the interplay of experiment and theory in the formation of lyotropic cholesteric states,' *Macromolecules*, **26**, 4551, 1993.

[608] J. Watanabe, H. Kamee & M. Fujiki, 'First observation of thermotropic cholesteric liquid crystal in helical polysilane,' *Polym. J.*, **33**, 495, 2001.

[609] Y. Wang, J. Xu, Y. Wang & H. Chen, 'Emerging chirality in nanoscience,' *Chem. Soc. Rev.*, **42**, 2930, 2013.

[610] M. Hentschel, M. Schäferling, X. Duan, H. Giessen & N. Liu, 'Chiral plasmonics,' *Sci. Adv.*, **3**, e1602735, 2017.

[611] G. Meier, E. Sackmann & J. G. Grabmaier, *Applications of Liquid Crystals* (Springer-Verlag, Berlin), 1st edition, 1975.

[612] J.-F. Janson, 'Applications of LCP Materials,' in A. A. Collyer (editor), *Liquid Crystal Polymers: From Structures to Applications*, chapter 9, pp. 447–463 (Springer, Dordrecht), 1st edition, 1992.

[613] S. J. Woltman, G. D. Jay & G. P. Crawford, 'Liquid-crystal materials find a new order in biomedical applications,' *Nat. Mater.*, **6**, 929, 2007.

[614] J. P. F. Lagerwall, C. Schütz, M. Salajkova, J. Noh, J. H. Park, L. Bergström & G. Scalia, 'Cellulose nanocrystal-based materials: From liquid crystal self-assembly and glass formation to multifunctional thin films,' *NPG Asia Mater.*, **6**, e80, 2014.

[615] E. Yashima, N. Ousaka, D. Taura, K. Shimomura, T. Ikai & K. Maeda, 'Supramolecular helical systems: Helical assemblies of small molecules, foldamers, and polymers with chiral amplification and their functions,' *Chem. Rev.*, **116**, 13752, 2016.

[616] N. Dal Mas, A. Ferrarini, P. L. Nordio, P. Styring & S. M. Todd, 'Prediction of pitch in twisted nematics: Puzzling cases,' *Mol. Cryst. Liq. Cryst. Sci. Technol. A.*, **328**, 391, 2007.

[617] A. B. Harris, R. D. Kamien & T. C. Lubensky, 'Molecular chirality and chiral parameters,' *Rev. Mod. Phys.*, **71**, 1745, 1999.

[618] S. Dussi, S. Belli, R. van Roij & M. Dijkstra, 'Cholesterics of colloidal helices: Predicting the macroscopic pitch from the particle shape and thermodynamic state,' *J. Chem. Phys.*, **142**, 074905, 2015.

[619] T. Gibaud, E. Barry, M. J. Zakhary, M. Henglin, A. Ward, Y. Yang, C. Berciu, R. Oldenbourg, M. F. Hagan, D. Nicastro, R. B. Meyer & Z. Dogic, 'Reconfigurable self-assembly through chiral control of interfacial tension,' *Nature*, **481**, 348, 2012.

[620] S. Iamsaard, S. J. Aßhoff, B. Matt, T. Kudernac, J. J. L. M. Cornelissen, S. P. Fletcher & N. Katsonis, 'Conversion of light into macroscopic helical motion,' *Nat. Chem.*, **6**, 229, 2014.

[621] W. Feng, J.-Y. Kim, X. Wang, H. A. Calcaterra, Z. Qu, L. Meshi & N. A. Kotov, 'Assembly of mesoscale helices with near-unity enantiomeric excess and light-matter interactions for chiral semiconductors,' *Sci. Adv.*, **3**, e1601159, 2017.

[622] B. Sung, A. De La Cotte & E. Grelet, 'Chirality-controlled crystallization via screw dislocations,' *Nat. Commun.*, **9**, 1405, 2018.

[623] H. H. Wensink & G. Jackson, 'Cholesteric order in systems of helical Yukawa rods,' *J. Phys.: Condens. Matter*, **23**, 194107, 2011.

[624] E. Frezza, A. Ferrarini, H. B. Kolli, A. Giacometti & G. Cinacchi, 'Left or right cholesterics? A matter of helix handedness and curliness,' *Phys. Chem. Chem. Phys.*, **16**, 16225, 2014.

[625] S. Dussi & M. Dijkstra, 'Entropy-driven formation of chiral nematic phases by computer simulations,' *Nat. Commun.*, **7**, 11175, 2016.

[626] A. B. Harris, R. D. Kamien & T. C. Lubensky, 'Microscopic origin of cholesteric pitch,' *Phys. Rev. Lett.*, **78**, 1476, 1997.

[627] R. Oda, I. Huc, M. Schmutz, S. J. Candau & F. C. MacKintosh, 'Tuning bilayer twist using chiral counterions,' *Nature*, **399**, 566, 1999.

[628] D. H. Van Winkle, M. W. Davidson, W.-X. Chen & R. L. Rill, 'Cholesteric helical pitch of near persistence length DNA,' *Macromolecules*, **23**, 4140, 1990.

[629] C. B. Stanley, H. Hong & H. H. Strey, 'DNA cholesteric pitch as a function of density and ionic strength,' *Biophys. J.*, **89**, 2552, 2005.

[630] Z. Dogic & S. Fraden, 'Smectic phase in a colloidal suspension of semiflexible virus particles,' *Phys. Rev. Lett.*, **78**, 2417, 1997.

[631] E. Barry, D. Beller & Z. Dogic, 'A model liquid crystalline system based on rodlike viruses with variable chirality and persistence length,' *Soft Matter*, **5**, 2563, 2009.

[632] Z. Zhang & E. Grelet, 'Tuning chirality in the self-assembly of rod-like viruses by chemical surface modifications,' *Soft Matter*, **9**, 1015, 2013.

[633] S. B. Murray & A. C. Neville, 'The role of pH, temperature and nucleation in the formation of cholesteric liquid crystal spherulites from chitin and chitosan,' *Int. J. Biol. Macromol.*, **22**, 137, 1998.

[634] P. De Sa Peixoto, A. Deniset-Besseau, M.-C. Schanne-Klein & G. Mosser, 'Quantitative assessment of collagen I liquid crystal organizations: Role of ionic force and acidic solvent, and evidence of new phases,' *Soft Matter*, **7**, 11203, 2011.

[635] J. P. Straley, 'Theory of piezoelectricity in nematic liquid crystals, and of the cholesteric ordering,' *Phys. Rev. A*, **14**, 1835, 1976.

[636] M. M. C. Tortora & J. P. K. Doye, 'Hierarchical bounding structures for efficient virial computations: Towards a realistic molecular description of cholesterics,' *J. Chem. Phys.*, **147**, 224504, 2017.

[637] F. Tombolato & A. Ferrarini, 'From the double-stranded helix to the chiral nematic phase of B-DNA: A molecular model,' *J. Chem. Phys.*, **122**, 054908, 2005.

[638] M. M. C. Tortora & J. P. K. Doye, 'Incorporating particle flexibility in a density functional description of nematics and cholesterics,' *Mol. Phys.*, **116**, 2773, 2018.

[639] R. Cortini, X. Cheng & J. C. Smith, 'The tilt-dependent potential of mean force of a pair of DNA oligomers from all-atom molecular dynamics simulations,' *J. Phys.: Condens. Matter*, **29**, 084002, 2017.

[640] S. Fraden, 'Phase Transitions in Colloidal Suspensions of Virus Particles,' in M. Baus, L. F. Rull & J. P. Ryckaert (editors), *Observation, Prediction and Simulation of Phase Transitions in Complex Fluids*, chapter 3, pp. 113–164 (Kluver Academic Publishers, Dordrecht), 1995.

[641] S. Tomar, M. M. Green & L. A. Day, 'DNA-protein interactions as the source of large-length-scale chirality evident in the liquid crystal behavior of filamentous bacteriophages,' *J. Am. Chem. Soc.*, **129**, 3367, 2007.

[642] F. C. Bawden, N. W. Pirie, J. D. Bernal & I. Fankuchen, 'Liquid crystalline substances from virus-infected plants,' *Nature*, **138**, 1051, 1936.

[643] D. A. Marvin, L. C. Welsh, M. F. Symmons, W. R. P. Scott & S. K. Straus, 'Molecular structure of fd (f1, M13) filamentous bacteriophage refined with respect to X-ray fibre diffraction and solid-state NMR data supports specific models of phage assembly at the bacterial membrane,' *J. Mol. Biol.*, **355**, 294, 2005.

[644] D. S. Thiriot, A. A. Nevzorov, L. Zagyanskiy, C. H. Wu & S. J. Opella, 'Structure of the coat protein in Pf1 bacteriophage determined by solid-state NMR spectroscopy,' *J. Mol. Biol.*, **341**, 869, 2004.

[645] A. L. Hitt, A. R. Cross & R. C. Williams, Jr., 'Microtubule solutions display nematic liquid crystalline structure,' *J. Biol. Chem.*, **265**, 1639, 1990.

[646] H. Dietz, S. M. Douglas & W. M. Shih, 'Folding DNA into twisted and curved nanoscale shapes,' *Science*, **325**, 725, 2009.

[647] C. De Michele, G. Zanchetta, T. Bellini, E. Frezza & A. Ferrarini, 'Hierarchical propagation of chirality through reversible polymerization: The cholesteric phase of DNA oligomers,' *ACS Macro Lett.*, **5**, 208, 2016.

[648] D. M. Hall, I. R. Bruss, J. R. Barone & G. M. Grason, 'Morphology selection via geometric frustration in chiral filament bundles,' *Nat. Mater.*, **15**, 727, 2016.

[649] H. Shen, J. A. Fallas, E. Lynch, W. Sheffler, B. Parry, N. Jannetty, J. Decarreau, M. Wagenbach, J. J. Vicente, J. Chen, L. Wang, Q. Dowling, G. Oberdorfer, L. Stewart, L. Wordeman, J. De Yoreo, C. Jacobs-Wagner, J. Kollman & D. Baker, 'De novo design of self-assembling helical protein filaments,' *Science*, **362**, 705, 2018.

[650] P. W. K. Rothemund, 'Folding DNA to create nanoscale shapes and patterns,' *Nature*, **440**, 297, 2006.

[651] B. E. K. Snodin, J. S. Schreck, F. Romano, A. A. Louis & J. P. K. Doye, 'Coarse-grained modelling of the structural properties of DNA origami,' *Nucleic Acids Res.*, **47**, 1585, 2019.

[652] R. R. Sinden, *DNA Structure and Function* (Academic Press, London), 1st edition, 1994.

[653] J. N. Milstein & J. C. Meiners, 'Worm-Like Chain (WLC) Model,' in *Encyclopedia of Biophysics* (Springer, Berlin), 2013.